

CRANFIELD UNIVERSITY

School of Applied Sciences

PhD THESIS

ALUMINIUM-BASED COATINGS  
FOR CADMIUM REPLACEMENT

Emanuele Cardilli

CRANFIELD UNIVERSITY  
School of Applied Sciences

PhD THESIS

Academic Years 2005-2008

Emanuele Cardilli

ALUMINIUM-BASED COATINGS  
FOR CADMIUM REPLACEMENT

Supervisor: Dr. M. J. Robinson

June 2008

# CONTENTS

<b>ABSTRACT .....</b>	<b>V</b>
<b>LIST OF FIGURES .....</b>	<b>VII</b>
<b>LIST OF TABLES .....</b>	<b>XIV</b>
<b>INTRODUCTION.....</b>	<b>1</b>
<b>1 LITERATURE REVIEW .....</b>	<b>7</b>
<b>1.1 Introduction .....</b>	<b>7</b>
<b>1.2 Electrochemical nature of aqueous corrosion .....</b>	<b>7</b>
1.2.1 Corrosion potential and current density .....	11
1.2.2 Electrochemical nature of galvanic corrosion.....	14
1.2.2.1 Two-metals galvanic corrosion .....	14
1.2.2.2 Cathodic protective coatings .....	16
<b>1.3 Cadmium sacrificial coatings and alternatives to cadmium .....</b>	<b>17</b>
1.3.1 Introduction.....	17
1.3.2 Previous studies on cadmium replacement at Cranfield University.....	17
1.3.3 Ion Vapour Deposition (IVD) aluminium.....	22
1.3.4 Electrodeposited Zn-Ni.....	23
1.3.5 Chromate conversion coatings (CCCs) on aluminium and steel substrate.....	25
1.3.6 Electroplated Aluminium.....	26
1.3.7 Modified aluminium coatings by addition of Zn or Mg.....	27
<b>1.4 Hydrogen embrittlement.....</b>	<b>27</b>
1.4.1 Barrier effect of coatings.....	31
1.4.2 Solubility of hydrogen in metals .....	33
<b>1.5 Health risk of cadmium.....</b>	<b>34</b>
1.5.1 Cadmium toxicity.....	34
1.5.1.1 Occupational hazard definition .....	35
<b>2 METHODS .....</b>	<b>37</b>
<b>2.1 Materials.....</b>	<b>37</b>
2.1.1 Substrates .....	37
2.1.2 Coatings .....	38
2.1.2.1 SermeTel coatings .....	39
2.1.2.2 New SermeTel Coatings.....	40

2.1.2.3	Zn-Ni coatings.....	41
2.1.2.4	Electroplated aluminium .....	41
<b>2.2</b>	<b>Corrosion testing .....</b>	<b>42</b>
2.2.1	Corrosion Potential Measurements .....	43
2.2.2	Linear Polarisation Measurement (LPR).....	43
2.2.3	Galvanic test for steel substrate coatings .....	46
2.2.4	Galvanic test for aluminium/bronze coatings.....	46
2.2.5	Polarisation behaviour test .....	47
2.2.6	Marine Exposure.....	49
<b>2.3</b>	<b>Selective attack and coatings characterization .....</b>	<b>49</b>
2.3.1	Corrosion micromonitoring-EDX SEM analysis .....	50
2.3.2	Focus Ion Beam (FIB).....	50
2.3.3	X-Ray Diffraction .....	51
2.3.3.1	Rocking curve .....	51
2.3.4	Coating thicknesses.....	51
<b>2.4</b>	<b>Mechanical testing.....</b>	<b>52</b>
2.4.1	Hydrogen Re-embrittlement Testing.....	52
<b>3</b>	<b>RESULTS .....</b>	<b>53</b>
<b>3.1</b>	<b>Sacrificial coating for steel substrate .....</b>	<b>53</b>
3.1.1	LPR Measurements .....	53
3.1.2	Galvanic Coupling Measurement.....	67
3.1.3	Marine exposure.....	93
3.1.4	Hydrogen Re-embrittlement Tests .....	96
3.1.4.1	Uncoated Control Specimens .....	96
3.1.4.2	SermeTel CR984-LT Coatings.....	96
3.1.4.3	SermeTel CF1725 Chromium Free Coatings .....	98
3.1.4.4	Electrodeposited cadmium coatings .....	100
3.1.4.5	Aluminium alloy 7075 sprayed coatings.....	102
3.1.4.6	Zn modified 984 coatings.....	103
3.1.4.7	Mg/Al modified 984 coatings.....	104
3.1.4.8	IVD aluminium coatings .....	105
3.1.5	Selective attack and coating characterization.....	106
3.1.5.1	Optical-thickness measurement.....	106
3.1.5.2	SEM analysis and Focused Ion Beam on 984A .....	110
3.1.5.3	SEM-EDX analysis .....	118
3.1.5.4	X-ray diffraction.....	124



<b>3.2</b>	<b>Compatibility coatings .....</b>	<b>127</b>
3.2.1	Galvanic test Results and Discussion.....	127
3.2.1.1	Galvanic test between aluminium alone.....	127
3.2.1.2	Mixed potentials.....	128
3.2.1.3	Galvanic currents .....	130
3.2.1.4	Appearance of the panels after the galvanic corrosion test .....	138
3.2.1.5	Repetition of the galvanic test.....	141
3.2.2	Polarisation curves .....	141
3.2.3	Linear polarisation resistance.....	159
<b>4</b>	<b>DISCUSSION.....</b>	<b>164</b>
<b>4.1</b>	<b>Selection of sacrificial coatings for high strength steel substrate .....</b>	<b>166</b>
4.1.1	Extent of the problem.....	167
4.1.2	Corrosion potentials of the alternative coatings.....	168
4.1.3	Summary of self-corrosion rates .....	170
4.1.4	Appearance of red rust .....	172
4.1.5	Hydrogen re-embrittlement risk.....	173
4.1.5.1	IVD coating detachment.....	177
4.1.6	Effect of applied cathodic potential .....	178
4.1.7	Effect of the exchange current density on the hydrogen re-embrittlement .....	181
4.1.8	Increase of the amount of the hydrogen absorbed in the porosity of the coating .....	183
4.1.9	Advantage of the use of aluminium in terms of metal loss .....	185
4.1.10	Total corrosion.....	187
4.1.11	Selection of the coating.....	189
<b>4.2</b>	<b>Selection of the compatibility coatings for aluminium/bronze assembly .....</b>	<b>193</b>
4.2.1	Extent of the problem.....	193
4.2.2	Effect of applying a coating .....	193
4.2.3	Comparison of the charge produced by each coating.....	194
4.2.4	Time to coating reversal.....	195
4.2.5	Potentials of the coatings .....	195
4.2.6	Corrosion control .....	197
4.2.7	Lifetime of the coatings .....	202
<b>4.3</b>	<b>Overall discussion.....</b>	<b>204</b>
<b>5</b>	<b>CONCLUSIONS .....</b>	<b>209</b>
<b>5.1</b>	<b>Alternative sacrificial coatings for high strength steel substrate .....</b>	<b>209</b>
<b>5.2</b>	<b>Alternative compatible coatings for aluminium/bronze assemblies.....</b>	<b>210</b>

5.3	General conclusions.....	211
5.4	Future Work .....	212
	<b>APPENDIX.....</b>	<b>214</b>
A)	Interpretation of polarisation curves .....	214
B)	Stern-Geary values .....	217
C)	Weibull Model of Failure Times.....	218
	<b>REFERENCES.....</b>	<b>220</b>

## **ABSTRACT**

Cadmium electroplating is widely used in the aerospace industry for the corrosion protection of high strength steels. Cadmium is also used as compatible coating to reduce the galvanic corrosion generated in the assembly of components manufactured with different materials. However, environmental and safety concerns over the high toxicity of cadmium has led to the investigation of suitable replacements.

Aluminium coatings are promising coatings for the replacement of electroplated cadmium. Previous studies have shown that the use of SermeTel 984, a commercial aluminium sprayed coating, is beneficial in eliminating the hydrogen direct embrittlement without increasing the risk of re-embrittlement. However, the coating has shown to be prone to passivation in the mild corrosive environment. The addition of active zinc and magnesium particles are thought to avoid the passivation of the aluminium. A range of modified SermeTel 984 coatings, containing 0.5%, 3%, 10% and 50% of zinc, and SermeTel 984 modified with the addition of 30% and 50% of Mg/Al alloy particles in weight have been evaluated as possible alternatives. Chromium free SermeTel 984 and a SermeTel 984 modified with aluminium alloy 7075 particles together with IVD aluminium coatings have also been included in the project.

The sacrificial protection of the new coatings has been evaluated together with the associated risk of hydrogen re-embrittlement and compared with the electroplated cadmium.

Zinc modified SermeTel 984, containing 1% of zinc and 5% of zinc electroplated aluminium, IVD aluminium and electroplated Zn-Ni coatings have been studied as alternative coatings to cadmium as compatible coatings.

Slow strain rate testing has been performed to study the effect of hydrogen on the re-embrittlement of steel substrate as a result of the corrosion of the aluminium-based coatings in 3.5% NaCl. Linear polarisation testing in 3.5% NaCl has been used to

evaluate the self-corrosion rates of the coatings; galvanic coupling measurements have been used in the case of steel substrate to evaluate the sacrificial properties or, in the case of bronze/aluminium assembly, to evaluate the compatibility properties of the coatings. Polarisation behaviour tests have been used to study the anodic or cathodic control of the corrosion mechanisms. Total corrosion, calculated as the addition of self-corrosion and galvanic corrosion, has been calculated to evaluate the duration of the coating in service compared to electroplated cadmium.

## LIST OF FIGURES

Figure 1. Anodic and cathodic half-cell reactions present simultaneously on a corroding zinc surface .....	12
Figure 2. Polarisation of anodic and cathodic half-cell reactions for zinc in acid solution to give a mixed potential, $E_{corr}$ , and a corrosion rate (current density), $i_{corr}$ .....	13
Figure 3. Galvanic Series of seawater. Yellow box indicate behaviour for active-passive alloys. (From Denny A. Jones – Principles and Prevention of Corrosion, p.169, 1992).....	14
Figure 4. Schematic polarisation in a galvanic couple between corroding metals M (anode) and N(cathode). (From Denny A. Jones – Principles and Prevention of Corrosion, p.175, 1992) .....	15
Figure 5. Hydrogen evolution and absorption [29].....	30
Figure 6. Example of polarisation curves recorded at different times for CF1725 coating after 44 hours (bottom graph), 76 hours (middle graph) and after 102 hours (top graph) .....	44
Figure 7. Example of $R_p$ calculation from a polarisation resistance measurement on CF1725 coating .....	45
Figure 8. Three metal galvanic corrosion measurement configuration.....	47
Figure 9. Three star configuration for polarisation behaviour test.....	48
Figure 10. Sample preparing procedure for interface observation.....	51
Figure 11 .Dimensions of slow strain rate tensile specimens .....	52
Figure 12. Corrosion potentials of 984 commercial coating compared with electroplated Cd. Tested in naturally aerated 3.5% NaCl solution. ....	53
Figure 13. Corrosion rate of 984 commercial coating compared with electroplated Cd. Tested in naturally aerated 3.5% NaCl solution .....	54
Figure 14. Appearance of unmodified 984 on the left and Cd electroplated on the right. Tested for ten days in naturally aerated 3.5% NaCl solution.....	55
Figure 15. Corrosion potentials of Zn modified 984 coatings compared with electroplated Cd and unmodified 984. Tested in naturally aerated 3.5% NaCl solution .....	55
Figure 16. Appearance of 50%Zn modified 984 on the left and 10%Zn modified 984 on the right. Tested for ten days in naturally aerated 3.5% NaCl solution.....	56
Figure 17. Corrosion rate of Zn modified 984 coatings compared with unmodified 984 and electroplated Cd. Tested in naturally aerated 3.5% NaCl solution. ....	56
Figure 18. Appearance of 3%Zn modified 984 on the left and 0.5%Zn modified 984 on the right. Tested for ten days in naturally aerated 3.5% NaCl solution.....	57
Figure 19. Corrosion potentials of Zn modified 984 coatings compared with electroplated Cd and unmodified 984. Tested in naturally aerated 3.5% NaCl solution .....	58
Figure 20. Corrosion rate of Mg modified 984 coatings compared with unmodified 984 and electroplated Cd. Tested in naturally aerated 3.5% NaCl solution .....	59
Figure 21. Appearance of 50%Mg modified 984 on the left and 30%Mg modified 984 on the right. Tested for ten days in naturally aerated 3.5% NaCl solution.....	59

Figure 22. Corrosion potentials of aluminium alloy 7075 coating compared with electroplated Cd and unmodified 984 tested in naturally aerated 3.5% NaCl solution.....	60
Figure 23 Corrosion rate of 7075 coating compared with unmodified 984 and electroplated Cd tested in naturally aerated 3.5% NaCl solution. ....	61
Figure 24. Appearance aluminium alloy 7075 coating on the left and chromium free 1725 on the right. Tested for ten days in naturally aerated 3.5% NaCl solution.....	61
Figure 25. Corrosion potentials of chromium free 1725 coating compared with electroplated Cd and unmodified 984 tested in naturally aerated 3.5% NaCl solution.....	62
Figure 26. Corrosion rate of chromium free 1725 coating compared with unmodified 984 and electroplated Cd tested in naturally aerated 3.5% NaCl solution.....	63
Figure 27. Corrosion potentials of pure aluminium IVD coatings compared with electroplated Cd and unmodified 984 tested in naturally aerated 3.5% NaCl solution.....	64
Figure 28 Corrosion rate pure aluminium IVD coatings compared with unmodified 984 and electroplated Cd tested in naturally aerated 3.5% NaCl solution.....	65
Figure 29. Appearance pure aluminium IVD1 on the left, IVD2 in the middle and IVD3 on the right. Tested for ten days in naturally aerated 3.5% NaCl solution.....	65
Figure 30. Couple potential of 984, 50% Zn 984 and Cd with steel .....	67
Figure 31. Couple potential of 50% Zn 984 with steel (blue line) and galvanic current (yellow line) .	68
Figure 32. Appearance of 50% Zn 984 and steel panels after ten days of testing. Coated panel on the left and steel panel on the right. ....	68
Figure 33. Couple potential of 984, 10% Zn 984 and Cd with steel .....	69
Figure 34. Couple potential of 10% Zn 984 with steel (blue line) and galvanic current (yellow line) .	70
Figure 35. Appearance of 10% Zn 984 and steel panels after ten days of testing. Coated panel on the left and steel panel on the right. ....	70
Figure 36. Couple potential of 3% Zn 984 with steel .....	71
Figure 37. Couple potential of 3% Zn 984 with steel (blue line) and galvanic current (yellow line) ...	72
Figure 38. Appearance of 3% Zn 984 and steel panel after ten days of testing. Coated panel on the left and steel panel on the right .....	72
Figure 39. Couple potential of 0.5% Zn 984 with steel .....	73
Figure 40. Couple potential of 0.5% Zn 984 with steel (blue line) and galvanic current (yellow line)	74
Figure 41. Appearance of 0.5% Zn 984 and steel panels after ten days of testing. Coated panel on the left and steel panel on the right.....	74
Figure 42. Couple potential of 50% Mg 984 with steel .....	75
Figure 43. Couple potential of 50% Mg 984 with steel (blue line) and galvanic current (yellow line) .....	76
Figure 44. Appearance of 50% Mg 984 and steel panels after ten days of testing. Coated panel on the left and steel panel on the right.....	76
Figure 45. Couple potential of 30% Mg 984 with steel .....	77

Figure 46. Couple potential of 30% Mg 984 with steel (blue line) and galvanic current (yellow line)	78
Figure 47. Appearance of 30% Mg 984 and steel panels after ten days of testing. Coated panel on the left and steel panel on the right	78
Figure 48. Couple potential of 7075 with steel	79
Figure 49. Couple potential of 7075 with steel (blue line) and galvanic current (yellow line)	80
Figure 50. Appearance of 7075 and steel panels after ten days of testing. Coated panel on the left and steel panel on the right	80
Figure 51. Couple potential of 984 with steel	81
Figure 52. Couple potential of 984 with steel (blue line) and galvanic current (yellow line)	82
Figure 53 Appearance of 984 and steel panels after ten days of testing. Coated panel on the left and steel panel on the right	82
Figure 54. Couple potential of 1725 with steel	83
Figure 55. Couple potential of Chromium Free 1725 with steel (blue line) and galvanic current (yellow line)	84
Figure 56. Appearance of 1725 and steel panels after ten days of testing. Coated panel on the left and steel panel on the right	84
Figure 57. Couple potential of IVD1 with steel	85
Figure 58. Couple potential of IVD1 with steel (blue line) and galvanic current (yellow line)	86
Figure 59 Appearance of IVD1 and steel panels after ten days of testing. Coated panel on the left and steel panel on the right	86
Figure 60. Couple potential of IVD2 with steel	87
Figure 61. Couple potential of IVD2 with steel (blue line) and galvanic current (yellow line)	88
Figure 62 Appearance of IVD2 and steel panels after ten days of testing. Coated panel on the left and steel panel on the right	88
Figure 63. Couple potential of IVD3 with steel	89
Figure 64. Couple potential of IVD3 with steel (blue line) and galvanic current (yellow line)	90
Figure 65 Appearance of IVD3 and steel panels after ten days of testing. Coated panel on the left and steel panel on the right	90
Figure 66. Couple potential of Cd with steel	91
Figure 67. Couple potential of Cd with steel (blue line) and galvanic current (yellow line)	92
Figure 68 Appearance of Cd and steel panels after ten days of testing. Coated panel on the left and steel panel on the right	92
Figure 69. Appearance of A-50%Zn, B-10%Zn and C-3%Zn modified 984 after four months in marine exposure	93
Figure 70. Appearance of D-0.5%Zn, E-50%Mg/Al and F-30%Mg/Al modified 984 after four months in marine exposure	94
Figure 71. Appearance of G-7075, unmodified H-984 and CF1725 after four months in marine exposure	94

Figure 72. Appearance of IVD1, IVD2 and IVD3 after four months in marine exposure .....	95
Figure 73. Appearance of IVD3 and electroplated Cd after four months in marine exposure .....	95
Figure 74. Weibull plot for uncoated AISI 4340 specimens tested in air .....	96
Figure 75 .Weibull plot showing the re-embrittlement of CR984-LT coated specimens tested in 3.5% NaCl solution .....	97
Figure 76 . Comparison of Load/time graphs for specimens coated with CR984-LT tested in 3.5%NaCl and an uncoated control tested in air .....	98
Figure 77. Weibull plot showing the effect of additional heat treatment at 243°C for 24 hours on failure times of uncoated AISI 4340 .....	99
Figure 78 .Weibull plot comparing re-embrittlement of specimens coated with CR984-LT and CF1725 .....	100
Figure 79 .Weibull plot showing re-embrittlement of cadmium plated specimens tested in 3.5% NaCl solution .....	102
Figure 80. Weibull plot for times to failure of 7075(2) coated specimens vs. uncoated specimens ...	103
Figure 81. Weibull plot for times to failure of Zn modified 984 coated specimens vs. uncoated specimens.....	104
Figure 82. Weibull plot for times to failure of magnesium modified 984 coatings vs. uncoated specimens.....	105
Figure 83. Weibull plot for times to failure of magnesium IVD aluminium coatings vs. uncoated specimens.....	106
Figure 84. Optical image of 984A (50%Zn) cross section. Magnification 40x. ....	107
Figure 85. Optical image of 984E (50%Mg/Al) cross section. Magnification 40x.....	107
Figure 86. Optical image of 7075 aluminium alloy coating cross section. Magnification 40x.....	108
Figure 87. Optical image of 984H free cross section. Magnification 40x. ....	109
Figure 88. Optical image of IVD2 cross section. Magnification 40x. ....	109
Figure 89. Optical image of electroplated Cd cross section. Magnification 40x. ....	110
Figure 90. SEM Secondary Electrons top view of “as made” 984 A surface”. Bias voltage 15kV....	111
Figure 91. Secondary Electrons image of “as made” 984A cross section on the left and zinc mapping on the right. Bias voltage 15kV. ....	112
Figure 92. FIB section of 984 A “as made”. Bias voltage 15kV. ....	113
Figure 93. Back Scattered Electrons image of FIB section for 984 A after 10 days in 3.5% NaCl. Bias voltage 15kV.....	114
Figure 94. Secondary Electrons image of FIB section for 984 A after 10 days in 3.5% NaCl .....	115
Figure 95. SEM Secondary Electrons image of FIB for 984 A 10 days in 3.5% NaCl solution. Particular of the coating surface. Bias voltage 5kV. ....	117
Figure 96. Etched area by FIB for 984A (50%Zn) after 10 days in 3.5% NaCl solution. View of the coating interface with the steel substrate on the left. Zinc mapping on the right. ....	118
Figure 97. Area marked by four Vickers indentations. Bias voltage 15kV. ....	119
Figure 98. ES SEM image of 984A after polishing. Bias voltage 15kV.....	120



Figure 99. ES SEM image of 984A after 4 days in 3.5% NaCl. Bias voltage 15kV.....	122
Figure 100. From left to right zinc and chlorine mapping by EDX of 984 A (50%Zn) surface after 4 days in 3.5% NaCl solution. Bias voltage 15kV.....	123
Figure 101. Iron mapping by EDX of 984 A (50%Zn) surface after 4 days in 3.5% NaCl solution. Bias voltage 15kV.....	124
Figure 102. Diffraction pattern of 984 A after 10 days of exposure in 3.5% NaCl in aerated solution. ....	125
Figure 103. Iron oxide and chloride reference pattern in blue. ....	125
Figure 104. Diffraction pattern of 984 A after 10 days of exposure in 3.5% NaCl in aerated solution. NaCl reference pattern in green colour. ....	126
Figure 105. Comparison for different incident angles between a corrosion compound main peak and aluminium main peak.....	127
Figure 106. Galvanic corrosion measurement between the bronze and the aluminium panels. Surface area of 16 cm <sup>2</sup> for both the panels.....	128
Figure 107. Mixed potential of the galvanic couples during the ten days of galvanic test. ....	129
Figure 108. Three metal galvanic corrosion measurements. Bronze-Aluminium-Passivated Cadmium. ....	131
Figure 109. Galvanic currents. Bronze-Aluminium-Unpassivated Cadmium. ....	132
Figure 110. Galvanic currents. Bronze-Aluminium-ZiNi coating. ....	133
Figure 111. Galvanic currents. Bronze-Aluminium-Electroplated Aluminium. ....	134
Figure 112. Galvanic currents. Bronze-Aluminium-984 (1% Zinc) coating.....	135
Figure 113. Galvanic currents. Bronze-Aluminium-984 (5% Zinc) coating.....	136
Figure 114. Galvanic currents. Bronze-Aluminium-IVD Aluminium. ....	137
Figure 115. Appearance of the panels after the galvanic test. 10 days in 3.5% NaCl solution. ....	138
Figure 116. Appearance of the panels after the galvanic test. 10 days in 3.5% NaCl solution. ....	140
Figure 117. Polarisation curves before starting the galvanic current measurement. Aluminium and bronze panel with same surface area.....	142
Figure 118. Polarisation curves after ten day. Aluminium and bronze panel with same surface area.....	143
Figure 119. Passivated cadmium, bronze and aluminium. Galvanic currents and mixed potential. ...	144
Figure 120. Polarisation curves after one day. Passivated cadmium, aluminium panel and bronze panel. One resistor setup in continuous lines, three resistors setup in dashed lines. ....	145
Figure 121. Polarisation curves after ten days. Passivated cadmium, aluminium panel and bronze panel. One resistor setup in continuous lines, three resistors setup in dashed lines. ....	146
Figure 122. Unpassivated cadmium, bronze and aluminium. Galvanic currents and mixed potential. ....	147
Figure 123. Polarisation curves after one. Unpassivated cadmium, aluminium and bronze. One resistor setup in continuous lines, three resistors setup in dashed lines.....	148
Figure 124. Polarisation curves after ten days. Unpassivated cadmium, aluminium and bronze. One resistor setup in continuous lines, three resistors setup in dashed lines. ....	148

Figure 125. Electroplated aluminium, bronze and aluminium. Galvanic currents and mixed potential. ....	149
Figure 126. Polarisation curves after one day. Electroplated aluminium, aluminium panel and bronze panel. One resistor setup in continuous lines, three resistors setup in dashed lines. ....	150
Figure 127. Polarisation curves after ten days. Electroplated aluminium, aluminium panel and bronze panel. One resistor setup in continuous lines, three resistors setup in dashed lines. ....	150
Figure 128. IVD aluminium, bronze and aluminium. Galvanic currents and mixed potential. ....	151
Figure 129. Polarisation curves after one day of. IVD aluminium, aluminium and bronze. One resistor setup in continuous lines, three resistors setup in dashed lines. ....	152
Figure 130. Polarisation curves after ten days. IVD aluminium, aluminium and bronze. One resistor setup in continuous lines, three resistors setup in dashed lines. ....	152
Figure 131. Zn-10% Ni, bronze and aluminium. Galvanic currents and mixed potential. ....	153
Figure 132 Polarisation curves after one day. Zn-10% Ni, aluminium and bronze. One resistor setup in continuous lines, three resistors setup in dashed lines. ....	154
Figure 133. Polarisation curves after ten days. Zn-10% Ni, aluminium and bronze. One resistor setup in continuous lines, three resistors setup in dashed lines. ....	154
Figure 134. 984-1% zinc, bronze and aluminium. Galvanic currents and mixed potential. ....	155
Figure 135. Polarisation curves after one day. 984-1% zinc, aluminium and bronze. One resistor setup in continuous lines, three resistors setup in dashed lines. ....	156
Figure 136. Polarisation curves after ten days. 984-1% zinc, aluminium and bronze. One resistor setup in continuous lines, three resistors setup in dashed lines. ....	156
Figure 137. Zn-10% Ni, bronze and aluminium. Galvanic currents and mixed potential. ....	157
Figure 138. Polarisation curves after one day. 984-5% zinc, aluminium and bronze. One resistor setup in continuous lines, three resistors setup in dashed lines. ....	158
Figure 139. Polarisation curves after ten days. 984-5% zinc, aluminium panel and bronze panel. One resistor setup in continuous lines, three resistors setup in dashed lines. ....	158
Figure 140. Open circuit potentials of 984-1% zinc, 984-5% zinc, Zn-10% Ni and unpassivated cadmium compared with the aluminium and the bronze. ....	160
Figure 141. Corrosion rates for unpassivated cadmium, 984-1% zinc, 984-5% zinc and Zn-10% Ni. ....	161
Figure 142. Open circuit potentials for passivated cadmium, electroplated aluminium and IVD aluminium compared with aluminium and bronze. ....	162
Figure 143. Corrosion rates of passivated cadmium, unpassivated cadmium, electroplated aluminium and IVD aluminium. ....	163
Figure 144. Effect of the sacrificial coating potential on the corrosion of the steel and on the risk of hydrogen re-embrittlement. ....	165
Figure 145. Total charge density passed by self-corrosion of coatings in 10 days in quiescent 3.5% NaCl solution. ....	171

Figure 146. Average coupling potential during the first day, average current over the first day and time of appearance of signs of red rust. ....	173
Figure 147. Weibull Plot of all the coatings .....	174
Figure 148. Re-embrittlement indices of all the coating.....	175
Figure 149. IVD1. Secondary electrons SEM image on the left and iron mapping on the right. Bias 15kV. ....	178
Figure 150. Comparison of mean failure times for specimens with freely corroding coatings and applied cathodic potentials. From [4] fig.7 p.31. ....	179
Figure 151. Comparison of mean failure times for specimens with freely corroding coatings and applied cathodic potentials.....	179
Figure 152. $E_0$ is the equilibrium electrode potential at the pH of the experiment .....	182
Figure 153. Hydrogen formation, adsorption and absorption on the steel substrate.....	183
Figure 154. Decrease of metal loss of the alternative aluminium-based coatings compared to electroplated cadmium in terms of metal loss expressed in percentages .....	187
Figure 155. Charge density for self-corrosion, galvanic corrosion and total corrosion calculated over a period of one day .....	188
Figure 156. Metal loss for galvanic corrosion and total corrosion calculated over a period of one day .....	189
Figure 157. Total charge density provided by the coatings during the galvanic test. ....	194
Figure 158. Illustration of the effect of the cathodic curve gradient on the corrosion currents compared with a situation of complete cathodic control (dashed line).....	202
Figure 159. Total corrosion after 3-days' exposure before reversal of any coating took place. ....	203
Figure 160. Total corrosion after 10-days' exposure .....	203
Figure 161. Polarisation behaviour curves between copper and steel. Area steel 24 cm <sup>2</sup> , area copper 8 cm <sup>2</sup> .....	215
Figure 162. Polarisation behaviour curves between copper and steel. Area steel 48 cm <sup>2</sup> , area copper 8 cm <sup>2</sup> .....	215
Figure 163. Polarisation behaviour curves between copper and steel. Area steel 24 cm <sup>2</sup> , area copper 24 cm <sup>2</sup> .....	216
Figure 164. Schematic Weibull plot of failure times .....	219

## LIST OF TABLES

Table 1. Standard Electrode Force Potentials	10
Table 2. Cadmium safety data sheet, from International Labour Organization database (Cadmium ICSC 0200 April 2005).	35
Table 3. Composition of AISI 4340 Steel in weight %	37
Table 4. Composition of the aluminium and aluminium/bronze panels for the study of aluminium/bronze assemblies	38
Table 5. Summary of coating types and nominal compositions	39
Table 6. Electroplated aluminium specifications	42
Table 7. Appearance of the solutions and the coating surfaces from the first to the tenth day. WP=White Products of corrosion, RR=Red rust, WS=White solution, RS=Red solution, DP=dark pits on the coating, GC=Gel on the coating, UD=uniform darkening.	66
Table 8. Coatings thickness. Values measured from coatings cross sections.	110
Table 9. EDX analysis of the area marked in Figure 90.	111
Table 10. EDX analysis of area selected in Figure 91.	112
Table 11. EDX analysis of points marked in Figure 94. Percentages in weight	116
Table 12. EDX analysis of area selected in Figure 96. All the other elements except Zn and Al have been omitted. Percentages in weight.	118
Table 13. Point analysis of Spectrum2 and Spectrum3 as marked in Figure 98.	121
Table 14. Point analysis of Spectrum2 and Spectrum3 as marked in Figure 99.	123
Table 15. Summary of times to current reversal	141
Table 16. Initial corrosion potential of the coatings	168
Table 17. Corrosion potential of the coatings after 10 days	168
Table 18. Corrosion potential average in ten days and standard deviation in percentage	169
Table 19. Student's t-test on time to failure means for a 95% level of confidence. Green=coatings distributions belong to different populations; Red=coatings distributions do not belong to different populations	176
Table 20. Student's t-test on time to time to failure means for a 95% level of confidence. Green=coatings distributions belong to different populations; Red=coatings distributions do not belong to different populations	177
Table 21. Physical characteristics of some of the main elements of coatings	186
Table 22. Physical characteristics of the coating for the calculation of the metal loss	186
Table 23. Appearance of red rust in the galvanic test, metal loss caused by self-corrosion rate and hydrogen re-embrittlement indices	190
Table 24. Current averages over the first three days.	193
Table 25. Summary of times to current reversal	195
Table 26. OCPs of the coating, aluminium and bronze after one day of testing.	196
Table 27. OCPs of the coating, aluminium and bronze after ten days of testing.	196

Table 28. Zn-Ni and IVD coatings OCPs and mixed potentials after one day. Type of corrosion control after one day.	197
Table 29. Passivated Cadmium and Unpassivated Cadmium OCPs and mixed potentials after one day. Type of corrosion control after one day.	198
Table 30. 984-1% Zn and 984-5% Zn OCPs and mixed potentials after one day. Type of corrosion control after one day.	198
Table 31. Electroplated aluminium OCP and mixed potential after one day. Type of corrosion control after one day.	199
Table 32. Comparison between calculated current and measured current on the basis of the experimental Tafel constant	200
Table 33. $b_a$ and $b_c$ values used to calculate the Stern-Geary constants	217

## INTRODUCTION

The electrochemical characteristics of cadmium are currently utilised for the cathodic protection of individual mechanical components or to limit the problem of galvanic corrosion produced by the coupling of different metals. Due to its toxicity the use of cadmium will be limited in the future and alternative coatings have been studied as substitutes.

High strength steels used for some aeronautical components, are usually protected by the electrodeposition of a cadmium layer that avoids the contact between the steel and the corrosive environment. Moreover the electrochemical potential of the coating, i.e. more active than the potential of the steel, provides sacrificial protection where the coating is slightly damaged because of the presence of scratches, pores or other defects that could expose the substrate to corrosion phenomena. The use of sacrificial protective coatings in the aeronautical field is necessary in order to preserve the physical and chemical integrity of materials which are designed to provide good reliability of the different components for a long time.

Generally the use of sacrificial protective coatings does not cause any side effects to the substrate but in the case of high strength steels there is a problem related to the embrittlement, caused by hydrogen, which reduces the exceptional mechanical characteristics of these types of steel. The hydrogen responsible for the embrittlement could come from the chemical reactions related to the deposition of electrodeposited coatings or subsequently, from the reactions characteristic of the cathodic protection, regardless from the deposition technique utilised. In the first case, we will refer to “hydrogen embrittlement” and in the second case to “hydrogen re-embrittlement”.

The embrittlement can be effectively eliminated by thermal treatment and it has been proved by previous studies [1] that a baking treatment at 200°C for 24 hours is fully effective in the de-embrittlement of those steel specimens that had been electroplated.

The re-embrittlement is instead related to the protection that the coating provides to the metal and cannot be eliminated without reducing the development of hydrogen in the reactions or the penetration of the element through the coating.

The amount of hydrogen produced is dependent on the electrochemical characteristics of the coating and primarily on the potential of the coating. A different study [2] has shown that an additional under-layer of nickel, deposited between the protective coating and the steel substrate, is beneficial in decreasing the diffusion of hydrogen toward the steel because of the low diffusivity coefficient of the hydrogen in the metal. Nevertheless, the barrier effect that any coatings can provide as opposition to the hydrogen produced on its surface which is diffusing to the substrate, is a characteristic that also depends on its thickness and porosity and not only on the diffusion coefficient of the hydrogen in the material.

However, the possibility of effectively interposing a layer of nickel should still be accurately studied in the future to understand the consequences of the corrosion protection of the sacrificial coating. In the selection of the sacrificial coating to be used, it is important to correctly balance the protection provided with the negative effects due to the risk of hydrogen re-embrittlement, which is associated with the electrochemical characteristics of the coating and with its ability to reduce the diffusion of the hydrogen.

Most modern aerospace structural components are designed from low alloy high strength steels. These alloys generally have exceptional mechanical properties including yield and ultimate tensile strengths around 1800 and 2000 MPa, respectively.[1-3] The strength levels of these low alloyed steels are higher than virtually any other structural alloy, with approximately 40% strength to weight advantage over 7000 aluminium series, and superior mechanical properties compared to most titanium alloys.

The high strength steel selected for the project is one of the most commonly used low alloyed high strength steels for modern aerospace structural components. It is the

AISI-4340, a nickel-chromium-molybdenum low alloy steel, heat treated to reach tensile strength levels of approximately 1800 MPa. The alloy has a good combination of tensile strength (1700 to 2000 MPa), toughness and fatigue resistance for structural applications.

However, the main drawback of high strength steels is their intrinsic susceptibility to delayed failure, caused by hydrogen embrittlement (HE), stress corrosion cracking SCC, or fatigue.

The common sacrificial coating for the AISI 4340 is electroplated cadmium. Cadmium is a sacrificial coating to the steel, as its open-circuit potential is more negative than that of steel, suggesting that if the coating is damaged, cadmium will preferentially corrode instead of the exposed substrate.

Recent research at Cranfield University [1] has demonstrated that severe hydrogen re-embrittlement of high strength steel can occur when sacrificial protective coatings undergo corrosion. This finding could have important safety implications for high strength steel components used on aircraft. The extent of re-embrittlement is influenced by the corrosion potential of the coating and it is recommended that the potential should not be more active than is necessary to provide adequate protection of the steel.

Aluminium-based coatings have corrosion potentials that are similar to that of cadmium and the research to date has shown that they cause slightly less re-embrittlement. However, a disadvantage of some aluminium-based coatings is that they can passivate in mildly corrosive conditions, which leads to loss of their sacrificial properties. For these reasons, further research is required on aluminium-based coatings to obtain the optimum balance of their properties.

The aluminium-based coatings, examined in the programme as possible alternatives to Cd, were SermeTel CR984-LT and Alcotec Galvano-Aluminium.



A later study [3] considered different alternatives to electroplated cadmium, electroplated Zinc-14%Nickel alloys and aluminium-based coating SermeTel® 1140/962, which were strong candidates for the replacement of electroplated cadmium due to their promising characteristics.

In the two projects the two SermeTel coatings, showed the advantage of being able to eliminate the problem related to the hydrogen direct embrittlement caused by the electrodeposition. Despite the important results obtained by these studies with the alternative coatings, the tendency to passivation of 984 coatings in marine atmosphere exposure underlined the risk in using this coating as a good sacrificial coating. The addition of more active elements in this project has been thought to overcome the tendency to passivation of SermeTel 984.

A range of new coatings based on SermeTel CR984-LT, aluminium IVD coatings and aluminium alloy coatings, have been produced and their compositions have been modified to seek optimum properties. Suitable coatings need to be sufficiently active to provide adequate sacrificial protection to a steel substrate without passivating in service and without promoting excessive hydrogen uptake, which could lead to re-embrittlement.

SermeTel CR984 will therefore be modified by the addition of zinc and magnesium, which are more active metals than aluminium. These additions are expected to improve the resistance of the coating to passivation. The commercial coating CR984 will also be modified by eliminating chromium from its formulation since this element could be prohibited in the future for aeronautical applications. Pure aluminium IVD coatings will be studied because they could result in an alternative deposition technique to electroplating and sprayed metal coatings. Additionally, a spray coating produced by using the aluminium alloy 7075 has been introduced into the study as this alloy is expected to give perfect galvanic compatibility with many parts of the airframe, when produced with the same aluminium alloy.

Electrochemical tests supported by marine atmosphere exposure and mechanical test under corrosive conditions to evaluate the risk of hydrogen re-embrittlement of the steel will be used in order to study the alternative coatings.

The aims of the research can be summarised as follows:

[I] To develop novel sprayed metal particle coatings of the SermeTel type with compositions chosen to minimise the risk of hydrogen re-embrittlement of high strength steel, while avoiding the problem of coating passivation and loss of sacrificial protection.

[II] To study the extent of hydrogen re-embrittlement of high strength steel that is caused by corrosion of aluminium-based coatings. Both metal particle and PVD coatings will be included.

[III] To evaluate the corrosion performance of selected aluminium-based coatings in conditions that are representative of aircraft in service.

A second important application regarding sacrificial coatings is their use as compatibility coatings and electroplated cadmium has been successfully used also for this purpose.

It is quite common in aerospace applications for bronze bushes and bearings to be pressed into aluminium forgings. This type of assembly could cause serious galvanic corrosion of the aluminium component in service conditions and it is essential that the surface of the noble bronze component is coated with a metal that reduces its inherently cathodic behaviour.

Without the protection, and because the materials are electrochemically more active, the aluminium would increase its corrosion rate with serious consequences on durability. In the assembly of bronze components with aluminium ones, the aluminium, which is more active than the bronze, would increase its corrosion rate. By coating the bronze with a material with an electrochemical potential similar to the aluminium, the corrosion rate of the aluminium component would be significantly reduced. Ideally the coating to be used should have a potential identical to the

aluminium although small variations around this potential are possible. In this study, different coatings with different characteristics from cadmium will be evaluated, i.e. studying materials with electrochemical potentials that are not necessarily more active than the aluminium.

The electrochemical potential, its stability, and other factors such as the anodic or cathodic control of the corrosion will be evaluated in order to study in detail possible alternative coatings to cadmium and to identify the guidelines for the correct choice of a compatibility coating for this and for other different applications that require a compatibility coating.

On the basis of the experience gained from the study of alternative coatings for high strength steels [1, 4], aluminium coatings are thought to be promising alternatives to cadmium as well as in different applications in which the coating is applied for compatibility purposes.

SermeTel coatings containing 1% and 5% in weight of zinc, IVD aluminium and electroplated aluminium have been selected for the project. Together with these aluminium based coatings, an electroplated Zn-Ni coating, with a deposit containing between 8% and 14% nickel, has been included in this project. Zn-Ni coating has been studied in the past as a possible alternative to cadmium for high strength steel substrate [5, 6] showing electrochemical characteristics which could be suitable for the new application.

# 1 LITERATURE REVIEW

## 1.1 INTRODUCTION

Metal alloys commonly used for structures or mechanical components, like aluminium, copper, iron, zinc etc., are intrinsically unstable. In many environments in which they are exposed, their carbonates, hydroxides, oxides, sulphides, sulphates, and many other salts are potentially more stable than the metal itself. These compounds are in many conditions thermodynamically more stable and the conversion can be driven by a large negative free energy. The physical or mechanical properties, such as strength, ductility and tenacity of the metals, can be seriously changed by the formation of corrosion products, leading to the failure of the components. Corrosion in metals that are prone to corrode is rarely completely eliminated but can be reduced to allow the materials to attain their expected lifetime.

## 1.2 ELECTROCHEMICAL NATURE OF AQUEOUS CORROSION

Corrosion in aqueous solutions has been found to involve electron or charge transfer. Thermodynamics gives an understanding of the energy changes providing the driving force and controlling the spontaneous direction for chemical reaction. When corrosion is possible, however, thermodynamics cannot predict the rate.

When immersing zinc in hydrochloric acid, the corrosion of zinc is represented by the following reaction



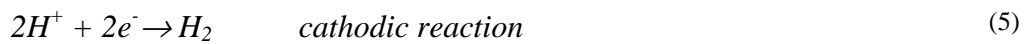
And, in ionic form, the reaction is



Eliminating  $\text{Cl}^-$  from both sides of the reaction gives



Reaction 3 can be separated as follows:



All corrosion reactions in water involve an anodic reaction such as Reaction 4  
Thus, for corroding metals, the anodic reaction is of the form



Cathodic reactions are few in number. The simplest one of the most common is reduction of hydrogen ions in acid solution (reaction 1). Another is reduction of an oxidised ion in solution as the reduction of ferric to ferrous ions,



The reduction of dissolved oxygen is often observed in neutral and acid solution exposed to ambient air. The respective reduction reactions are



and



In the absence of all other reduction reactions, water will be reduced by



which is equivalent to Reaction 5 assuming dissociation of water to  $H^+$  and  $OH$  and subtracting  $OH$  from both sides of the reaction.

The free-energy change,  $\Delta G$ , associated with any chemical reaction, may be associated with an electrochemical potential,  $E$ , at equilibrium, by the fundamental relationship

$$\Delta G = -nFE \quad (11)$$

Where  $n$  is the number of electrons (or equivalents) exchanged in the reaction, and  $F$  is Faraday's constant, 96,500 coulombs per equivalent. For Reaction 5,  $n$  is 2, i.e. the electron number change in the reaction.

Table 1 shows a list of Standard Electrode Potentials.

	Reaction	Standard Potential, $e^\circ$ (volts vs. SHE)
Noble	$\text{Au}^{3+} + 3e^- = \text{Au}$	+1.498
	$\text{Cl}_2 + 2e^- = 2\text{Cl}^-$	+1.358
	$\text{O}_2 + 4\text{H}^+ + 4e^- = 2\text{H}_2\text{O}$ (pH 0)	+1.229
	$\text{Pt}^{3+} + 3e^- = \text{Pt}$	+1.2
	$\text{O}_2 + 2\text{H}_2\text{O} + 4e^- = 4\text{OH}^-$ (pH 7) <sup>a</sup>	+0.82
	$\text{Ag}^+ + e^- = \text{Ag}$	+0.799
	$\text{Hg}_2^{2+} + 2e^- = 2\text{Hg}$	+0.788
	$\text{Fe}^{3+} + e^- = \text{Fe}^{2+}$	+0.771
	$\text{O}_2 + 2\text{H}_2\text{O} + 4e^- = 4\text{OH}^-$ (pH 14)	+0.401
	$\text{Cu}^{2+} + 2e^- = \text{Cu}$	+0.337
	$\text{Sn}^{4+} + 2e^- = \text{Sn}^{2+}$	+0.15
	$2\text{H}^+ + 2e^- = \text{H}_2$	0.000
	$\text{Pb}^{2+} + 2e^- = \text{Pb}$	-0.126
	$\text{Sn}^{2+} + 2e^- = \text{Sn}$	-0.136
	$\text{Ni}^{2+} + 2e^- = \text{Ni}$	-0.250
	$\text{Co}^{2+} + 2e^- = \text{Co}$	-0.277
	$\text{Cd}^{2+} + 2e^- = \text{Cd}$	-0.403
	$\text{Fe}^{2+} + 2e^- = \text{Fe}$	-0.440
	$\text{Cr}^{3+} + 3e^- = \text{Cr}$	-0.744
	$\text{Zn}^{2+} + 2e^- = \text{Zn}$	-0.763
$2\text{H}_2\text{O} + 2e^- = \text{H}_2 + 2\text{OH}^-$	-0.828	
Active	$\text{Al}^{3+} + 3e^- = \text{Al}$	-1.662
	$\text{Mg}^{2+} + 2e^- = \text{Mg}$	-2.363
	$\text{Na}^+ + e^- = \text{Na}$	-2.714
	$\text{K}^+ + e^- = \text{K}$	-2.925

**Table 1. Standard Electrode Force Potentials**

The half-cell reactions 4 and 5 also have free-energy changes analogous to  $\Delta G$  and corresponding potentials  $e_a$  and  $e_c$ . The algebraic sum of these potentials is equal to  $E$ , that is

$$E = e_a + e_c \quad (12)$$

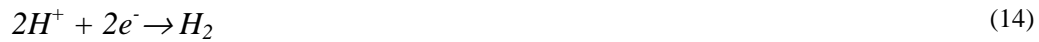
$e_a$  and  $e_c$  are not absolute values and a zero point must be assumed. The arbitrary zero point is the electrochemical potential of the half cell  $\text{H}^+/\text{H}_2$  and the reference half-cell potential is established with the easily constructed *standard hydrogen electrode (SHE)*. Table 1 shows a list of Standard Electrode Potentials.

### 1.2.1 Corrosion potential and current density

When a metal such as zinc is corroding in an acid solution, both the anodic,



and the cathodic,



half-cell reactions occur simultaneously on the surface. Each has its own half-cell electrode potential and exchange current density as shown in Figure 1, where  $i_o$  is the *exchange current density* equivalent to the reversible rate at equilibrium of any chemical reaction.

The two half-cell potentials  $e_{\text{Zn}/\text{Zn}^{2+}}$  and  $e_{\text{H}^{+}/\text{H}_2}$  cannot coexist separately on an electrically conductive surface. Each must polarise or change potential to a common intermediate value,  $E_{\text{corr}}$ , which is called corrosion potential.  $E_{\text{corr}}$  is referred to as a mixed potential since it is a combination or mixture of two half-cell electrode potentials reactions. Figure 2 shows graphically the polarisation of anodic and cathodic half-cell reactions for zinc in acid solution.



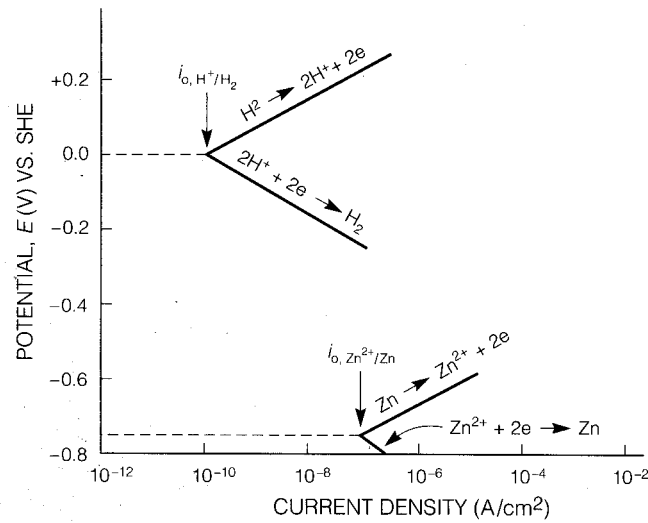


**Figure 1. Anodic and cathodic half-cell reactions present simultaneously on a corroding zinc surface**

A list of different  $E_{\text{corr}}$  of different half-cells coupled with the same reference half-cell is called Galvanic Series. Figure 3 shows a Galvanic Series measured in seawater and in respect of a Saturated Calomel Electrode. Galvanic Series should not be confused with emf. The emf is a list of half-cells proportional to the free-energy changes of the corresponding reversible half-cell reactions for standard (unit activity) conditions. The Galvanic Series is a list of corrosion potentials, each of which is formed by the polarisation of two half cell reactions to a common mixed potential,  $E_{\text{corr}}$ , on the corroding surface.

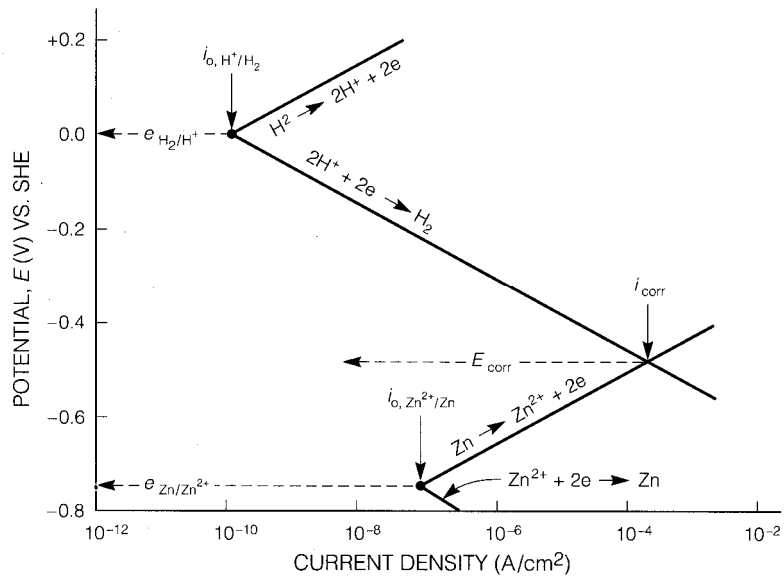


**Figure 2. Polarisation of anodic and cathodic half-cell reactions for zinc in acid solution to give a mixed potential,  $E_{corr}$ , and a corrosion rate (current density),  $i_{corr}$**

The Galvanic Series are available for useful alloys and pure metals, and a selection of alloys with a minimum potential difference will minimise corrosion in a Galvanic Series. The Galvanic Series depend on the electrolytic solution and do not give any information about the corrosion rates of either the cathode or anode.

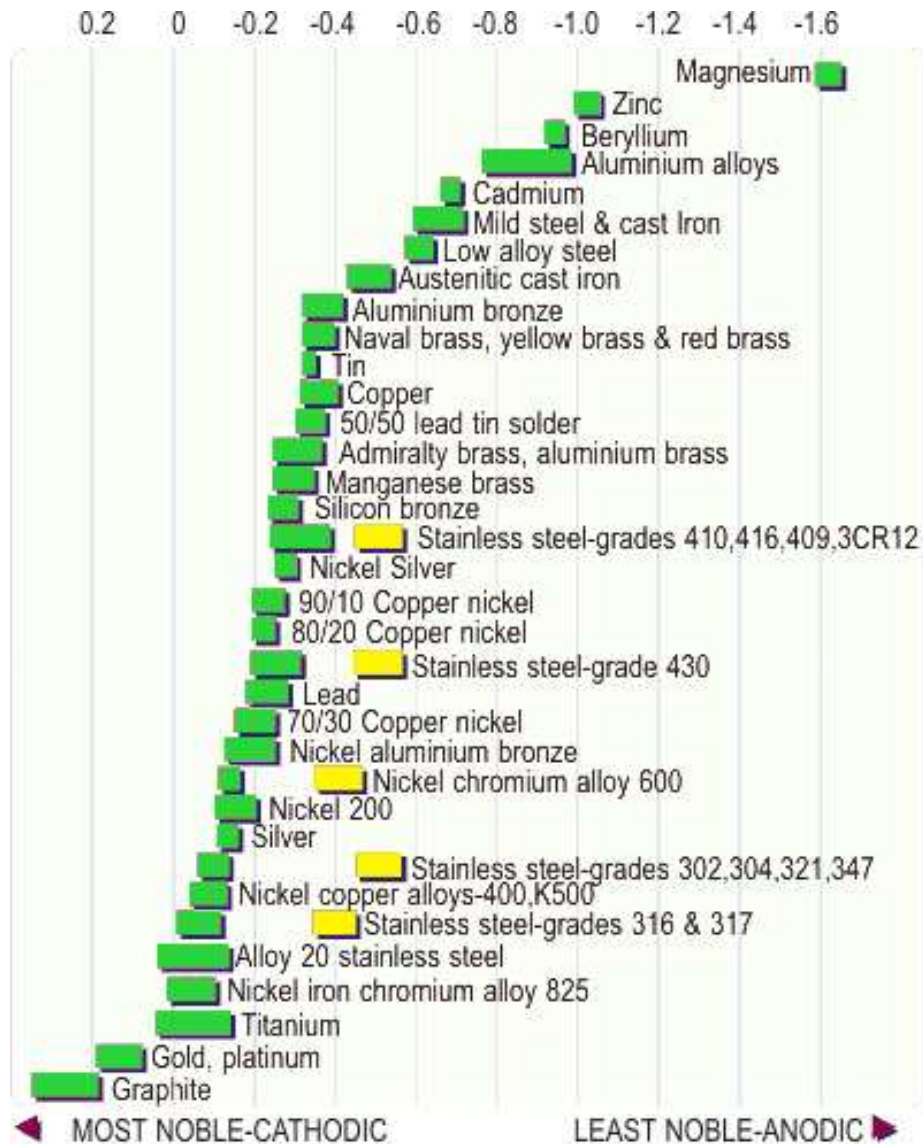


Figure 3. Galvanic Series of seawater. Yellow box indicate behaviour for active-passive alloys. (From Denny A. Jones – Principles and Prevention of Corrosion, p.169, 1992)

## 1.2.2 Electrochemical nature of galvanic corrosion

### 1.2.2.1 Two-metals galvanic corrosion

Any metal or alloy has a unique corrosion potential,  $E_{corr}$ , when immersed in a corrosive electrolyte. When any two different alloys are coupled together, the one with more negative or active  $E_{corr}$  has an excess activity of electrons, which are lost

to the more positive alloy. In a couple between two metals, M and N, the anodic dissolution or corrosion reaction



of the active metal, M, has its rate increased by loss of electrons. M thus becomes the anode in the galvanic cell. The more positive or noble alloy, N, has the rate of its cathodic reaction



decreased due to the excess of electrons drawn from M. N is the cathode of the galvanic cell, and the corrosion-rate decrease is the basis of cathodic protection by sacrificial anode alloy such as M.

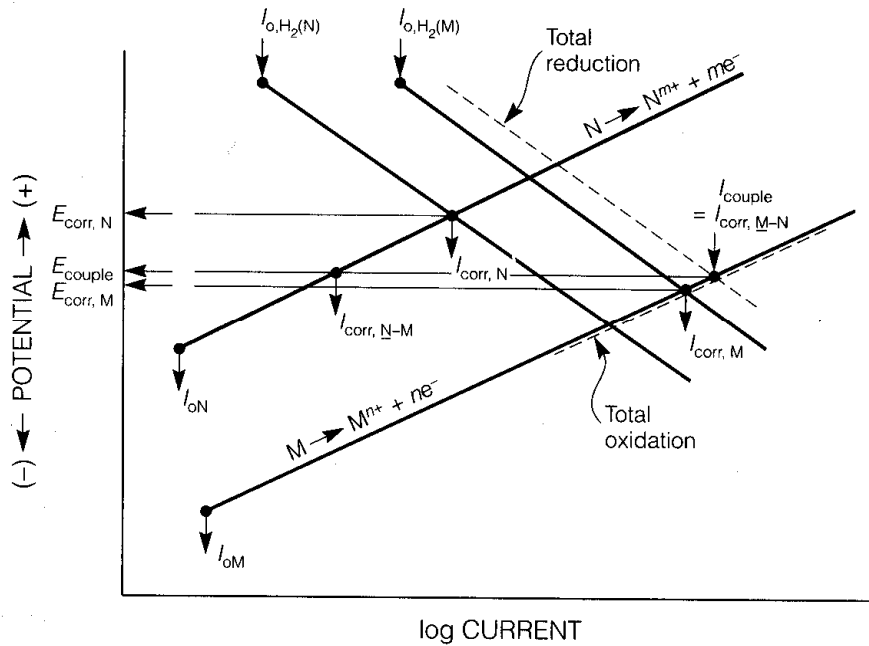


**Figure 4. Schematic polarisation in a galvanic couple between corroding metals M (anode) and N(cathode). (From Denny A. Jones – Principles and Prevention of Corrosion, p.175, 1992)**

In  $E_{\text{corr}}$  of M, the anode shifts to a more positive value, while  $E_{\text{corr}}$  of N shifts to a more negative value, until both the potentials reach the same intermediate potential  $E_{\text{couple}}$ . The effect can be explained by anode and cathode polarisation between the couple. Figure 4 schematises the galvanic coupling between corroding metals M (anode) and N (cathode).

At  $E_{\text{couple}}$  the anodic dissolution rate for M has increased from  $I_{\text{corr}(M)}$  to  $I_{\text{corr}(M-N)}$ , and that for N, the cathode, has decreased from  $I_{\text{corr}(N)}$  to  $I_{\text{corr}(M-N)}$  as shown in Figure 4.

### 1.2.2.2 Cathodic protective coatings

In galvanic couples involving two corroding metals, the potential of the couple always falls between the uncoupled corrosion potentials of the two metals. The corrosion rate of the metal with the more active corrosion potential, the anode, is always increased, while the corrosion rate of the one with more noble potential, the cathode, is always decreased. Decreased corrosion of the cathode at the expense of increased anode corrosion is the basis for cathodic protection by sacrificial anodes. The same principle can be used for sacrificial coatings in aqueous corrosion, where more active coatings are applied on the surface of a more noble metal that needs protection. The metal continues to be protected by the sacrificial coating even after a scratch on or damage to the coating surface.

Cathodic protection increases the amount of hydrogen produced by the cathodic reaction. Part of the hydrogen produced by the cathodic reaction



can be adsorbed by the surfaces to diffuse into the bulk. Some metal alloys such as high strength steel are susceptible to hydrogen embrittlement with a consequent decrease of their mechanical properties.

## 1.3 CADMIUM SACRIFICIAL COATINGS AND ALTERNATIVES TO CADMIUM

### 1.3.1 Introduction

Different publications about alternative coatings to cadmium have shown that aluminium, modified aluminium and Zn-Ni coatings can provide improved sacrificial protection to steel components. Although the results are good in terms of corrosion, some of the alternatives can be deposited by expensive techniques that can limit the real utilisation. In this project, particle sprayed coatings were introduced to modified aluminium coating, where the additional active element is present in the coating not in terms of alloy but as individual particles. The use of sprayed coatings allows the production of a less expensive coating while optimising the composition of the sprayed coatings.

### 1.3.2 Previous studies on cadmium replacement at Cranfield University

Chalaftris and Robinson [1], studied two aluminium based coatings as alternatives to electroplated cadmium coatings. Their research was focused on the corrosion characteristics of the coatings and on the permeation of hydrogen in the steels. In their research, high strength AISI 4340 steel was used as testing material in the mechanical testing (SSRTs), whilst low-carbon steel shims were applied in hydrogen permeation measurements. The aluminium-based coatings, examined in the programme as possible alternatives to Cd, were SermeTel CR984-LT and Alcotec Galvano-Aluminium. Hydrogen re-embrittlement caused by the two alternative coatings was compared with the re-embrittlement caused by electroplated cadmium and re-embrittlement tests were carried out on uncoated hydrogen charged unplated steel tensile specimens. Electrochemical permeation measurements were used to determine the amount of absorbed hydrogen by unplated steel membranes, potentiostatically charged at the potential of a corroding coating, in order to simulate the hydrogen absorption during the re-embrittlement of corroding coated tensile specimens.

A wide range of corrosion tests were used in the work to evaluate the possibility of replacing electroplated cadmium with the alternative aluminium coatings, i.e. galvanic corrosion test, polarisation behaviour test, together with 1000h salt fog test and marine atmosphere exposure. In the latter two tests, coated tensile specimens were tested together with a coated panel, in order to evaluate the risk of re-embrittlement subsequent to the exposure in the corrosive environment.

The exposure to the corrosive environment either preceded the SSRT (Slow Strain Rate Test) or occurred during the test. Immersion in 3.5% NaCl solution and neutral salt spray tests, complying with the ASTM B117-94 standard, were used in the laboratory. Moreover, other tensile specimens were exposed to a coastal marine atmosphere for two years at a QinetiQ test site in Weymouth, Dorset, as marine atmosphere exposure is considered to represent most closely the service conditions on an aircraft. Additional uncoated steel tensile specimens were exposed to 3.5% NaCl solution and held at the electrochemical potential of a corroding coating to investigate the effects of electrolytic hydrogen charging when a coating corrodes in service.

It was found that cadmium electroplating caused severe direct hydrogen embrittlement to the quenched and tempered AISI 4340 high strength steel. In contrast, no reduction in times to failure was observed by the application of the SermeTel CR984-LT coating. On the other hand, the electrodeposition of Galvano-Aluminium Alcotec in an organic electrolyte introduced a very small amount of embrittlement, which was proven to be statistically insignificant.

Direct embrittlement is the damage caused to the steel during the deposition typical of the electrodeposition processes. It is intrinsic in the methodology utilised for the deposition. The term re-embrittlement, in contrast, refers to the hydrogen produced during the sacrificial protection provided by the coating to the steel during the service. Direct embrittlement has been proved to be removable by a baking treatment at 200°C for 24 hours. This was found to be fully effective in the de-embrittlement

of the steel specimens that had been electroplated with cadmium, as well as coated with Alcotec.

No embrittling effect was observed in the case of unplated steel specimens that were potentiostatically charged and then stressed in air. The range of the applied potentials was more negative than the free corrosion potentials of Alcotec, SermeTel and cadmium.

Re-embrittlement occurred when uncoated AISI 4340 steel specimens were strained and simultaneously potentiostatically charged at a cathodic potential to simulate the corrosion of a sacrificial coating. A higher degree of re-embrittlement was observed at more active potential values, showing that the potential of a corroding sacrificial coating is an important factor influencing the extent of re-embrittlement.

Hydrogen permeation measurements showed that there is more hydrogen uptake by steel substrates at more negative applied potentials. Moreover, it was found that there is good correlation between the degree of re-embrittlement and the amount of hydrogen absorbed by steel, following a logarithmic relationship for a wide range of applied potentials.

The corrosion of cadmium, SermeTel and Alcotec caused a substantial amount of hydrogen re-embrittlement to AISI 4340 steel when exposed to 3.5% NaCl solution during slow strain rate tests. The severity of re-embrittlement was in the order Cadmium > SermeTel > Alcotec.

A second major factor affecting the amount of re-embrittlement is the barrier properties of the coating. Although Alcotec was the most active coating, it caused the least re-embrittlement, because it was the densest coating, and it is thought that it contained fewer pores where the steel substrate was exposed and hydrogen charging could take place. On the other hand, cadmium was quite porous, allowing hydrogen an easier access to the steel substrate and, as a result, its corrosion caused the largest amount of hydrogen re-embrittlement.



A small amount of hydrogen re-embrittlement occurred in coated steel tensile specimens that had been exposed to a marine atmosphere for two years prior to the slow strain rate tests, showing that corrosion under applied stress is not a prerequisite for re-embrittlement to occur, which can take place even if aircraft components are only stressed intermittently. The severity of the marine environment in re-embrittlement was in the order Alcotec > SermeTel > Cadmium. These results are particularly pertinent as marine atmosphere exposure testing is thought to be most representative of service conditions on aircraft.

Open circuit potential measurements of the investigated coatings showed that Alcotec was the most active coating, while SermeTel was fluctuating between more noble values, and cadmium was the most noble coating among them.

According to linear polarisation resistance results, the self-corrosion rate of the studied coatings in 3.5% NaCl solution was in the order Alcotec < SermeTel < Cadmium. In particular, the corrosion rate of the isolated cadmium coating was far higher than that of the aluminium-based coatings.

The galvanic corrosion rate of the examined coatings when coupled to steel after 1000 hours of exposure to 3.5% NaCl solution was in the order Alcotec > Cadmium > SermeTel. In particular, the dissolution rate of Alcotec was far higher than the galvanic corrosion rate for the other two coatings.

Cadmium and Alcotec both performed well in marine atmosphere exposure, but SermeTel appeared to passivate in these conditions and after 12 months red rust was visible in scribed regions, as well as in the corners and at the edges of the panels.

Although there were many good results obtained by the authors using the alternative coatings, the tendency to passivation of 984 coatings in marine atmosphere exposure underlined the risks in using this coating as a good sacrificial coating. However, the

addition of more active elements in the new project should overcome the tendency to passivation of SermeTel 984.

Following Chalaftris and Robinson [1], Figueroa [3] studied different alternatives to electroplated cadmium, electroplated zinc-14%nickel alloys and aluminium-based coating SermeTel<sup>®</sup>1140/962, which represented strong candidates for the replacement of electroplated cadmium due to their promising characteristics. The aluminium based coating together with a ceramic inorganic binder (coating system 962) were applied by spray painting and subsequently cured at temperatures up to 315°C. Further application of a modified polyurethane top-coat layer (top-coat system 1140) was applied on the coating. Although the work was mainly focused on the 300M and AerMet<sup>®</sup>100 high strength steels, alternative alloys GifloM2000 and CSS-42L<sup>™</sup> were also considered in some tests.

It was shown that a thin layer of nickel which had been applied before the cadmium acted as a barrier to hydrogen uptake by the GifloM2000 steel. This alloy displayed no susceptibility to hydrogen re-embrittlement, ( $EI=-0.05$ ), when the cadmium coating, applied after the '*nickel strike*' process, was corroding in 3.5% NaCl solutions. It appears that a thin nickel layer beneath the sacrificial coating would provide a promising method for controlling both direct hydrogen embrittlement and hydrogen re-embrittlement. Alternatively, the second group of cadmium-plated, baked and corroded GifloM2000, which did not receive a nickel strike treatment, showed to be susceptible to hydrogen re-embrittlement, displaying  $EI$  of 0.19.

The alternative sacrificial coating, SermeTel<sup>®</sup>1140/962, proved to have an advantage over the electroplated cadmium and the zinc-nickel based on the lack of direct embrittlement produced by its deposition process.

The levels of re-embrittlement susceptibilities displayed by the high strength steels due to the corrosion of the three sacrificial coatings were associated with two main factors: 1) the electro-negativity and 2) the barrier properties of the coating. The electrochemical activity of the coatings increased in the order SermeTel<sup>®</sup>1140/962 <

Cadmium < Zinc-Nickel coating. In relation to this finding, permeation measurements showed that the hydrogen uptake increased in an exponential rate as the potential was lowered from -0.90 to -1.15 V (SCE).

After the study of Chalafris and Robinson [1], the study of Figueroa [3] which was more focused on the steel susceptibility of different steel to hydrogen re-embrittlement, confirmed the good characteristics of the aluminium based coatings as alternatives to electrodeposited cadmium. However the risk of passivation of the alternative aluminium coating was not evaluated and concerns remain regarding the risk of passivation of this coating and its possible use as sacrificial coating.

### 1.3.3 Ion Vapour Deposition (IVD) aluminium

Historically, IVD was developed in the 1970s for use on fatigue-critical aircraft parts. The aluminium coating provides good fatigue resistance because it is soft and thus is less prone to serve as a crack initiation layer [7]. However, its benefits as an environmentally friendly coating have become increasingly appreciated as the use of heavy metals, such as cadmium, have become more highly regulated. The IVD process is similar to the familiar physical vapour deposition (PVD), with one major difference: during plating, the substrate is held at a high negative potential with respect to the vacuum chamber and evaporation source. This potential produces a DC glow discharge of inert argon gas in the deposition chamber. A number of the evaporated aluminium atoms are ionised by this argon glow discharge and accelerated toward the cathode (substrate). This produces stronger adhesion and increases the uniformity of the aluminium coating.

Aluminium coatings applied by PVD, including IVD, show good substrate adhesion. However, they tend to be highly porous, and consequently, glass beading is necessary to compact the structure, as well as improve the corrosion resistance and protection performance of the IVD coatings. The IVD process has been commercially known for many years, with the McDonnell Douglas aircraft company

developing the IVADIZE process to coat landing gear parts, engine mountings and fasteners with aluminium.

Drawbacks of the IVD technique can be avoided by applying another vacuum technique, termed as Unbalanced Magnetron Sputtering (UMS). Steel parts are cleaned, placed in a vacuum chamber, and afterwards sputter-cleaned under an argon atmosphere prior to coating with aluminium. A major advantage of this technique is that the aluminium coatings are very dense. Aluminium–magnesium alloys have recently proved able to be deposited by the UMS technique, and have also displayed an improved corrosion resistance at an approximately 20–wt% Mg [5].

#### 1.3.4 Electrodeposited Zn-Ni

Zinc based coatings have been used for years in the automotive industry to protect ferrous substrates from the effects of corrosion. Production is well established in the surface coatings industry. The early commercialisation of the UK zinc nickel market occurred in the mid-1980's, with the installation of the first acidic based technology [8]. This metal can be readily deposited through a number techniques such as electrodeposition, mechanical plating and hot dip galvanising. The resultant coatings are anodic to iron and steel, providing sacrificial protection. The application of conversion coatings on to the zinc deposit extends the time to oxide formation which greatly enhances the overall corrosion protection.

Studies on the toxicology of chromium are more than 40 years old. In the *Food and Cosmetics Toxicology* journal, published by Elsevier, the first studies about the toxicology of chromium are dated 1963 [9]. For this reason many efforts have been made to find alternatives to the chromatisation of zinc. The addition of nickel to zinc alloys to enhance their corrosion resistance started independently from the production of electrodeposited coating. In 1986, Suzuki and Enjuzi [10] studied the effects of the addition of several elements, i.e. Ni, Cu, Sn, Ti, Cr, Bi and Nb additions on 25% Fe-Zn and measured the corrosion rate of the alloy when compared with the compactness of corrosion layer. They found that titanium, chromium, bismuths, copper and niobium tended to precipitate their compounds on the zinc

alloy surface instead of playing a role in compacting the zinc compounds such as zinc hydroxide and basic zinc chloride. Apart from Cu all the other elements produced a corrosion layer less dense than the one obtained adding Ni.

The first commercially modified zinc coatings were realised by adding small quantities of nickel, typically 5-7% of nickel. The first major UK commercial development of the electrodeposited alkaline zinc nickel alloy occurred during 1992 with the installation of a large production volume of low alloy having a typical deposit composition of 5-7% nickel [8]. In the same year, the research into alternative for CrVI passivation replacement was brought to the study of high alloy zinc nickel. Baldwin and Robinson [11] [6] carried out an extensive study on different concentrations of nickel addition to electrodeposited zinc. They found that Zn alloys containing 14% Ni by weight can afford an optimum level of corrosion resistance to steel in neutral salt fog tests. In open-circuit potential measurements they noticed that Zn-Ni alloys become more noble with immersion time, which was attributed to the preferential dissolution of zinc.

In this work Zn-Ni coatings will not be proposed as sacrificial coatings for the steel because further studies have confirmed the risk of dezincification [12] and concerns have arisen about the integrity of the coatings due to residual stress generated by the dealloying mechanism. Gavrilă et al. [13] noticed that after 48 hours of immersion in the neutral aerated saline solution, the Zn-Ni had shown varying degrees of cracking. The surface had become a network of cracks which was mainly dense and developed. The same author in the same publication concludes that ‘whichever Zn–Ni alloy is considered, its corrosion behaviour is very different to the cadmium deposit which it will replace. The cadmium samples corrode more slowly and uniformly, whereas the Zn–Ni deposits corrode in a localised manner with the appearance of surface cracking and partial dezincification’.

In this project Zn-Ni coating will be proposed as a compatibility coating for the aluminium-bronze assembly. The addition of nickel to zinc has been proven to increase the electrochemical potential of the pure coating [6] and this could result in

a better galvanic compatibility with the aluminium forging alloys generally more noble than pure zinc.

### 1.3.5 Chromate conversion coatings (CCCs) on aluminium and steel substrate

Conversion coatings can provide corrosion protection by converting some of the base metal to a coating in which ions of the base metal are a component. The chromium passivating ion is reported by different authors as the most efficient passivator known [14], [15]. However, due to health and environmental concerns associated with hexavalent chromium, alternatives have been studied for years.

Aluminium alloys can be protected by chromate conversion coatings. Exposure of Al to a dichromate-containing CCC solution results in simultaneous oxidation of Al and reduction of the chromate to Cr(III) [16], [17]:



Zhao et al. [18] showed that chromate is released by CCCs and migrates and protects a nearby uncoated area in an artificial scratch cell. In their experiment they mounted a freshly polished, uncoated surface of AA2024-T3 in epoxy resin in close proximity (1.8mm gap) to a CCC-coated surface. The CCC surface was obtained by exposure to Alodine powder, a commercial solution widely used for chromating aluminium alloys. The whole sample was exposed immersed in an NaCl solution for different times and the self-corrosion rates of the unmodified Al 2024-T3 surfaces was measured. After exposure in the artificial scratch cell for 96 hours the unmodified Al surface showed very little corrosion. In contrast, the control sample exposed to an artificial scratch cell without the CCC-treatment was heavily corroded. Furthermore, they measured the corrosion rate of the aluminium surface after the test for the three samples, the two with the CCC-treated sample, with and without electrical connection between the surfaces, and the one without the presence of the CCC-

treated sample. The polarisation resistance is seen to increase for the samples exposed to a cell with the CCC-treated sample. The presence of chromium oxides or hydroxide on the aluminium surface was not proved by the author, but the increase in the corrosion resistance even when the aluminium has been removed from the scratch-cell seems to suggest that the aluminium surface has been modified maybe by the presence of a protective film [ $\text{Cr}_2\text{O}_3$  or  $\text{Cr}(\text{OH})_3$ ].

Similar mechanisms have been proposed for the steel. Forsgren [14] has reported possible mechanisms for the protection of steel that was proposed by Rosenfeld et al. [19]. " *$\text{CrO}_4^{2-}$  are absorbed onto the steel surface, where they are reduced to trivalent ions. These trivalent ions participate in the formation of the complex compound  $\text{FeCr}_{12}\text{O}_{14-n}(\text{OH})_n$ , which in turns forms a protective film. Largin and Rosenfeld have proposed that chromates do not merely form a mixed oxide film, accompanied by a considerable increase in the bond energy between the iron and oxygen atoms. This leads to an increase in the protective properties of the film*" [20].

### 1.3.6 Electroplated Aluminium

There are few publications regarding the use of electroplated aluminium as sacrificial coating. The use of electrodeposited aluminium is limited to the difficulty of the deposition process. Electrodeposited Al coatings could not be obtained in aqueous solutions since hydrogen evolution occurs before the deposition of the metal.

Currently, there are two main types of media available for the electrodeposition of aluminium i.e. nonaqueous organic solvents and molten salts. Organic solvents as aromatic hydrocarbons and ethers are usually inflammable, volatile, and have relatively low conductivity and a narrow electrochemical window. Inorganic molten salts such as  $\text{AlCl}_3/\text{NaCl}/\text{KCl}$  systems operate at relatively high temperatures (above  $150^\circ\text{C}$ ), while organic molten salts (also called ionic liquids) such as  $\text{AlCl}_3/\text{N}$ -(1-butyl) pyridinium chloride and  $\text{AlCl}_3/1$ -methyl-3-ethylimidazolium chloride operate at near room temperatures.

Kautek [21] studied the galvanic interaction between carbon steel and six galvanic coating materials including electroplated aluminium, cadmium, zinc and duplex combinations with copper, nickel and tin using potentiodynamic techniques and continuous monitoring of the galvanic current. Results for different galvanic couples were reported in the publication for immersion in argon and air saturated sulphate and chloride solutions of various acidity. Kautek found that steel can cathodically be protected not only by cadmium and zinc, but also by electroplated aluminium, in moist urban, industrial and marine atmospheres. He also evaluated the influence of ultrathin intermediate layers in duplex coatings of e.g. nickel or tin, and concluded that they have a practically negligible influence on the aluminium top layer and the steel base.

### 1.3.7 Modified aluminium coatings by addition of Zn or Mg

Enders et al. [22] studied the electrochemical characteristics of aluminium and aluminium alloy coatings containing magnesium for uniform and local pitting corrosion protection of low carbon steel substrates. Their results show that corrosion protection of aluminium coating on steel substrate can be improved by the use of Mg and Zn addition. In their study, the authors used the ion-beam-assisted deposition (IBAD) technique. This deposition method allows a good control of the deposition parameter but is slow and expensive and not suitable for complex shapes and large components.

## 1.4 HYDROGEN EMBRITTLEMENT

Hydrogen embrittlement of steel under load might result from the exposure of the sample to a hydrogen-rich environment. It can be defined as the loss of ductility or delayed fracture caused by absorbed hydrogen within the material during the application of load. In this process, the material manifests a non-ductile fracture mode or loss of ductility, sometimes together with a reduction of tensile strength due to the hydrogen trapped into its microstructure. Hydrogen embrittlement was initially found in steels but there are studies regarding the mechanical properties of other



metals and alloys which show they can deteriorate by hydrogen under certain conditions [23].

The vulnerability of steels to hydrogen embrittlement usually increases as the tensile strength increases. Consequently, high strength steel components are particularly prone to this phenomenon by failing prematurely and rapidly with serious consequences [24-26] and even relatively small amounts of hydrogen can deleteriously control their mechanical properties. Slow strain rate specimens can exhibit a decrease in tensile strength due to HE with a concurrent reduction in area but their yield strength is not significantly affected.

Hydrogen can be absorbed during metal processing and fabrication processes such as electroplating, solidification, forging and welding [27]. Furthermore, hydrogen absorption may occur in specific offshore conditions, such as corrosion and cathodic protection. Slow strain rates and moderately elevated temperatures increase HE, suggesting that the phenomenon is under the control of the lattice diffusion of hydrogen .

Hydrogen embrittlement is a reversible phenomenon and post-baking treatments can relieve hydrogen-containing steels from hydrogen. Such processes facilitate hydrogen to escape to the atmosphere or diffuse to microstructural traps within the steel, but the temperature and duration of the treatment has to be controlled to avoid loss of strength. During these treatments the duration of the exposure in the range of temperature of 400-500°C should be reduced as much as possible to prevent the diffusion of hydrogen in inclusions and grain boundaries, where hydrogen may reduce carbides and oxide inclusions to form methane gas (decarburisation) or water, a phenomenon identified as hydrogen attack.

Before hydrogen can produce any embrittlement to the steel, it has to be situated within the vicinity of the surface, to be absorbed and finally transported to the bulk of the alloy. This growth and entry of hydrogen into the metal is the preliminary stage of the hydrogen embrittlement process [28].

The mechanism is illustrated in Figure 5 [29]:

- 1) Transport of the hydrated proton ( $\text{H}_3\text{O}^+$ ) to the electrical double layer that exists at the iron-electrolyte interface
- 2) Loss of water of hydration shield in the vicinity of the double layer
- 3) Adsorption of the proton to the electrode surface
- 4) Discharge of the proton to an adsorbed hydrogen atom
- 5) Combination which can occur in two ways, chemically (5a) or electrochemically (5b)
  - 5a) two adjacent adsorbed hydrogen atoms can combine to form a hydrogen molecule with a possibility of surface migration between the discharge and recombination site
  - 5b) an adsorbed hydrogen atom can combine with a proton – which is reduced by an electron, hence forming a hydrogen atom – and consequently forms a hydrogen molecule
- 6) Desorption of hydrogen molecule, which will develop as hydrogen bubbles (HER) or absorption of atomic hydrogen (HAR)
- 7) Diffusion of hydrogen into the metal bulk

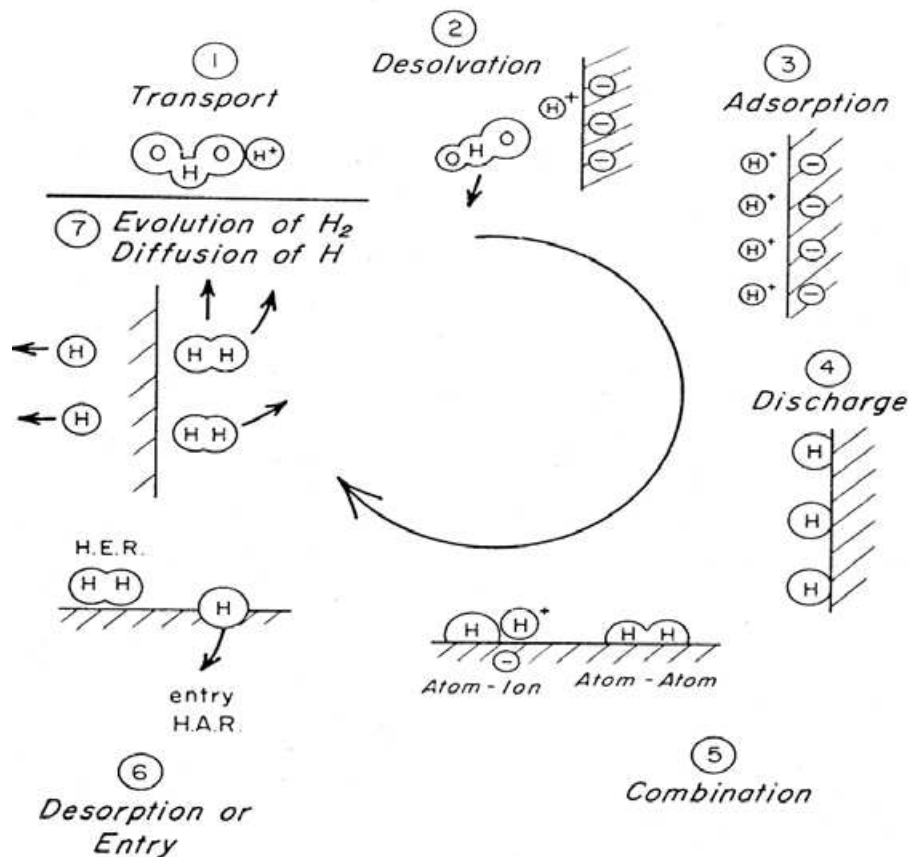
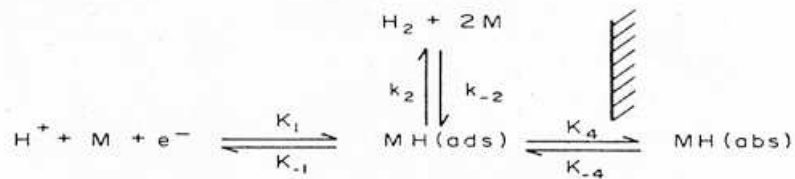


**Figure 5. Hydrogen evolution and absorption [29]**

Only a part of the evolved hydrogen really diffuses into the lattice to stay in the bulk. The access mechanism of hydrogen into the steel (step 7) is still under discussion and there are several theories. Two of these mechanisms are illustrated in Figure 13. Hydrogen entering the metallic crystal lattice could come from the adsorbed hydrogen on the surface, or could directly go through the metal as proton species [28].

(A) Absorption from  $H(ads)$



(B) Absorption from  $H^+$

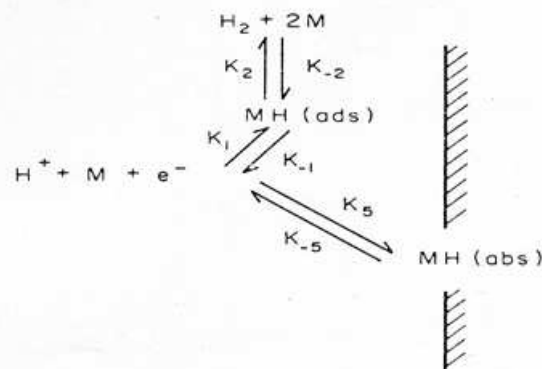


**Figure 14. Models for hydrogen entry into metals: (A) Absorption from atomic hydrogen and (B) absorption from protons [29]**

One part of the hydrogen entering into the metal forms a solid solution with the iron and another part is trapped in lattice defects, such as vacancies, dislocations, inclusion boundaries or microcracks, where the hydrogen is segregated. It is reported that hydrogen is responsible for the weakening of the bonding strength between atoms in the crack tip or for the cohesive strength decrease in the cleavage planes [30]; the lattice decohesion and the formation of cracks take place as an effect of the interaction between the accumulated hydrogen atoms and iron atoms.

#### 1.4.1 Barrier effect of coatings

When evaluating the risk of hydrogen re-embrittlement caused by sacrificial coating, it is important to consider the barrier effect of the coating to hydrogen. Some metals like nickel have been proven to act as a barrier to hydrogen and even a very thin layer of this metal between the substrate and the protective coatings can reduce the amount of hydrogen that can permeate to the substrate through the coating. Hillier

and Robinson [2] in their research on electroplated zinc-cobalt alloys for high strength steels proved that nickel acts like a barrier to hydrogen, reducing the risk of hydrogen re-embrittlement when using nickel as an interlayer between the substrate and the protective coating. In their work they investigated the extent to which electroplating with zinc-cobalt alloys causes hydrogen embrittlement of high strength steel. Slow strain rate tests were carried out on plated tensile specimens to measure the effect of the absorbed hydrogen on the loss of the steel's mechanical properties and the effectiveness of post-plating baking treatments in restoring these properties. For comparison, further tests were conducted on specimens plated with pure zinc, Zn-10%Ni and cadmium and also with Zn-12%Co-9%Fe to investigate ways in which hydrogen uptake could be controlled by the coating composition.

During their work, Hillier and Robinson [2] found a very low embrittlement caused by Zn-10%Ni compared to cadmium. Their results showed that electrodeposited Zn-1%Co coatings promoted high levels of hydrogen embrittlement in a susceptible high strength steel substrate. This embrittlement was much greater than that caused by Zn-10%Ni plating but not quite as severe as that for pure zinc or cadmium. The lower risk of embrittlement from zinc-10%nickel coatings was attributed to the deposition of a nickel-rich layer in the first stages of electroplating. Nickel is an effective barrier to hydrogen uptake by the steel from the coating as it has a very low coefficient for hydrogen diffusion. Their conclusions were supported by the results for the dual bath treatments in which a 0.5  $\mu\text{m}$  layer of nickel deposited beneath a zinc-1%cobalt layer reduced hydrogen embrittlement to the level caused by zinc-10%nickel alone.

The barrier effect of the coatings, which is dependent on the hydrogen diffusion coefficient, should be considered when comparing the re-embrittlement caused by sacrificial coatings. Some metals, such as nickel, could reduce the penetration of hydrogen through the coating, resulting in a beneficial reduction in the amount of re-embrittlement.

### 1.4.2 Solubility of hydrogen in metals

Crystal structure analysis and diffusion studies reveal that the first series of non-metallic elements, i.e. H, B, C, N, upon combining with transition metals, form interstitial solid solutions and compounds [31]. The small size of the non-metal atoms permits their packing into the interstices of the host metal structure. While hydrogen can occupy both octahedral and tetrahedral interstices the other interstitials are only incorporated into the octahedral interstices. The interstitial alloys retain many of the metallic properties of a metal-metal bond, such as electrical conductivity, metallic reflectivity and opacity, although properties such as the ductility and strength of the metallic bond may be profoundly altered.

According to Sievert's law the solubility of hydrogen  $C_H$  in a metal is

$$C_H = \eta(T)P(H_2)^{1/2} \quad (20)$$

where  $P(H_2)$  is the partial pressure of  $H_2$  in the atmosphere and  $\eta(T)$  a parameter depending on the temperature.

The solubility of hydrogen in  $\alpha$ - and  $\gamma$ - Fe in the form of the equation 21 and equation 22 respectively [32]

$$\text{Log } S \text{ (cm}^3\text{/g Fe)} = -0.205 - 1500/T + 0.5\text{log}P \text{ (torr)} \quad (21)$$

$$\text{Log } S \text{ (cm}^3\text{/g Fe)} = +0.018 - 1630/T + 0.5\text{log}P \text{ (torr)} \quad (22)$$

where  $T$  is the temperature in Kelvin.

## 1.5 HEALTH RISK OF CADMIUM

### 1.5.1 Cadmium toxicity

Cadmium is regarded as an occupational hazard [33] associated with industrial processes such as metal plating and the production of nickel-cadmium batteries, pigments, plastics and other synthetics. The primary route of exposure in industrial settings is inhalation. Cadmium has been defined as a human carcinogen by the International Agency for Research on Cancer and the US National Toxicology Program. Cadmium is one of six substances banned by the European Union's Restriction on Hazardous Substances (RoHS) directive. On the 1st July 2006 the Restriction of the Use of Certain Hazardous Substances in Electrical and Electronic Equipment Regulations 2006, implementing the European Directive, came fully into force. These regulations restrict the use of lead, cadmium, mercury, hexavalent chromium, PBE and PBDE in electronic and electrical equipment covered by the regulations. Table 2 shows part of the safety warnings proposed by the same international organisation.

<b>Important Data</b>	
<p><u>Physical State, appearance:</u></p> <p>Soft blue-white metal lumps or grey powder. Malleable. Turns brittle on exposure to 80°C and tarnished on exposure to moist air.</p>	<p><u>Routes of exposure:</u></p> <p>The substance can be absorbed into the body by inhalation of its aerosol and by ingestion.</p> <p>Inhalation risk A harmful concentration of airborne particles can be reached quickly when dispersed, especially if powdered.</p> <p>Effects of short-term exposure The fume is irritating to the respiratory tract. Inhalation of fume may cause lung oedema (see Notes). Inhalation of fumes may cause metal fume fever. The effects may be delayed. Medical observation is indicated.</p> <p>Effects of long-term or repeated exposure Lungs may be affected by repeated or prolonged exposure to dust particles. The substance may have effects on the kidneys, resulting in kidney impairment. This substance is carcinogenic to humans.</p>
<p><u>Physical dangers:</u></p> <p>Dust explosion possible if in powder or granular form, mixed with air.</p>	
<p><u>Occupational exposure limits:</u></p> <p>TLV: (Total dust) 0.01 mg/m<sup>3</sup>; (Respirable fraction) 0.002 mg/m<sup>3</sup>; as TWA; A2 (suspected human carcinogen); BEI issued; (ACGIH 2005). MAK: skin absorption (H); Carcinogen category: 1; Germ cell mutagen group: 3A; (DFG 2004).</p>	

**Table 2. Cadmium safety data sheet, from International Labour Organization database (Cadmium ICSC 0200 April 2005).**

### 1.5.1.1 Occupational hazard definition

Occupational safety and health (OSH) is a cross-disciplinary area concerned with protecting the safety, health and welfare of people engaged in work or employment. As a secondary effect, OSH may also protect co-workers, family members, employers, customers, suppliers, nearby communities, and other members of the public who are impacted by the workplace environment.

Since 1950, the International Labour Organization (ILO) and the World Health Organization (WHO) have shared a common definition of occupational health. It was adopted by the Joint ILO/WHO Committee on Occupational Health at its first session in 1950 and revised at its twelfth session in 1995. The definition reads:



"Occupational health should aim at: the promotion and maintenance of the highest degree of physical, mental and social well-being of workers in all occupations; the prevention amongst workers of departures from health caused by their working conditions; the protection of workers in their employment from risks resulting from factors adverse to health; the placing and maintenance of the worker in an occupational environment adapted to his physiological and psychological capabilities; and, to summarize, the adaptation of work to man and of each man to his job."

## 2 METHODS

### 2.1 MATERIALS

#### 2.1.1 Substrates

The material used for the hydrogen re-embrittlement tests was the high strength steel AISI 4340 with the composition shown in Table 3.

%C	%Mn	%Si	%Cr	%Ni	%Mo	%Cu	%S	%P
0.40	0.49	0.24	0.80	1.75	0.24	0.12	0.006	0.014

**Table 3. Composition of AISI 4340 Steel in weight %**

Carbon steel panels (40x40x1mm) were used to deposit the coatings for the series of corrosion tests.

Aluminium/bronze (40x40x2mm) panels were used as substrate for the deposition of the coatings for the study of alternative coating for bronze-aluminium assemblies. A second smaller group of uncoated aluminium/bronze panels (10x10x2mm), used to simulate the damage on the coatings, and 7075 aluminium alloy panels (40x40x1.5mm) panels were used for the galvanic corrosion test. The composition of the panels is shown in Table 4.

	Dim (mm)	% in weight										
		Si	Mn	Mg	Cr	Zn	Ti	Al	Fe	Ni	Cu	Total
7075 Al	40x40x1.5	0.4	0.3	2.1- 2.9	0.18- 0.28	5.1- 6.1	0.2	Rem.	0.5		1.2- 2.0	100.0
(10x10X2mm), Al/Br	10x10x2.5	-	-	-	-	-	-	8.4	4.2	4.6	Rem.	100.0
(40x40x2mm) Al/Br	40x40x2.5	-	-	-	-	-	-	9.0	5.5	5.4	Rem.	100.0

**Table 4. Composition of the aluminium and aluminium/bronze panels for the study of aluminium/bronze assemblies**

### 2.1.2 Coatings

Table 5 shows the coatings used for the high strength steel substrate and for the aluminium/bronze substrate, the type of coatings, the nominal composition and the coating deposition method.

	Nominal composition	Coating Type	Coating Method
Steel substrate			
984 (A)	Al 50% - Zn	Active additions	SermeTel metal particle coating
984 (B)	Al 90% - Zn 10%		
984 (C)	Al 97% - Zn 3%		
984 (D)	Al 99.5% - Zn 0.5%		
984 (E)	Al 50% - Al/Mg 50%		
984 (F)	Al 70% - Al/Mg 30%		
984 (G)	Al alloy 7075 – 100%	Active & noble additions	Ion Vapour Deposition coatings
984 (H)	CR984 - LT	Commercial coating	
CF1725	Al-100%	Cr free binder	
IVD1	Al – 100%		
IVD2	Al – 100% + wax	Dipped in acetyl alcohol	
IVD3	Al – 100% + PTFE	Low friction surface	
Un Cd	Unpassivated Cd	Control coating	Electrodeposited
Aluminium/Bronze substrate			
Pa Cd	Unpassivated Cd	Control coating	Electrodeposited
Un Cd	Passivated Cd	Control coating	Electrodeposited
984 1%Zn	Al 99% - Zn 1%	Active additions	SermeTel metal particle coating
984 5%Zn	Al 95% - Zn 5%		
EI Al	Al-100%	-	Electrodeposited
Zn-Ni	Zn85%-15%Ni	-	Electrodeposited
IVD	Al – 100%	-	Ion Vapour Deposition

**Table 5. Summary of coating types and nominal compositions**

### 2.1.2.1 SermeTel coatings

SermeTel CR984 – LT coating was produced by Sermatech International Inc of Lincoln. This coating consists of pure aluminium particles held in an inorganic chromate and phosphate binder. They were applied to abraded tensile specimens and steel corrosion test panels as a slurry and then cured by baking at 163-191°C. This temperature does not affect the microstructure of the tensile specimens as it was lower than the tempering temperature of 250°C. Furthermore, as the coating was not

applied electrolytically it does not introduce a risk of direct hydrogen embrittlement. SermeTel CR984 – LT has been included in the programme as a baseline coating.

### **2.1.2.2 New SermeTel Coatings**

Instead of pure aluminium particles, as used in currently available coatings, new formulations containing particles with a range of compositions have been produced to optimise the coating properties. Small additions different particles with different compositions have been made to the commercial aluminium particle coating in order to modify the electrochemical potential of the coating and reduce its tendency to passivation.

Two different approaches have been adopted in selecting the compositions of the different coating compositions.

(1) Addition of a more active alloying element. In the first case, additions of pure zinc particles have been made as zinc is known to have a more active corrosion potential than aluminium alone (-1000mV(SCE) compared to -750mV(SCE) for pure aluminium). Two further coatings have been produced with magnesium additions. As magnesium has a very negative potential (-1500mV(SCE)), which would be expected to lead to severe re-embrittlement, the additions were made in the form of an Al/Mg alloy to moderate its effect.

(2) Additions to promote self corrosion. An alternative method of overcoming passivation of the pure aluminium coating is to make additions that promote a controlled amount of corrosion and maintain an active surface. Copper is known to have this effect and coatings have been produced using a powder of the high strength aluminium alloy 7075 (Al-Zn-Mg-Cu). Clearly, this coating will possess excellent galvanic compatibility with the aluminium alloys used in the airframe. However, the research will need to examine not only if this coating maintains a suitable potential but whether it still has an acceptable life.

Nine new coating formulations have been produced for the project by Sermatech Inc in Pennsylvania, USA and their compositions are shown in Table 5. In addition, three types of IVD aluminium coatings have been produced by Acorn Surface Technology in Nottingham, UK. The first of these is 100% Al with a nominal thickness of 25  $\mu\text{m}$ . The second has the same composition but has been dipped in acetyl alcohol wax

after coating to improve its corrosion resistance. The third is duplex coating with a layer of PTFE deposited on the surface to reduce friction. Finally, further specimens have been electroplated with cadmium to act as a well established control coating for comparison purposes. All of the coatings in the programme have been supplied in the unpassivated condition so that the properties of the coatings themselves can be studied directly.

#### **2.1.2.3 Zn-Ni coatings**

The ZnNi was produced by the acid zinc/nickel Corroban process with a deposit containing between 8 and 14% nickel.

#### **2.1.2.4 Electroplated aluminium**

Electroplated aluminium coatings were produced in Germany by Aluminal Oberflächentechnik & Co. KG with the specification shown in Table 6.

Coating deposition standard	DIN 50898		
Coating	Electroplated aluminium Cr(VI) free		
Min layer thickness	10 $\mu\text{m}$		
Layer thickness		Middle	Edge
Coatings identification number	1	14.9	21.7
	2	13.5	23.5
	3	13.9	21.6
	4	12	18.5
	5	13.6	17.9
	6	12.6	17.9
	7	11.5	16.1
	8	12.9	19.6
	9	11.1	16.4

**Table 6. Electroplated aluminium specifications**

## 2.2 CORROSION TESTING

The corrosion tests were carried out using the ASTM designation G 71-81 (Reapproved 2003) for “Conducting and Evaluating Galvanic Corrosion Tests in Electrolytes”. Although the standard refers to Galvanic Corrosion Tests, part of the standard, was applied, where possible, to the other corrosion tests. In particular the ratio surface area exposed/solution volume was selected according to the ASTM standard.

A computer controlled multiplexer Solartron 1281 was used together with a Solartron Galvanostat/Potentiostat SI 1280 to perform the Corrosion Potential Measurement and the Linear Polarisation Measurement.

A 12-channels Zero Resistance Ammeter, ACM Galvogill 12, was used to carry out the Galvanic Corrosion Tests.

All the SCE electrodes were compared before each test with an unused reference SCE and the results corrected. This procedure was necessary because of the small fluctuation that can affect the SCE potential after long usage.

### 2.2.1 Corrosion Potential Measurements

Steel or Aluminium/Bronze panels (40x40x1mm or 40X40X2mm) that had been coated with the coatings listed in Table 5 before were suspended in 3.5% NaCl solution so that the bottom half was immersed. Their free corrosion potentials were measured against a saturated calomel reference electrode (SCE) and the values were recorded on a data logger at one minute intervals.

### 2.2.2 Linear Polarisation Measurement (LPR)

Steel panels or Aluminium/Bronze panels (40x40x1mm or 40X40X2mm) had been coated with all the coatings described in Table 5. They had been coated on both faces with a total surface area of 32 cm<sup>2</sup>. Panels were partially (70% of their surface) immersed in quiescent 3.5% NaCl solution for ten days. Specimens were polarized from -15 mV versus open circuit potential (free corrosion potential) to +15 mV versus open circuit potential and back again to -15 mV with a polarisation rate of 0.1667 mV/sec; thus resulting a cycle of 360 seconds. On each coating the polarisation measurement was repeated at approximately 45 minutes intervals, depending on the number of coatings tested. An electronic filter was used to stabilize the output signal (current) and a filter frequency was chosen depending on the activity of the coating. A Stern-Geary constant (see Appendix) of 16 mV was used for Cadmium and 18mV was used for the remaining coatings.

All the potentials reported are referred to the Standard Calomel Electrode, which has a potential of +241 mV vs. Normal Hydrogen Electrode.

Linear Polarisation Resistance consists in applying controlled overvoltage on corroding electrode to calculate the polarisation resistance  $R_p$  as the inverse of the slope of the  $I_{app}$  vs.  $E$  data near the Open Circuit potential.  $I_{corr}$  can be estimated using Stern-Gear relationship, shown in Equation 23.



$$I_{corr} = \frac{B_a \times B_c}{2.3(B_a + B_c)R_p} = \frac{B}{R_p} \quad (23)$$

where  $B_a$  and  $B_c$  are the cathodic and anodic Tafel constants that depend on the materials tested and must be estimated experimentally. Figure 6 shows three of the several polarisation curves obtained for coating CF1725 tested for this report after 44, 76 and 102 hours from the beginning of the test.

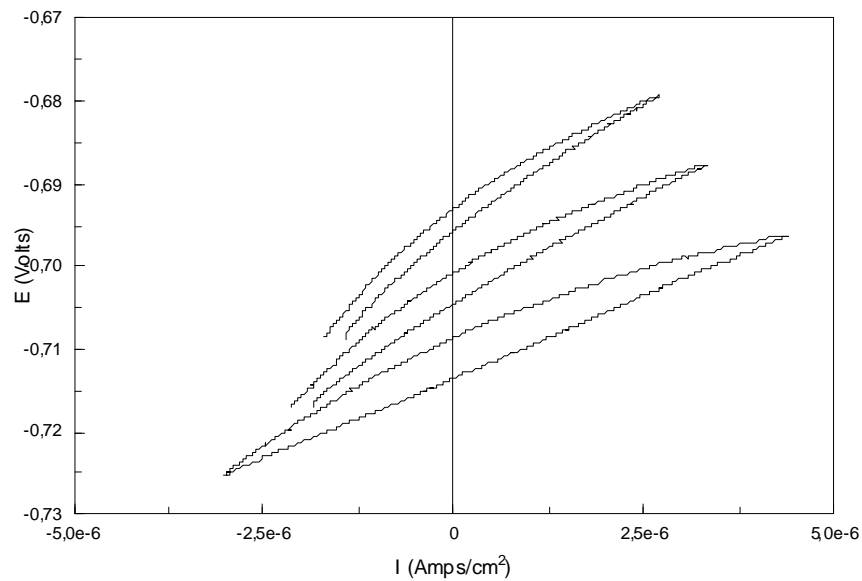


**Figure 6. Example of polarisation curves recorded at different times for CF1725 coating after 44 hours (bottom graph), 76 hours (middle graph) and after 102 hours (top graph)**

The gradient of the trend line is  $R_p$  as showed in Figure 7

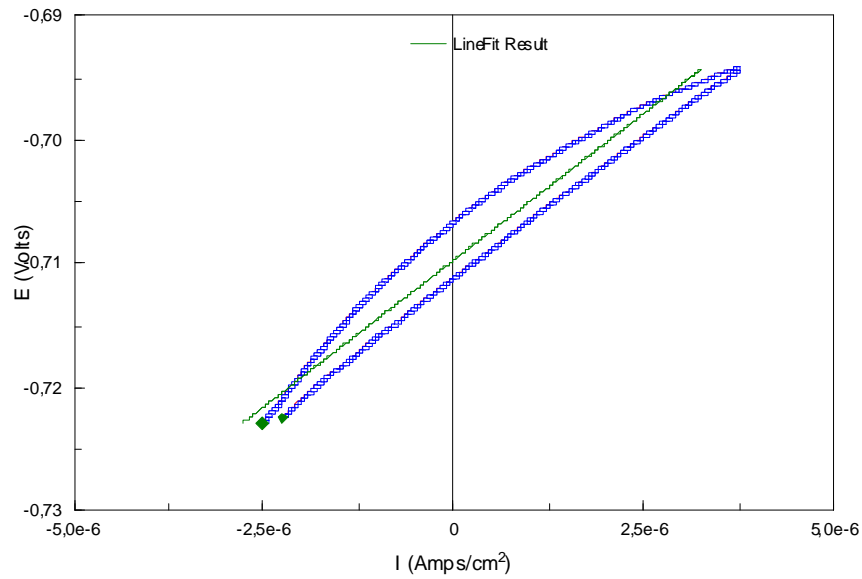


**Figure 7. Example of  $R_p$  calculation from a polarisation resistance measurement on CF1725 coating**

For every coating one of these curves was plotted approximately every hour for a period of ten days. For every curve the  $R_p$  was calculated from the trend line to calculate the corrosion rate.

Equation 24 was used to calculate the corrosion rate  $R$

$$R(mmPY) = \frac{I_{corr}(A/cm^2) \times EquivWeight(g/eq) \times 10(mm/cm)}{Density(g/cm^3) \times 96500(coulomb/eq)} \times 3.1536 \cdot 10^7 (s) \quad (24)$$

Linear polarisation resistance measurements were carried out to measure self corrosion rates of the coatings. It was assumed that the coating gave protection to the steel substrate for all the test duration. However, if the coating passivated during the test it would become too noble and could stop giving cathodic protection to the steel. In this case the steel substrate could start to corrode changing LPR corrosion rate measurement. If the steel starts corroding its corrosion rate will influence the measurement. In this case the Stern-Geary value should be changed to the new

condition in addition to the density and the equivalent weight used for the calculation.

In practice, the area of corroding steel was small, even at the end of the test, and any error is not thought to have been very significant.

### 2.2.3 Galvanic test for steel substrate coatings

The coated and uncoated panels were connected to a zero resistance ammeter and immersed in quiescent 3.5% NaCl solution. Coupling potential and galvanic current were recorded every minute. The tests lasted for ten days and were carried out on all the coated panels shown in Table 5.

### 2.2.4 Galvanic test for aluminium/bronze coatings

In the case of the Aluminium/Bronze substrate a three metal configuration was used to simulate the galvanic compatibility between the aluminium components, the bronze bush and the coating applied to the bush. The three panels were connected to a zero resistance ammeter and immersed in quiescent 3.5% NaCl solution. The couple potential and galvanic current were recorded every minute and all the tests lasted ten days.

The zero resistance ammeter (ZRA) was used to measure a current between two points of a circuit without interposing any resistance. In a galvanic corrosion measurement this allows the current flowing between two metals to be recorded while maintaining them at the same potential.

In these tests the bronze panel was coupled with both the aluminium and the coated panel and all the three panels were immersed in the same beaker. This test was designed to record the galvanic compatibility between the coating, the bronze substrate and the aluminium forging. Samples of the coating under test, the bronze and the aluminium alloy were prepared to give surface areas that are representative of service conditions. The aluminium alloy and the coated panel had the largest area ( $16 \text{ cm}^2$ ) while that of the bronze was relatively small ( $1 \text{ cm}^2$ ). Two currents, Al/Bronze and Coating/Bronze, were measured, while the third current, exchanged between the aluminium panel and the coated one was calculated using the First Kirchoff's Law for the electrical nodes.

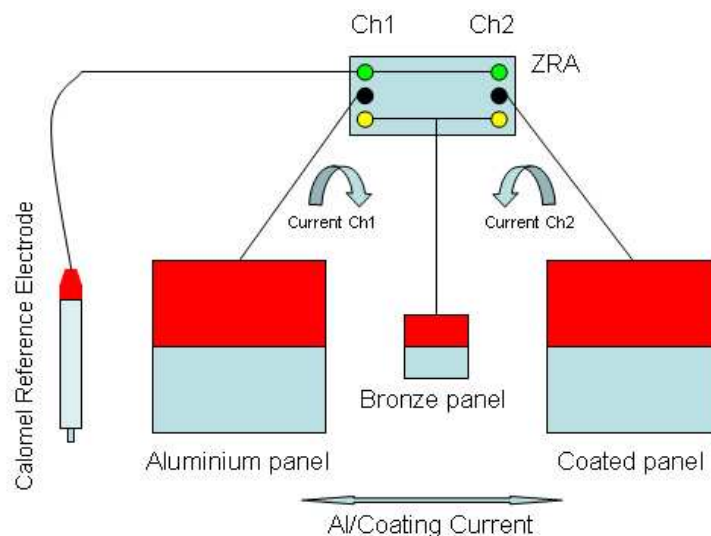


**Figure 8. Three metal galvanic corrosion measurement configuration.**

Ch1: measured Al/Bronze current

Ch2: measured Coating/Bronze current

Al/Coating Current: calculated through the First Kirchoff's Law,  $I_{Al/Coating} = -I_{Ch1} - I_{Ch2}$

Electrochemical potentials:  $Ch1 = Ch2 = Al/Bronze/Coating$  electrochemical potential vs. Standard Calomel Electrode

### 2.2.5 Polarisation behaviour test

The ability of a sacrificial coating to supply a protective current to another metal to which it is coupled depends on its anodic polarisation characteristics. Ideally, the coating would supply the required current without its potential being changed excessively. The polarisation characteristics of the coating have been measured at intervals during the galvanic coupling experiments after one day, five days and ten days of testing. The test was carried out during the second galvanic corrosion measurement repetition on the aluminium/bronze substrate coatings. The three panels were disconnected and three resistors were placed between them using a star configuration. The resistor values were changed from 10 Mohm to 10 ohm, following a logarithmic scale. The difference in potential at the ends of the resistors was measured at each step, the currents were calculated and the results were plotted on a graph with potential vs. log current axes.

In the usual two-metal configuration the resistor is simply placed between the two panels; the anode and the cathode. When three panels need to be tested, two of them should be short circuited in order to keep the same set up. With this configuration the two panels showing the same anodic or cathodic behaviour should be connected so that the three-metal experiment assumes the same set up as the common two-metal experiment. Nevertheless, this setup does not allow monitoring of the current flowing between the two panels that are joined together.

Using the new setup shown in Figure 9 it is possible to monitor the three currents at the same time. The three panels were connected to the points A, B and C and the reference electrode connected through a voltmeter to the node. The three resistors were controlled to have the same values, so that  $R = R_A = R_B = R_C$ .  $V_N$ ,  $V_A$ ,  $V_B$  and  $V_C$  were measured by a voltmeter vs. a SCE. Knowing the value of the resistance the currents  $I_A$ ,  $I_B$  and  $I_C$  were easily calculated being  $I = V/R$ .

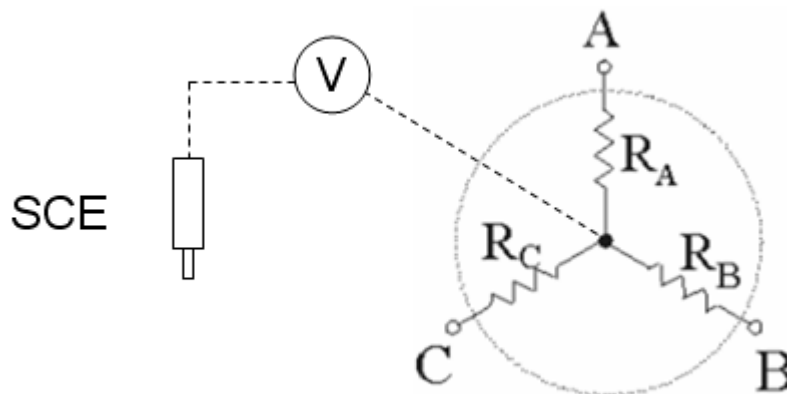


**Figure 9. Three star configuration for polarisation behaviour test.**

The measurement described was repeated for each coating during the galvanic corrosion test after one, five and ten days. Both the two-panel and three-panel configuration were used at each stage.

### 2.2.6 Marine Exposure

This test was performed on the steel substrate coatings. Coated panels were exposed at testing site on the coast, as this environment is considered to represent most closely the service condition on an aircraft. The effectiveness of the coatings was assessed by a visual inspection after four months of exposure.

In June 2005 thirteen coatings were scratched on one side and sent to QinetiQ Bin Cleaves, in Weymouth, Dorset. The panels were held by nylon nuts, bolts and spacer so that they are clear of the holder. Finally, the holders were mounted on frames at the test site.

After four months, photographs of the panels were taken to evaluate the appearance of signs of corrosion.

## 2.3 SELECTIVE ATTACK AND COATINGS CHARACTERIZATION

The study of a possible selective attack in the SermeTel zinc-aluminium coatings for the steel substrate and the structural and micro-structural characterization of some coatings before and after the corrosive exposure were carried out using a combination of different techniques.

SEM and EDX was used to analyze the 50%Zn modified 984 before and after the corrosion exposure to investigate the possibility of a significant zinc particles preferential oxidation resulting in a premature deterioration of the coating in use.

FIB images and EDX analysis were used to investigate the status of corrosive attack to the coating and to the substrate after ten days of exposure in 3.5% NaCl.

XRD was used on “as made” and corroded 984A SermeTel coating to investigate the formation of corrosion compounds. Additionally to normal XRD setup a technique called “Rocking Curve” was used to locate the presence of the corrosion compounds on the coating surface rather than in the coating bulk.

Optical microscope cross section analysis was carried out on all the coatings in order to measure their thickness and, in the case of SermeTel coatings, to investigate their particles morphology.

### 2.3.1 Corrosion micromonitoring-EDX SEM analysis

The surface was polished with an alumina suspension and four micro-Vickers indentations were used to identify a square of 400  $\mu\text{m}$  side. This area was observed with a SEM and analyzed with the EDX. The analysis was repeated after polishing the sample and after 4 days of exposure in quiescent 3.5% NaCl solution. The micro analysis was repeated on the same aluminum and zinc particles to make a comparison between them. An EDX mapping was plotted to identify preferential corrosion in the identified area.

### 2.3.2 Focus Ion Beam (FIB)

Focus Ion Beam allows one to etch small pits into the coating to look at its microstructure and, if deep enough, at the coating interface with the substrate. Although this is an attractive possibility, the time required to etch a pit can make this process too long and expensive when working with thick and hard coatings.

To overcome this problem the use of FIB was combined with the traditional mechanical grinding. The ion beam was basically used to polish a small area of the specimen after it had been mechanically ground. This new technique allows looking at the specimen without any need of tilting the specimen in the SEM chamber Figure 10 shows a scheme of the procedure used to polish the specimen interface using the FIB.

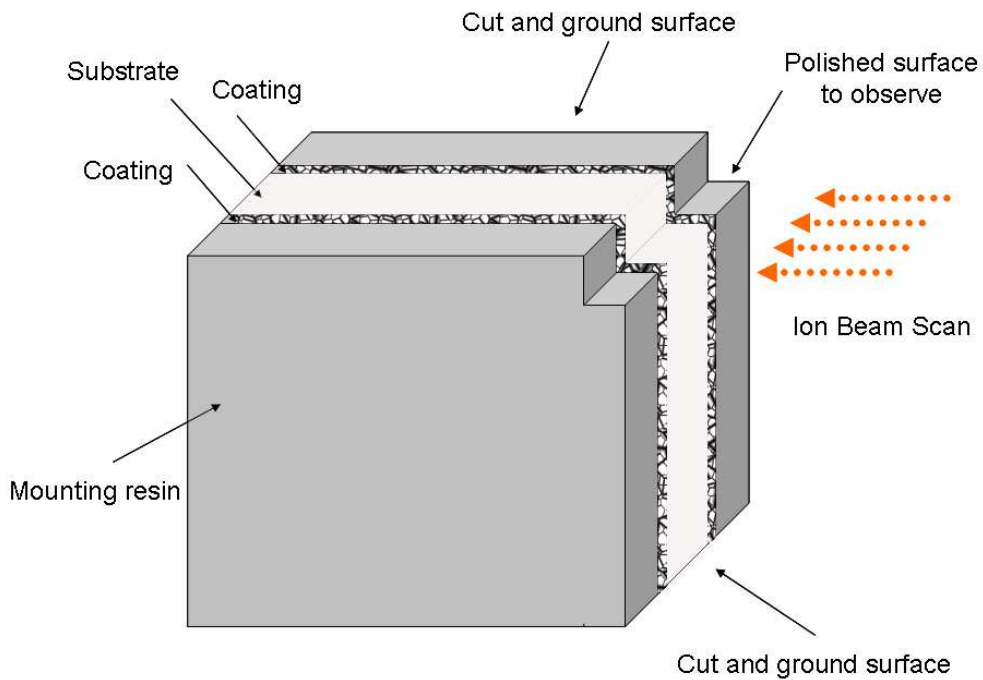


**Figure 10. Sample preparing procedure for interface observation.**

### 2.3.3 X-Ray Diffraction

X-ray diffraction was carried out on 984 and 984A as “made panels” and “after 10 days in 3.5% NaCl solution” panels. The configuration used was a conventional X-ray (Cu K-alpha) - Bragg Brentano with  $\text{Cu K } [\alpha] = 1.5406 \text{ \AA}$ .

#### 2.3.3.1 Rocking curve

Different incident angle scans were performed with  $2\theta$  in the range  $9.5^\circ$ - $12.5^\circ$  with a resolution of  $0.15^\circ$  and  $37.5^\circ$ - $39.5^\circ$  with a resolution of  $0.20^\circ$ . For both of them, three different incident angles were used,  $3^\circ$ ,  $6^\circ$  and  $9^\circ$  and 25 seconds as time for step.

### 2.3.4 Coating thicknesses

Samples were cut on the cross section mounted with bakelite ground and polished with alumina powder. The cross sections were observed with standard optical microscope to measure the thickness of the coatings. Images were taken at 40x magnification for all the specimens.



## 2.4 MECHANICAL TESTING

### 2.4.1 Hydrogen Re-embrittlement Testing

Tensile specimens were produced from the AISI 4340 steel by CNC machining to give a gauge length of 25 mm and diameter of 2.25 mm, as shown in Figure 11. They were then hardened by Holt Brothers of Halifax to give a tempered martensitic microstructure by first heating in a neutral salt bath for 30 minutes at 850°C, followed by an oil quench and then tempering three times for 2 hours at 250°C. The mean UTS of the specimens was 1800 MPa.

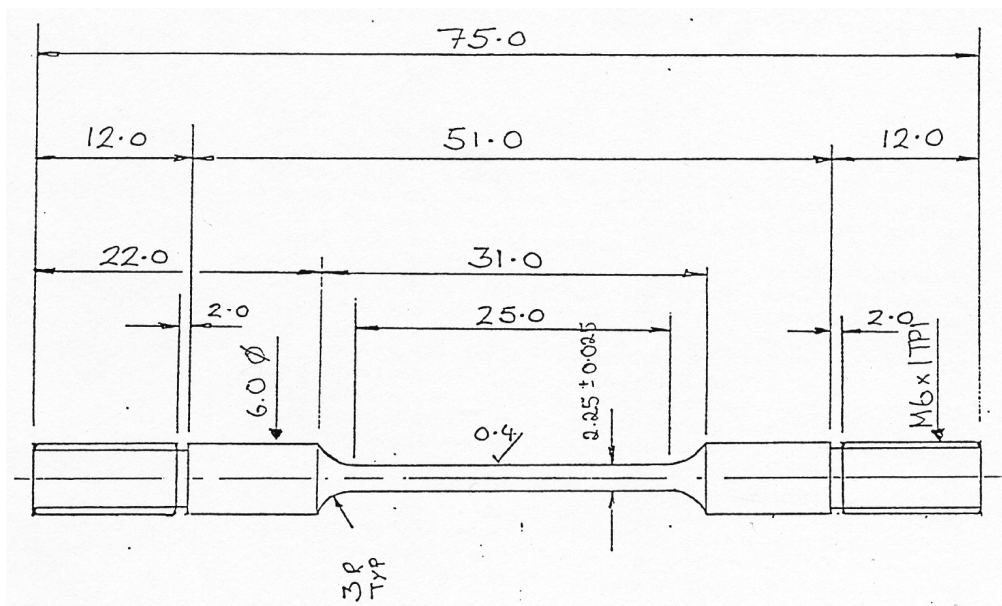


**Figure 11 .Dimensions of slow strain rate tensile specimens**

Slow strain rate tests were performed on the tensile specimens at a strain rate of  $9.7 \times 10^{-7} \text{ s}^{-1}$ . A load/time graph was recorded using a data logger and five or more replicate tests were conducted for each experimental condition.

The failure times of uncoated specimens tested in air were compared with those of coated specimens that had been scribed in the centre of the gauge length and tested in 3.5% NaCl solution. The reduction in time to failure of the coated specimens was a sensitive measure of the effects of re-embrittlement and in each case an embrittlement index (EI) was calculated, as follows:

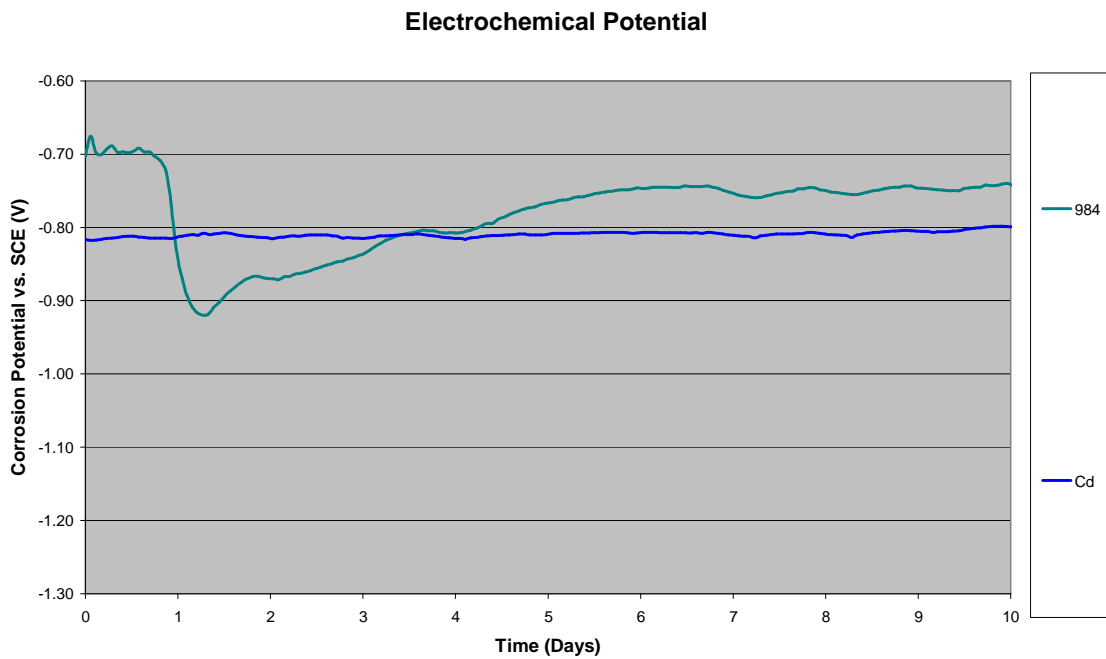
$$EI = 1 - (t_{tf(\text{coated})} / t_{tf(\text{uncoated})}) \quad (25)$$

### 3 RESULTS

#### 3.1 SACRIFICIAL COATING FOR STEEL SUBSTRATE

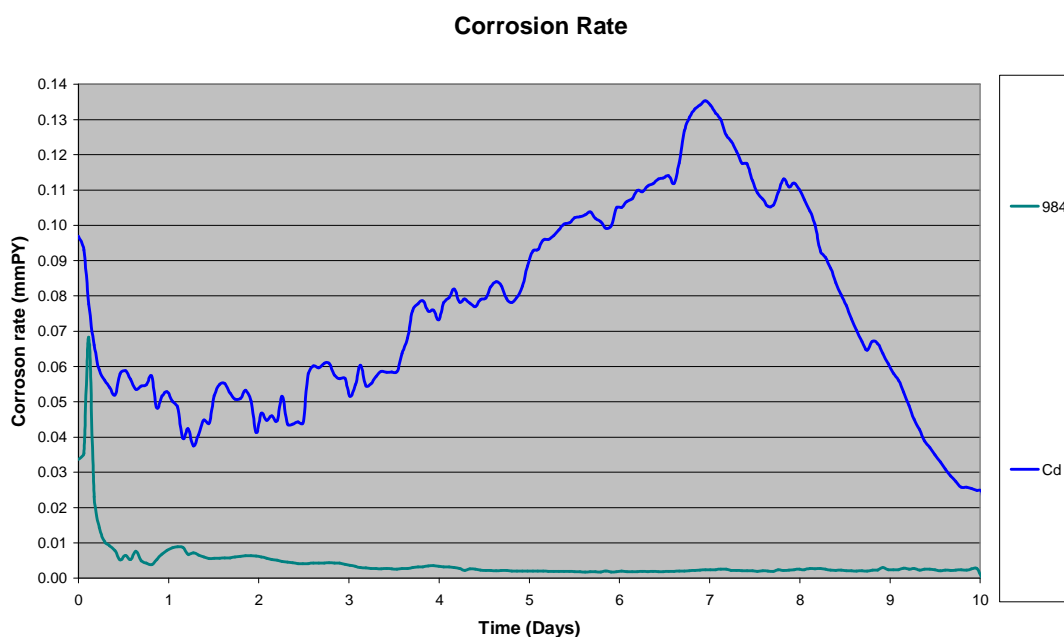
##### 3.1.1 LPR Measurements

Figure 12 shows the electrochemical potentials of 984 commercial coating and electroplated Cd. For the 984 the initial value was  $-703\text{ mV (SCE)}$  while for Cd it was  $-816\text{ mV (SCE)}$ .



**Figure 12. Corrosion potentials of 984 commercial coating compared with electroplated Cd. Tested in naturally aerated 3.5% NaCl solution.**

The potential of 984 started to decrease after 17 hours to reach the minimum of  $-918\text{ mV (SCE)}$  after 30 hours. Then gradually the potential increased to stabilize around  $-750\text{ mV (SCE)}$  after six days. The last final potential was  $-740\text{ mV (SCE)}$ . Cd showed a quite constant potential that ranged between  $-817$  and  $-798\text{ mV (SCE)}$  for all the duration of the test.



**Figure 13. Corrosion rate of 984 commercial coating compared with electroplated Cd. Tested in naturally aerated 3.5% NaCl solution**

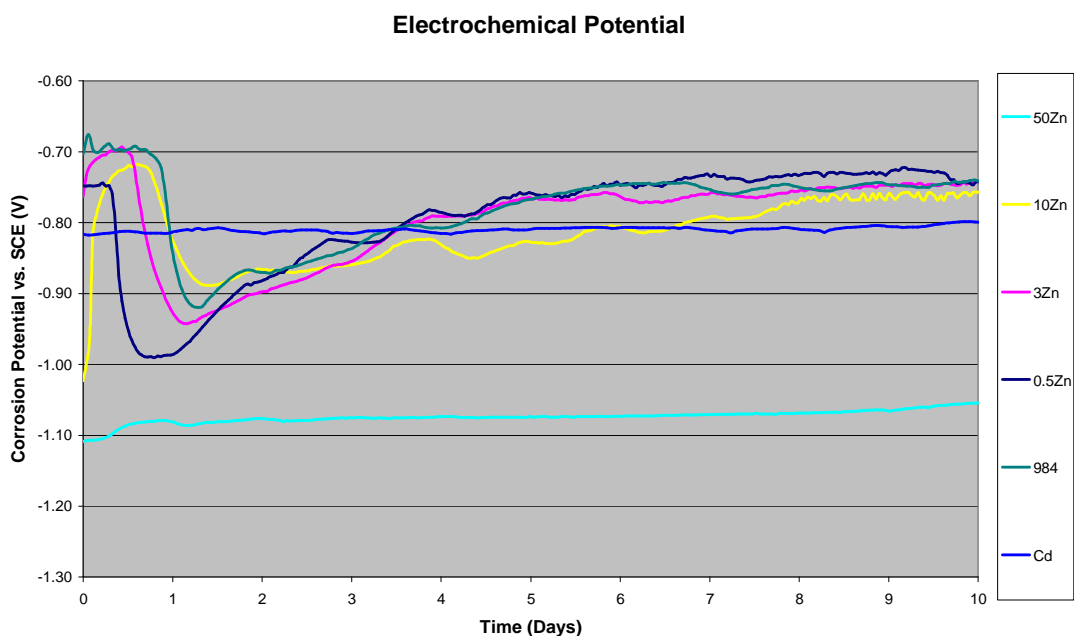
Figure 13 shows the self corrosion rates of 984 commercial coating and electroplated Cd. After the first ten hours, during which the corrosion rate increased and decreased very quickly, 984 showed a corrosion rate that ranged between 9  $\mu\text{m}/\text{yr}$  and 1.7  $\mu\text{m}/\text{yr}$  from the second to the last day. The last value recorded was 2.8  $\mu\text{m}/\text{yr}$ .

Cd showed a different behaviour with higher values. The initial corrosion rate was 99  $\mu\text{m}/\text{yr}$  and the last value recorded was 25  $\mu\text{m}/\text{yr}$ . The appearance of the panels at the end of the test is shown in Figure 14. Cadmium panel became darker during the test. The difference in the colour can be noticed looking at the top of the panels that was the surface kept out of the solution and covered with Lacomit. Both of them showed no signs of red rust at the end of the test.



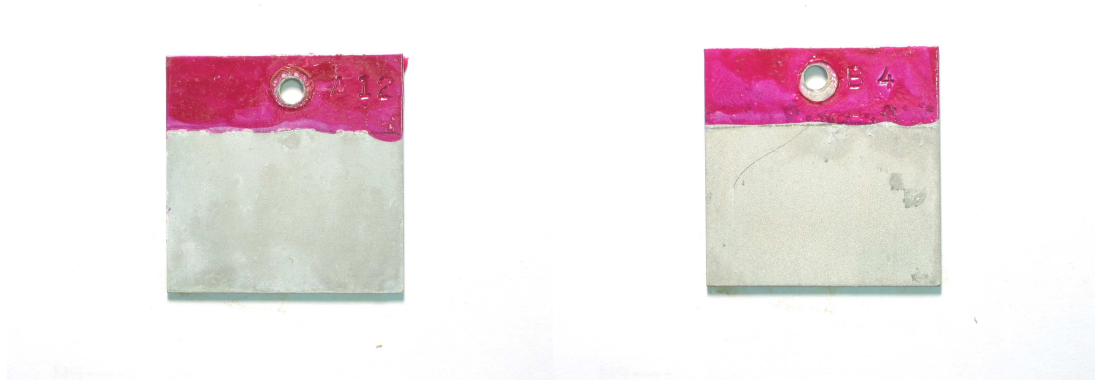
**Figure 14. Appearance of unmodified 984 on the left and Cd electroplated on the right. Tested for ten days in naturally aerated 3.5% NaCl solution**

Figure 15 shows the comparison between the four Zn modified 984 coatings with unmodified 984 and Cd. The initial potential values are respectively -1108 mV (SCE), -1023 mV (SCE), -762 mV (SCE) and -748 mV (SCE) for 50% Zn 984, 10%Zn 984, 3%Zn 984 and 0.5%Zn 984. The final values were -1051 mV (SCE), -773 mV (SCE), 760 mV (SCE) and -746 mV (SCE).



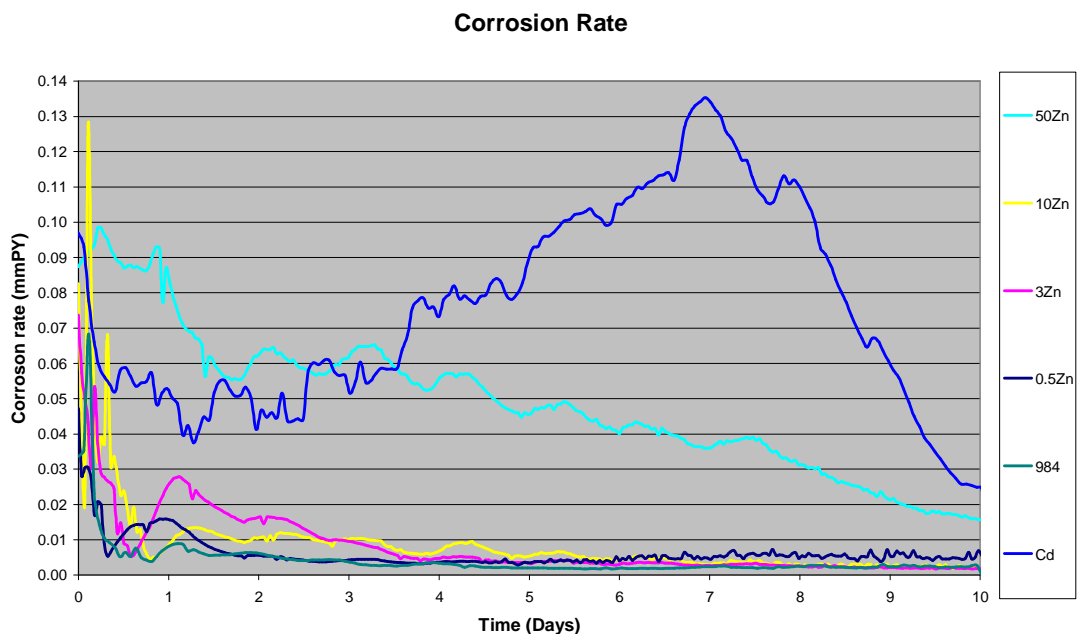
**Figure 15. Corrosion potentials of Zn modified 984 coatings compared with electroplated Cd and unmodified 984. Tested in naturally aerated 3.5% NaCl solution**

The appearance of 50% Zn 984 and 10% Zn 984 after the test is shown in Figure 16. Neither of them showed signs of red rust at the end of the test.



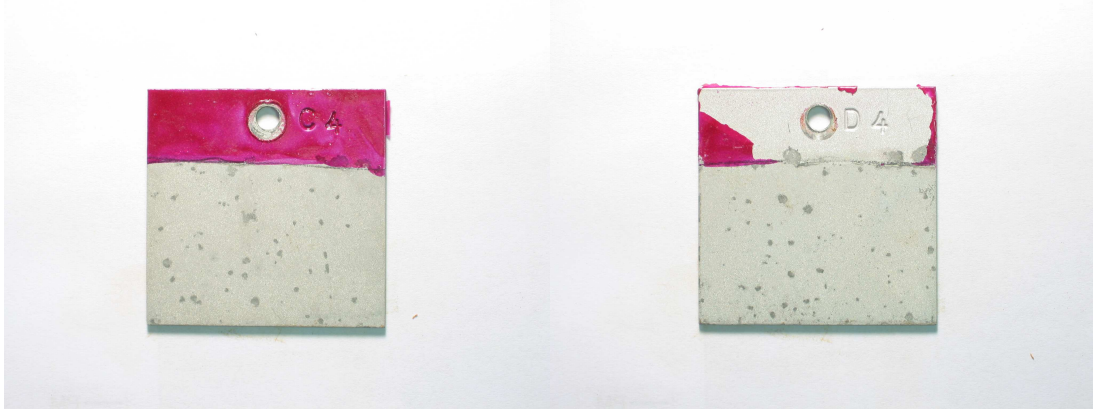
**Figure 16. Appearance of 50%Zn modified 984 on the left and 10%Zn modified 984 on the right. Tested for ten days in naturally aerated 3.5% NaCl solution**

Figure 17 shows the self corrosion rates of Zn modified 984 compared with unmodified 984 and electroplated Cd. The final corrosion rates for 50% Zn, 10%Zn, 3%Zn and 0.5%Zn were respectively 18  $\mu\text{m}/\text{yr}$ , 3  $\mu\text{m}/\text{yr}$ , 3  $\mu\text{m}/\text{yr}$  and 6  $\mu\text{m}/\text{yr}$ . The corrosion rate of 50% Zn seemed to be still decreasing when the test was stopped.



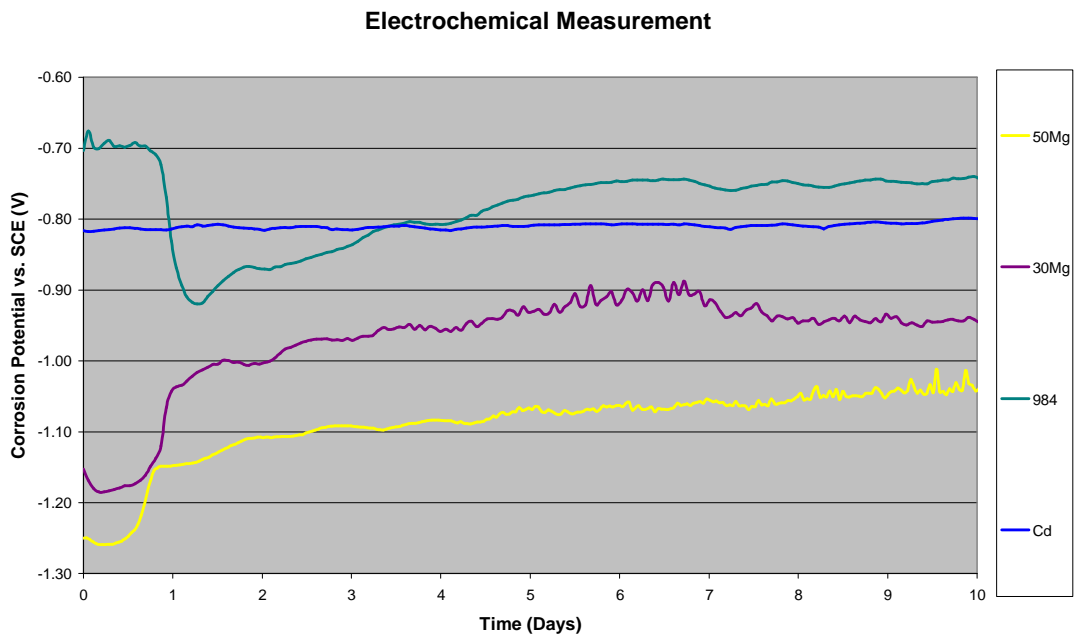
**Figure 17. Corrosion rate of Zn modified 984 coatings compared with unmodified 984 and electroplated Cd. Tested in naturally aerated 3.5% NaCl solution.**

The appearance of 3% 984 and 0.5% 984 is shown in Figure 18. Both the coatings showed corrosion pits that had not been shown on the unmodified 984 or from 50% Zn 984 and 10% Zn 984.



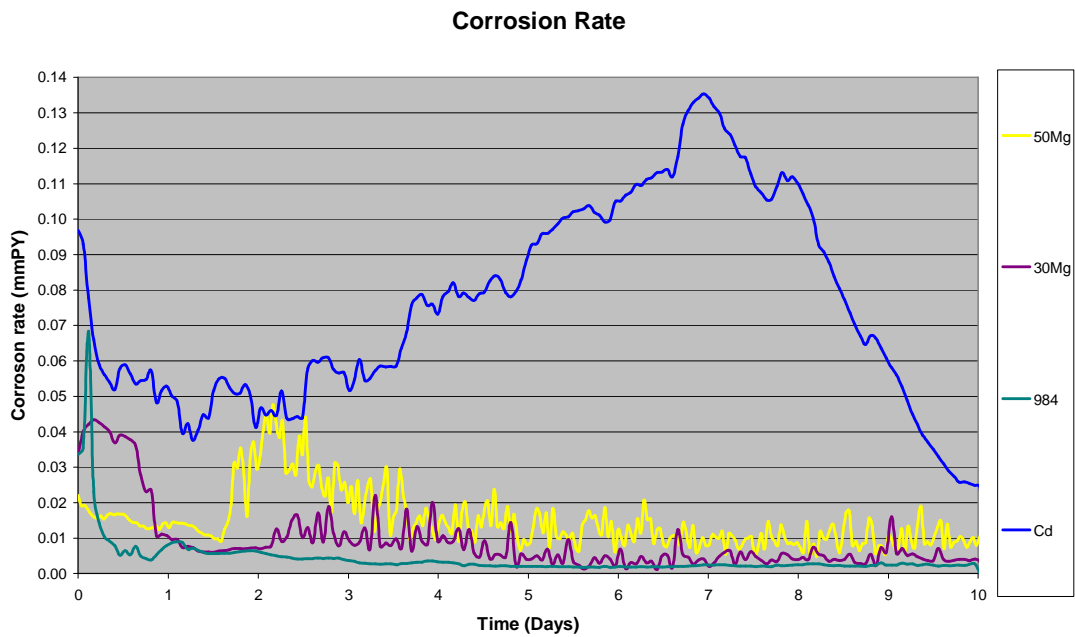
**Figure 18. Appearance of 3%Zn modified 984 on the left and 0.5%Zn modified 984 on the right. Tested for ten days in naturally aerated 3.5% NaCl solution**

Figure 19 shows the electrochemical potential of Mg modified 984 compared with unmodified 984 and electroplated Cd. 50% Mg showed a more active curve for all the duration of the test. Its initial potential was -1250 mV (SCE) and after the first day started to increase slowly to reach values ranged between -1090 and -1014 mV (SCE) from the fifth to the last day. The curve seemed to be still increasing when the test was stopped. The coating modified with 30% Mg showed an initial potential of -1152 mV (SCE), less active than 50% Mg, as was expected because of the smaller amount of Mg. Otherwise 30% Mg seemed to reach a plateau at the end of the test with values ranging around -940 mV (SCE).



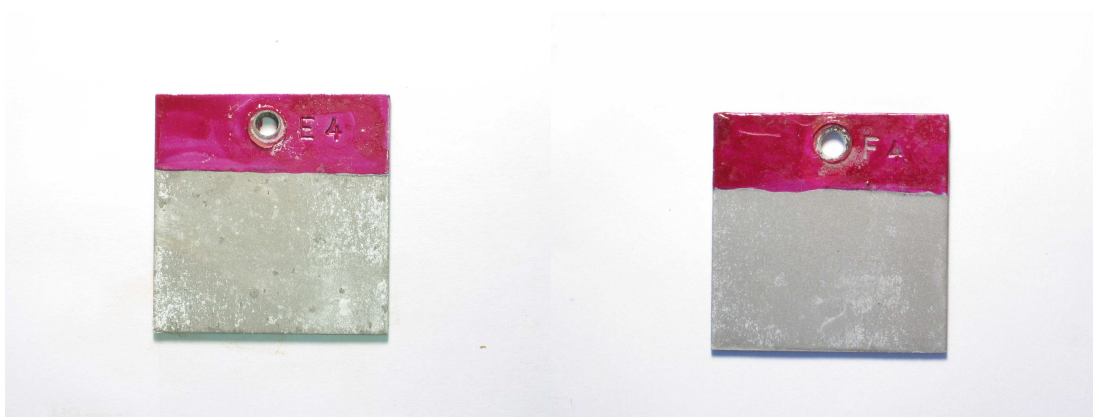
**Figure 19. Corrosion potentials of Zn modified 984 coatings compared with electroplated Cd and unmodified 984. Tested in naturally aerated 3.5% NaCl solution**

Figure 20 shows the corrosion rates of Mg modified coatings compared with unmodified 984 and Cd electroplated. Both of them after five days showed low corrosion rates, lower than 20  $\mu\text{m}/\text{yr}$  for 50% Mg and 10  $\mu\text{m}/\text{yr}$  for 30% Mg for most of the last five days.



**Figure 20. Corrosion rate of Mg modified 984 coatings compared with unmodified 984 and electroplated Cd. Tested in naturally aerated 3.5% NaCl solution**

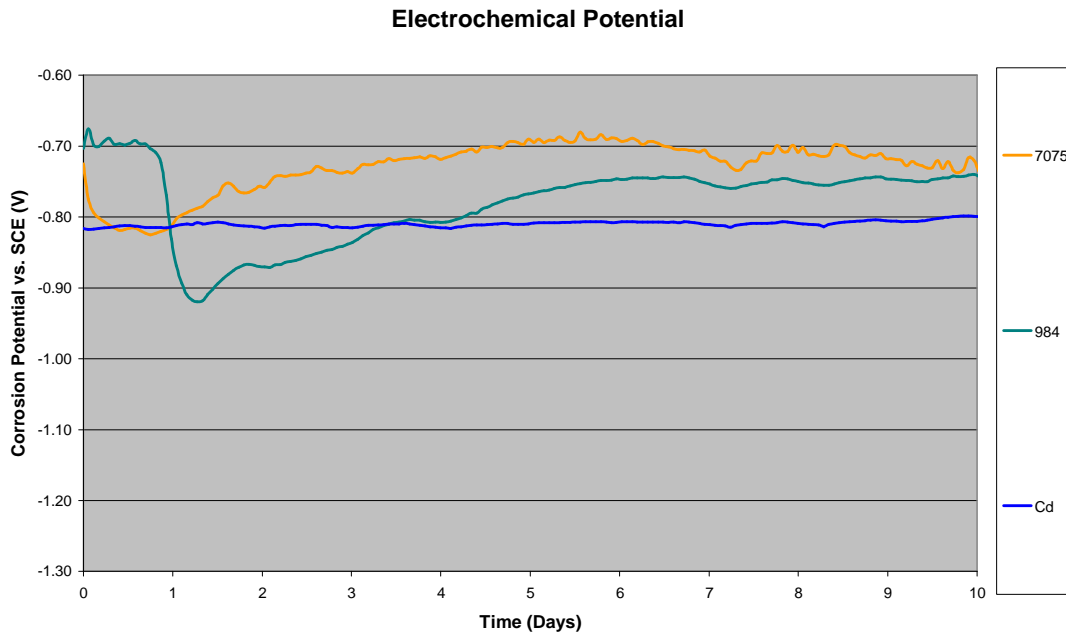
Figure 21 shows the appearance of 50% Mg modified 984 on the left and 30% Mg modified 984 on the right. Neither of them showed signs of red rust at the end of the test but white corrosion products are visible on 50% Mg.



**Figure 21. Appearance of 50%Mg modified 984 on the left and 30%Mg modified 984 on the right. Tested for ten days in naturally aerated 3.5% NaCl solution**

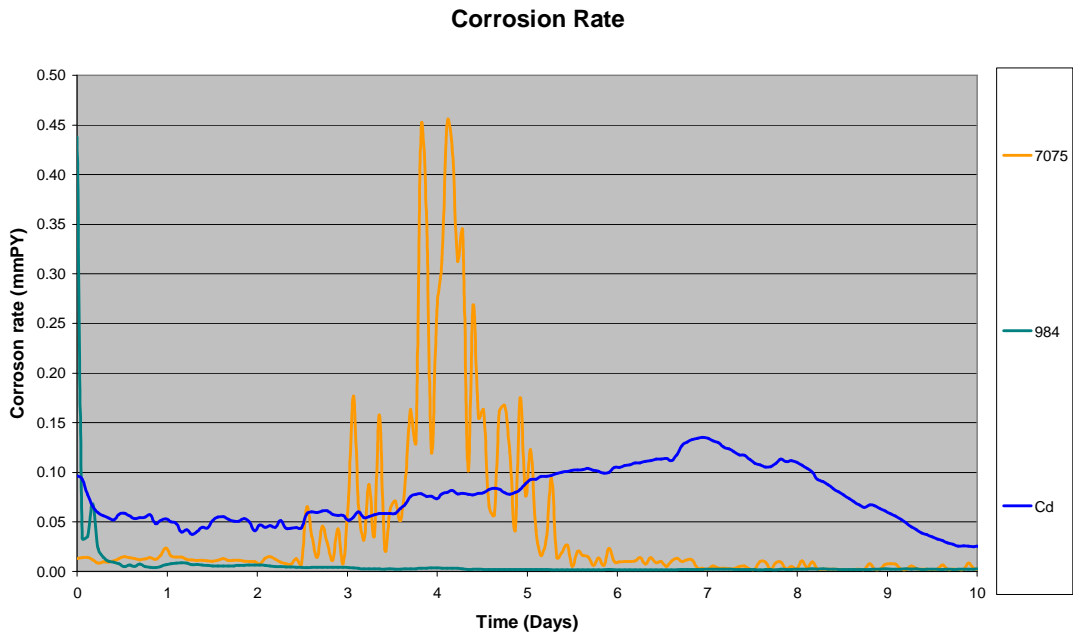


Figure 22 shows the electrochemical potential of aluminium alloy 7075 coating compared with unmodified 984 and electroplated Cd. The initial potential was -724 mV (SCE) and after four days it reached values ranging between -680 mV (SCE) and -740 mV (SCE) by the end of the test.



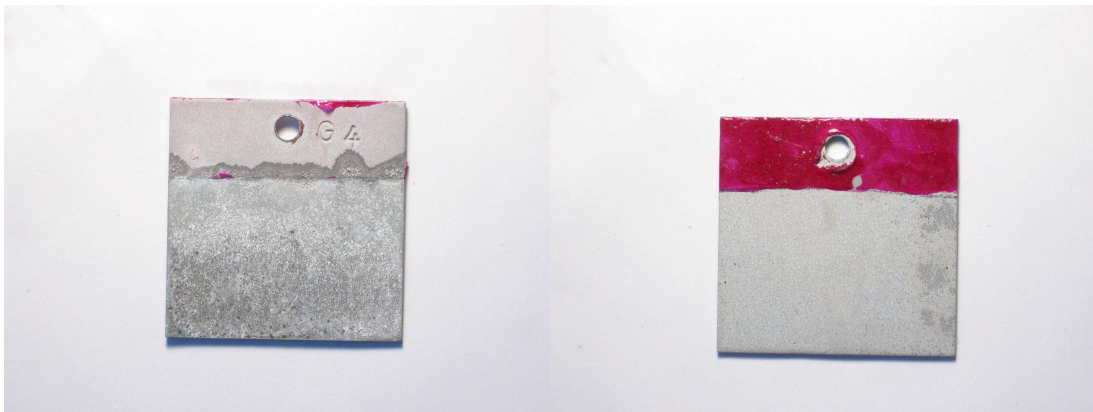
**Figure 22. Corrosion potentials of aluminium alloy 7075 coating compared with electroplated Cd and unmodified 984 tested in naturally aerated 3.5% NaCl solution.**

Figure 23 shows the corrosion rate of aluminium alloy 7075 coating compared with unmodified 984 and electroplated Cd. The scale on the graph is larger than previously because of the high corrosion rate of the 7075 between the fourth and fifth day. During that time the coating reached 450  $\mu\text{m}/\text{yr}$ , to stabilise around values comparable with those of unmodified 984 from the seventh day to the end.



**Figure 23 Corrosion rate of 7075 coating compared with unmodified 984 and electroplated Cd tested in naturally aerated 3.5% NaCl solution.**

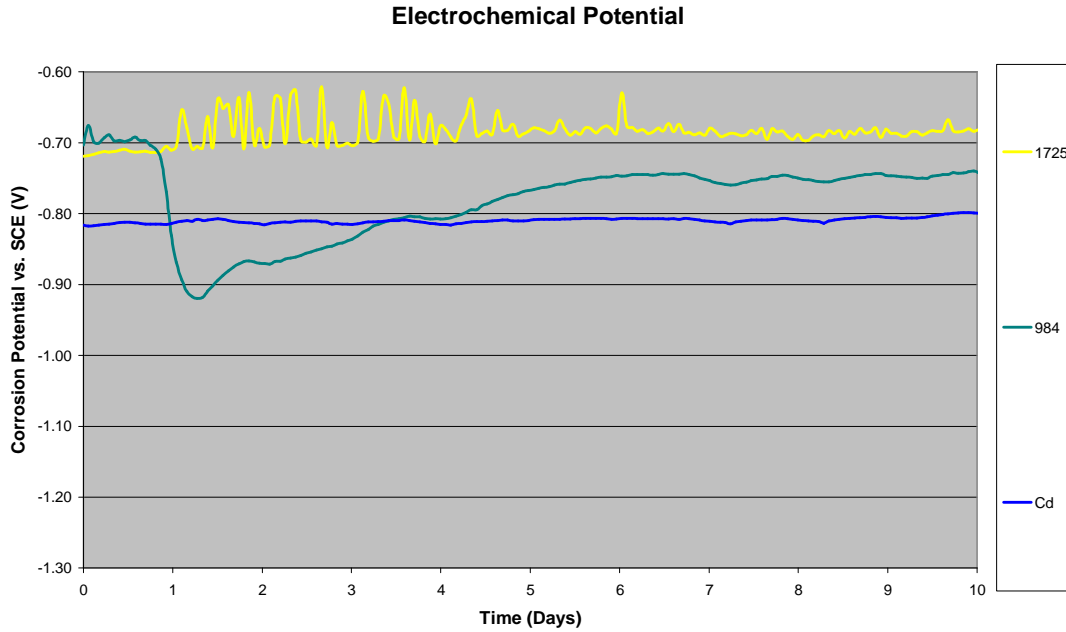
The appearance of 7075 is shown in Figure 24 on the left. A mix of white rust and darker spots is visible on its surface.



**Figure 24. Appearance aluminium alloy 7075 coating on the left and chromium free 1725 on the right. Tested for ten days in naturally aerated 3.5% NaCl solution**

Figure 25 shows the electrochemical potential of chromium free 1725. This coating differs from unmodified 984 due to the absence of chromium in its composition. Apart from a lower initial potential, that was -718 mV (SCE) instead of -703 mV (SCE) for the 984, from the second day it showed a more noble potential for all the

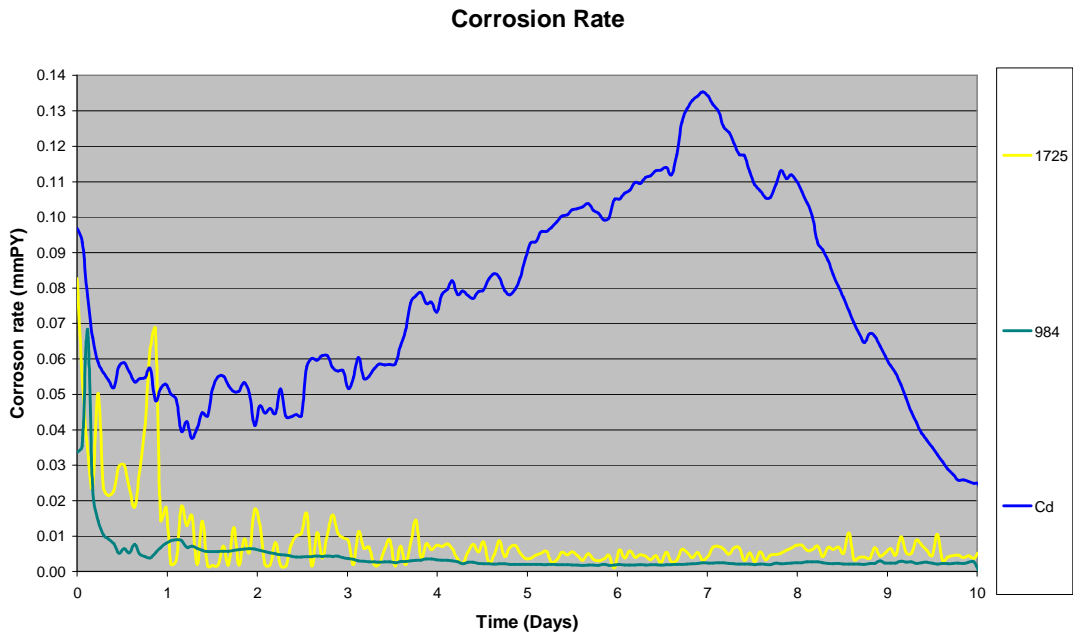
duration of the test. After the first four days the curve became smoother and it stabilized around -680mV (SCE).



**Figure 25. Corrosion potentials of chromium free 1725 coating compared with electroplated Cd and unmodified 984 tested in naturally aerated 3.5% NaCl solution.**

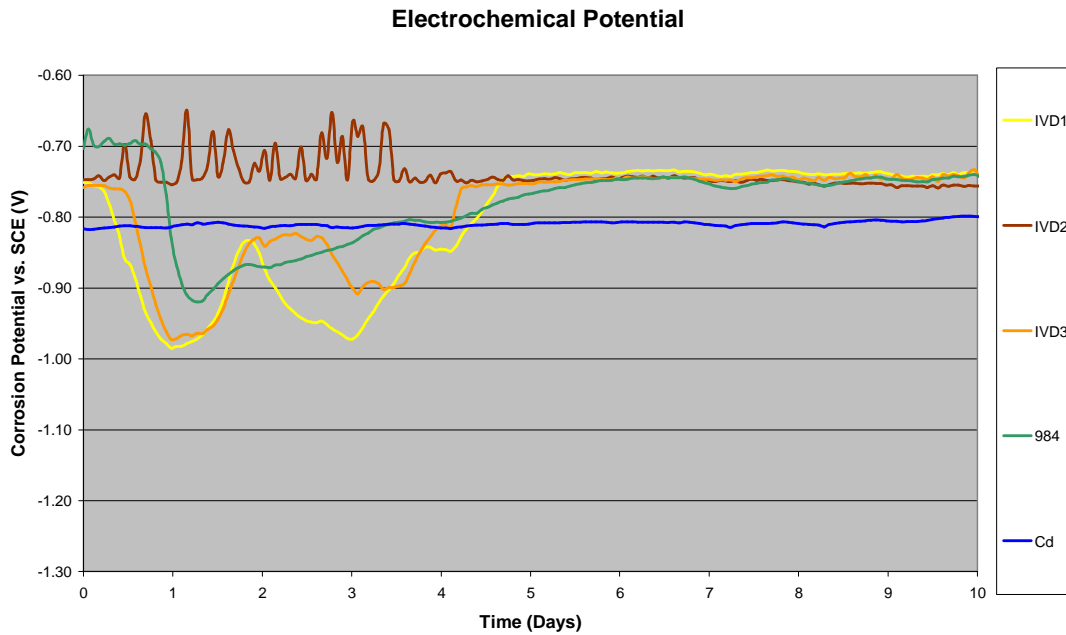
Chromium free 1725 corrosion rate is shown in Figure 26. After the first four days of decreasing values the corrosion rate settled above 10  $\mu\text{m}/\text{yr}$  for most of the last five days.

The appearance of 1725 is shown in Figure 24 on the right. After ten days of testing it did not show visible signs of corrosion on the steel substrate although white products were noticed on its surface.



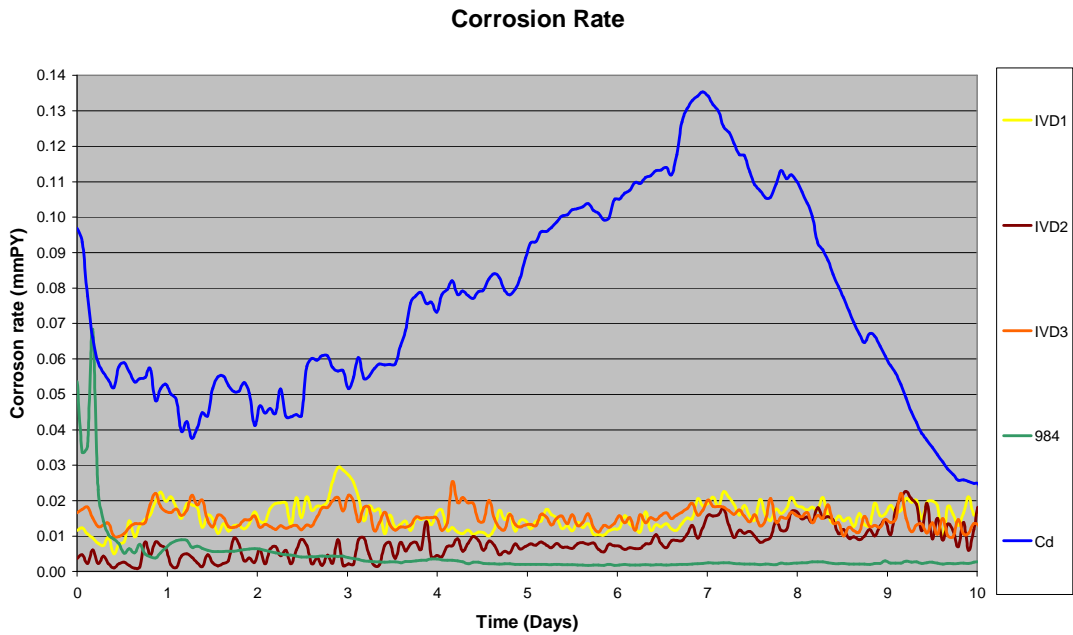
**Figure 26. Corrosion rate of chromium free 1725 coating compared with unmodified 984 and electroplated Cd tested in naturally aerated 3.5% NaCl solution.**

Figure 27 shows the corrosion potential of pure aluminium IVD coatings. IVD1 is the basic IVD coating while IVD2 has a layer of wax on its surface and IVD3 a layer of PTEF designed to reduce its friction coefficient. All the three initial potentials are very close to -750 mV (SCE), but IVD2 showed a different behaviour during the first four days remaining more noble and constant despite of a more scattered plot. This is thought to have been caused by the barrier properties of the wax layer.



**Figure 27. Corrosion potentials of pure aluminium IVD coatings compared with electroplated Cd and unmodified 984 tested in naturally aerated 3.5% NaCl solution.**

Figure 28 shows the corrosion rate of the same coatings, still compared with unmodified 984 and electroplated Cd. IVD2 showed a lower corrosion rate for the first eight day of the test with values almost always lower than 10  $\mu\text{m}/\text{yr}$  during the first eight days and lower than 20  $\mu\text{m}/\text{yr}$  during the last two days. IVD1 and IVD2 showed values that ranged between 10  $\mu\text{m}/\text{yr}$  and 20  $\mu\text{m}/\text{yr}$  for most of the ten days. The appearance of the three coatings is shown in Figure 29 with, from the left to the right IVD1, IVD2 and IVD3.



**Figure 28 Corrosion rate pure aluminium IVD coatings compared with unmodified 984 and electroplated Cd tested in naturally aerated 3.5% NaCl solution.**



**Figure 29. Appearance pure aluminium IVD1 on the left, IVD2 in the middle and IVD3 on the right. Tested for ten days in naturally aerated 3.5% NaCl solution**

Table 7 describes the appearance of the coatings and of the solutions during the test. During the fourth day 7075 became darker, 1725 IVD1 and IVD3 showed white products of corrosion on their surface and, consequently, the solution became white. IVD2 showed small black pits on its surface during the same day but the solution became slightly white during the fifth day. During the sixth day 50%Mg showed white gel on the coating surface and a white film appeared floating on top of the solution. During the seventh day 7075 showed black and white deposits on its

surface and all the IVD coatings showed gel on their surfaces. The 30%Mg 984, the unmodified 984 and Cd did not show significant changes during the test. However Cd became progressively and uniformly darker during the ten days. Regarding the dark pit of the surface of 3%Zn and 0.5%Zn in Figure 18 they were not noticed during the test and it is not possible to say when they appeared for the first time.

	<i>1st</i>	<i>2nd</i>	<i>3rd</i>	<i>4th</i>	<i>5th</i>	<i>6th</i>	<i>7th</i>	<i>8th</i>	<i>9th</i>	<i>10th</i>
50%Zn	-	-	-	-	-	-	-	-	-	-
10%Zn	-	-	-	-	-	-	-	-	-	-
3%Zn	-	-	-	-	-	-	-	-	-	-
0.5%Zn	-	-	-	-	-	-	-	-	-	-
50%Mg	-	-	-	-	-	GC	-	-	-	-
30%Mg	-	-	-	-	-	-	-			
7075	-	-	-	UD	-	-	WR- DP	RS		
CR984	-	-	-	-	-	-	-	-	-	-
CF1725	-	-	-	WP- WS			GC			
IVD1				WP- WS			GC			
IVD2				DP	WP		GC			
IVD3				WP- WS			GC			
Cd	-	-	-	-	-	-	-	-	-	-

**Table 7. Appearance of the solutions and the coating surfaces from the first to the tenth day. WP=White Products of corrosion, RR=Red rust, WS=White solution, RS=Red solution, DP=dark pits on the coating, GC=Gel on the coating, UD=uniform darkening.**

### 3.1.2 Galvanic Coupling Measurement

The coated and uncoated panels were connected to a zero resistance ammeter and immersed in quiescent 3.5% NaCl solution. The galvanic current and the couple potential were recorded over a ten day period.

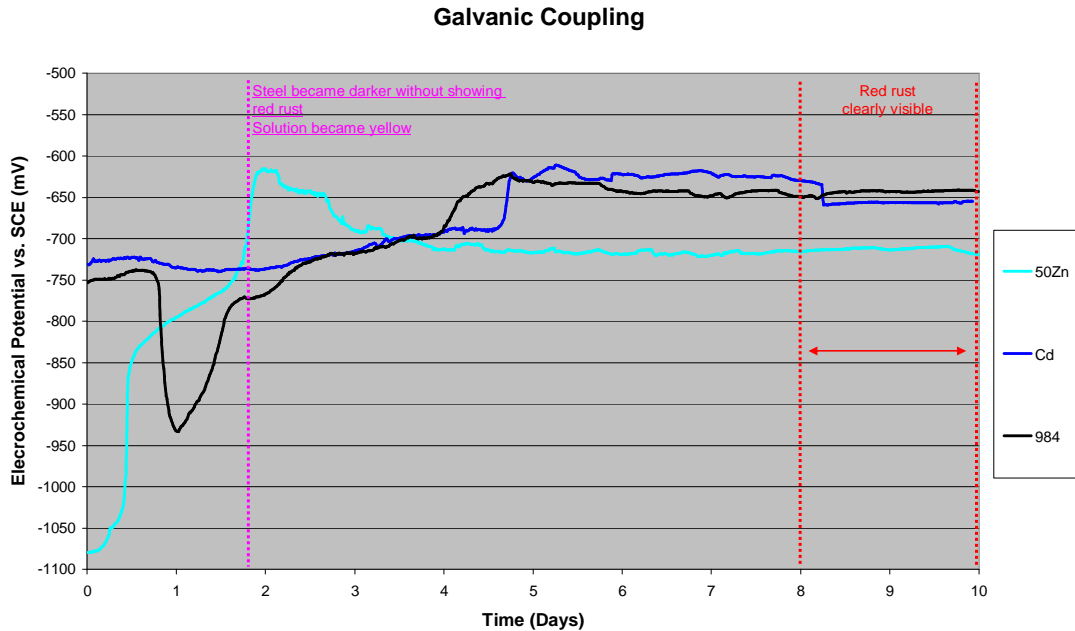


**Figure 30. Couple potential of 984, 50% Zn 984 and Cd with steel**

After reaching a maximum the couple potential decreased progressively to stabilize after 4 days between -720 and -710 mV (SCE) until the end of the test.

The galvanic current between the two panels is shown in Figure 31. Current decreased quickly in the first three days from the maximum value of 1070  $\mu\text{A}$  reached in the first few hours to 40  $\mu\text{A}$ . From the fourth day to the last one the current continued to decrease slowly until 10  $\mu\text{A}$  in the last day.



### Galvanic Coupling

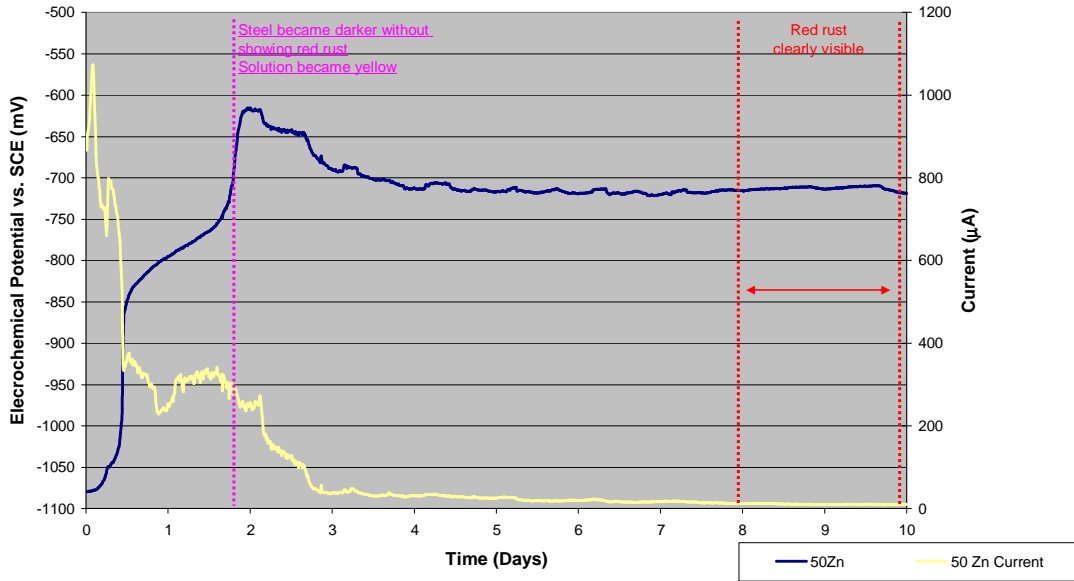


**Figure 31. Couple potential of 50% Zn 984 with steel (blue line) and galvanic current (yellow line)**



**Figure 32. Appearance of 50% Zn 984 and steel panels after ten days of testing. Coated panel on the left and steel panel on the right.**

Concerning the appearance of both panels and the solution, the steel panel became darker between the first and the second day and the colour of the solution changed to a light yellow. The appearance remained the same until the last two days in which

the steel panel clearly showed signs of red rust on its surface and the solution became red.

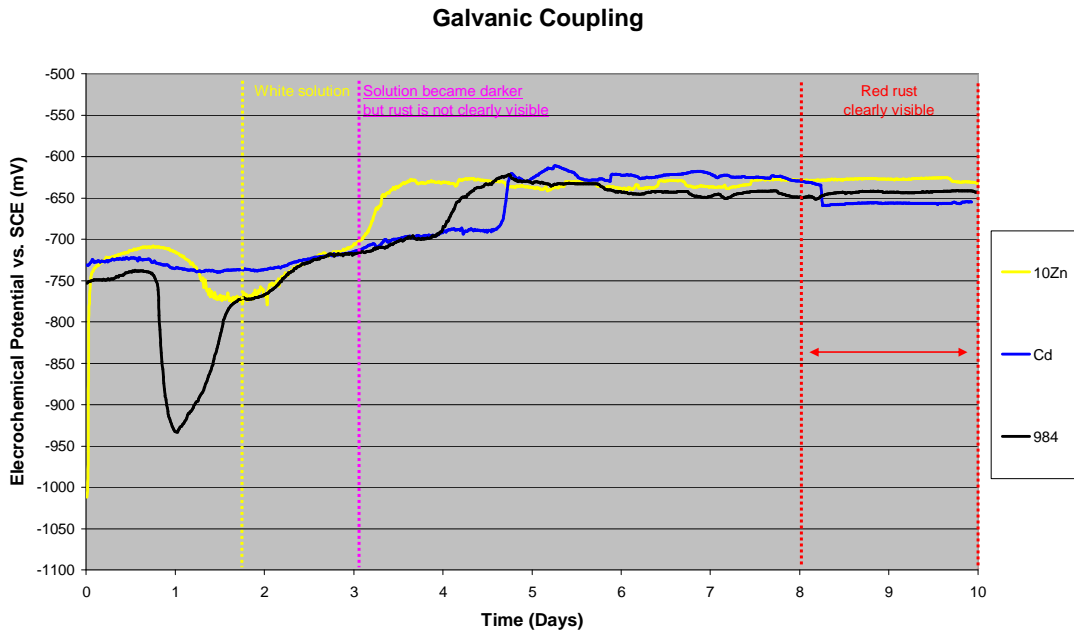


**Figure 33. Couple potential of 984, 10% Zn 984 and Cd with steel**

Figure 33 shows the trend of coupled potential of 10% Zn 984 with steel, compared with the coupling of Cd with steel and 984 with steel. The low initial potential of the couple, -1012 mV (SCE) increased quickly to higher values in approximately two hours. For three days the potential stayed between -780 and -710 mV (SCE) to increase after the third day to a range around -630 mV (SCE).

Figure 34 shows the galvanic current the two panels. The current stabilized in the first three days. Despite of the periodical oscillations with a period of one day, the trend line of the current became constant after three days around the value of 300  $\mu$ A. The oscillation almost disappeared after eight days when the panels started to show red rust.

### Galvanic Coupling

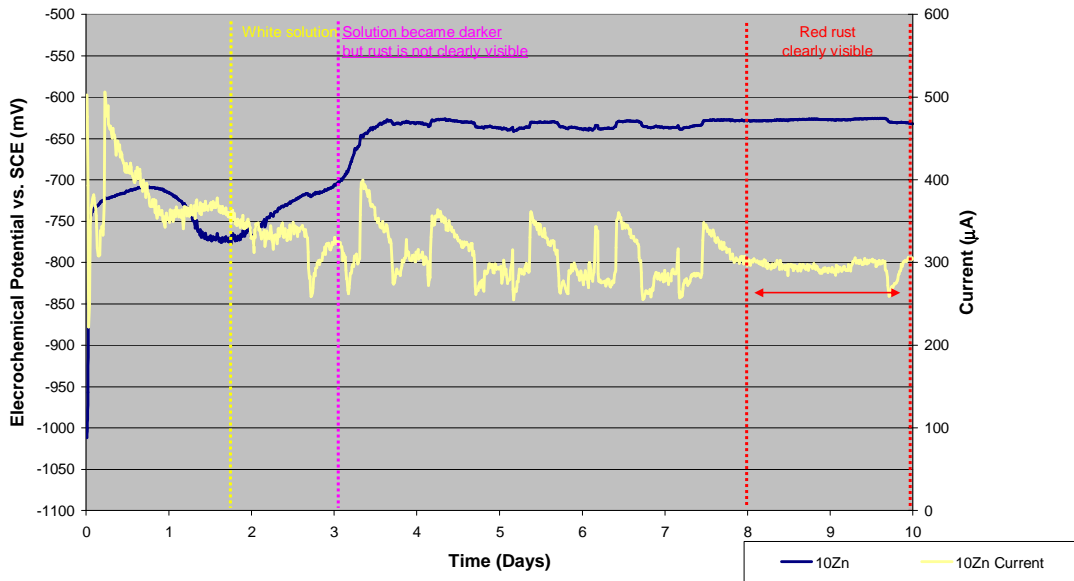


**Figure 34. Couple potential of 10% Zn 984 with steel (blue line) and galvanic current (yellow line)**



**Figure 35. Appearance of 10% Zn 984 and steel panels after ten days of testing. Coated panel on the left and steel panel on the right.**

Concerning the appearance of the panels, the solution showed white precipitation during the second day. After the third day the solution became darker but red rust was still not clearly visible on both the panels. During the ninth and tenth day both the panels became rusty.

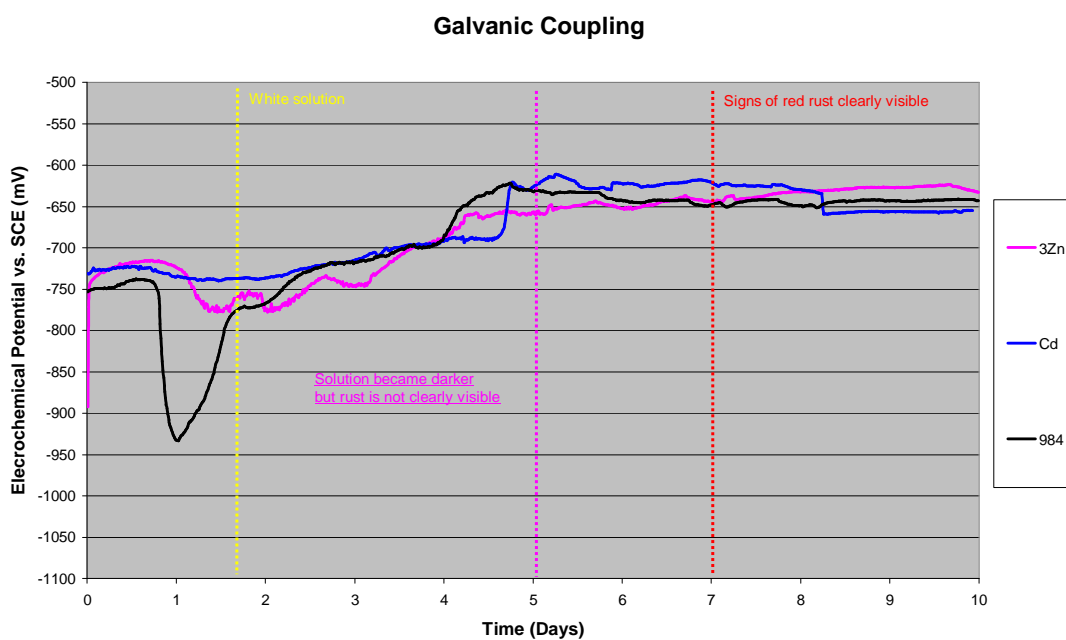


**Figure 36. Couple potential of 3% Zn 984 with steel**

Figure 36 shows the trend of coupled potential of 3% Zn 984 with steel, compared with the coupling of Cd with steel and 984 with steel. The low initial potential of the couple, -892 mV (SCE) increased quickly to higher values in approximately one hour. For three days the potential remained between -780 and -720 mV (SCE) to increase slower than 10% Zn to the plateau value around -630 mV (SCE).

Figure 37 shows the plot of the galvanic current compared with the couple potential. Despite several high peaks the current trend line is around 300  $\mu$ A. As for the 10% Zn these high peaks disappeared after the panels showed red rust.

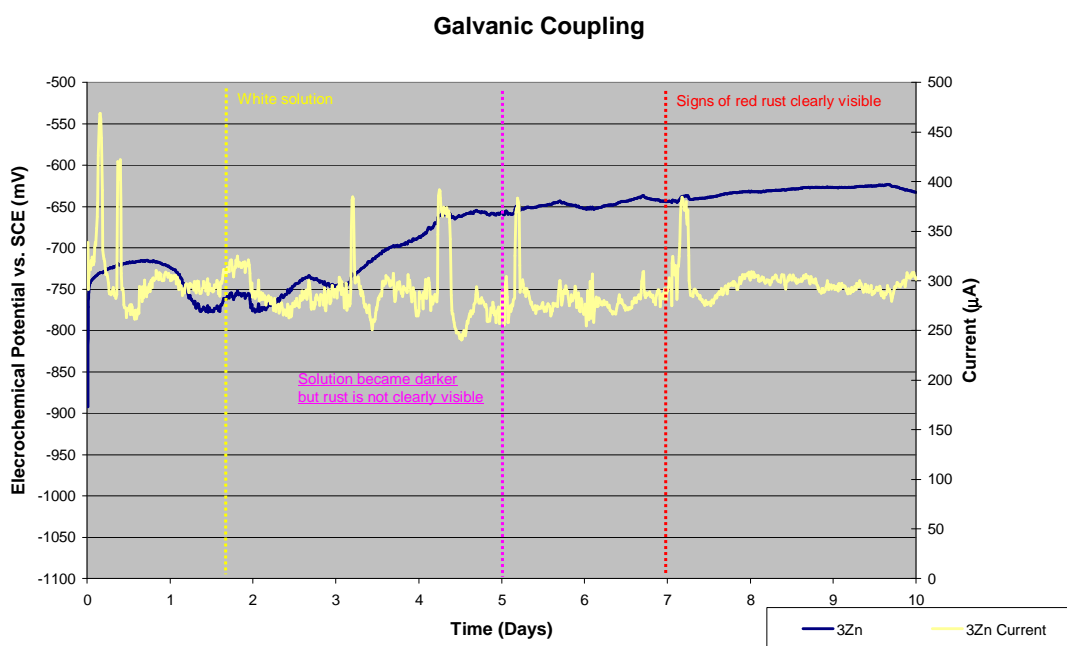


**Figure 37. Couple potential of 3% Zn 984 with steel (blue line) and galvanic current (yellow line)**



**Figure 38. Appearance of 3% Zn 984 and steel panel after ten days of testing. Coated panel on the left and steel panel on the right**

Concerning the appearance of the panels, the solution showed white precipitation during the second day. After the fifth day the solution became darker but red rust was

still not clearly visible on both the panels. After seven days signs of red rust became clearly visible.

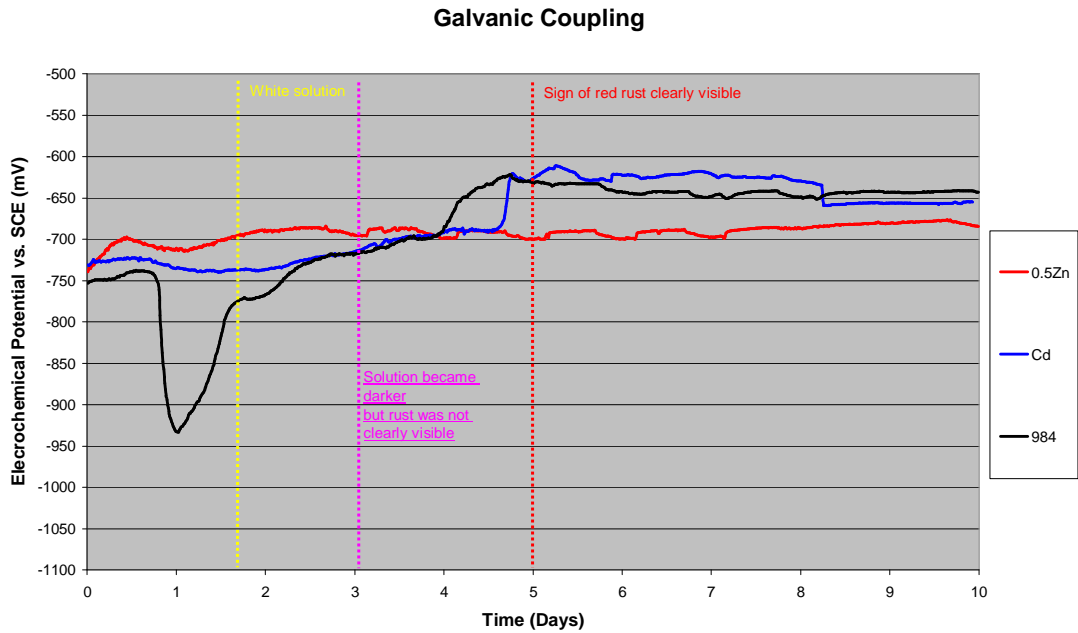


**Figure 39. Couple potential of 0.5% Zn 984 with steel**

Figure 39 shows the trend of coupled potential of 0.5%Zn 984 with steel, compared with the coupling of Cd with steel and 984 with steel. Starting from the value of -733 mV (SCE) the potential ranged between -700 and -690 mV (SCE) from approximately the third to the eighth day of testing to increase slightly up to -675 mV (SCE) in the last two days.

Figure 39 shows the plot of the galvanic current of the coupling. Between the fourth and the tenth day the trend line of the current seems to be slightly lower than what showed by 10% Zn and 3 %Zn but also in this plot periodical peaks are clearly visible from the fourth to the seventh day. The period of the peaks is of one day so probably the experiment was influenced by the periodical fluctuations of the temperature.

### Galvanic Coupling

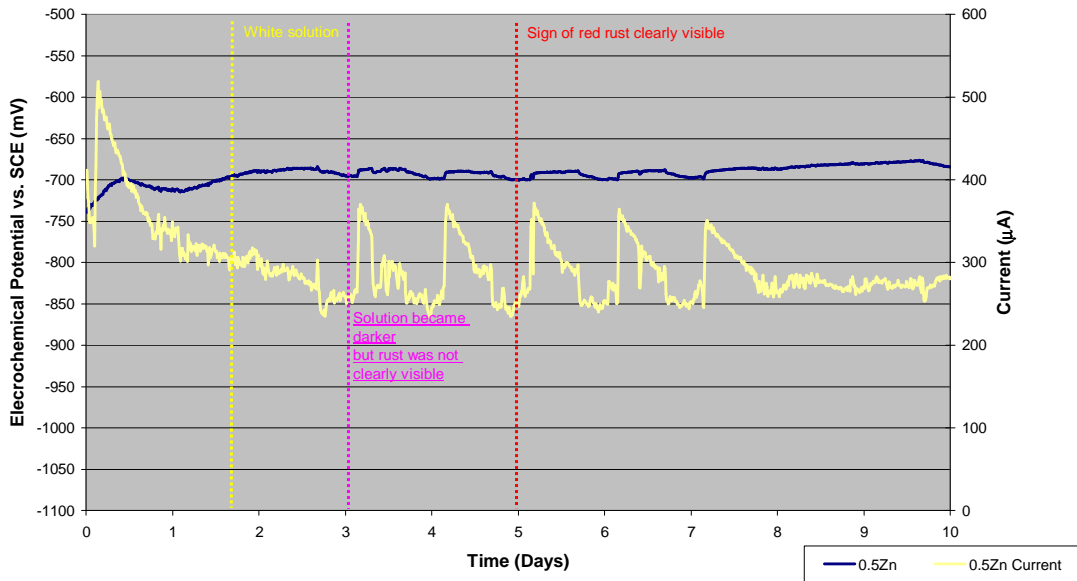
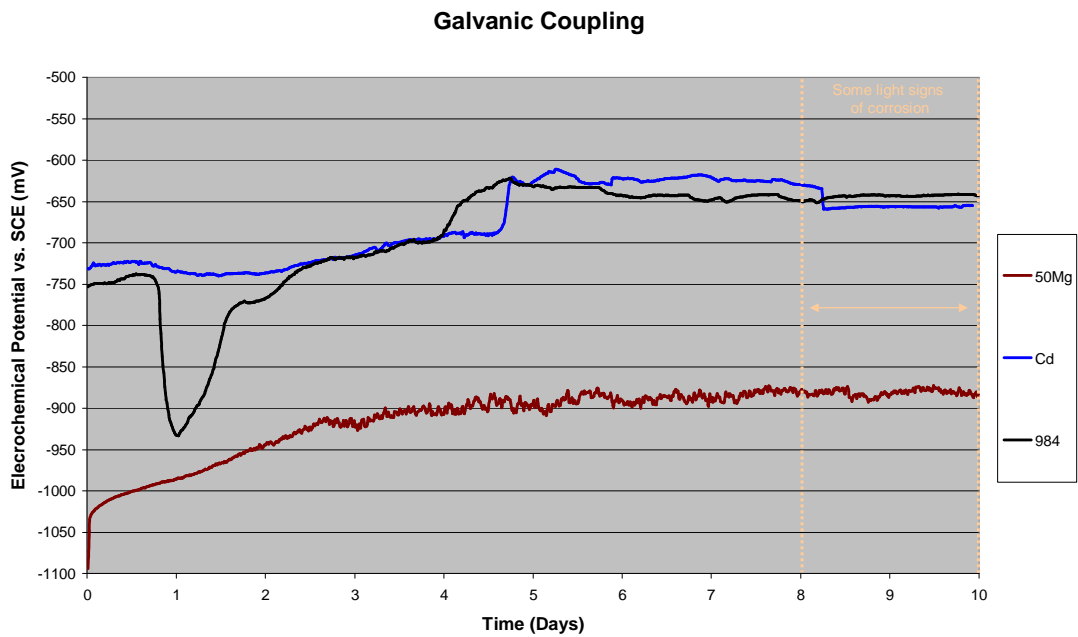


**Figure 40. Couple potential of 0.5% Zn 984 with steel (blue line) and galvanic current (yellow line)**



**Figure 41. Appearance of 0.5% Zn 984 and steel panels after ten days of testing. Coated panel on the left and steel panel on the right**

Concerning the appearance of the panels, the solution showed white precipitation during the second day. After the second day the solution became darker but red rust was not clearly visible on both the panels. After five days first signs of red rust became clearly visible.



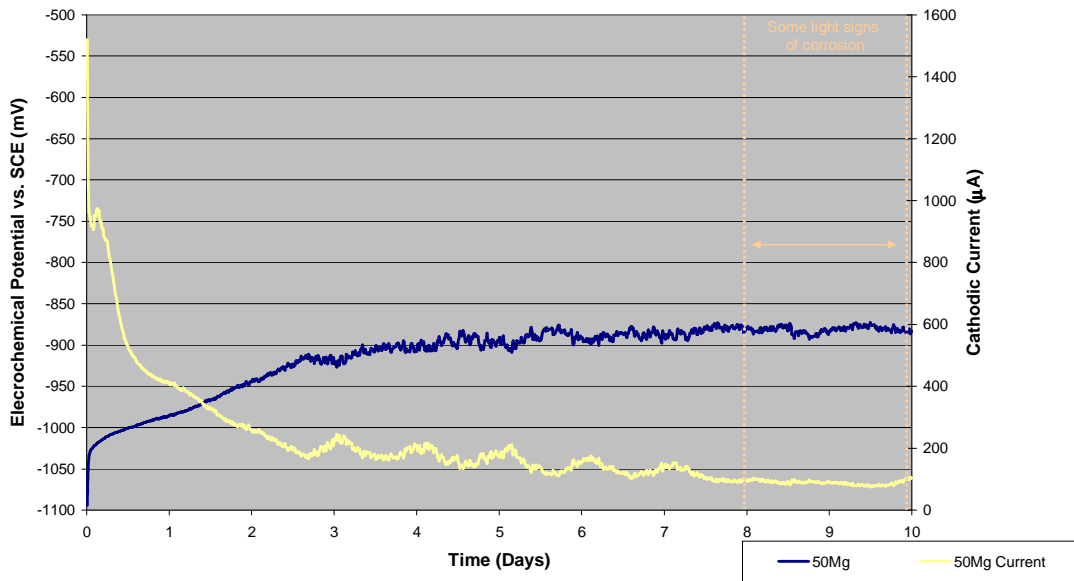
**Figure 42. Couple potential of 50% Mg 984 with steel**

Figure 42 shows the trend of coupled potential of 50% Mg 984 with steel, compared with the coupling of Cd with steel and 984 with steel. Starting from the value of -1093mV (SCE) the potential increased quickly in the first hour and then progressively in the first three days to stabilize around the value of -890, -870 mV (SCE) after the fourth-fifth day.

Figure 43 shows the plot of the galvanic current of the coupled panels. In this plot the current is clearly linked to the potential trend. As the potential became less active the current decreased until values smaller than 100  $\mu$ A in the last three days.



### Galvanic Coupling



**Figure 43. Couple potential of 50% Mg 984 with steel (blue line) and galvanic current (yellow line)**



**Figure 44. Appearance of 50% Mg 984 and steel panels after ten days of testing. Coated panel on the left and steel panel on the right**

Concerning the appearance of the panels the solution did not show change in colour and remained clean and transparent for the entire duration of the test. During the last two days some slight signs of rust appeared on the steel panel and the coated panel showed white products of corrosion on its surface.

### Galvanic Coupling

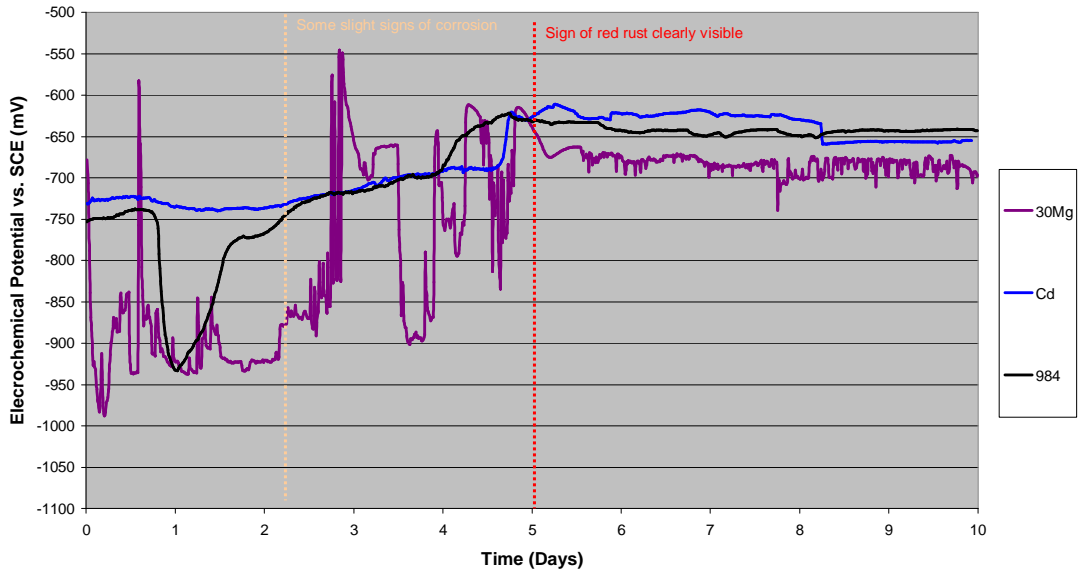


**Figure 45. Couple potential of 30% Mg 984 with steel**

Figure 45 shows the trend of coupled potential of 30% Mg 984 with steel, compared with the coupling of Cd with steel and 984 with steel. The initial potential was not as low as expected and from the beginning the measurement was not very stable. In the first two days the potential remained below -800 mV (SCE) except than for an high peak in the first day that reached a value of 585 mV (SCE). From the third to the fifth day the potential was still unstable but during the sixth day it stabilized around -690, -680 mV (SCE), still showing some scattering.

Figure 46 shows the plot of the galvanic current. Despite of the scattering of both the potential and the current, especially in the first five days, the trend line of current decreased as the trend line of the potential increased, that is when the potential became less active. With the formation of red rust the current decreased close to zero.

### Galvanic Coupling

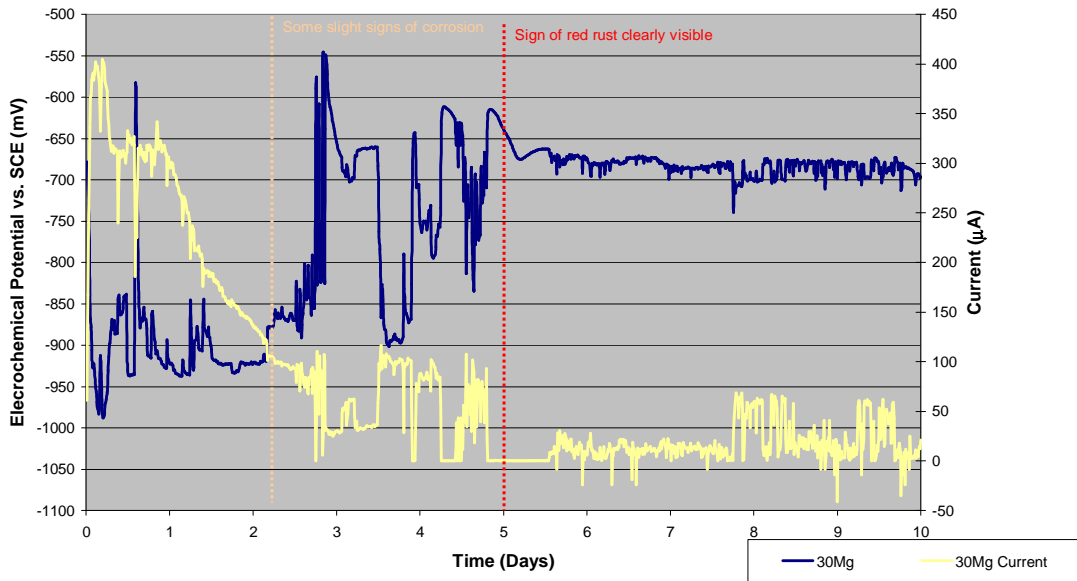


**Figure 46. Couple potential of 30% Mg 984 with steel (blue line) and galvanic current (yellow line)**



**Figure 47. Appearance of 30% Mg 984 and steel panels after ten days of testing. Coated panel on the left and steel panel on the right**

Concerning the appearance of the panels, during the second day some slight signs of rust appeared but they became clearly visible after the fifth day of testing. The solution did not show evident change of colour.

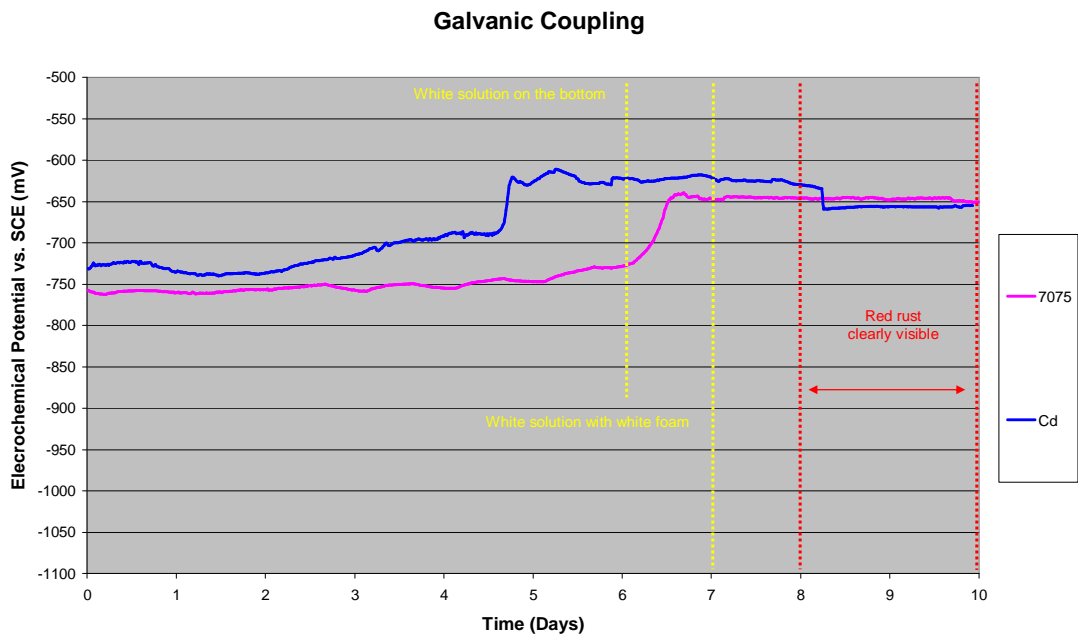


**Figure 48. Couple potential of 7075 with steel**

Figure 48 shows the trend of coupled potential of aluminium alloy 7075 coating with steel. The initial value of the potential was  $-759$  mV (SCE) and it remained almost stable at similar values for five days. During the sixth day it started to increase to reach again stable values around  $-645$  mV (SCE) until the end of the test.

Figure 49 shows the plot of the galvanic current. From the third to the fifth day and part of the sixth one, the current ranged approximately between  $300$  and  $400$   $\mu$ A. During the sixth day its trend line started to decrease as the potential started to become less active.

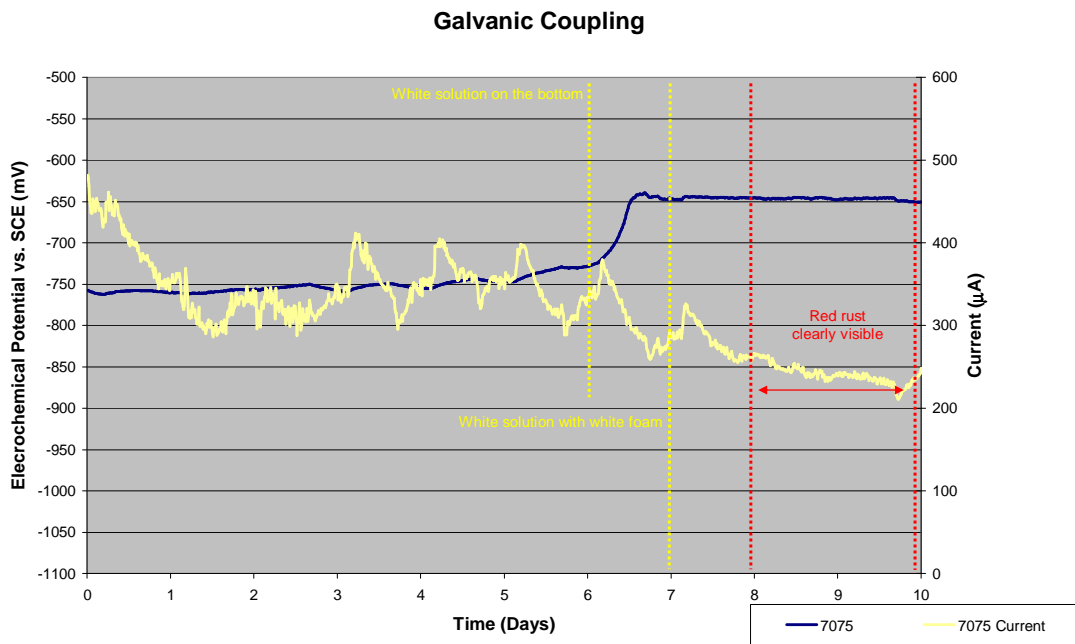


**Figure 49. Couple potential of 7075 with steel (blue line) and galvanic current (yellow line)**



**Figure 50. Appearance of 7075 and steel panels after ten days of testing. Coated panel on the left and steel panel on the right**

Concerning the panels and solution appearance, after six days the solution showed white corrosion deposits on the bottom of the cell and after another day a white precipitate started to float on the water line. Red rust became visible during the last two days of testing.

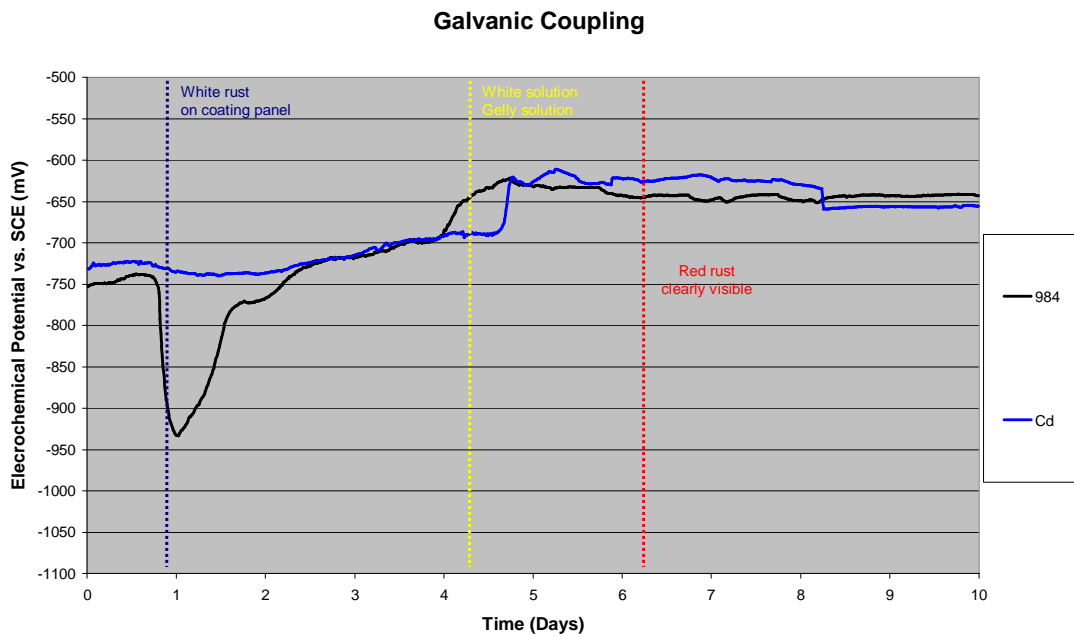


**Figure 51. Couple potential of 984 with steel**

Figure 51 shows the trend of coupled potential of 984 coating with steel compared with the couple Cd-steel. The couple potential started from the initial value of -751 mV (SCE). After less than one day it started to decrease quickly reaching -930 mV (SCE). From this minimum value the potential increased continuously for four days to settle above -650 mV (SCE). In the last five days of testing the couple potential ranged between -649 and -624 mV (SCE).

Figure 52 shows the plot of the galvanic current. For all the test the current ranged between 413 and 286  $\mu\text{A}$ , showing a decrease of the trend line during the fourth and fifth that coincided with change of the slope of the potential trend line.

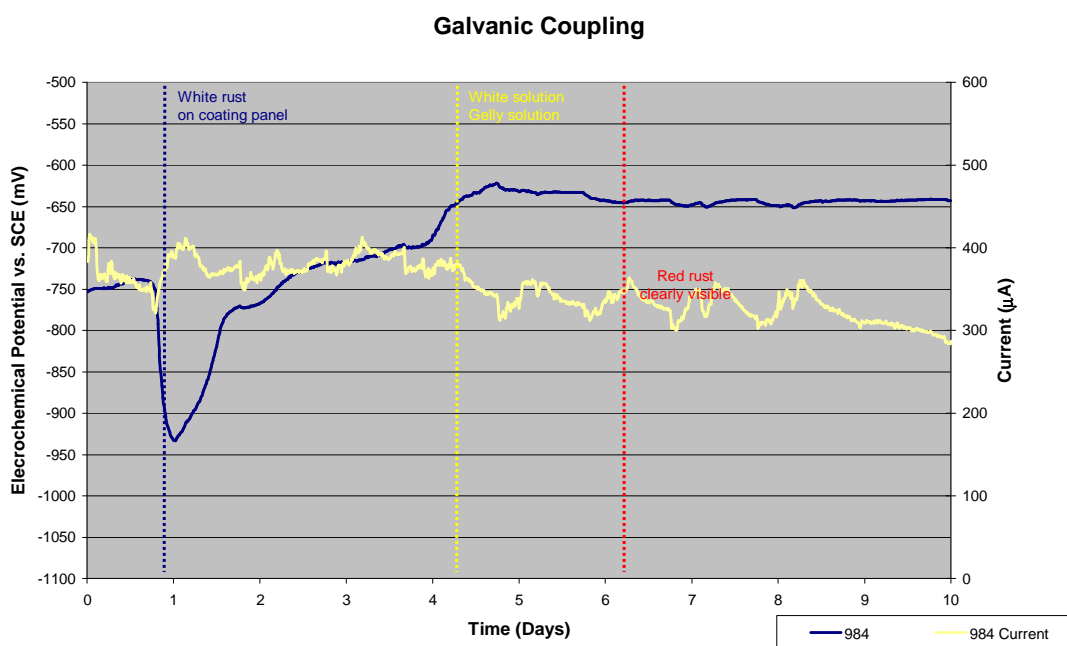


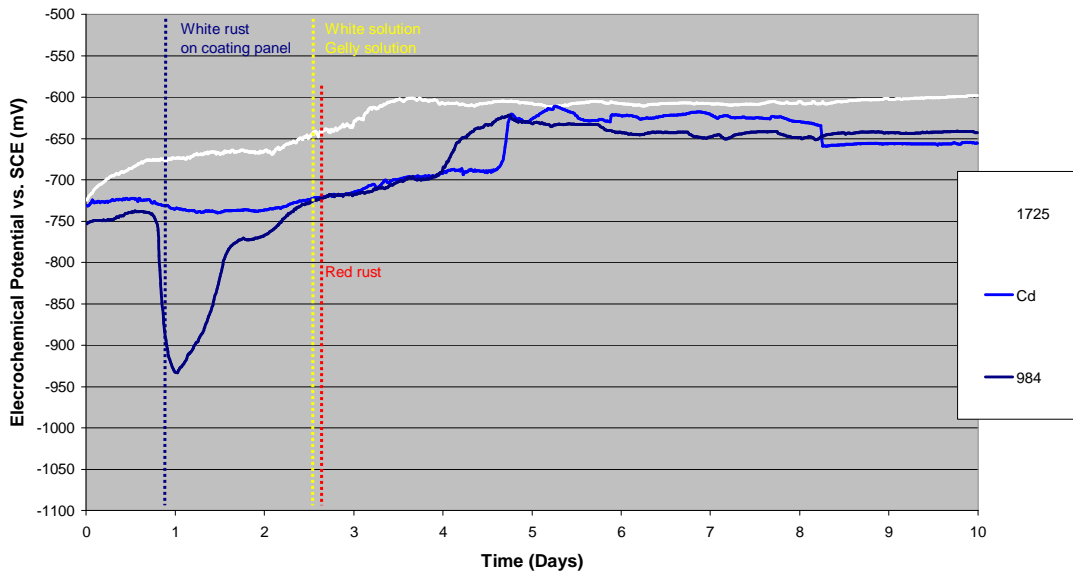
**Figure 52. Couple potential of 984 with steel (blue line) and galvanic current (yellow line)**



**Figure 53 Appearance of 984 and steel panels after ten days of testing. Coated panel on the left and steel panel on the right**

The coated panel showed slight signs of white rust during the first day. During the fifth day, due to white products of corrosion, the solution became white and jelly-like corrosion deposits became visible on the coating surface. First signs of red rust appeared after six days.

### Galvanic Coupling



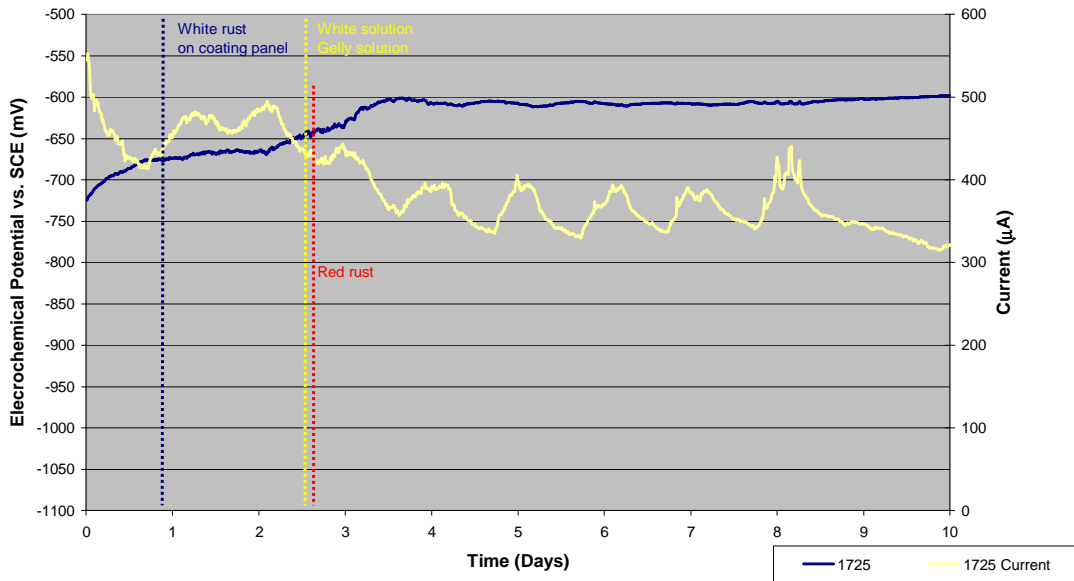
**Figure 54. Couple potential of 1725 with steel**

Figure 54 shows the trend of coupled potential of chromium free 1725 coating with steel. From the initial value of -718 mV (SCE) the potential increased progressively for three days. In the fourth day it reached the maximum of -601 mV (SCE) to remain just below -600 mV (SCE) for the rest of the test.

Figure 55 shows the plot of the galvanic current the panels. In the first two days the current ranged between 550 and 415  $\mu\text{A}$ . Then the current started to decrease and from the fifth to the eighth day it stayed between 405 and 340  $\mu\text{A}$  to continue to decrease during the ninth and the tenth day until 319  $\mu\text{A}$ .



### Galvanic Coupling



**Figure 55. Couple potential of Chromium Free 1725 with steel (blue line) and galvanic current (yellow line)**



**Figure 56. Appearance of 1725 and steel panels after ten days of testing. Coated panel on the left and steel panel on the right**

The coated panel showed slight signs of white rust during the first day. After two days of testing the solution became white with gelly-like products on the coating

surface and first signs of red rust appeared on the coated panel. After another day, during the fifth day red rust appeared on the steel panel as well.

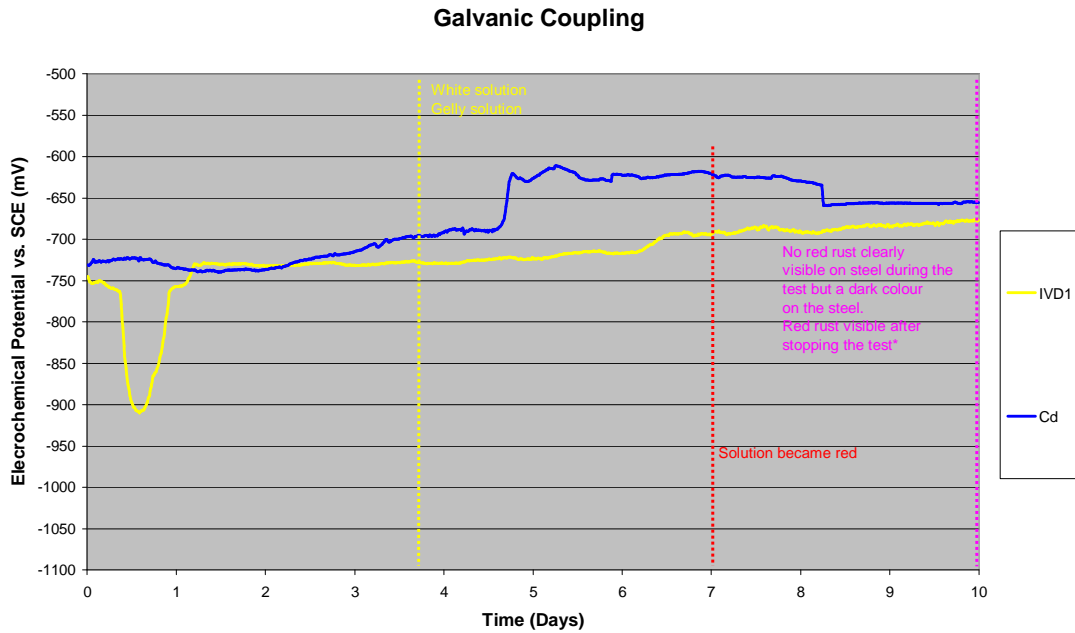


**Figure 57. Couple potential of IVD1 with steel**

Figure 57 shows the trend of coupled potential IVD1 coating with steel. From the initial value of -752 mV (SCE) potential reached a minimum at -906 mV (SCE) in less than one day to increase quickly to -730 mV (SCE) in less than one day and an half. It maintained values around -730 mV (SCE) for six days and during the seventh day it started to increase again, up to -677 mV (SCE) at the end of the test.

Figure 58 shows the galvanic current of IVD1 coupled with steel. The graph reflects very well the inverse trend of the potential and current changes. For the first seven days, before red rust appeared the current did not go lower than 361  $\mu$ A. For most of the test it ranged between 350 and 450  $\mu$ A.

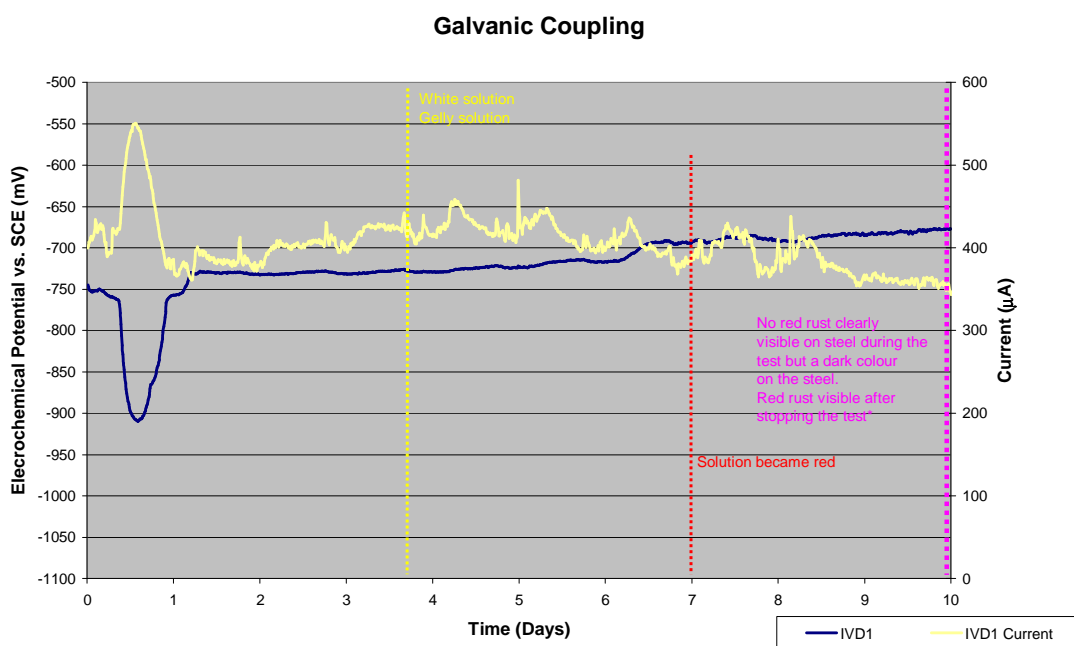


**Figure 58. Couple potential of IVD1 with steel (blue line) and galvanic current (yellow line)**



**Figure 59 Appearance of IVD1 and steel panels after ten days of testing. Coated panel on the left and steel panel on the right**

The solution of IVD1 and steel became white, gelly-like deposits and white precipitates floating on the solution appeared during the fourth day. After seven days the solution became red. At the end of the test red rust was not clearly visible on the

panels, probably because of the same colour of the solution. Some signs of red rust became visible after the test was stopped and the panels were removed from the solution and left to dry. The red rust visible on the coating in Figure 59 appeared above the water line where the solution had decreased level.

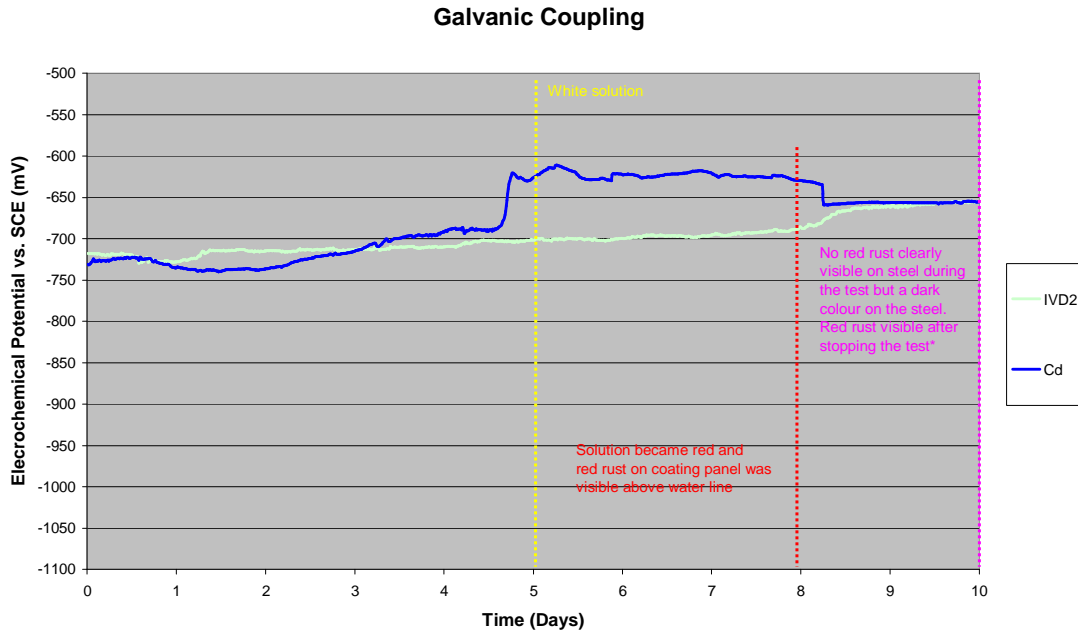


**Figure 60. Couple potential of IVD2 with steel**

Figure 60 shows the trend of couple potential of IVD2 and steel. IVD2 differs from IVD1 in the presence of a layer of wax applied on its surface. From the initial value of -711 mV (SCE) the potential did not decrease distinctly like IVD1 and IVD3. From the second day to the seventh its potential ranged between -710 and -690 mV (SCE). During the eighth day it started to increase gradually to reach -654 mV (SCE) by the end of the test.

Figure 61 shows the galvanic current of IVD2 couple with steel. Comparing it to the plots of IVD1 and IVD3 this coating did not show the minimum during the first day of testing. The current ranged between 290 and 460  $\mu\text{A}$  for all the duration of the test.

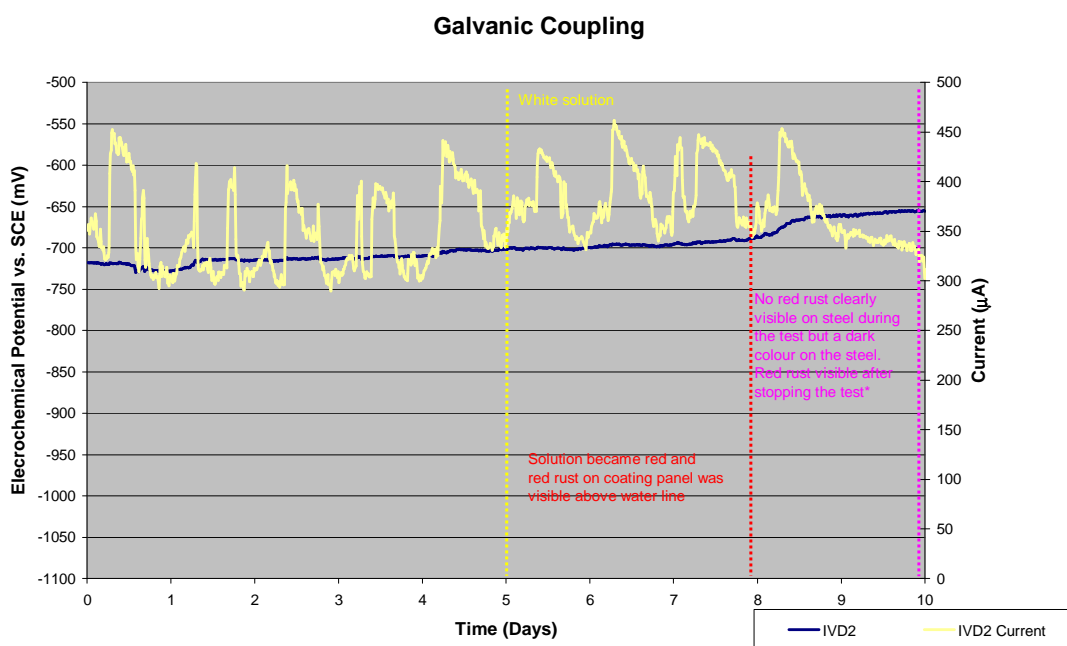


**Figure 61. Couple potential of IVD2 with steel (blue line) and galvanic current (yellow line)**



**Figure 62 Appearance of IVD2 and steel panels after ten days of testing. Coated panel on the left and steel panel on the right**

Compared to IVD1 the solution did not show gelly-like deposits but the solution became white during the fourth day showing a white precipitates floating on the solution. After eight days the solution became red and red rust appeared on the coating above the water line. At the end of the test red rust was not clearly visible on the panels because of the red colour of the solution. Some signs of red rust became

visible after the test was stopped and the panels were removed from the solution and left to dry.

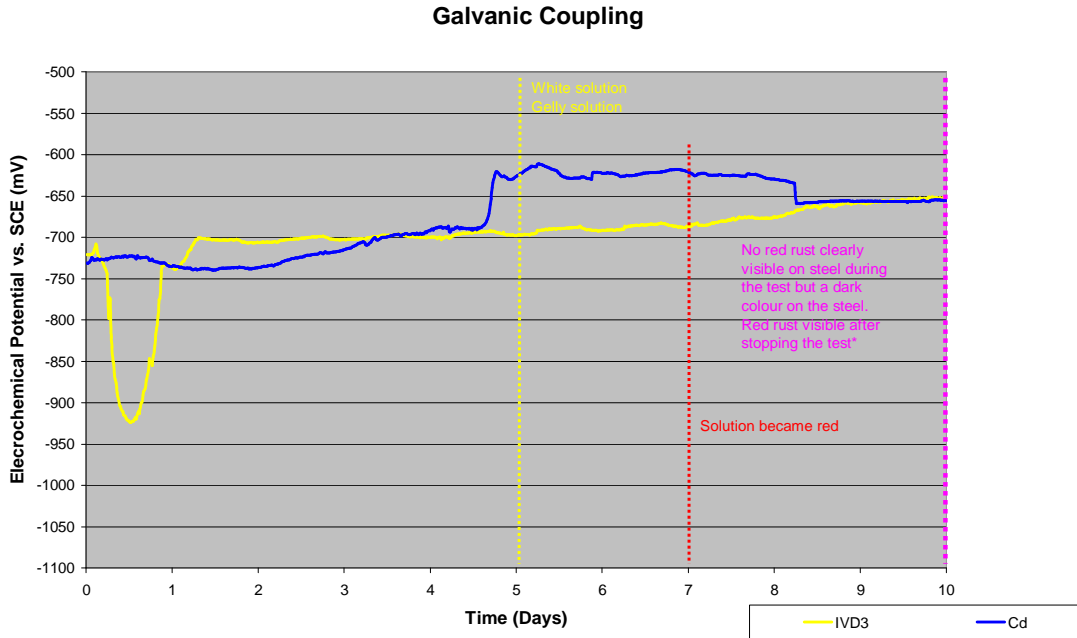


**Figure 63. Couple potential of IVD3 with steel**

Figure 63 shows the trend of coupled potential IVD3 coating with steel. The initial potential was -730 mV (SCE) and in one day the potential reached the minimum of -930 mV (SCE) to increase and settle around -700 mV until the seventh day. Only during the eighth day the potential started to increase slowly to reach -655 mV (SCE) by the end of the test.

Figure 64 shows the plot of the galvanic current. This plot is similar to IVD1 but with more pronounced peaks. In the first day we found a maximum in the galvanic current, which corresponded with the most active couple potential.

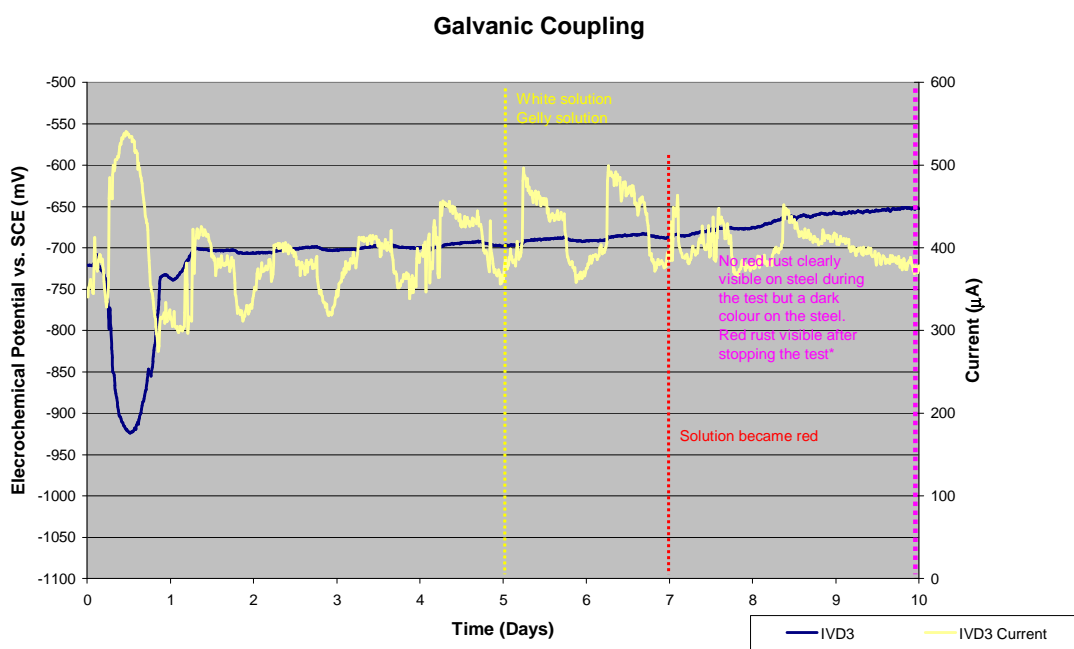


**Figure 64. Couple potential of IVD3 with steel (blue line) and galvanic current (yellow line)**



**Figure 65 Appearance of IVD3 and steel panels after ten days of testing. Coated panel on the left and steel panel on the right**

Compared to IVD1 the solution did not show gelly-like deposits but the solution became white after the same period of time, during the fourth day of testing. The

solution became red after seven days of testing. The red rust on the coating in Figure 65 was not noticed during the test because of a precipitate on the water line after four days. At the end of the test red rust was not clearly visible on the panels, maybe because of the colour of the solution that became red after seven days. Some signs of red rust became visible after the test was stopped and the panels were removed from the solution and left to dry

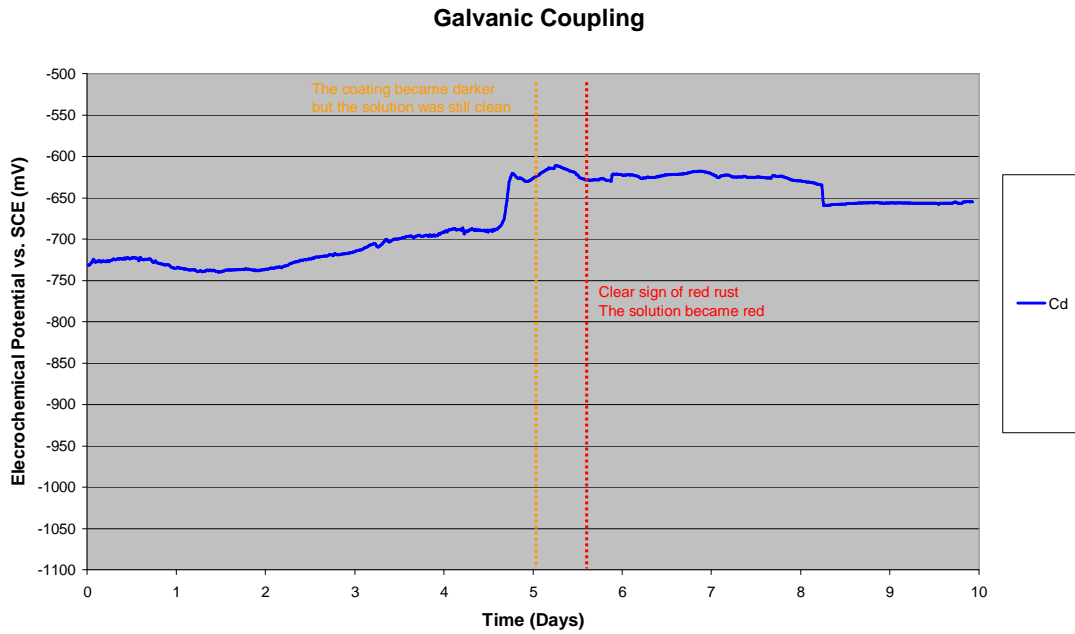


**Figure 66. Couple potential of Cd with steel**

Figure 66 shows the couple potential of Cd-steel. The initial potential was -728 mV (SCE). The potential remained between -740 and -690 mV (SCE) for almost five days and then it began to increase. At the end of the fifth day it increased very quickly to reach values between -630 and -610 mV (SCE) until the end of the eighth day. After that it decreased by approximately 30 mV.

Figure 67 shows the galvanic current. The initial value of the current is 376  $\mu\text{A}$  and the last value at the end of the test is 230  $\mu\text{A}$  lower than the same value for IVD1 (345  $\mu\text{A}$ ) IVD2 (360  $\mu\text{A}$ ) and IVD3 (302  $\mu\text{A}$ ).



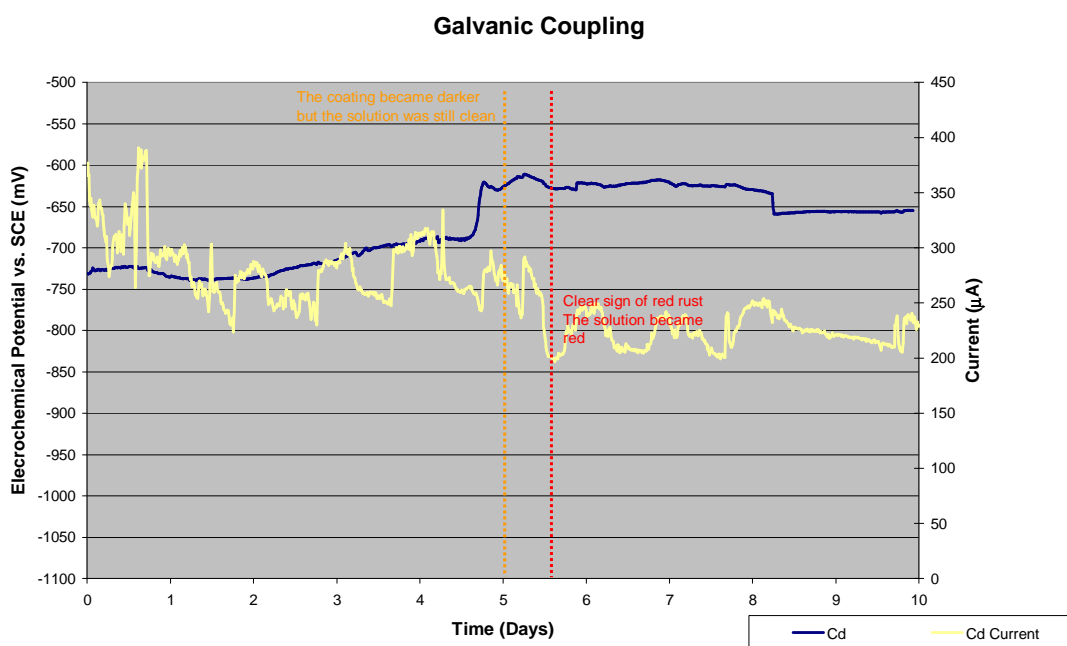


**Figure 67. Couple potential of Cd with steel (blue line) and galvanic current (yellow line)**



**Figure 68 Appearance of Cd and steel panels after ten days of testing. Coated panel on the left and steel panel on the right**

Concerning the panels and solution appearance, after five days the coated panel became darker but the solution was still clean. During the sixth day the solution became red and the coated panel started to show red rust. At the end of the test red rust was not clearly visible on the steel panel because of the colour of the solution.

Anyway some signs of red rust became visible on the steel panel after the test was stopped and the panels were removed from the solution and left to dry.

### 3.1.3 Marine exposure

Pictures of marine exposure are shown below.

Picture of the coated test panels after 4 months of marine exposure are shown below.

In general, the trends observed are similar to those seen in the laboratory tests but less extensive corrosion has taken place at this stage. For example, some corrosion of the 984 panel is visible in the scribed region suggesting passivation of the coating.

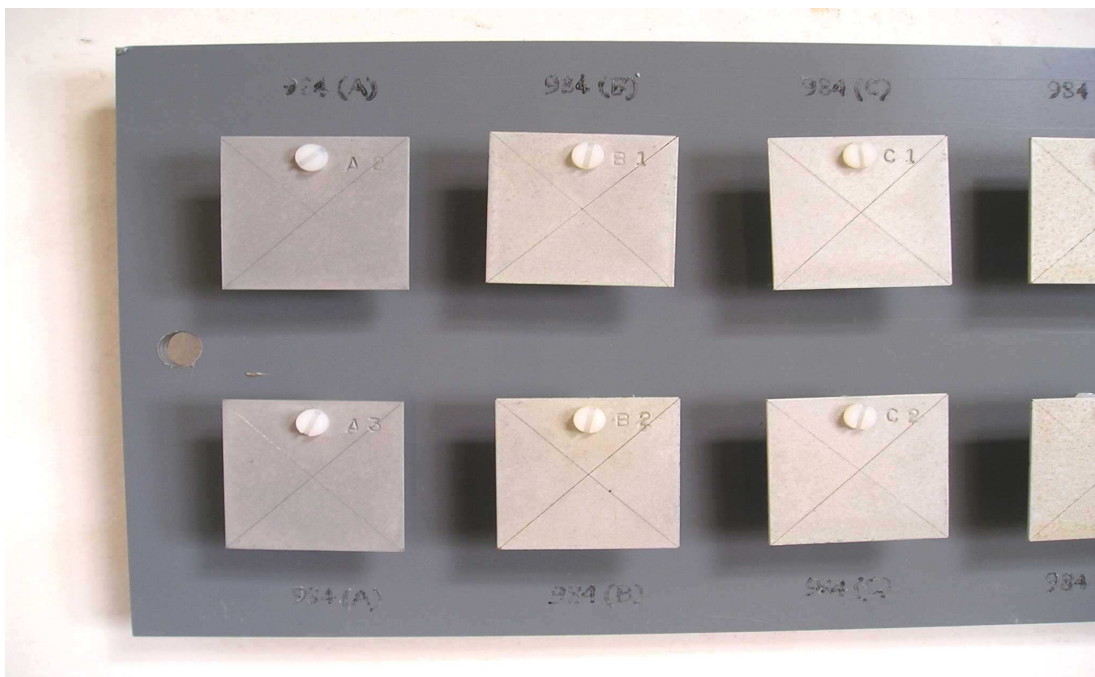


**Figure 69. Appearance of A-50%Zn, B-10%Zn and C-3%Zn modified 984 after four months in marine exposure**

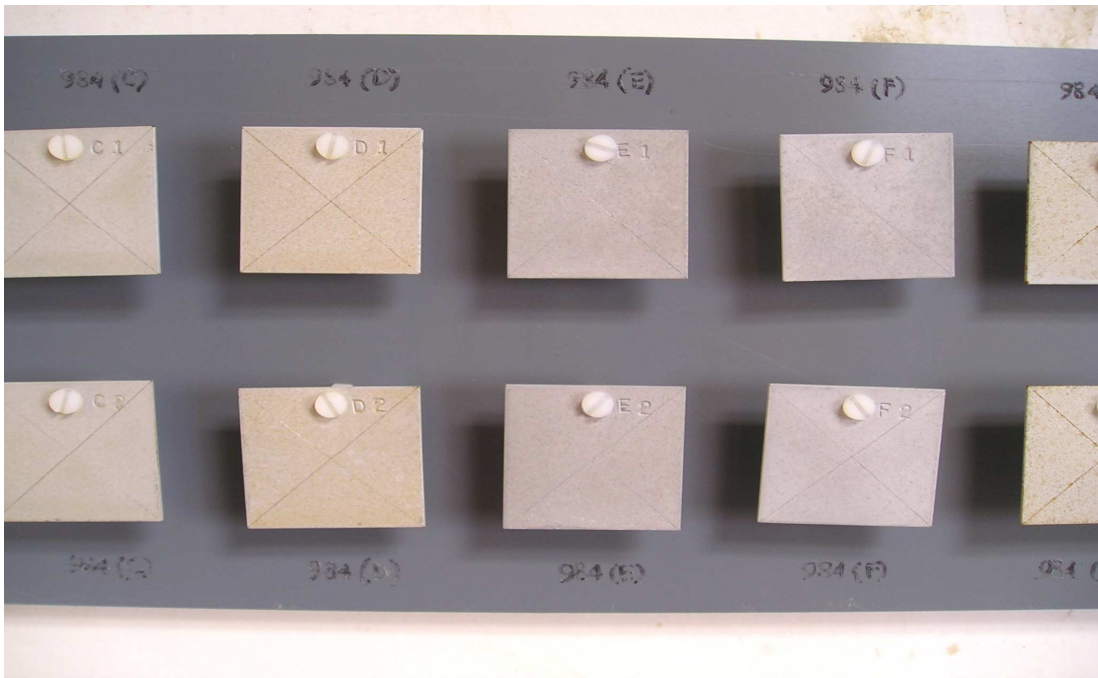


**Figure 70. Appearance of D-0.5%Zn, E-50%Mg/Al and F-30%Mg/Al modified 984 after four months in marine exposure**

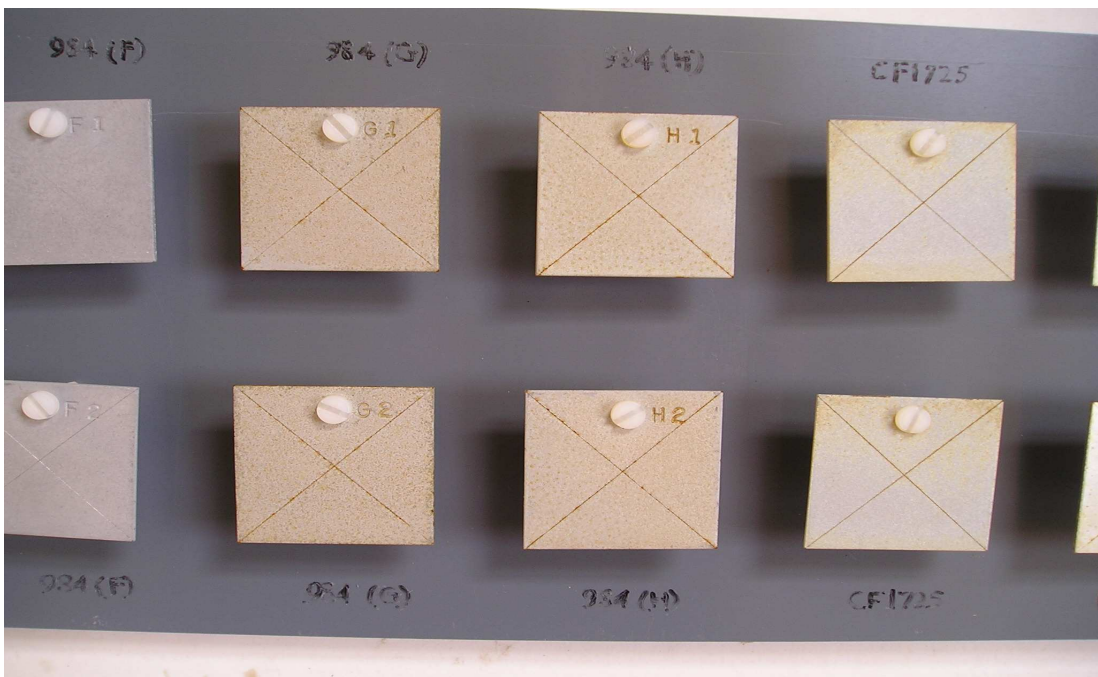


**Figure 71. Appearance of G-7075, unmodified H-984 and CF1725 after four months in marine exposure**

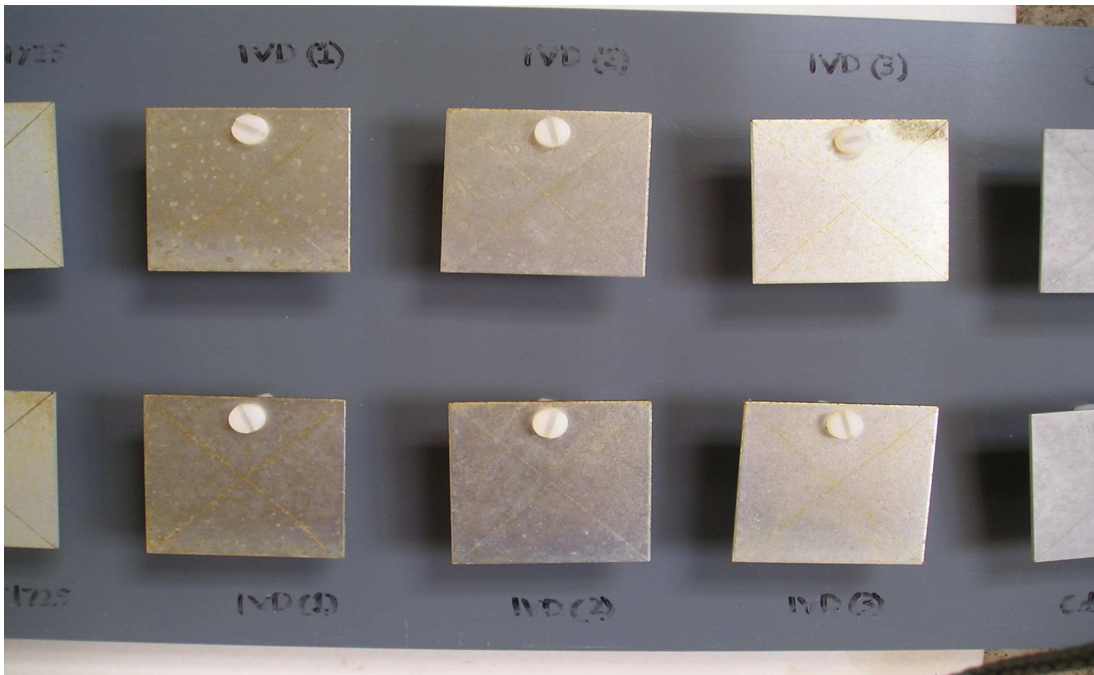


**Figure 72. Appearance of IVD1, IVD2 and IVD3 after four months in marine exposure**

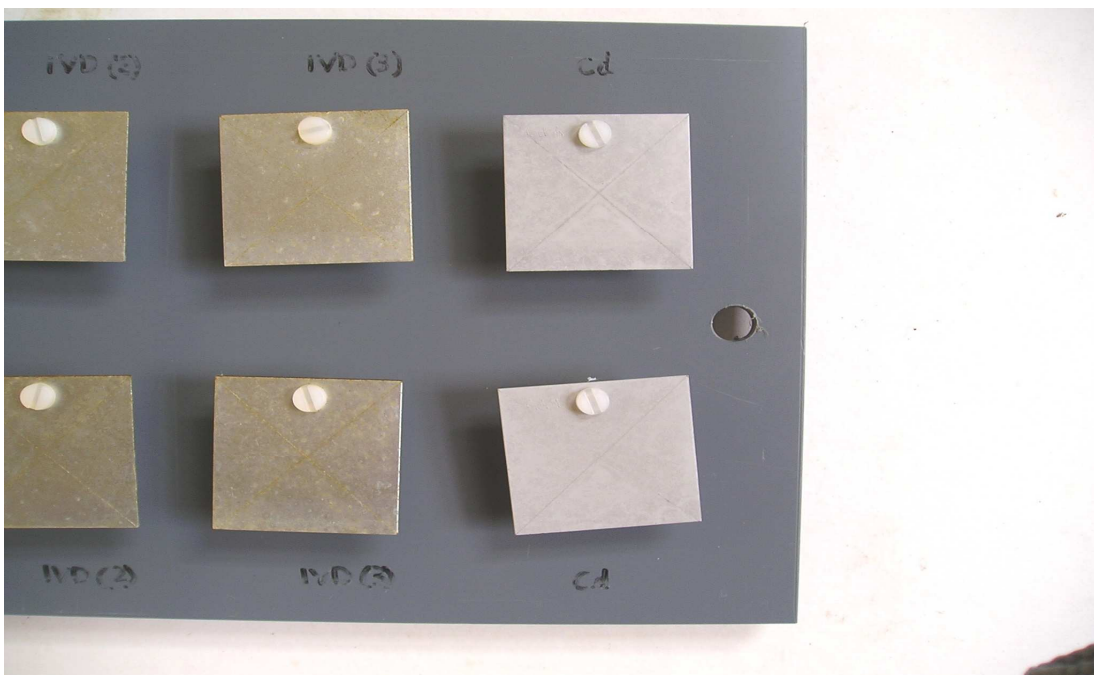


**Figure 73. Appearance of IVD3 and electroplated Cd after four months in marine exposure**



### 3.1.4 Hydrogen Re-embrittlement Tests

#### 3.1.4.1 Uncoated Control Specimens

A Weibull plot of the failure times of six uncoated control specimens tested in air is shown in Figure 74. Although the experimental conditions were the same in all of the tests the specimens failed in times ranging between 13.8 hrs and 16.6 hrs due to differences in the size and distribution of the microstructural flaws that they contained. The theoretical basis of the Weibull plot is described in the Appendix.

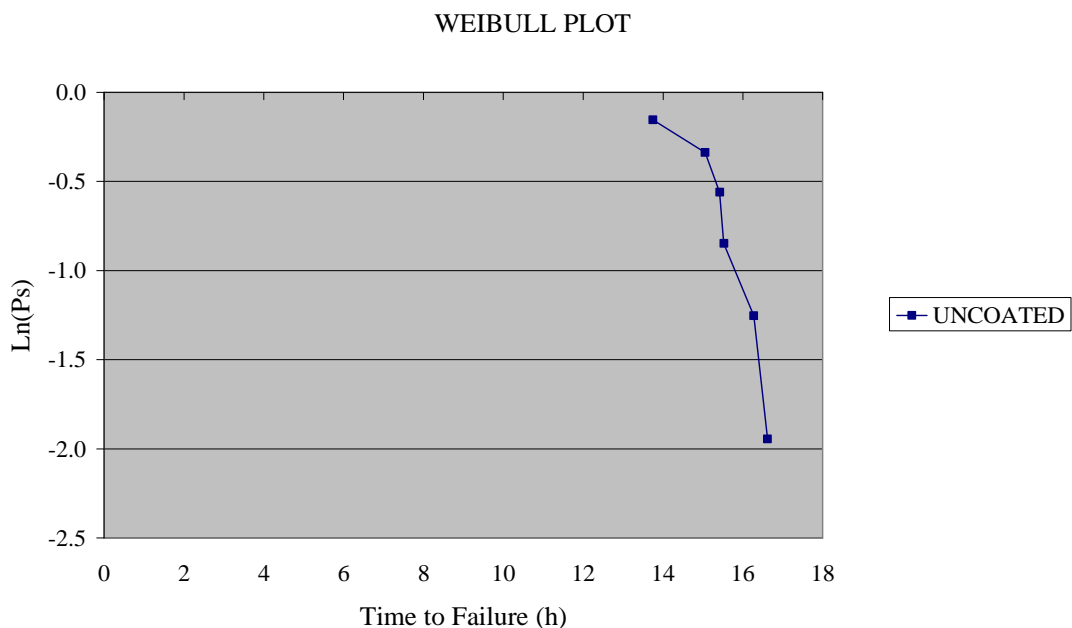


**Figure 74. Weibull plot for uncoated AISI 4340 specimens tested in air**

#### 3.1.4.2 SermeTel CR984-LT Coatings

Coated specimens tested in 3.5% NaCl solution failed in shorter times than the uncoated controls, as shown in Figure 75. The mean time to failure was reduced from 15.4 hours to 9.9 hours and fractures occurred in a brittle manner.

Although the specimens were scribed in the centre of the gauge length to remove the coating and expose the steel substrate, all of the failures occurred in the unscribed region near to the water line. It appears that sufficient hydrogen was generated on

the steel at pores in the coating for re-embrittlement to occur outside the scribed region at the site of the largest microstructural flaws within the gauge length.

Load/time graphs for the coated specimens are shown in Figure 76, together with the median uncoated specimen tested in air. The failures of the coated specimens occurred near the ultimate tensile stress, with very little necking.

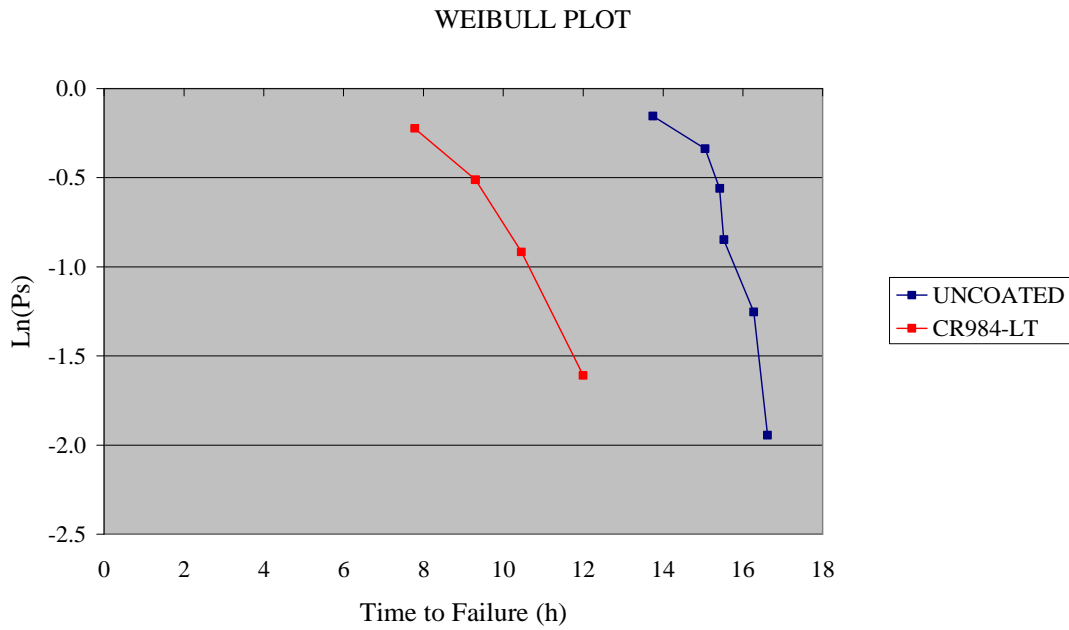


**Figure 75 .Weibull plot showing the re-embrittlement of CR984-LT coated specimens tested in 3.5% NaCl solution**

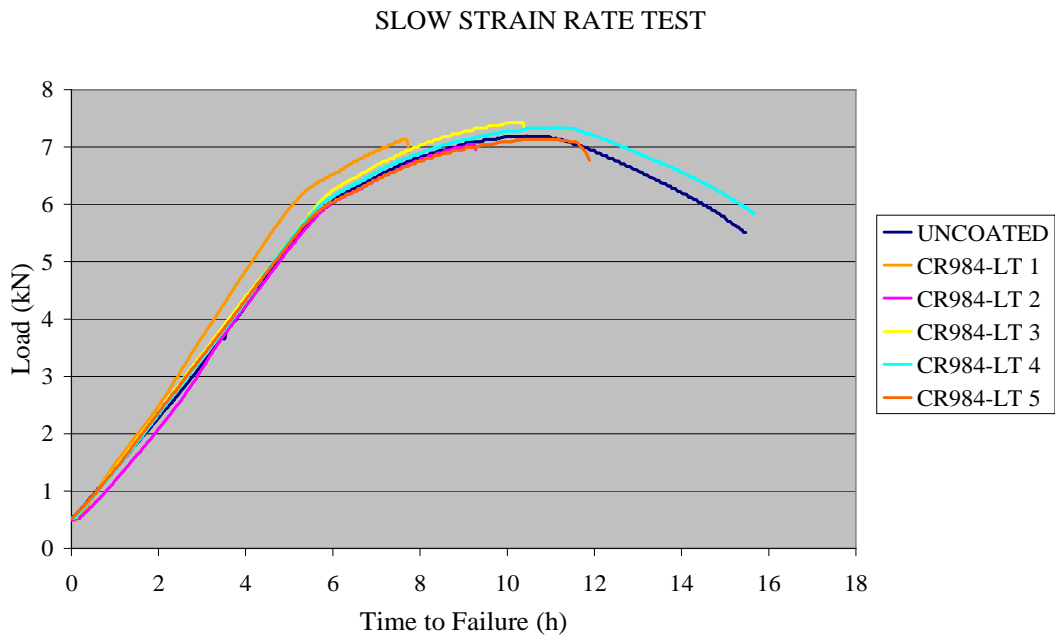


**Figure 76 . Comparison of Load/time graphs for specimens coated with CR984-LT tested in 3.5%NaCl and an uncoated control tested in air**

### 3.1.4.3 SermeTel CF1725 Chromium Free Coatings

The application process as this coating contains no chromium in the inorganic binder it needs to be applied to the steel under different conditions from the CR984-LT coating. The steel is usually preoxidised at 350°C to avoid a chemical reaction with phosphate in the binder but this temperature was considered too high as it would affect the mechanical properties of the AISI 4340 that had been tempered for 6 hours at 250°C. Trials were carried out by Sermatech Inc and it was found that preoxidation for 8 hours at 243°C was satisfactory. The CF1725 coating was subsequently applied in two layers and each of these involved curing for 8 hours at 243°C. In consequence, the specimens received heat treatment of 24 hours at 243°C in addition to the initial tempering. For this reason slow strain rate tests were carried out on further uncoated tensile specimens that had been given this heat treatment to investigate any effect on their mechanical properties. The results are shown in the Weibull plot in Figure 77.

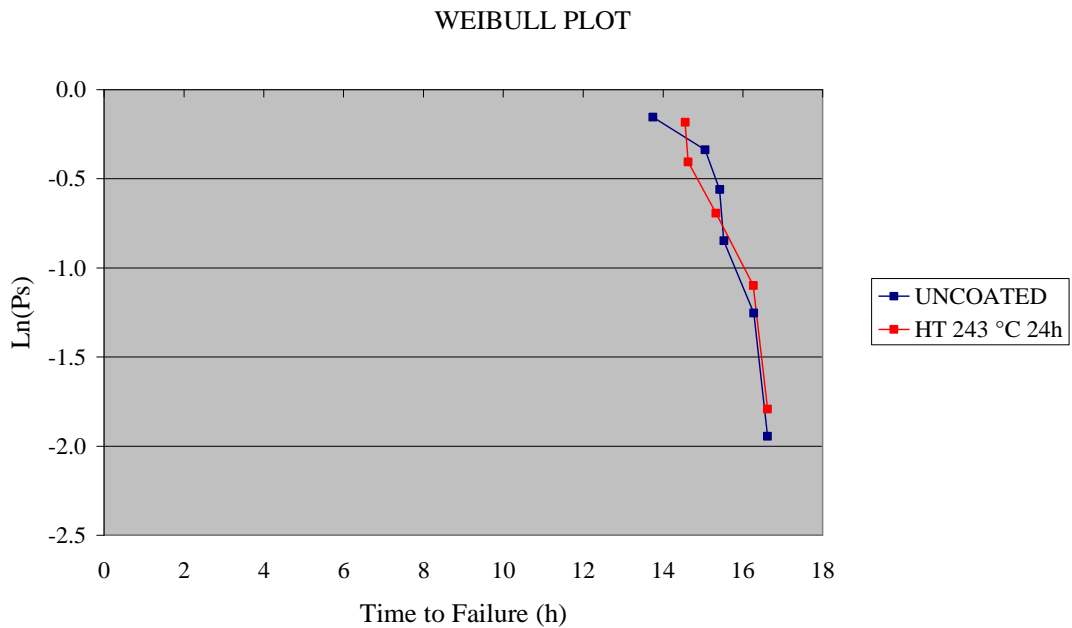


**Figure 77. Weibull plot showing the effect of additional heat treatment at 243°C for 24 hours on failure times of uncoated AISI 4340**

The mean time to failure for specimens with the additional heat treatment was 15.5 hours compared to 15.4 hours for the original condition. Student t-testing showed that, with a confidence of 95%, it was not possible to say that the two sets of data belonged to different populations.

The times to failure of specimens coated with CF1725 and tested in 3.5% NaCl solution are compared with results for the CR984-LT coating in Figure 78. The re-brittlement caused by the two coatings was similar and again it was not possible to say that they belonged to different populations. This finding is to be expected as both coatings had the same corrosion potential of -750mV(SCE).



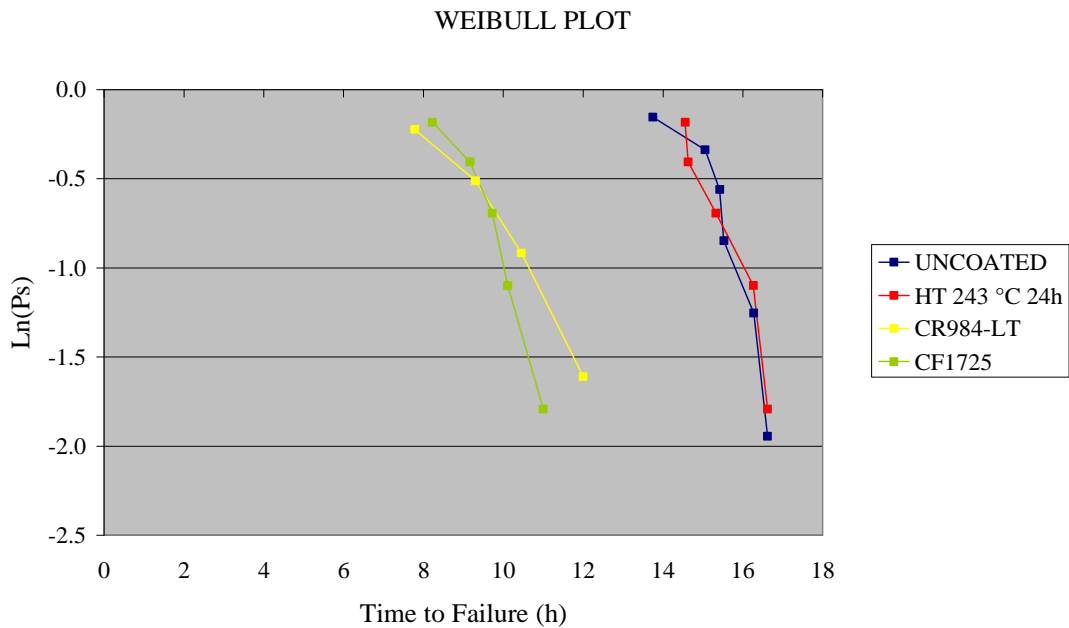


**Figure 78 .Weibull plot comparing re-embrittlement of specimens coated with CR984-LT and CF1725**

#### 3.1.4.4 Electrodeposited cadmium coatings

The re-embrittlement results for electroplated cadmium are shown in Figure 79. Of the five specimens tested, two failed in a brittle manner with reduced times and the other three displayed no re-embrittlement; their failure times were comparable with the uncoated controls. This behaviour was unexpected and the probable cause has been investigated.

A distribution of flaw sizes within the gauge length is to be expected and these different flaw sizes would affect the severity of re-embrittlement and times to failure. However, it would not be expected that any of the specimens would contain so few microstructural flaws that when charged with hydrogen during corrosion of the coating they would fail in a ductile manner before embrittlement occurred. Previous work on cadmium plated specimens has shown consistent times to failure and a high level of re-embrittlement.

Inconsistency in the composition and quality of the cadmium deposit is being considered as this could affect the generation, transport and uptake of hydrogen by the steel. However, the corrosion potential of the coating was monitored during the

SSR tests and shown to be approximately -790mV(SCE) in each case; close to the expected value for cadmium.

One of the specimens that did not display re-embrittlement was examined by metallography. It was shown that a thin layer of nickel had been deposited on the steel before it was electroplated with cadmium. (This treatment is sometimes used to improve the adhesion of the coating.) The nickel layer was 2-3 microns thick in most places but there were some areas where the thickness was about 10 microns.

The reason for the lack of re-embrittlement in three of the SSRT specimens is now clear. Nickel has a very low hydrogen diffusion coefficient ( $8 \times 10^{-10} \text{ cm}^2\text{s}^{-1}$  compared to approximately  $2 \times 10^{-7} \text{ cm}^2\text{s}^{-1}$  for AISI 4340). The nickel layer acted as an effective barrier to hydrogen generated by corrosion of the cadmium. All of the specimens received the same treatment and it is assumed that the two specimens that failed by re-embrittlement had an incomplete nickel layer on the surface so that hydrogen uptake by the steel occurred.

These results could have important practical implications. A thin nickel layer beneath the sacrificial coating would seem to be the answer to both direct embrittlement and re-embrittlement problems.

The Weibull plots for the SermeTel and cadmium coatings are compared in Figure 79.



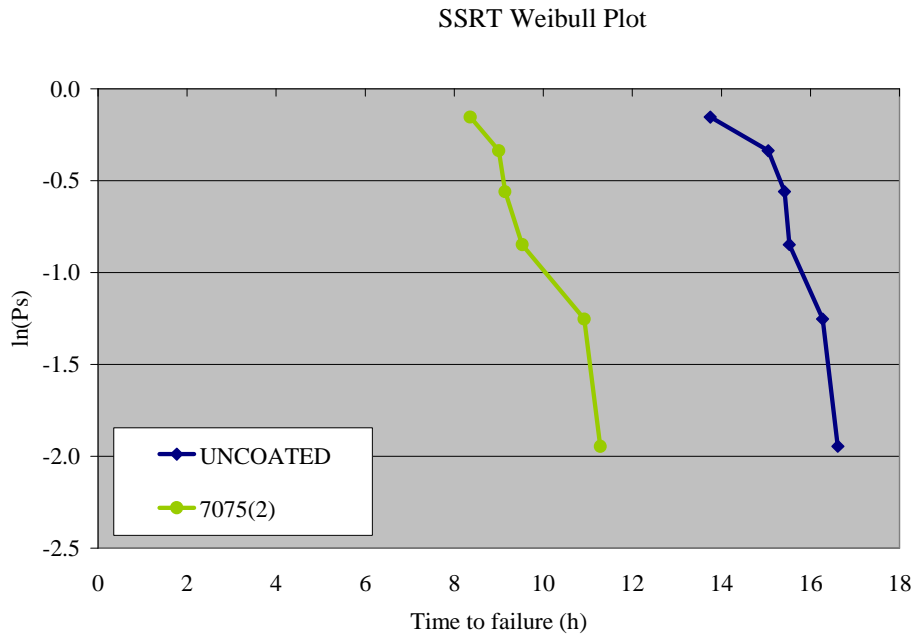


**Figure 80. Weibull plot for times to failure of 7075(2) coated specimens vs. uncoated specimens**

### 3.1.4.6 Zn modified 984 coatings

In each case, six specimens were tested for every Zn modified 984 coating. Specimens coated with 10%Zn-984 failed with a mean time of 10.5 hours while the means of time to failure for 3%Zn-984 and 0.5%Zn984 were 11.7 hours and 11.1 hours. Although 3%Zn-984 showed a longer time to failure than 0.5%Zn its standard deviation was 2.3 hours and higher than the 1.0 hour of 0.5%Zn-984. The standard deviations for 50%Zn-984 and 10%Zn-984 were of 2.2 hours and 2.3 hours. The 0.5%Zn-984 showed the smallest standard deviation between the three Zn modified 984 coatings and it was the same value as that calculated for uncoated specimens.

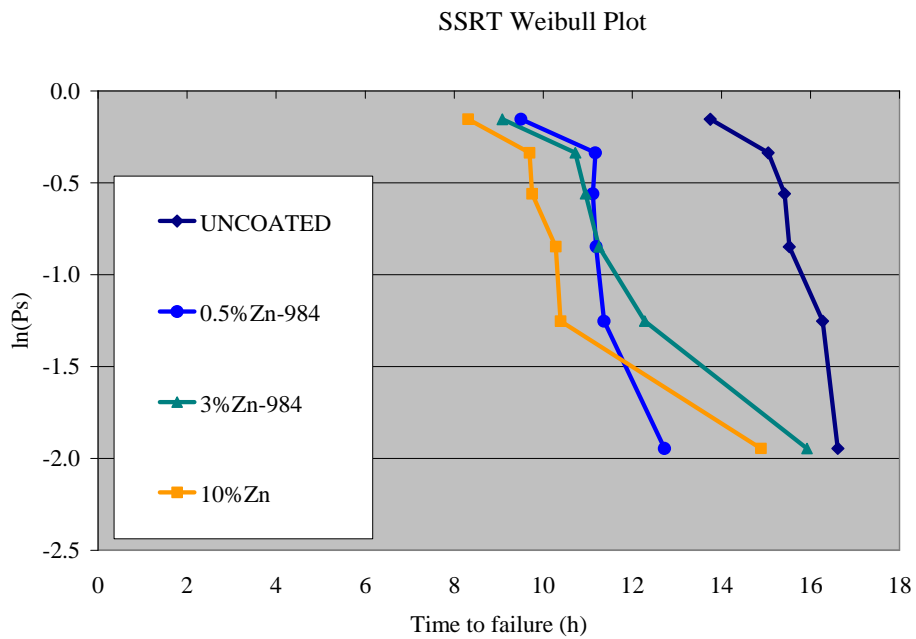


**Figure 81. Weibull plot for times to failure of Zn modified 984 coated specimens vs. uncoated specimens**

### 3.1.4.7 Mg/Al modified 984 coatings

30%Mg/Al 984 and 50%Mg/Al 984 coatings caused very high re-embrittlement on the steel specimen. The first coating time to failure ranged from 6.58 hours to 9.93 with an average value of 8.61. The 50%Mg/Al 984 showed very similar results with time to failure ranging between 5.56 hours and 9.73 and an average value of 8.56.

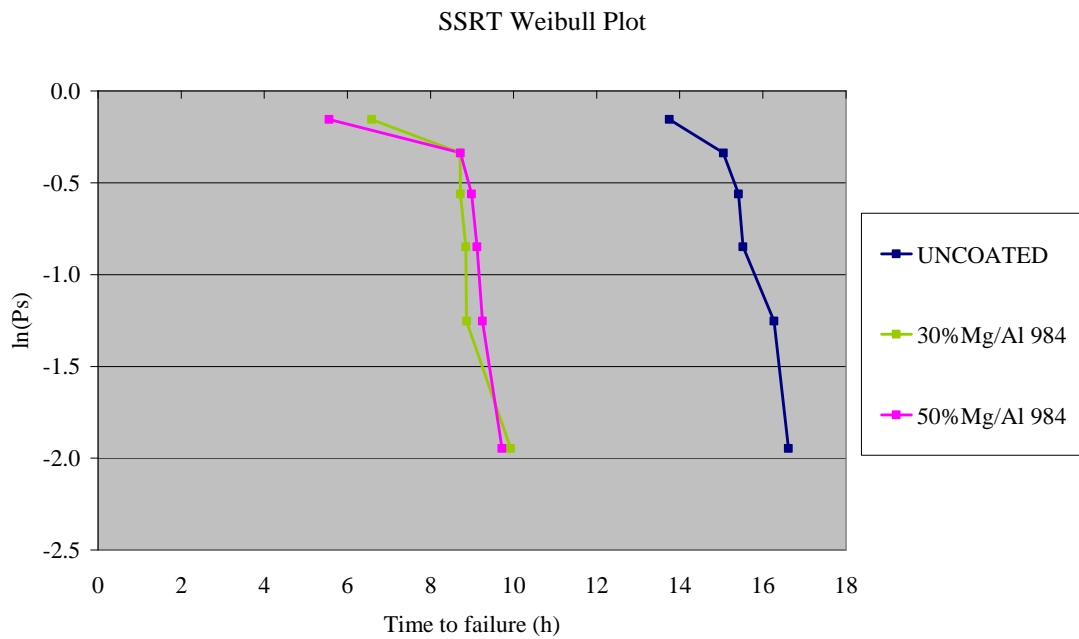


**Figure 82. Weibull plot for times to failure of magnesium modified 984 coatings vs. uncoated specimens**

### 3.1.4.8 IVD aluminium coatings

IVD aluminium coatings showed the longest time to failure between the coatings. Some IVD1 specimens showed time to failure greater than the uncoated specimens. All the specimens showed red rust after the test and fragments of the coating were noticed in the solution. The almost absence of re-embrittlement together with the signs of corrosion on the steel indicate that the coating detached from the steel because of the mechanical deformation stopping giving sacrificial protection to the substrate. SEM analysis was carried out on the surface of the specimens to investigate the condition of the IVD coating after the test.

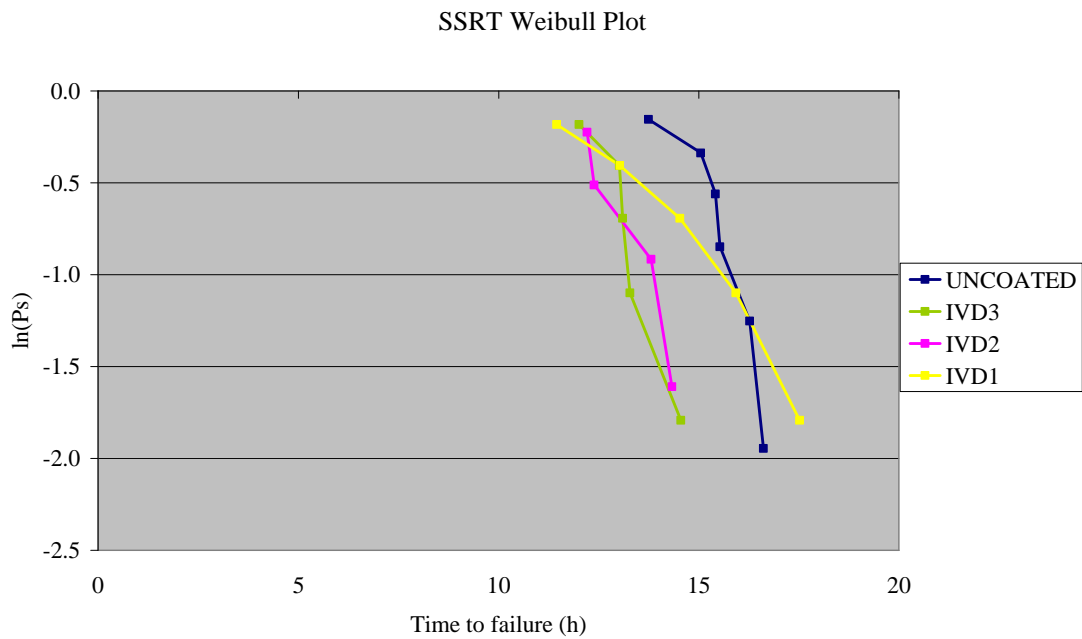
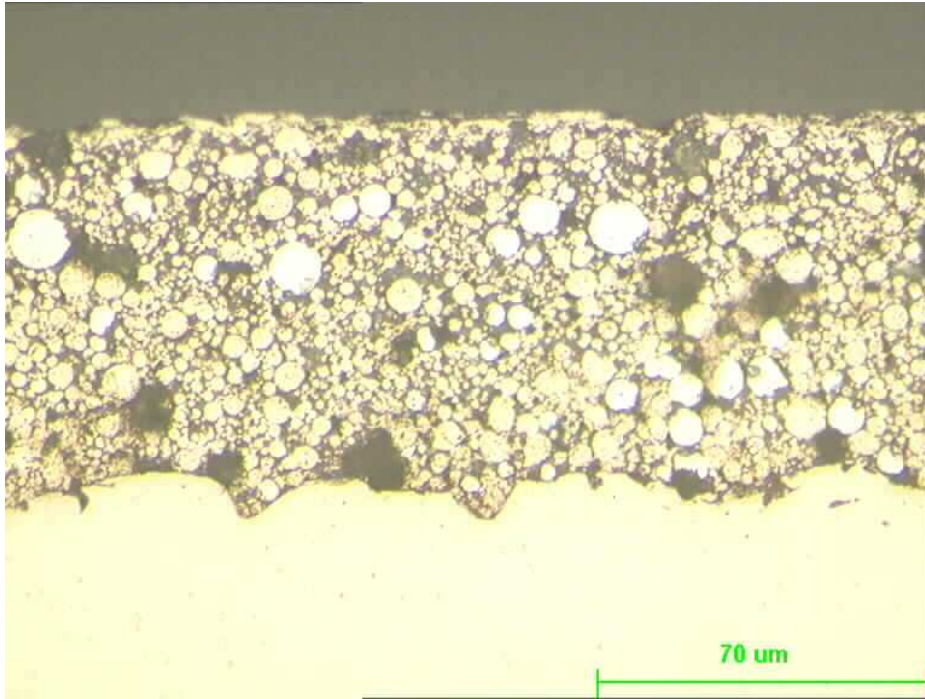


**Figure 83. Weibull plot for times to failure of magnesium IVD aluminium coatings vs. uncoated specimens**

### 3.1.5 Selective attack and coating characterization

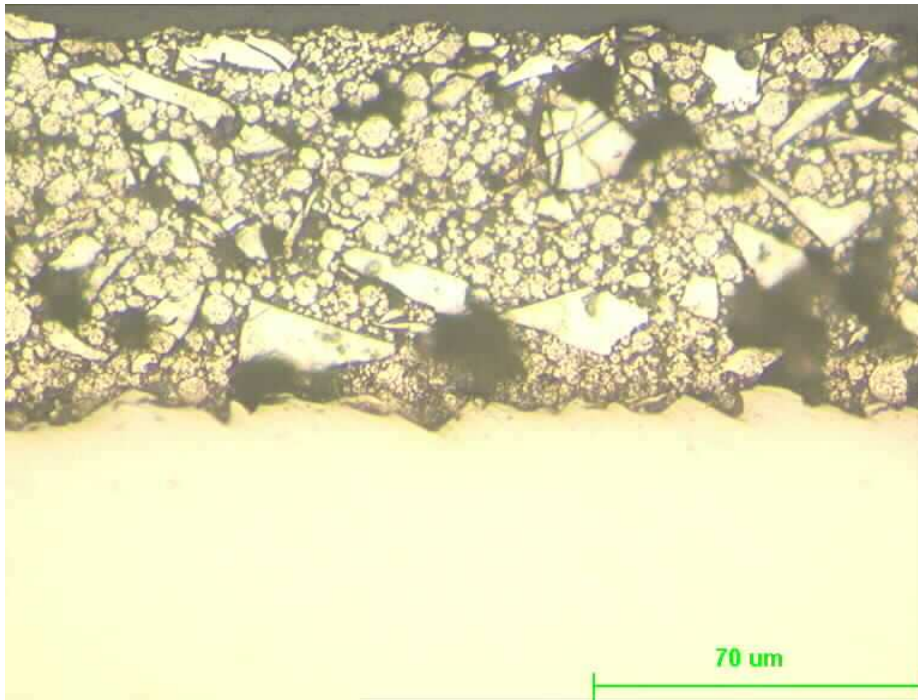
#### 3.1.5.1 Optical-thickness measurement

The cross sections of the specimens were observed with an optical microscope at 40x to measure their thickness. Figure 84 shows the cross section on 984A 50%Zn. In the observed area the thickness is in the range of 75-80  $\mu\text{m}$ . The bigger particles visible were afterwards found to be zinc particles.



**Figure 84. Optical image of 984A (50%Zn) cross section. Magnification 40x.**

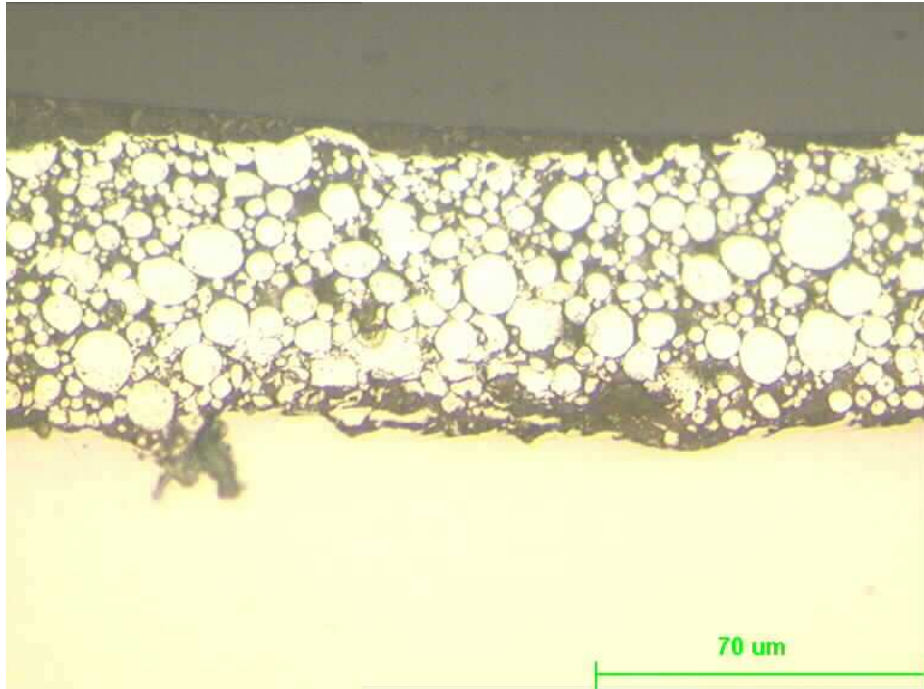
Figure 85 shows the cross section of 984E (50%Mg). Its thickness has been measured between 78-82  $\mu\text{m}$ . The not spherical particles were found to be Mg/Al particles by a following EDX analysis.



**Figure 85. Optical image of 984E (50%Mg/Al) cross section. Magnification 40x.**

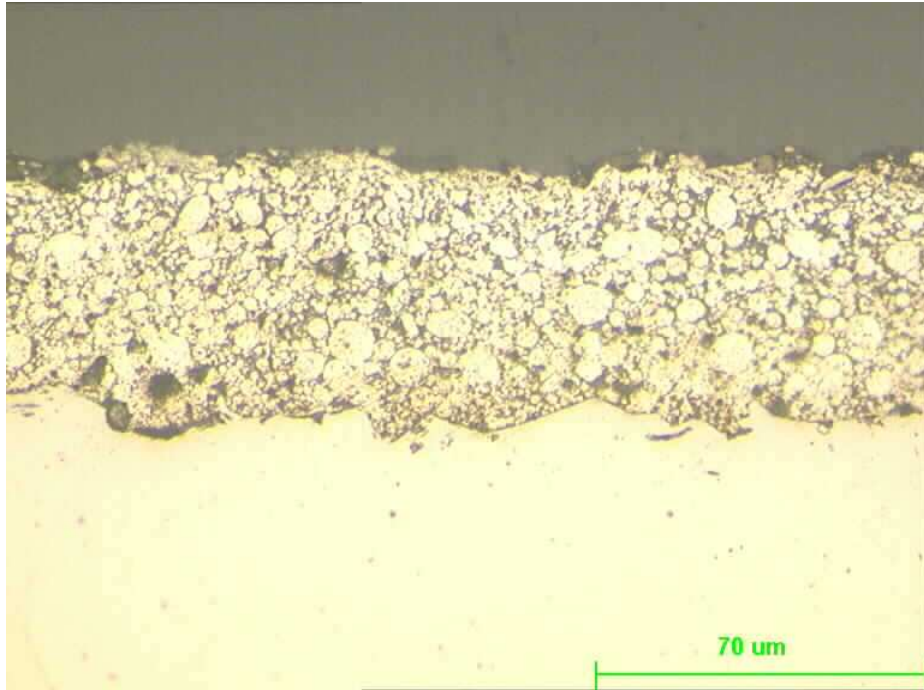


Figure 86 shows the cross section of aluminium coating 7075. Its thickness has been measured in the range of 55-60  $\mu\text{m}$ . This coating has been deposited using only one type of powder, the aluminum alloy 7075.



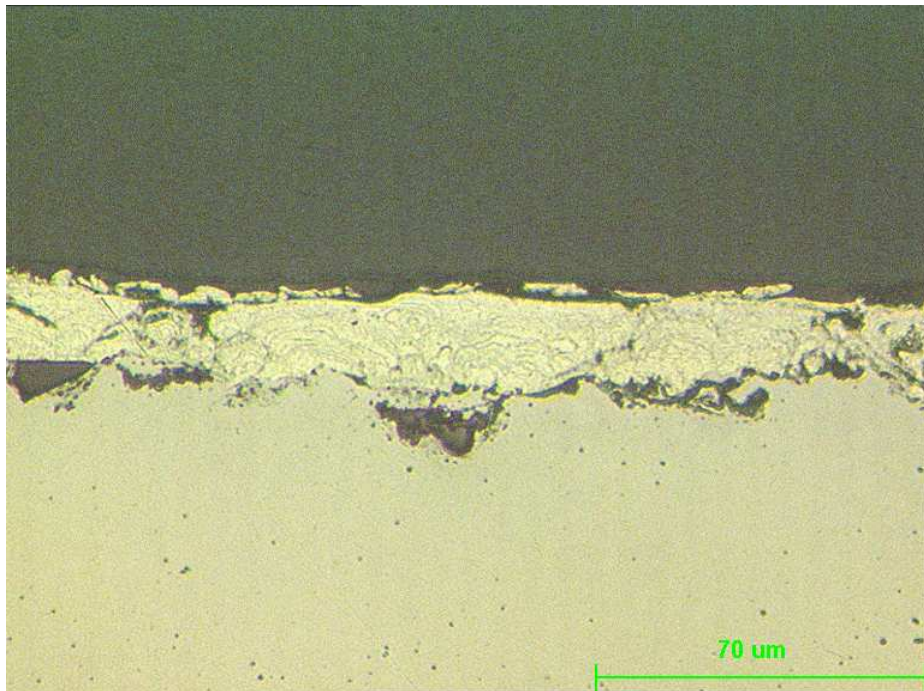
**Figure 86. Optical image of 7075 aluminium alloy coating cross section. Magnification 40x.**

Figure 87 show the 984H, the aluminium based commercial alloy from Sermatech. Thickness has been measured in a range of 55-60  $\mu\text{m}$ .



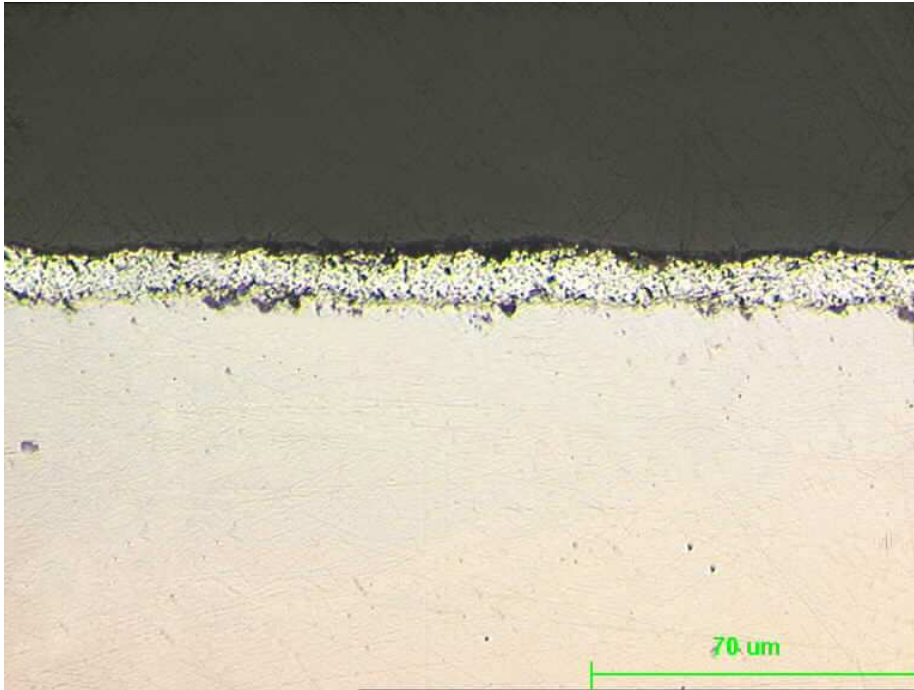
**Figure 87. Optical image of 984H free cross section. Magnification 40x.**

Figure 88 shows the cross section of IVD2 aluminium coating. This coating is clearly thinner than the 984 series coatings and its thickness was measured in a range of 12-27 $\mu\text{m}$ .



**Figure 88. Optical image of IVD2 cross section. Magnification 40x.**

Figure 89 shows the cross section of the electroplated cadmium coating. This coating thickness was measured between 10 and 13  $\mu\text{m}$ .



**Figure 89. Optical image of electroplated Cd cross section. Magnification 40x.**

Table 8 summarizes the thickness measurements of the coatings. The IVD coating are much thinner than the 984 spray coatings, as expected from the different deposition technique.

Coating	984A	984B	984C	984D	984E	984F	7075
Thickness ( $\mu\text{m}$ )	75-80	60-65	73-78	55-60	78-83	50-55	55-60
Coating	984H	1725	IVD1	IVD2	IVD3	Cd	
Thickness ( $\mu\text{m}$ )	55-60	62-67	12-25	12-27	5-30	10-13	

**Table 8. Coatings thickness. Values measured from coatings cross sections.**

### 3.1.5.2 SEM analysis and Focused Ion Beam on 984A

Figure 90 shows a secondary electrons image of the 984A surface for the “as made” coating and the EDX analysis of the area marked is showed in Table 9.

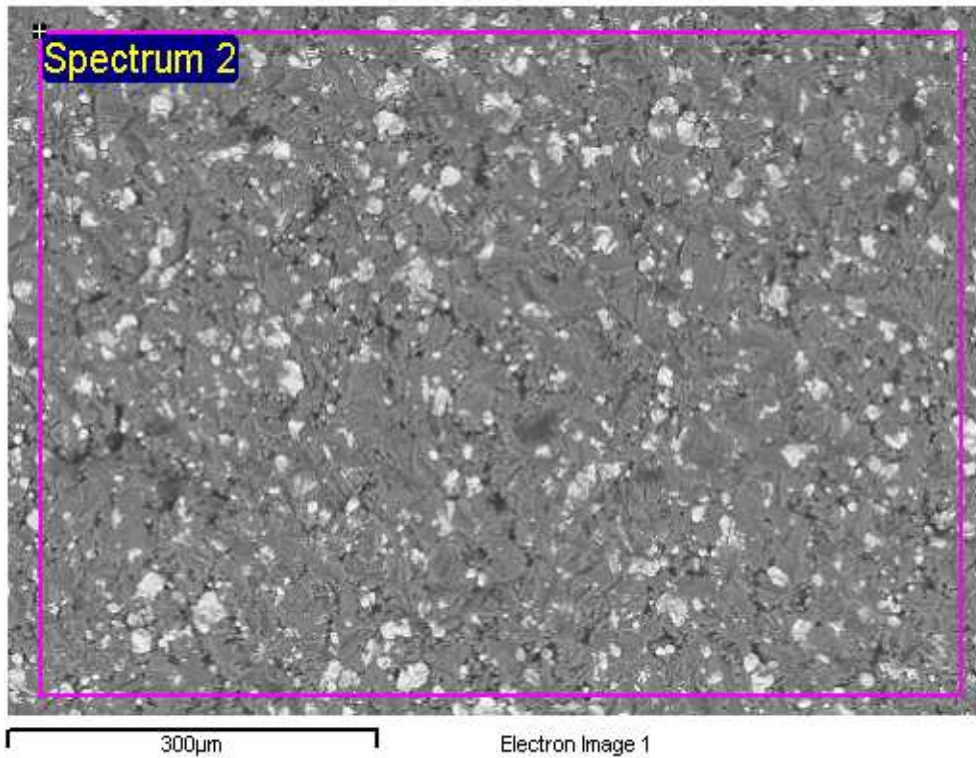


**Figure 90. SEM Secondary Electrons top view of “as made” 984 A surface”. Bias voltage 15kV.**

Element	Weight%	Atomic%
C	8.10	16.17
O	20.50	30.75
Al	47.78	42.48
P	4.46	3.46
Cr	1.71	0.79
Fe	0.35	0.15
Zn	16.59	6.09
Ag	0.51	0.11
Totals	100.00	100.00

**Table 9. EDX analysis of the area marked in Figure 90.**

Although the nominal concentration of zinc was 50% in weight the EDX shows a concentration of 16.58% for zinc and 47.78% for aluminium that means a ratio aluminium/zinc much smaller than what expected. This error in the concentration might be due to different factor:

- manufacturing process error
- zinc preferential oxidation on the surface
- segregation of the heavier zinc particles to the bottom before the curing.

Figure 91 shows the cross section of as made 984A and Table 10 the EDX analysis of the area. The amount of zinc detected was in this case higher than what detected from the top view analysis. This confirms zinc particles segregation.

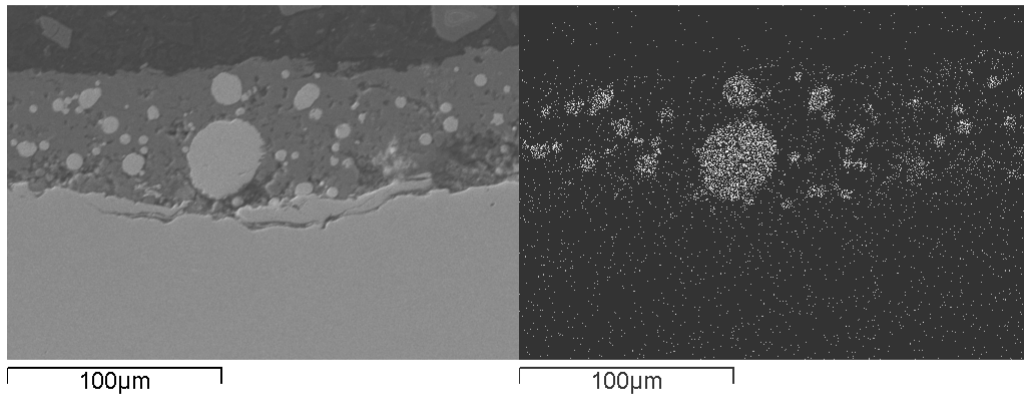


**Figure 91. Secondary Electrons image of “as made” 984A cross section on the left and zinc mapping on the right. Bias voltage 15kV.**

	Aluminium	Zinc
Sum Spectrum (% in weight)	62	38

**Table 10. EDX analysis of area selected in Figure 91.**

Figure 92 shows a FIB pit etched on the 984 A “as made”. EDX point analysis proved the big bright particle to be a zinc particle. Porosities are also clearly visible inside the coating while the etching seems have not reached the steel substrate. The coating substrate appears rough as expected from a spray coating.



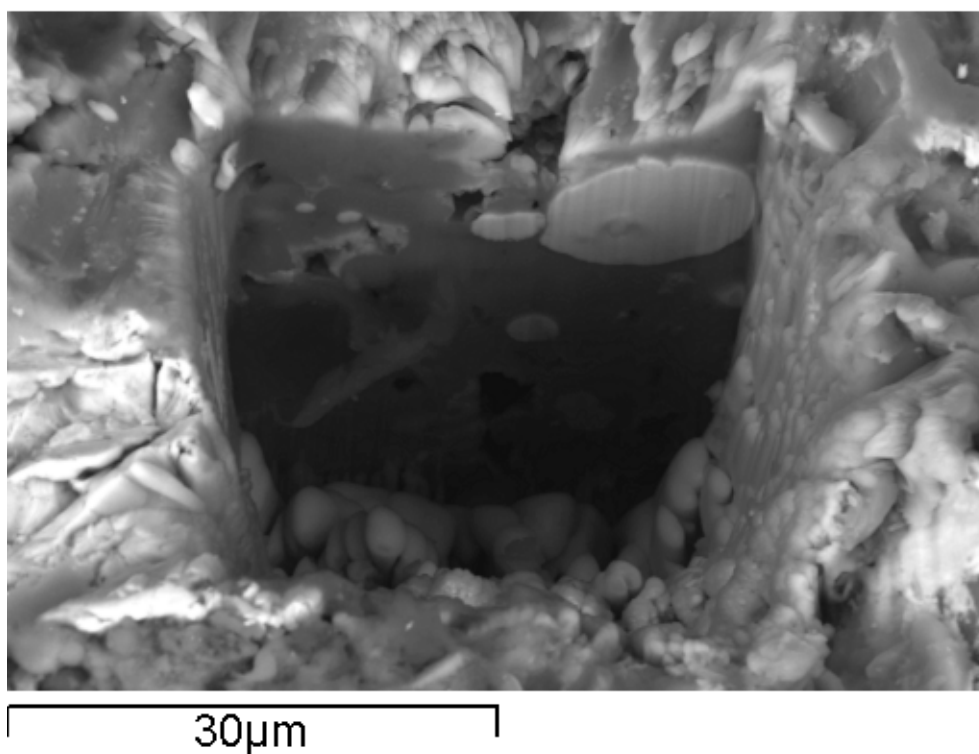


**Figure 92. FIB section of 984 A “as made”. Bias voltage 15kV.**

The same kind of analysis was repeated on a 984A panel after 10 days of exposure in 3.5% NaCl. Figure 93 shows the FIB pit for this second specimen. The coating surface visible in the upper part of the picture seems to be smoother than that in the “as made” coating. The brighter colour of the top of the coating from the BSE image also suggests a different composition of the area.

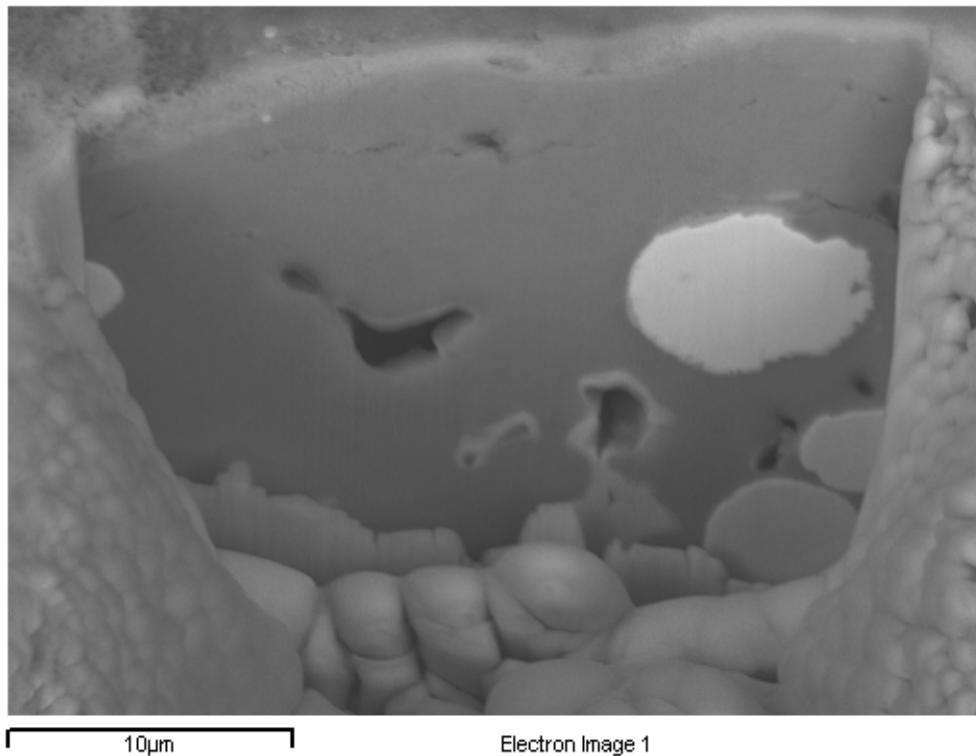


**Figure 93. Back Scattered Electrons image of FIB section for 984 A after 10 days in 3.5% NaCl. Bias voltage 15kV.**

The EDX analysis of the points marked in Figure 94 is shown in Table 11. It shows a ratio zinc/aluminium higher than the unit. The comparison of this result with the analysis before the exposure suggests the formation of a layer richer in zinc with some amount of Chlorine in it. The EDX analysis confirms the presence of Chlorine and an high amount of zinc on the surface. The higher amount of zinc compared to aluminium could be due to a preferential dissolution of aluminium compounds in the electrolytic solution during the corrosion test.

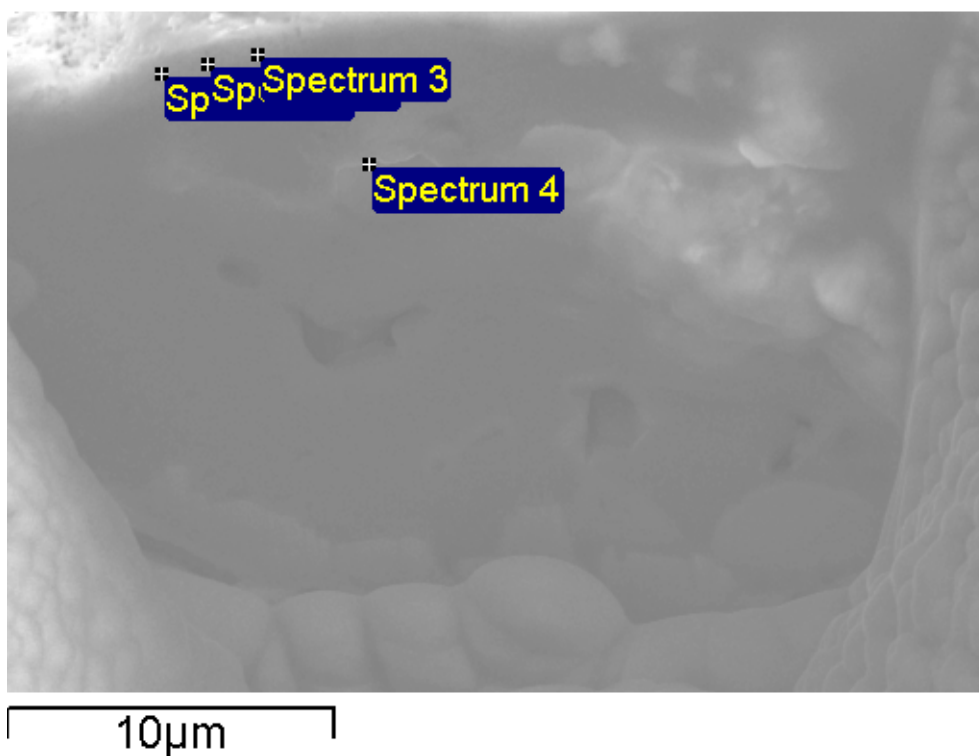


**Figure 94. Secondary Electrons image of FIB section for 984 A after 10 days in 3.5% NaCl**



	C	O	Na	Al	P	Cl	Cr	Zn	Ga	Re	Tot
Spectrum 1	-	30.97	-	20.31	1.73	6.53	-	40.46	-	-	100
Spectrum 2	4.36	32.35	-	19.11	2.22	6.13	-	35.83	-	-	100
Spectrum 3	-	32.35	-	17.77	6.14	5.65	3.15	31.37		0.32	100
Spectrum 4	-	25.68	1.85	48.89	6.84	-	5.85		10.90	-	100

**Table 11. EDX analysis of points marked in Figure 94. Percentages in weight**

The same top area of the coating is shown in Figure 95 at a bigger magnification. This last picture was taken using a low voltage of 5kV to avoid an excessive sample charging, but because the low Bias, it was impossible to carry out an EDX analysis in order to detect the zinc.

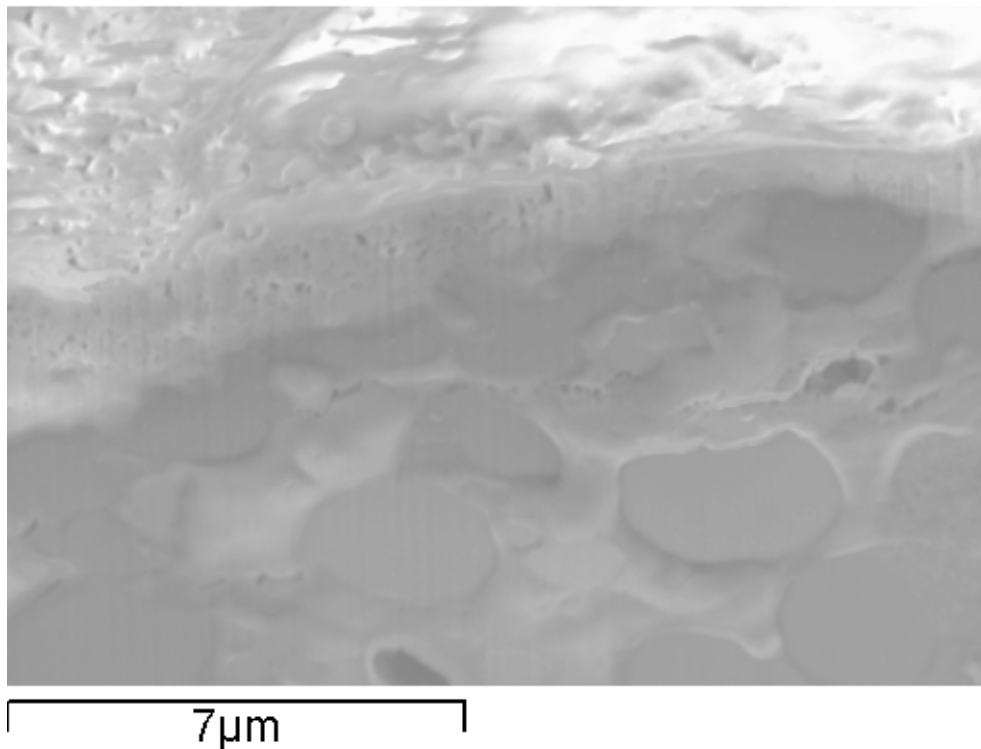


**Figure 95. SEM Secondary Electrons image of FIB for 984 A 10 days in 3.5% NaCl solution. Particular of the coating surface. Bias voltage 5kV.**

The FIB technique was also used, as described in the methodology section, to look at the interface between the coating and the steel substrate as shown in Figure 96. The zinc mapping by EDX is shown on the right side of the same picture and seems to confirm zinc particles segregation at the bottom of the coating.

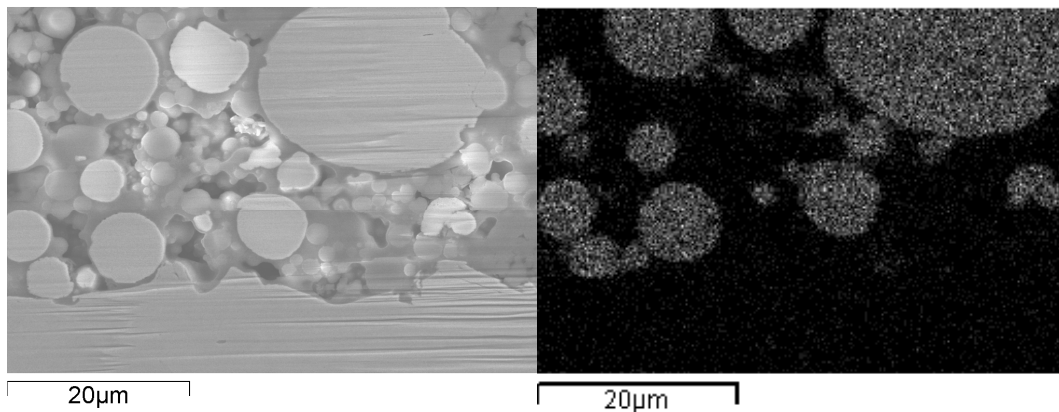


**Figure 96. Etched area by FIB for 984A (50%Zn) after 10 days in 3.5% NaCl solution. View of the coating interface with the steel substrate on the left. Zinc mapping on the right.**

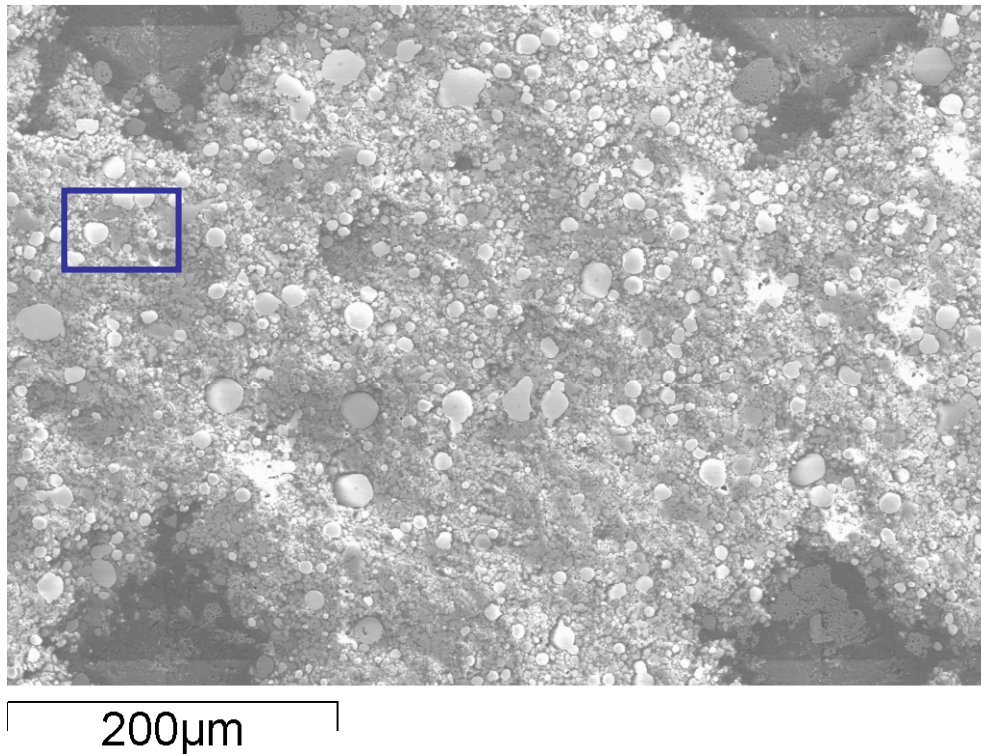
	Al	Zn	Total
Sum Spectrum	36.55	63.45	100

**Table 12. EDX analysis of area selected in Figure 96. All the other elements except Zn and Al have been omitted. Percentages in weight.**

Table 12 shows the composition of the area in Figure 96 where all the elements except zinc and aluminium have been removed from the analysis. The concentration ratio Zn/Al, higher than one, suggests a particles segregation probably due to the difference in density between the two metals.

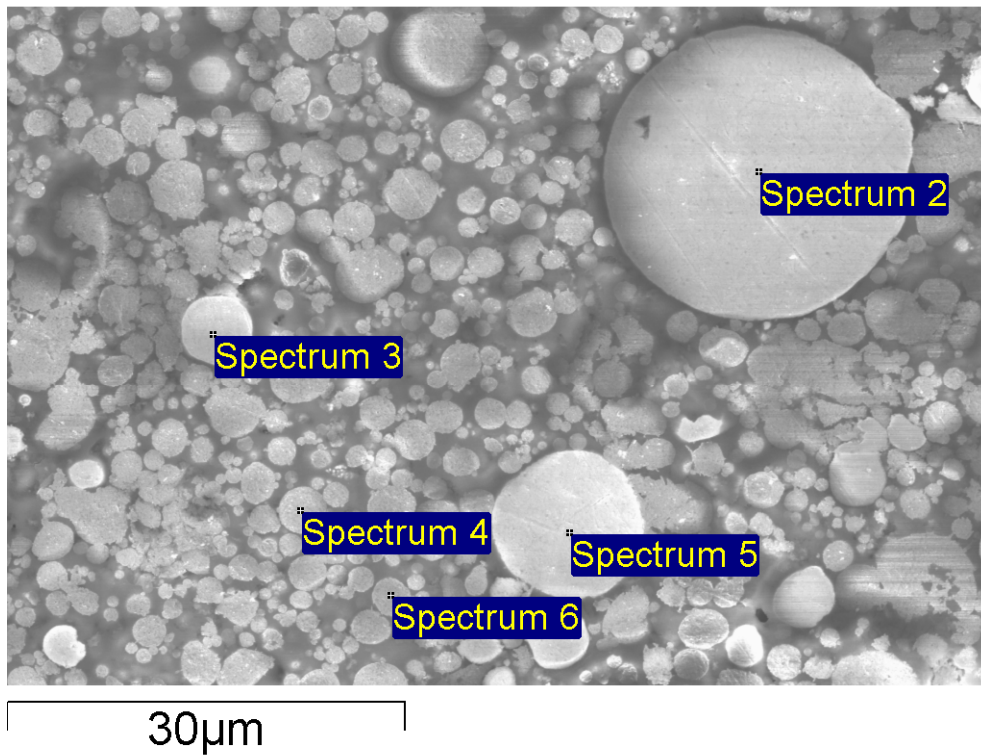
### **3.1.5.3 SEM-EDX analysis**

Figure 97 shows the four indentations used to identify a certain area, and inside that area, a smaller zone, marked in blue was identified to repeat the analysis after the exposure to 3.5% NaCl solution.



**Figure 97. Area marked by four Vickers indentations. Bias voltage 15kV.**

Figure 98 shows the 984A selected area after polishing. EDX point analysis has shown that Spectrum 2, Spectrum 3 and Spectrum 5 are zinc particles while Spectrum 4 and Spectrum 6 are both aluminum particles. Table 13 shows the analysis of zinc and aluminum particles. The amount of oxygen on the aluminum particle is higher than on the zinc particle. No Chlorine was found on any of the particles analyzed.



**Figure 98. ES SEM image of 984A after polishing. Bias voltage 15kV.**

Spectrum2 (Zinc particle)		Spectrum4 (Aluminium particle)	
Element	Weight%	Element	Weight%
C K	7.32	C K	--
O K	3.99	O K	19.46
Al K	--	Al K	76.89
P K	--	P K	2.50
Cr K	--	Cr K	0.46
Fe K	--	Fe K	--
Zn K	88.69	Zn K	0.45
Ag L	--	Ag L	0.24
Totals	100.00	Totals	100.00

**Table 13. Point analysis of Spectrum2 and Spectrum3 as marked in Figure 98.**

Figure 99 shows the secondary electrons image of the same area after 4 days of exposure in 3.5% NaCl in quiescent condition. EDX point analysis was repeated on some of the identified particles. The EDX of the same zinc and aluminium particles tested after the exposure is reported in Table 14. A bigger amount of oxygen was found on the zinc particle surface but it is not clear whether the oxygen is bonded to the zinc or maybe to the Iron, also present in the area selected. From the table it is also clear that chlorine is present on the zinc particle but not on the aluminium.

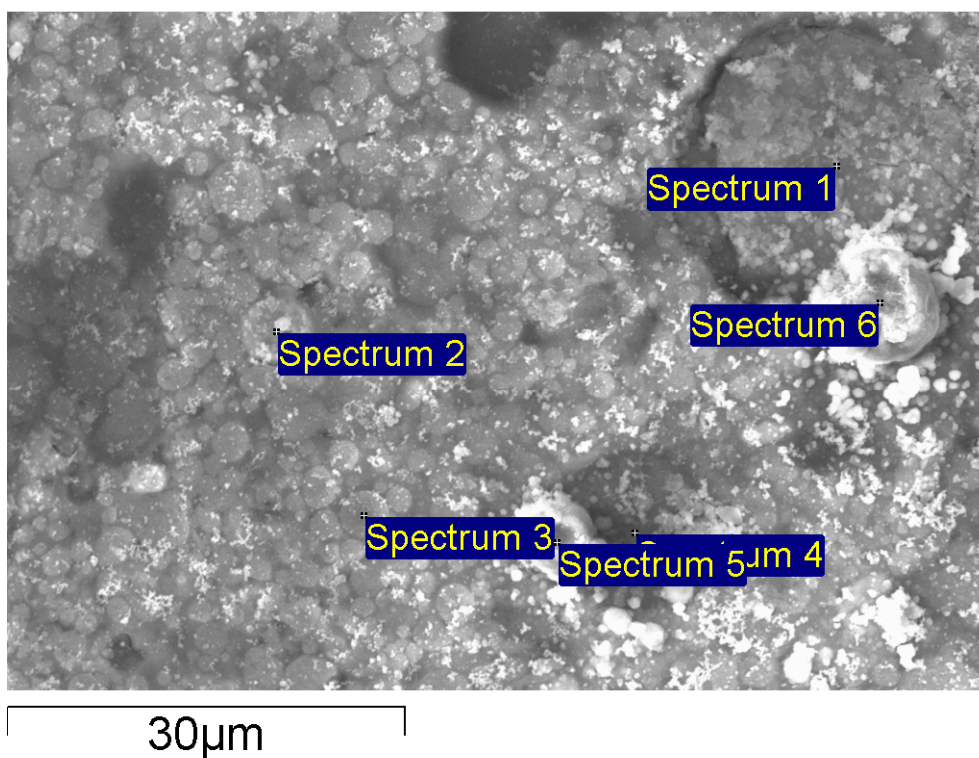


**Figure 99. ES SEM image of 984A after 4 days in 3.5% NaCl. Bias voltage 15kV.**

Spectrum1 (Zinc particle)		Spectrum3 (Aluminium particle)	
Element	Weight%	Element	Weight%
C K	-	C K	3.90
O K	30.49	O K	7.81
Al K	4.15	Al K	83.26
Si K	2.47	Si K	-
P K	0.00	P K	1.09
Cr K	0.00	Cr K	0.34
Cl K	4.95	Cl K	-
Fe K	20.94	Fe K	1.74
Zn L	37.00	Zn L	0.77
Ag L	-	Ag L	1.09
Totals	100.00	Totals	100.00

**Table 14. Point analysis of Spectrum2 and Spectrum3 as marked in Figure 99.**

Zinc, Iron and Chlorine mapping, after the exposure, is shown in Figure 100 and in Figure 101. Chlorine and iron seem to be present on the zinc particle but iron seems to be present mostly in correspondence with the white corrosion compounds while chlorine seems to be more uniformly spread on the zinc particle.

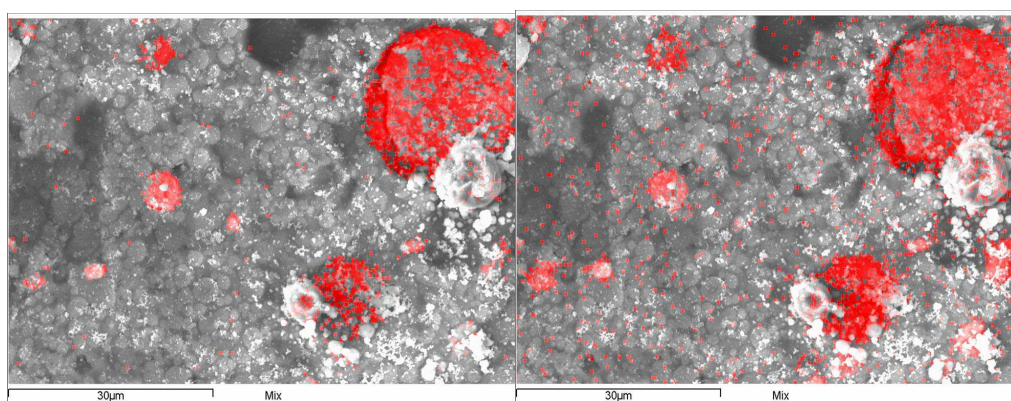


**Figure 100. From left to right zinc and chlorine mapping by EDX of 984 A (50%Zn) surface after 4 days in 3.5% NaCl solution. Bias voltage 15kV.**



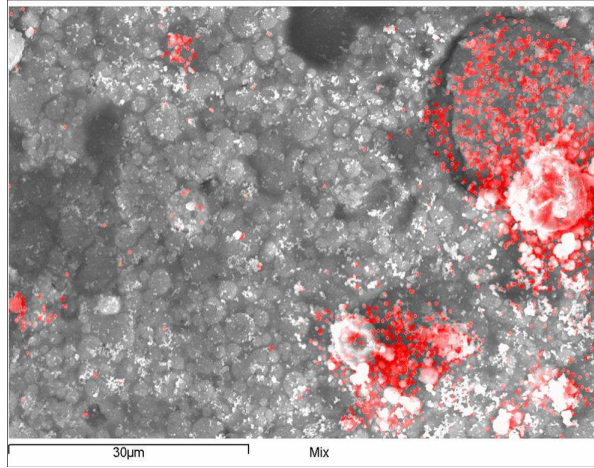


**Figure 101. Iron mapping by EDX of 984 A (50%Zn) surface after 4 days in 3.5% NaCl solution. Bias voltage 15kV.**

#### **3.1.5.4 X-ray diffraction**

The presence of a chlorine corrosion compound has been proved by the XRD analysis. Figure 102 shows the X-Ray diffraction pattern of the 984A after 10 days in 3.5% NaCl in aerated conditions. Apart from the presence of metallic zinc and aluminum, aluminum hydroxide, simonkolleite and zinc aluminum carbonate hydroxide hydrate were identified from the diffraction. The main peak of simonkolleite reference pattern is very close to the main peak of iron oxide chloride reference pattern, as shown in Figure 103, but the first compound seem to match the diffraction pattern much better than iron oxide chloride since it not only matches the main peak but at least two or three more secondary peaks.

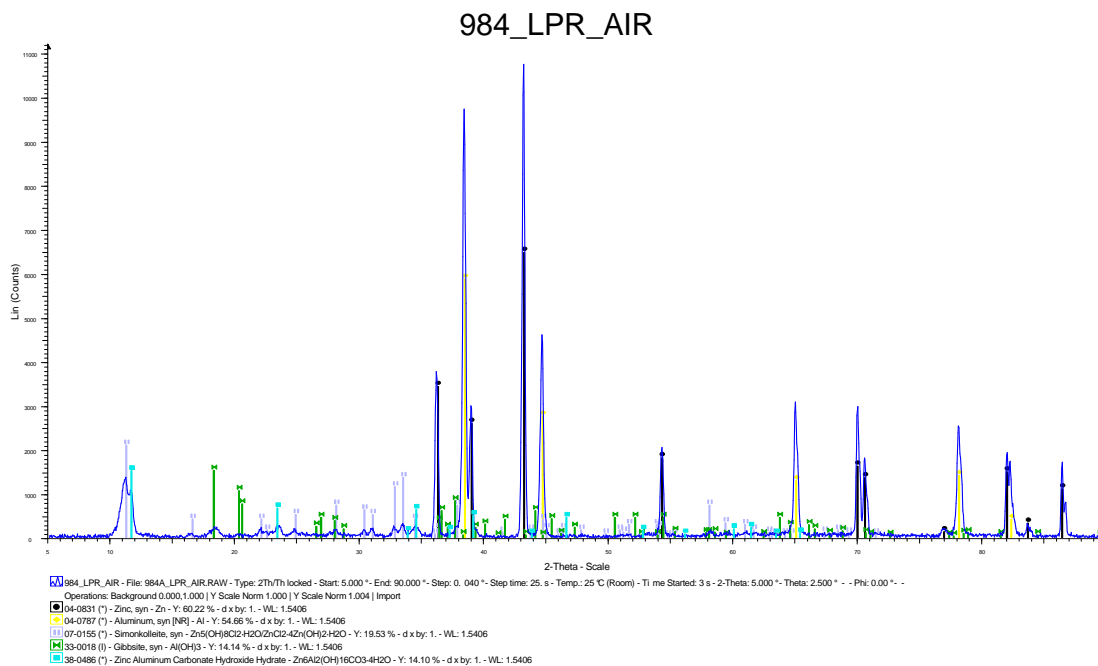


**Figure 102. Diffraction pattern of 984 A after 10 days of exposure in 3.5% NaCl in aerated solution.**

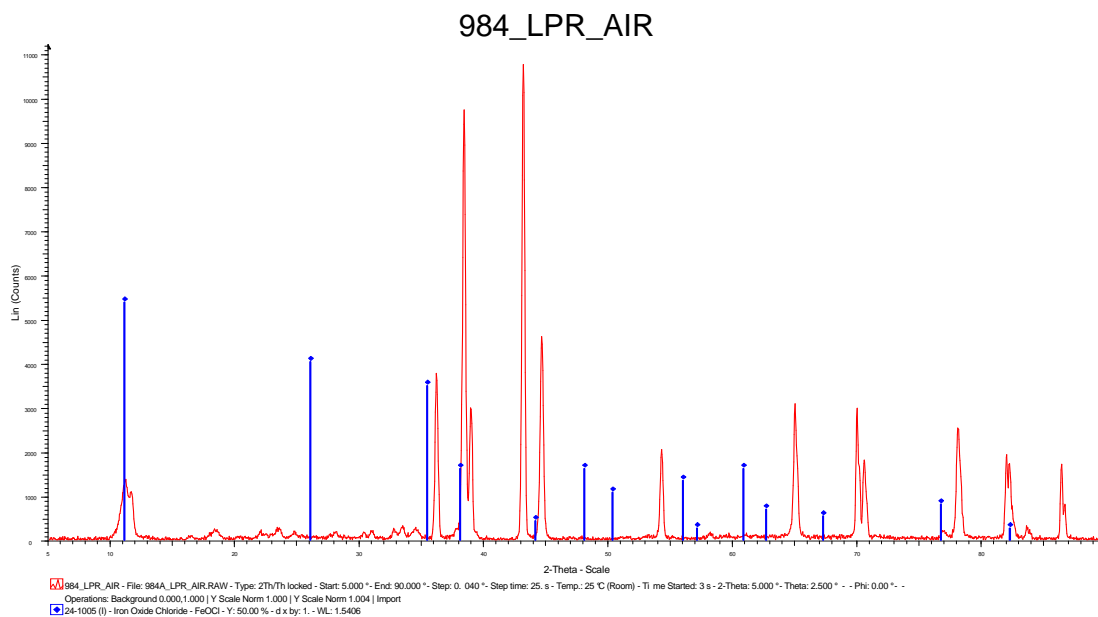


**Figure 103. Iron oxide and chloride reference pattern in blue.**

Although the sample has been rinsed before the analysis, the pattern of NaCl is shown in Figure 104 to disprove the presence of the salt on the surface.

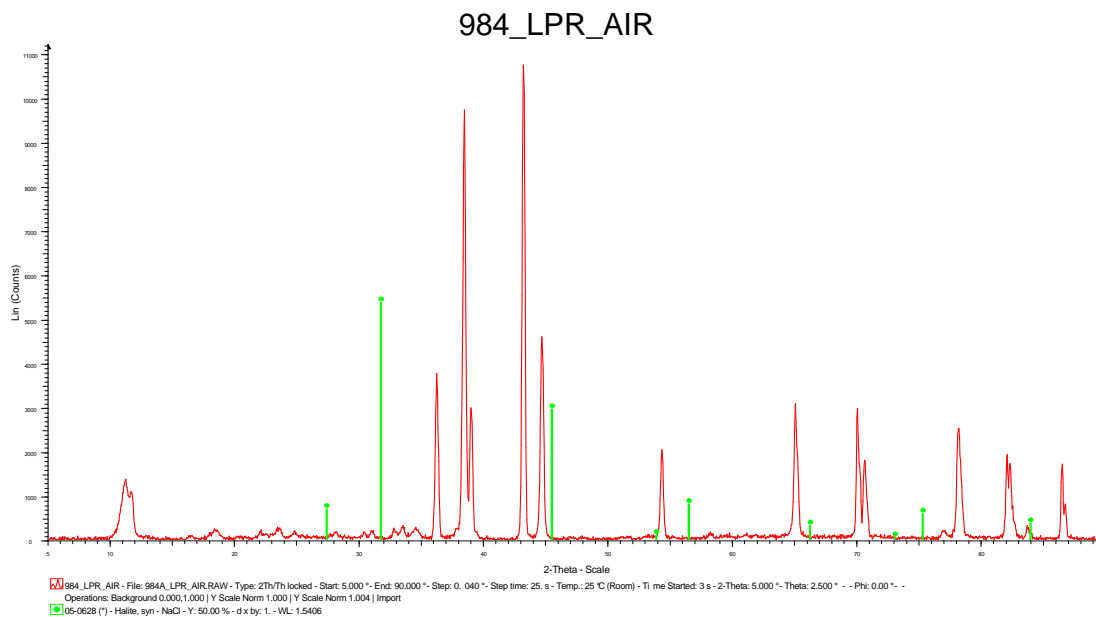


**Figure 104. Diffraction pattern of 984 A after 10 days of exposure in 3.5% NaCl in aerated solution. NaCl reference pattern in green colour.**

Figure 105 shows the diffraction patterns of the main peak of simonkolleite and aluminium. The corrosion compound main peak decreases with an increase of the incident angle while the aluminium peak increase. This proves that the corrosion compound is mostly present on the coating surface rather than in the coating bulk.

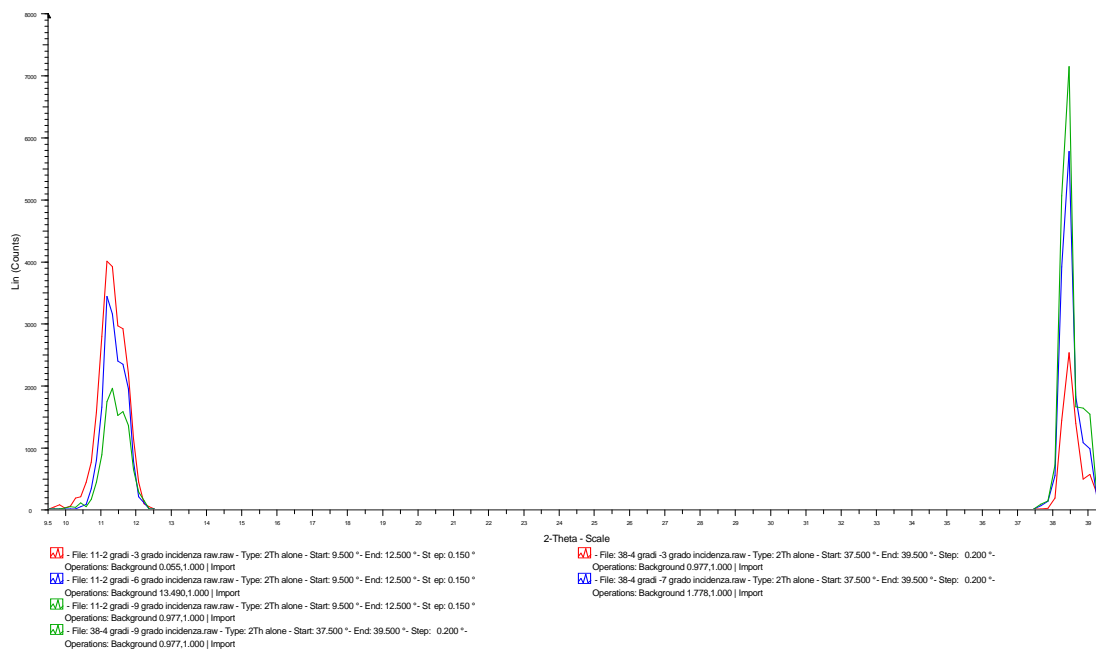


**Figure 105. Comparison for different incident angles between a corrosion compound main peak and aluminium main peak.**

## 3.2 COMPATIBILITY COATINGS

### 3.2.1 Galvanic test Results and Discussion

A preliminary galvanic measurement between only an aluminium and a bronze panel was carried out as a reference test for comparison with the following tests on the coatings.

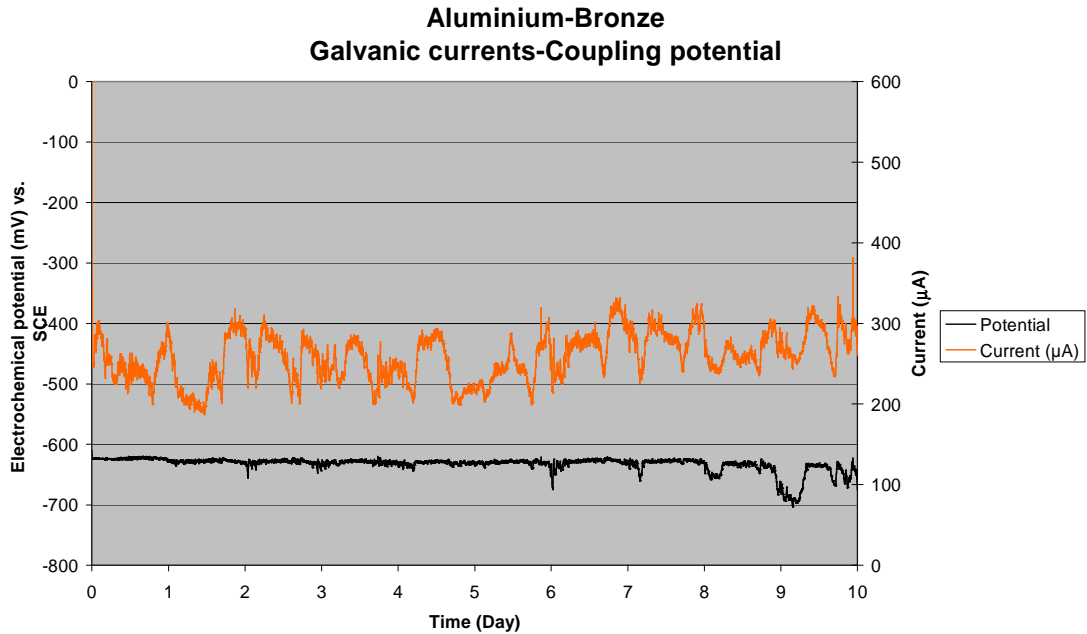
#### 3.2.1.1 Galvanic test between aluminium alone

Figure 106 shows the couple potential and the current flowing between the aluminium and the bronze panel over ten days, where both panels had the same surface area.

The open circuit potential was measured before the test and resulted in -300mV (SCE) for the bronze and -800mV (SCE) for the aluminium. After coupling, the mixed potential was as expected, between these two values, at -630 mV (SCE) for

most of the test. The aluminium behaved as an anode for the entire test, providing current to the more noble bronze.

The average current was 258  $\mu\text{A}$  and the average current density was calculated at 16  $\mu\text{A}/\text{cm}^2$ . This high current density indicates that accelerated corrosion would occur on the aluminium surface and it is to combat this problem that a coating for the bronze is being sought.



**Figure 106. Galvanic corrosion measurement between the bronze and the aluminium panels. Surface area of 16 cm<sup>2</sup> for both the panels.**

The following results will show how the application of a sacrificial coating is beneficial in terms of galvanic corrosion.

### 3.2.1.2 Mixed potentials

The mixed potential of the coatings coupled with the bronze and aluminium panels are shown in Figure 107. Passivated cadmium, unpassivated cadmium and electroplated aluminium were quite stable during the test, with potentials in the range between -800mV and -700mV (SCE). Similarly the Zn-Ni showed a potential in the same range for seven days, before increasing to almost -600mV (SCE) after nine

days. After this increase its potential stabilized around -610mV (SCE). This behaviour is thought to be due to zinc depletion during the test.

A different behaviour, in terms of potential, was shown by the IVD aluminium coating. In this case the mixed potential was unstable during the first three days when it decreased to very active values to then increase rapidly again. The potential settled around -730mV (SCE) from the third day to the end of the test. The active potential in the first three days explains the high anodic current of the coating at this time.

The zinc modified 984 were the most active coatings at the beginning of the test but their potentials increased in approximately one hour to values above -700mV (SCE). Both their potentials stabilized to around -600mV (SCE) after four days. The 1% zinc 984 remained, unexpectedly, more active then the 5% zinc until the end of the test. Only in the first hour was the 5% zinc 984 more active than the 1% zinc 984.

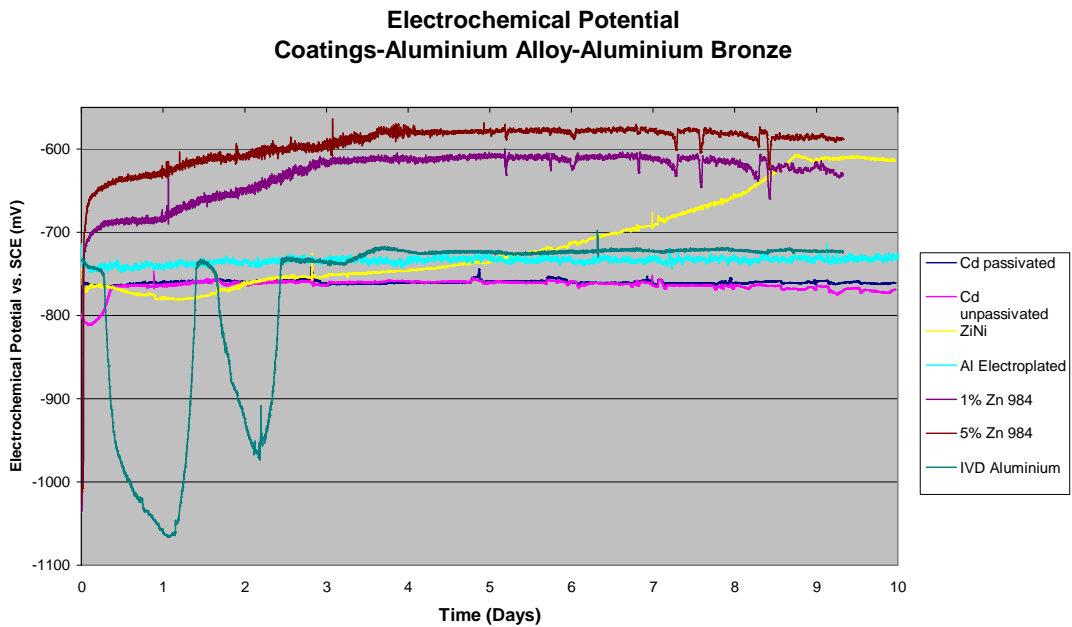


**Figure 107. Mixed potential of the galvanic couples during the ten days of galvanic test.**

From the potential plot and from the current plots, it seems that a value around -600mV (SCE) is the mixed potential at which the reversal of polarities between the coating and the aluminium panel occurs.

### 3.2.1.3 Galvanic currents

Each plot consists of three curves representing the currents flowing from or to the panel.

A positive current in the plot means that the metal is behaving as an anode while a negative value means that the metal is behaving as a cathode. For the majority of the plots the coating behaved as the anode providing current to both the bronze and the aluminium. Some of the coating, like the 984 1% zinc, the 984 5% zinc and the Zn-Ni became cathodic or provided very small current after a few days, while the aluminium became the anode. This is called reversal of polarities.

The results for passivated cadmium, are shown in Figure 108. This test will be used as the reference for the further comparisons.

The coating showed cathodic protection behaviour for the duration of the test, while both the aluminium and the bronze were protected. From the third to the last day the coating provided a protective current between 100  $\mu\text{A}$  and 150  $\mu\text{A}$ . The cathodic current on the bronze was around -50  $\mu\text{A}$  while the current on the aluminium was between -50 $\mu\text{A}$  and -100 $\mu\text{A}$  for the last seven days of the test.

One of the beneficial properties of cadmium is the stability of the electrochemical potential that seems to be confirmed in this case by a very protective current. The mixed potentials of all the coatings are shown in Figure 107. The blue line shows the passivated cadmium has one of the more stable potentials, together with the unpassivated cadmium and the electroplated aluminium.

The mixed potential is the potential of the three panels connected together so a stable mixed potential does not necessarily mean that the coating potential is stable. Anyway the first test between the aluminium and the bronze, in Figure 106, did not show any particular fluctuation in the mixed potential of these two panels so that it seems acceptable to think that any additional fluctuations in the coating-aluminium-bronze experiment is caused by the fluctuation of the potential of the coating.

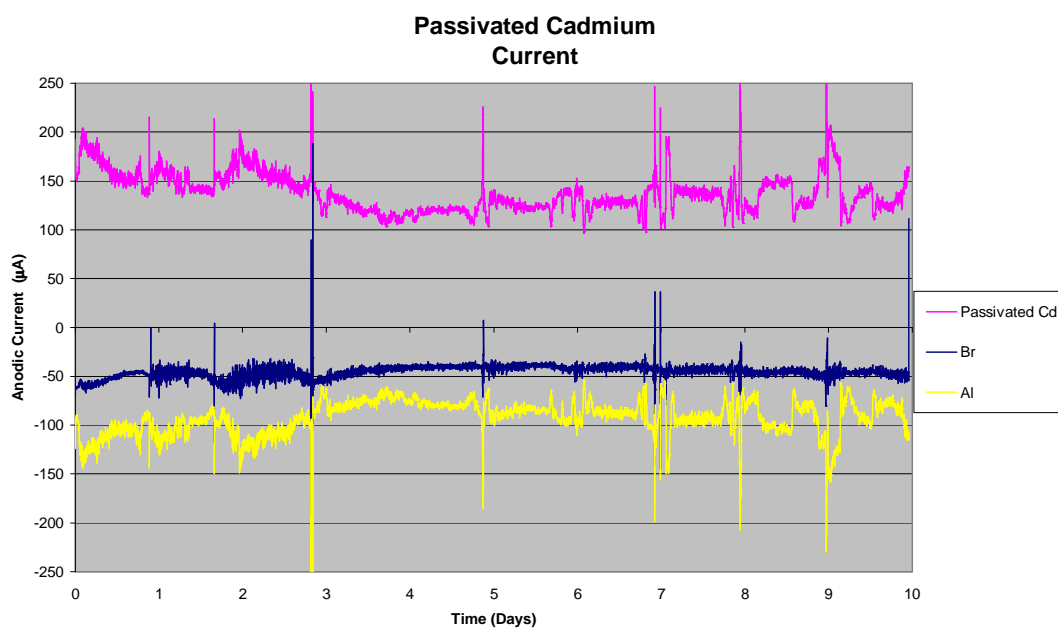


**Figure 108. Three metal galvanic corrosion measurements. Bronze-Aluminium-Passivated Cadmium.**

The unpassivated coating in Figure 109 showed a slightly lower anodic current that resulted in lower cathodic protection during the test.

As for the passivated cadmium, the currents became more stable after the first few days. A small fluctuation of the current is always expected in the first days of the tests, when all the surfaces are more reactive.



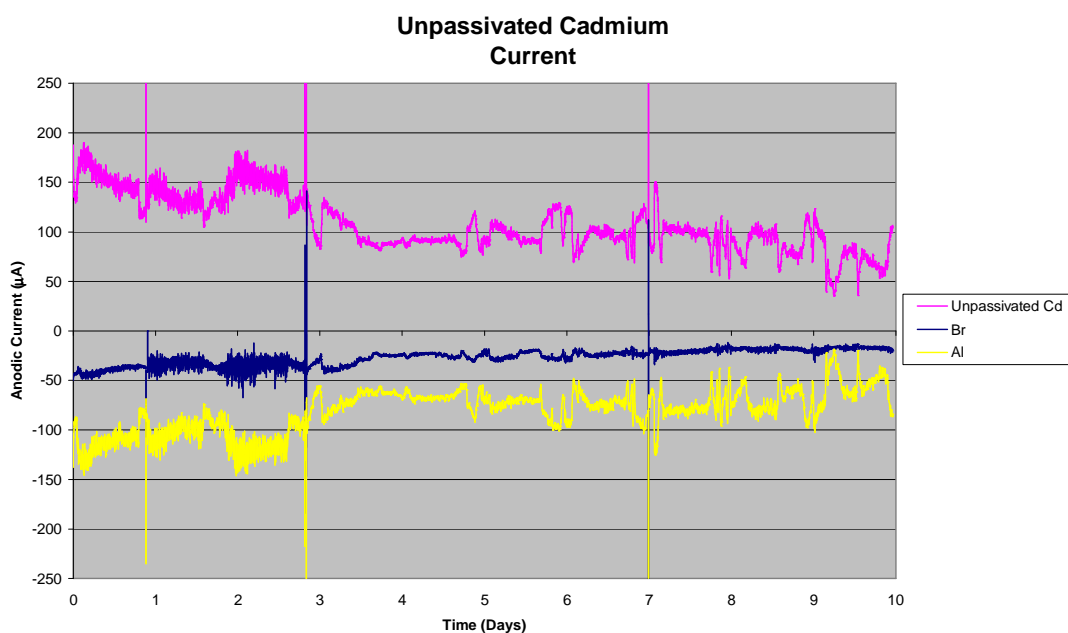


**Figure 109. Galvanic currents. Bronze-Aluminium-Unpassivated Cadmium.**

Figure 110 shows the galvanic currents between the Zn-Ni coating, the aluminium and the bronze panel. The Zn-Ni coating behaved as an anode for approximately eight days of testing, while in the last two days its current became cathodic and the aluminium started to be the anode. This reversal of polarities was probably due to coating ennoblement as a consequence of zinc depletion. After the reversal, the coating became cathodic, the same as the bronze. This means that the aluminium was now corroding and giving protection not only to the bronze but also to the coating, with an anodic current around 70  $\mu\text{A}$ . The cathodic behaviour of the coating after the reversal is not a benefit for the aluminium because it leads to an increase of its corrosion.

Comparing this result with the cadmium it is clear that, apart from the last few days, when the zinc had probably been completely depleted, the order of magnitude of the currents involved, both anodic and cathodic, was almost the same.

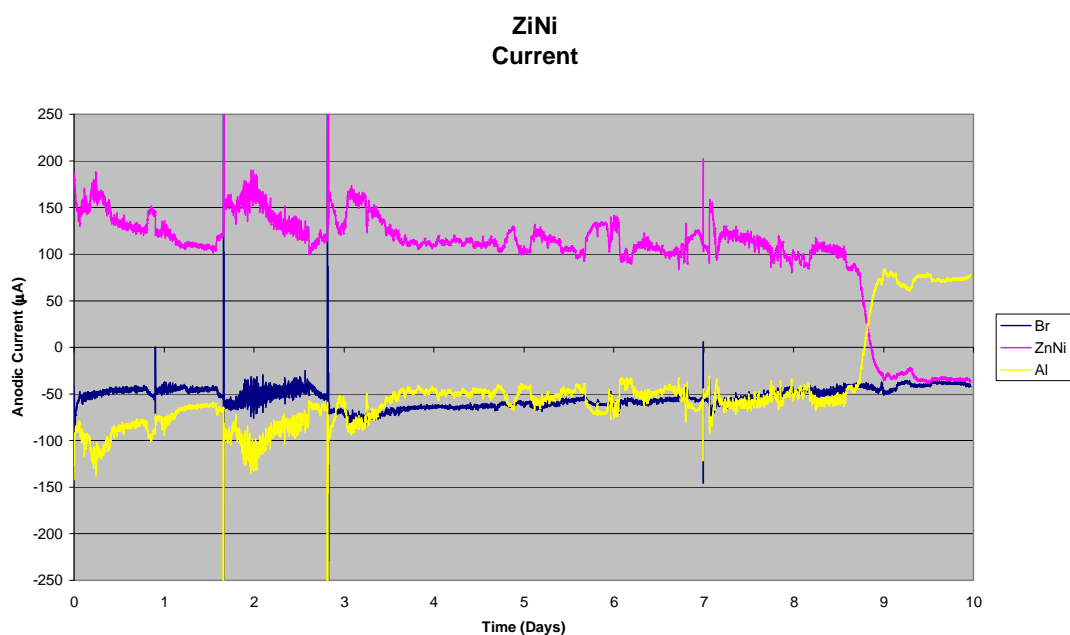


**Figure 110. Galvanic currents. Bronze-Aluminium-ZiNi coating.**

Figure 111 shows the currents exchanged in the cell containing the electroplated aluminium coating. The coating was anodic for the entire test while both the bronze panel and the aluminium panel were protected. The bronze panel showed, after two days, a cathodic current around 100  $\mu\text{A}$ ; that is much higher than the currents recorded for the bronze in the passivated and unpassivated cadmium and in the Zn-Ni cells. When the test was repeated the bronze did not show the same high cathodic current.

However, on the base of this first test, the electroplated aluminium seems to provide a good stable current, at least comparable with the cadmium, and more importantly, it did not show any reversal of polarity.

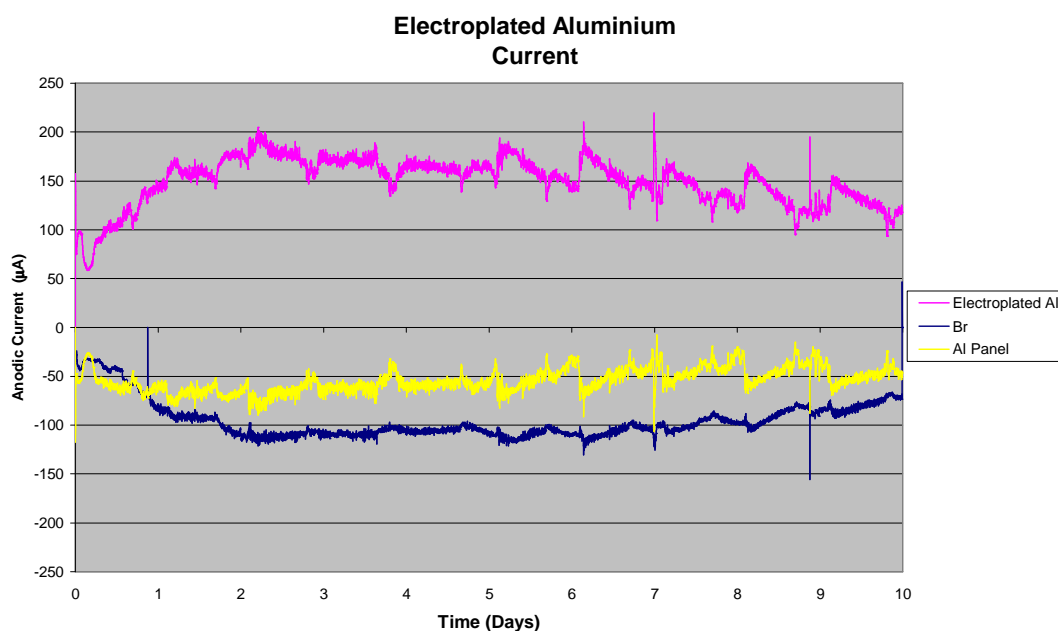


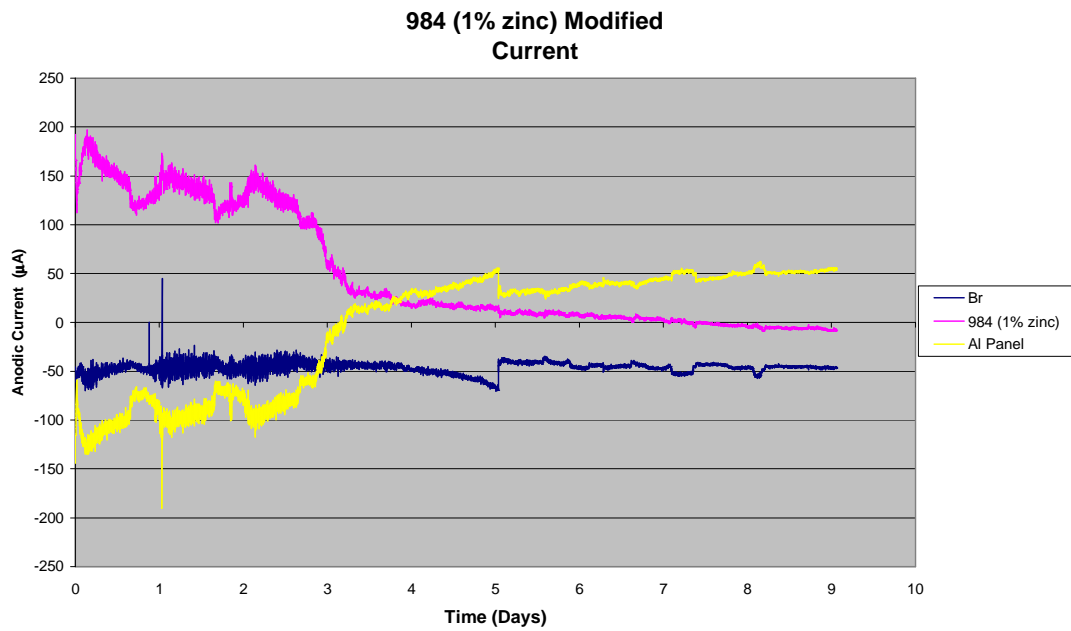
**Figure 111. Galvanic currents. Bronze-Aluminium-Electroplated Aluminium.**

Different behaviour was shown by the 1% zinc modified 984 (Figure 112). The coating started as anodic at the beginning of the test. After three days of testing the current on the coating decreased and the aluminium panel also became anodic. The coating showed the biggest anodic current for the first four days and then there was a reversal of the polarities with the aluminium panel starting to be more anodic than the coating. This was probably due to the depletion of the small amount of zinc in the coating. After seven days of testing the coating became cathodic and the aluminium panel remained the only anodic material.

In the last 5 days the coating exchanged very small currents. The coating was then behaving merely as a barrier layer on the bronze substrate, isolating it from exposure to the corrosive process. Compared to the Zn-Ni coating cell, the aluminium was corroding with a lower final anodic current, resulting in a small benefit for the component. This is due to the fact that in this case the coating did not rapidly reverse into the cathodic region and the only panel demanding current from the aluminium was the bronze.

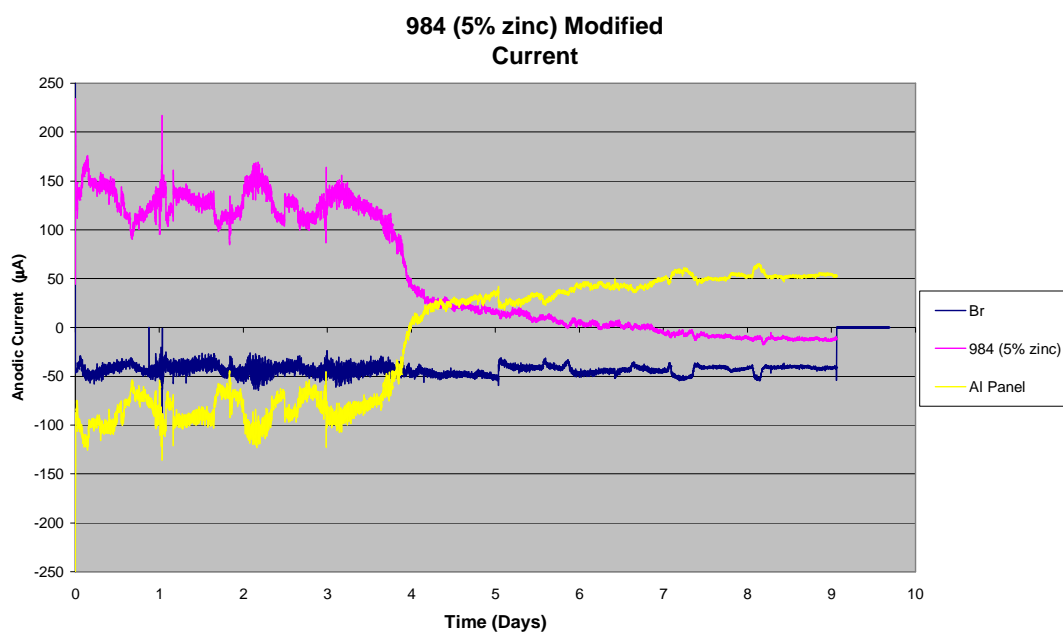
In this situation the bronze was under protection and the aluminium was corroding with a current that was approximately half of the currents recorded on the coating

before the reversal. The OCP of the coating should now be the mixed potential of the aluminium/bronze without the introduction of the coating. This potential was measured in around -630mV (SCE) during the galvanic corrosion test shown in Figure 106, for equal areas of bronze and aluminium. A reduction of the area of the bronze would probably change this value toward the aluminium OCP.



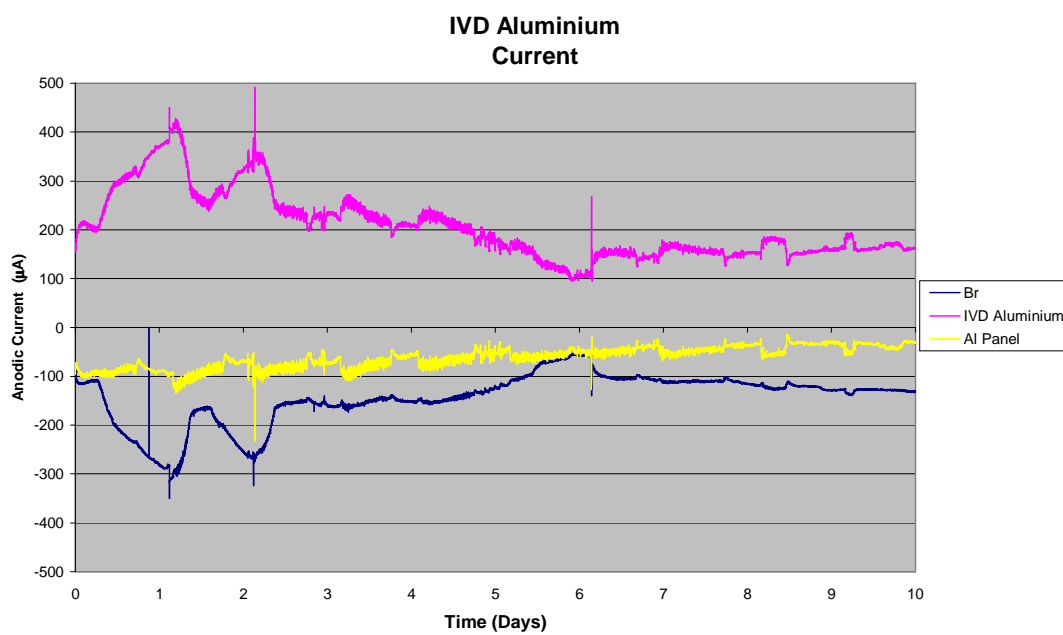
**Figure 112. Galvanic currents. Bronze-Aluminium-984 (1% Zinc) coating.**

Similar behaviour was shown by the 5% zinc 984, in Figure 113; the only difference being the point where the coating and aluminium lines cross each other occurred after a longer time.



**Figure 113. Galvanic currents. Bronze-Aluminium-984 (5% Zinc) coating.**

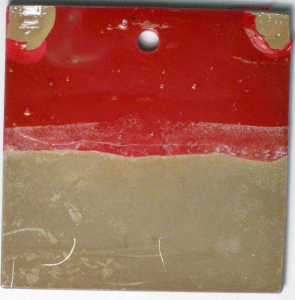










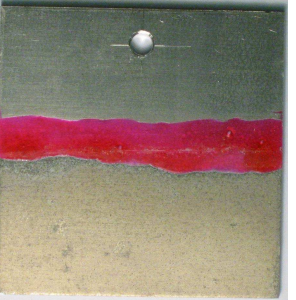
Figure 114 shows the galvanic currents for the IVD aluminium cell. The coating was anodic for the ten days and no reversal was observed during the entire test. The cathodic current of the bronze panel exceeded 100 µA for most of the test and the anodic current reached very high values during the first three days, classifying the IVD as the most active coating during initial exposure.



**Figure 114. Galvanic currents. Bronze-Aluminium-IVD Aluminium.**

### 3.2.1.4 Appearance of the panels after the galvanic corrosion test

The appearance of the panels after the test is shown in Figure 115 and in Figure 116.

<i>Coating</i>	<i>Bronze</i>	<i>Aluminium Panel</i>
		
Passivated cadmium		
		
Unpassivated cadmium		
		
Zn-Ni		
		
Electroplated aluminium		

**Figure 115. Appearance of the panels after the galvanic test. 10 days in 3.5% NaCl solution.**



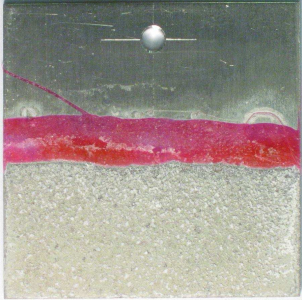


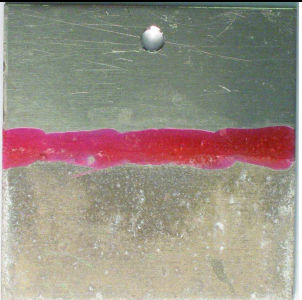



All of the coatings showed some signs of corrosion, to varying degrees. The IVD aluminium was most affected and this reflects the high anodic current from this coating. The electroplated aluminium also showed marked corrosion, particularly around the edges. Again, this coating produced a high anodic current.

Discoloration also occurred on all of the aluminium panels, even those that remained cathodic during the entire test. It should be remembered that aluminium is an amphoteric metal and is attacked in both acid and alkaline solutions. In this case, the increase in pH associated with the cathodic reaction was responsible for the observed corrosion of the panels.

In contrast, the aluminium became anodic towards the end of the test with the two zinc modified 984 coatings and these panels can be seen to have evidence of active corrosion. It should also be considered that self-corrosion of the aluminium can occur in cases where the galvanic currents due to corrosion of the sacrificial coating are insufficient to give full protection.

The bronze panels coupled with the passivated cadmium and unpassivated cadmium were discoloured after the test. The bronze panels coupled with electroplated aluminium and IVD aluminium were heavily discoloured while those coupled with Zn-Ni, 1% zinc 984 and 5% zinc 984 were lightly discoloured. Overall, the bronze panel coupled with 5% zinc 984 had the best appearance after the test, being only lightly discoloured.



<i>Coating</i>	<i>Bronze</i>	<i>Aluminium Panel</i>
		
1% zinc 984		
		
5% zinc 984		
		
IVD		

**Figure 116. Appearance of the panels after the galvanic test. 10 days in 3.5% NaCl solution.**

### 3.2.1.5 Repetition of the galvanic test

The galvanic test was repeated three times for each coating. Table 15 compares the times for reversal to occur in each.

The second and third series of tests were each interrupted for a few minutes on days one and five to take the polarisation measurement but this is not thought to have affected the overall galvanic behaviour.

	Pass Cd	Un Cd	984 1% Zn	984 5% Zn	Zn-Ni	IVD	El Al
1 <sup>st</sup> test	No rev	No rev	3 days	4 days	9 days	No rev	No rev
2 <sup>nd</sup> test	4 days	No rev	3 days	5 days	8 days	No rev	No rev
3 <sup>rd</sup> test	No rev	No rev	7 days	9 day	9 days	No rev	No rev

**Table 15. Summary of times to current reversal**

It is well confirmed that the coatings containing Zinc suffered reversal, probably because of the preferential oxidation of the Zinc. This seems to be an important result, especially for the Zn-Ni. In contrast to the modified 984 coatings, the Zn-Ni coating is not a novel coating and it is considered as one of the promising candidates for cadmium replacement. The effect of preferential oxidation of the zinc should be carefully considered to avoid the risk of an unexpected behaviour in service.

Apart from these zinc containing coatings, only the passivated cadmium showed a reversal of polarity in any of the three tests. This behaviour was unexpected.

In conclusion pure metal coatings, like cadmium or the two aluminium coatings seem to be safer in terms of avoiding risk of potential change in service.

### 3.2.2 Polarisation curves

Polarisation curves relative to Figure 106 are shown in the following two plots. Figure 117 shows the polarisation curves obtained before starting the galvanic current measurement while Figure 118 shows the same plot taken soon after the galvanic measurement was stopped. In both the plots the corrosion seems to be under mixed control. The OCPs of the aluminium and of the bronze became slightly more

active after ten days, probably due to a small reduction in the dissolved oxygen concentration in the cell, which caused more polarisation of the cathodic reaction.

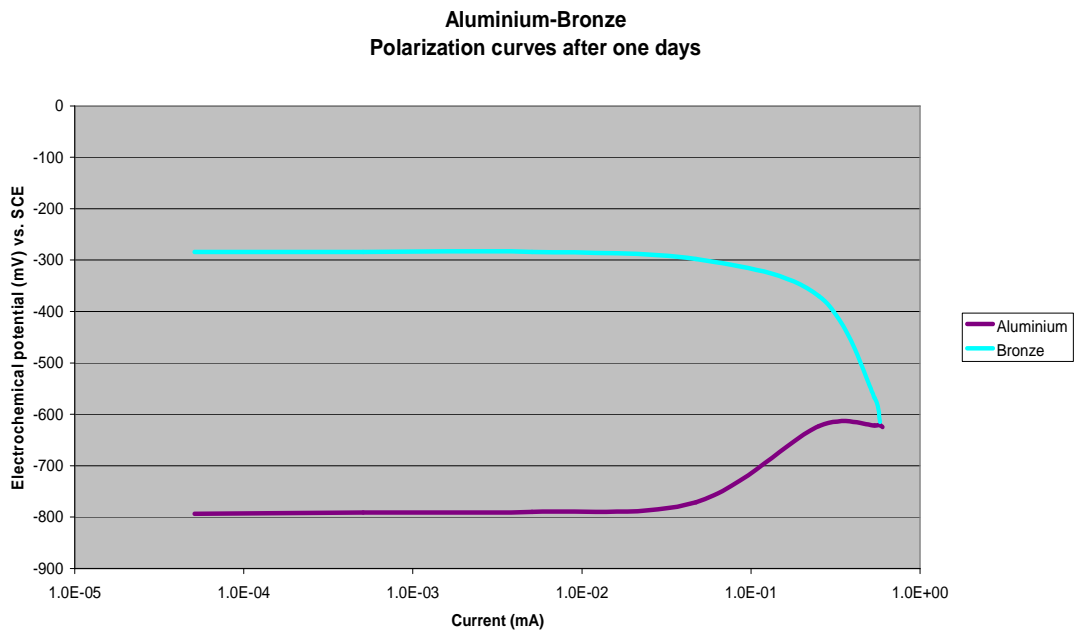


**Figure 117. Polarisation curves before starting the galvanic current measurement. Aluminium and bronze panel with same surface area.**

Aluminium Bronze  
Polarization curves after ten days

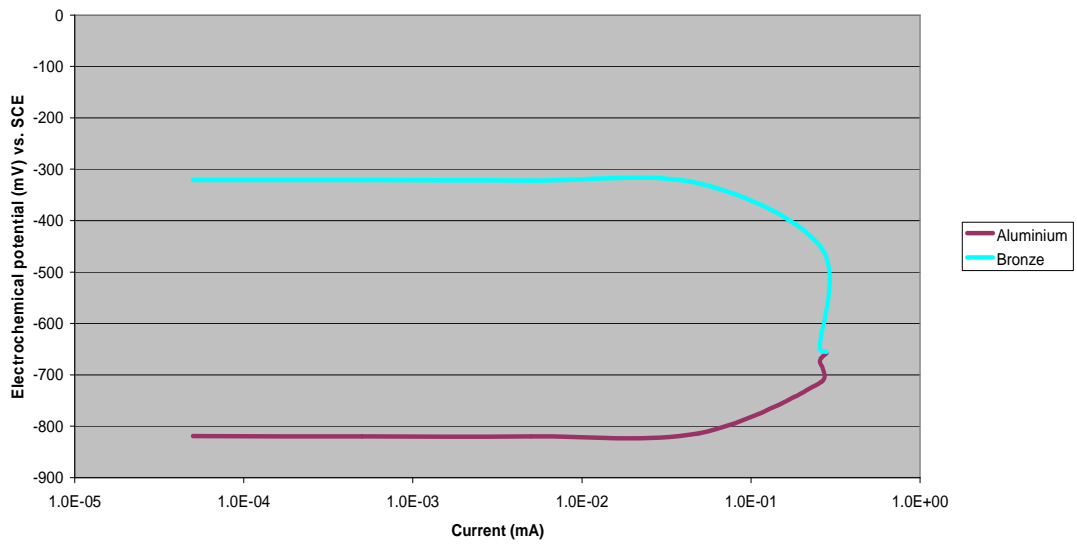


**Figure 118. Polarisation curves after ten day. Aluminium and bronze panel with same surface area.**

The following results show the second repetition of the galvanic corrosion measurement that was used to take the measurement for the polarisation behaviour curves of the coatings. It is useful to compare the second galvanic test repetition with the first one and to notice that, apart from the passivated cadmium, all the other results were in good agreement. The discussion regarding the controlling mechanism, explaining whether it is cathodic, anodic or mixed, always refers to the one-resistor setup that is shown on the plots in continues lines.

Figure 119 shows this second repetition of the galvanic corrosion test for the passivated cadmium that was used to take measurements for the polarisation behaviour curves. After four days the aluminium and the passivated cadmium showed a reversal of polarities. Before that, the passivated cadmium was the anode, while the bronze and the aluminium were the two cathodes. During the fourth day the aluminium and the passivated cadmium suddenly reversed their polarities and the aluminium became anodic until the end of the test. At the same time, the mixed potential rapidly increased to a more noble value of -620mV.

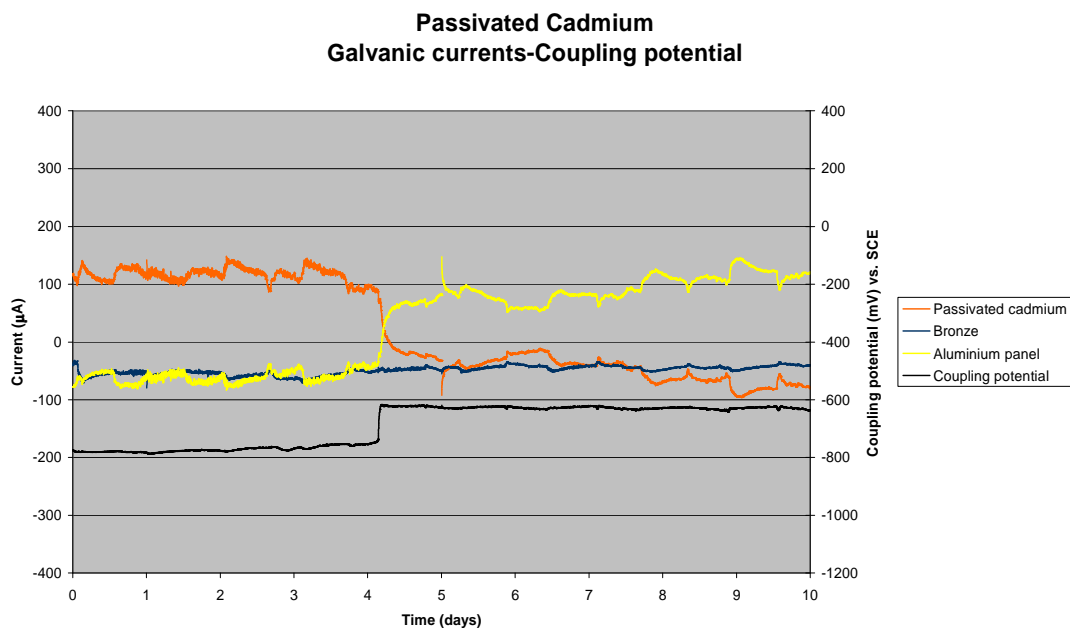
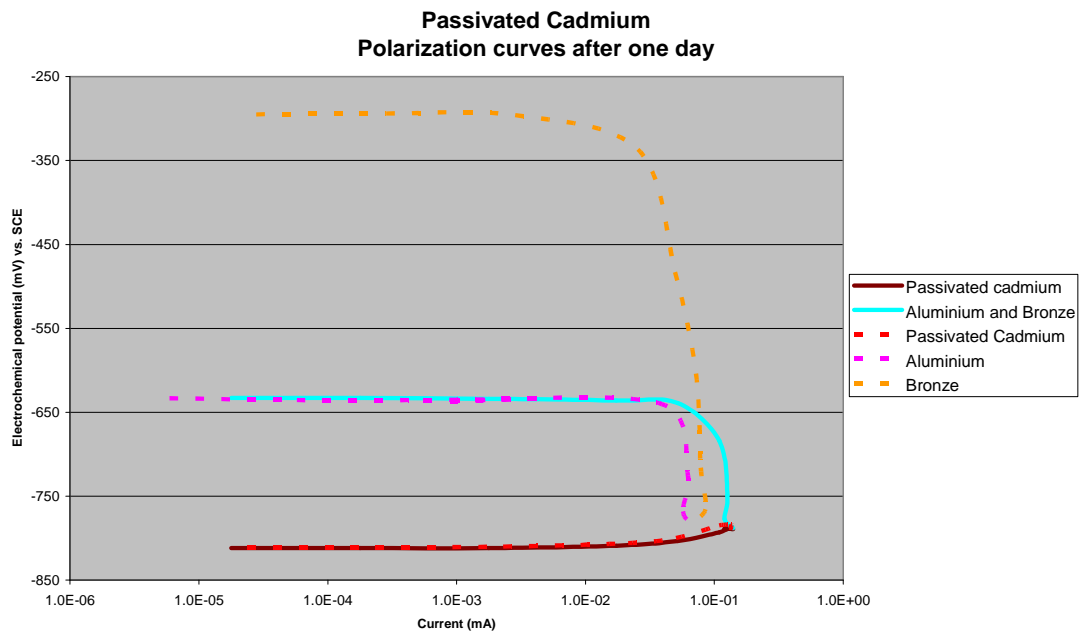


**Figure 119. Passivated cadmium, bronze and aluminium. Galvanic currents and mixed potential.**

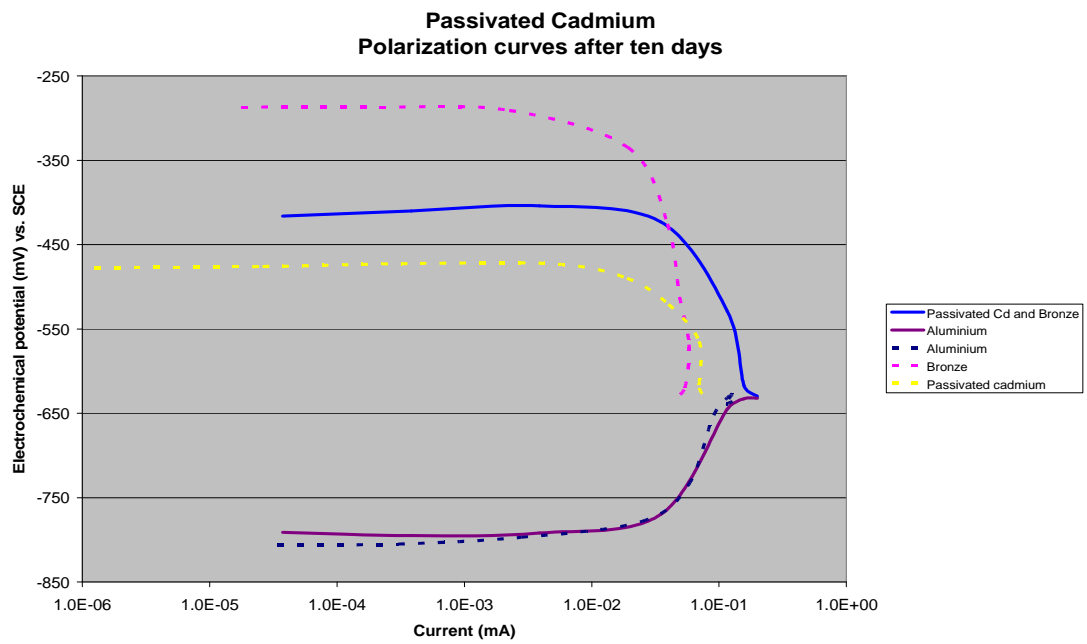
Comparison of Figure 120 and Figure 121 shows that OCP of the bronze did not substantially change. The passivated cadmium OCP showed a strong ennoblement

increasing from -812 mV to -477 mV vs. SCE while the aluminium open circuit potential decreased from -633 mV to -806 mV vs. SCE.

The control of corrosion changed from cathodic control to mixed control after the cadmium and the aluminium reversed their polarities.



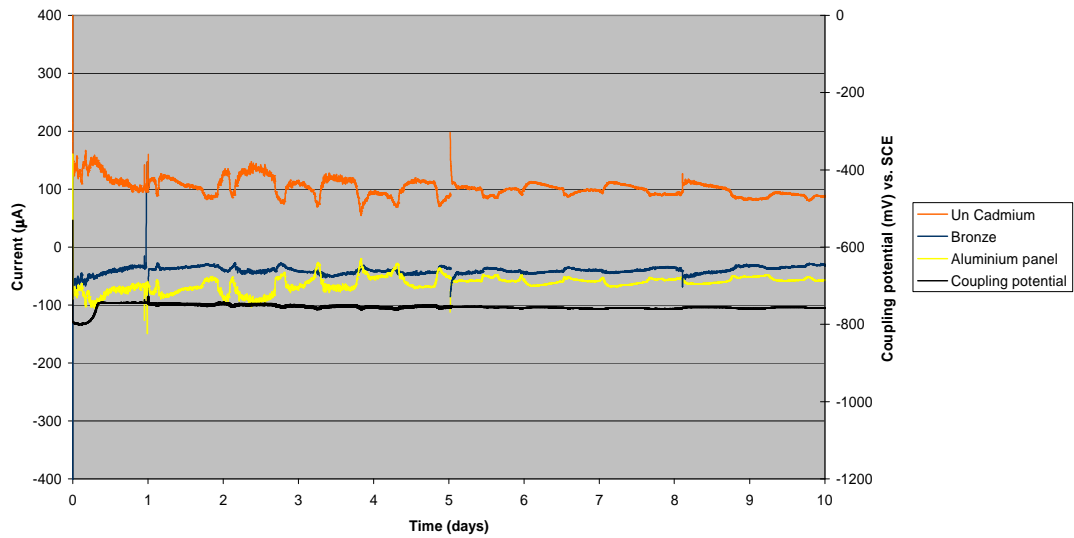
**Figure 120. Polarisation curves after one day. Passivated cadmium, aluminium panel and bronze panel. One resistor setup in continuous lines, three resistors setup in dashed lines.**



**Figure 121. Polarisation curves after ten days. Passivated cadmium, aluminium panel and bronze panel. One resistor setup in continuous lines, three resistors setup in dashed lines.**

Figure 122 shows the repetition of galvanic corrosion measurement for unpassivated cadmium. As in the first test, the unpassivated cadmium did not show any reversal of polarities. The coating behaved as an anode for the entire test and the bronze and the aluminium showed a stable cathodic behaviour.

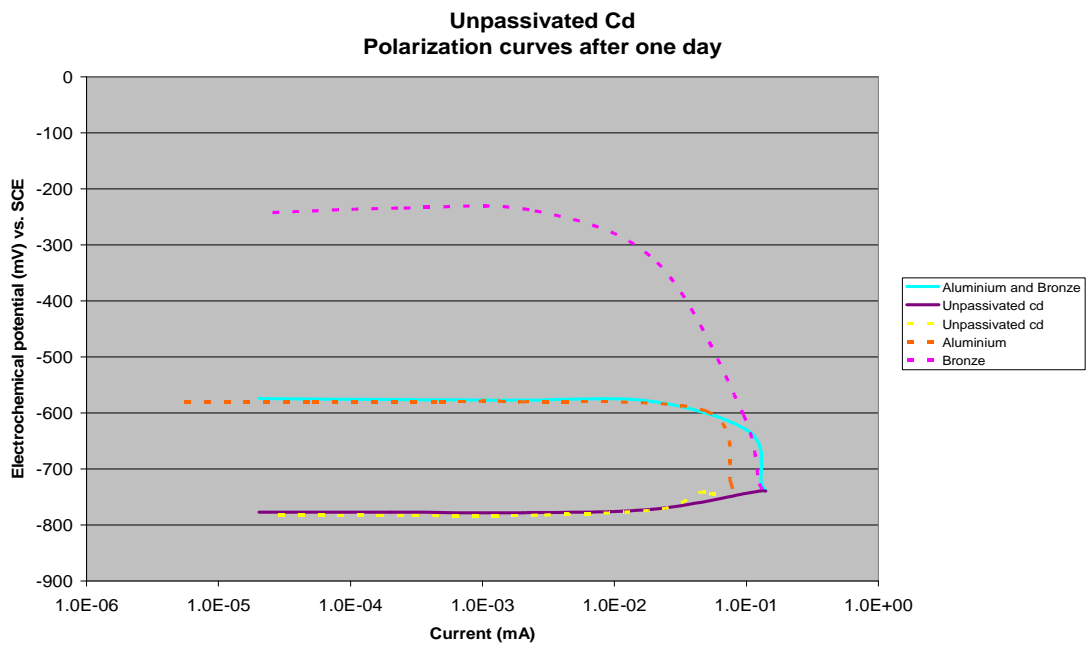
### Unpassivated Cadmium Galvanic currents-Coupling potential



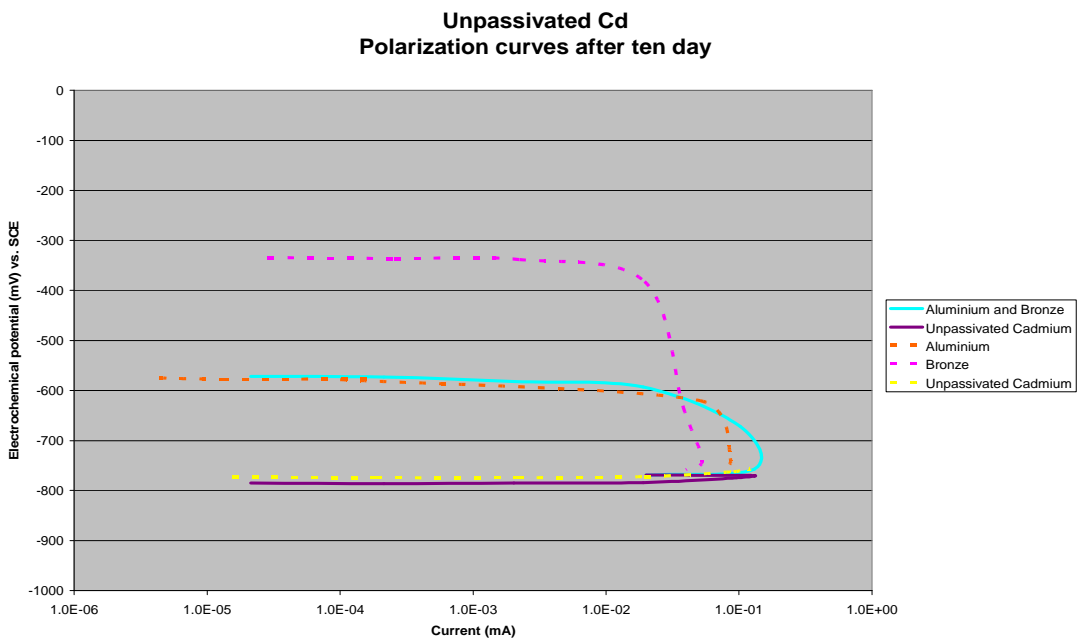
**Figure 122. Unpassivated cadmium, bronze and aluminium. Galvanic currents and mixed potential.**

Figure 123 and Figure 124 show the polarisation behaviour curves of the unpassivated cadmium, the bronze and aluminium. Both at the beginning and at the end of the test the galvanic corrosion is under cathodic control. The open circuit potentials of the unpassivated cadmium and of the aluminium did not significantly change while the bronze became less noble, moving from -242 mV to -334 mV vs. SCE



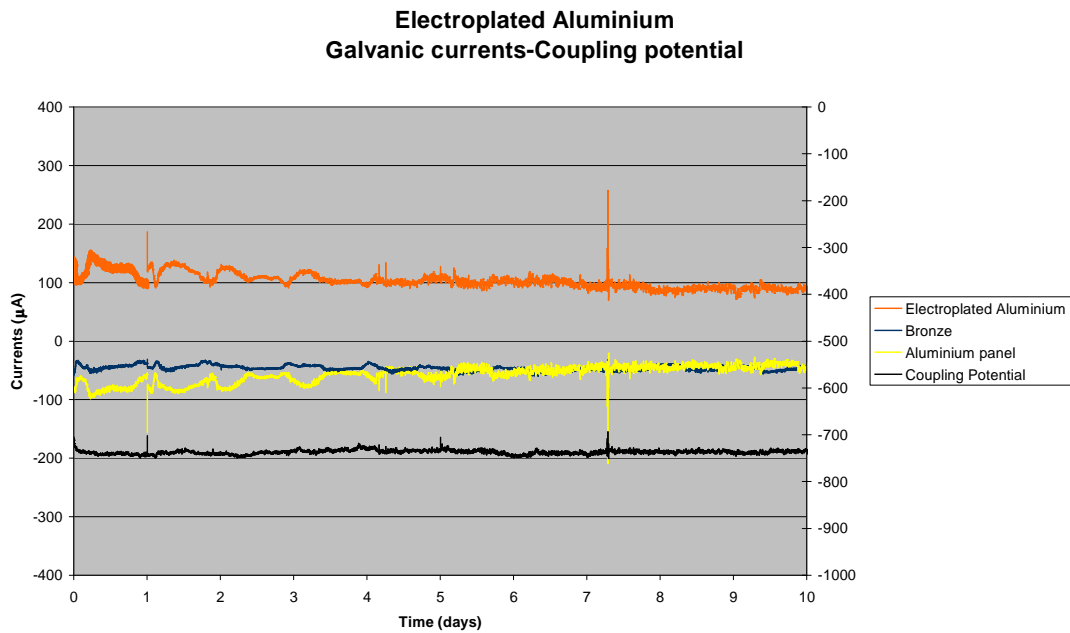


**Figure 123. Polarisation curves after one. Unpassivated cadmium, aluminium and bronze. One resistor setup in continuous lines, three resistors setup in dashed lines.**



**Figure 124. Polarisation curves after ten days. Unpassivated cadmium, aluminium and bronze. One resistor setup in continuous lines, three resistors setup in dashed lines.**

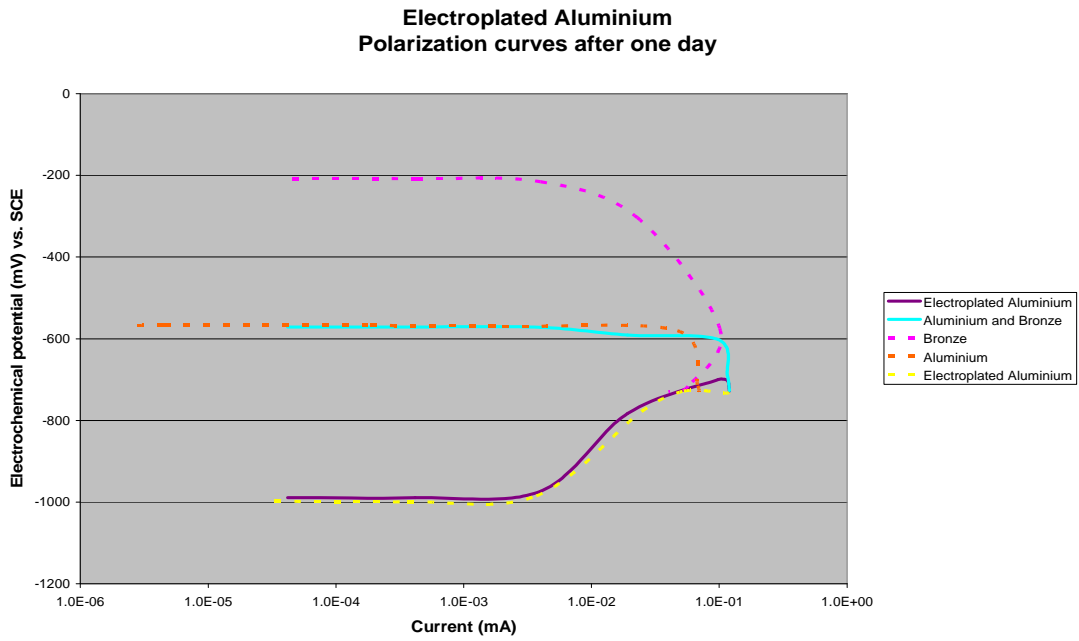
Figure 125 shows the repeated galvanic test for the electroplated aluminium. As in the previous one, no reversal of polarities was shown and the electroplated aluminium was confirmed to be a good protective coating, providing a current comparable with the ones of the unpassivated cadmium and of the passivated cadmium before the reversal of polarities.



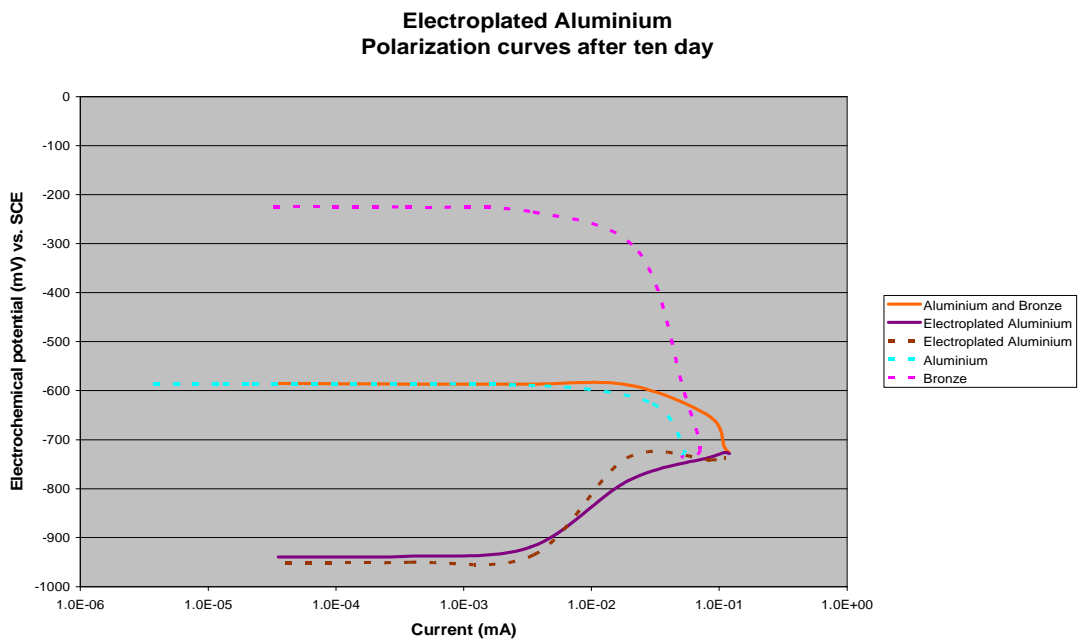
**Figure 125. Electroplated aluminium, bronze and aluminium. Galvanic currents and mixed potential.**

The coating behaved as an anode for the entire test, providing a stable current of around 100 μA. The mixed potential was measured at approximately -730 mV for the entire test.

Figure 126 and Figure 127 show the polarisation behaviour curves for the electroplated aluminium, the bronze and the aluminium panels. In the first plot the OCP of the electroplated aluminium increases from -983 mV to -731 mV while the OCP of cathodic couple decreases from -571 mV to -731 mV as the resistor was adjusted from 10 Mohm to the short circuit. The corrosion process seems to be under mixed control. Similar behaviour was found after ten days, with very similar values.

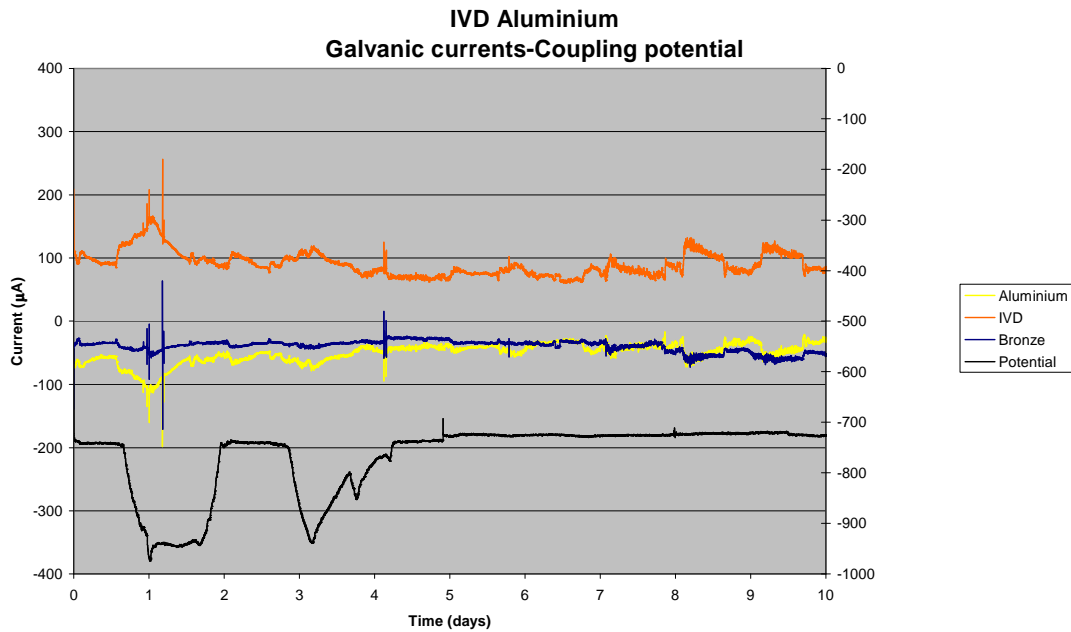


**Figure 126. Polarisation curves after one day. Electroplated aluminium, aluminium panel and bronze panel. One resistor setup in continuous lines, three resistors setup in dashed lines.**



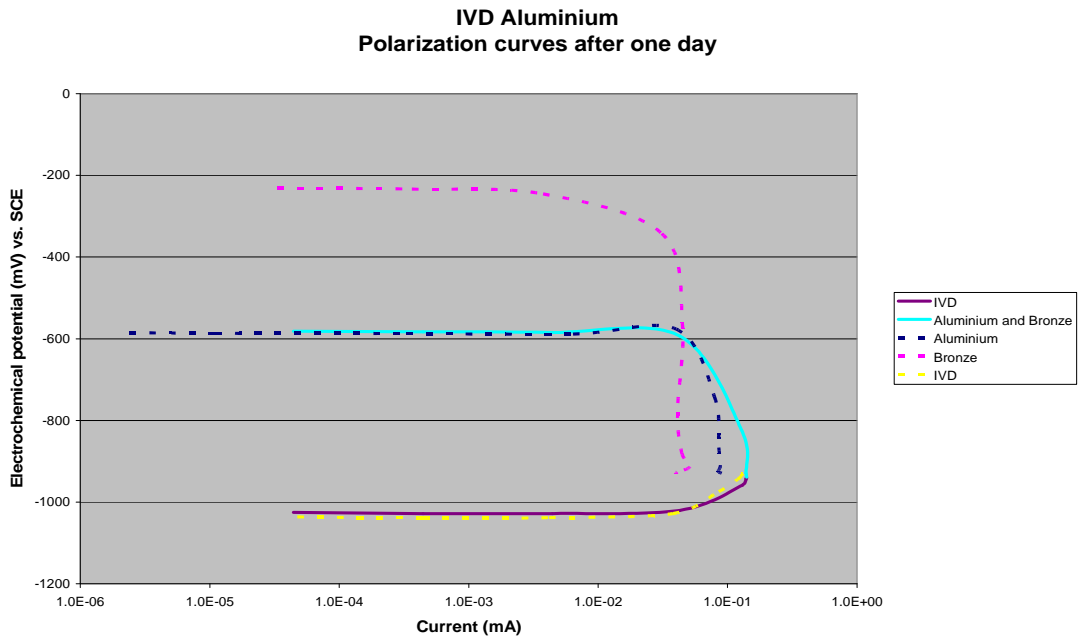
**Figure 127. Polarisation curves after ten days. Electroplated aluminium, aluminium panel and bronze panel. One resistor setup in continuous lines, three resistors setup in dashed lines.**

Figure 128 shows the galvanic corrosion measurement of the IVD aluminium, the bronze and the aluminium. As in the first repetition, the IVD aluminium showed big potential fluctuations during the first five days. At the same time, the current followed the trend of the potential, increasing when the coatings became more active. After the first days the mixed potential stabilized around -730 mV and the protective current at -80  $\mu\text{A}$ . In ten days the coating did not show any reversal of polarities, with the coating remaining the anode.

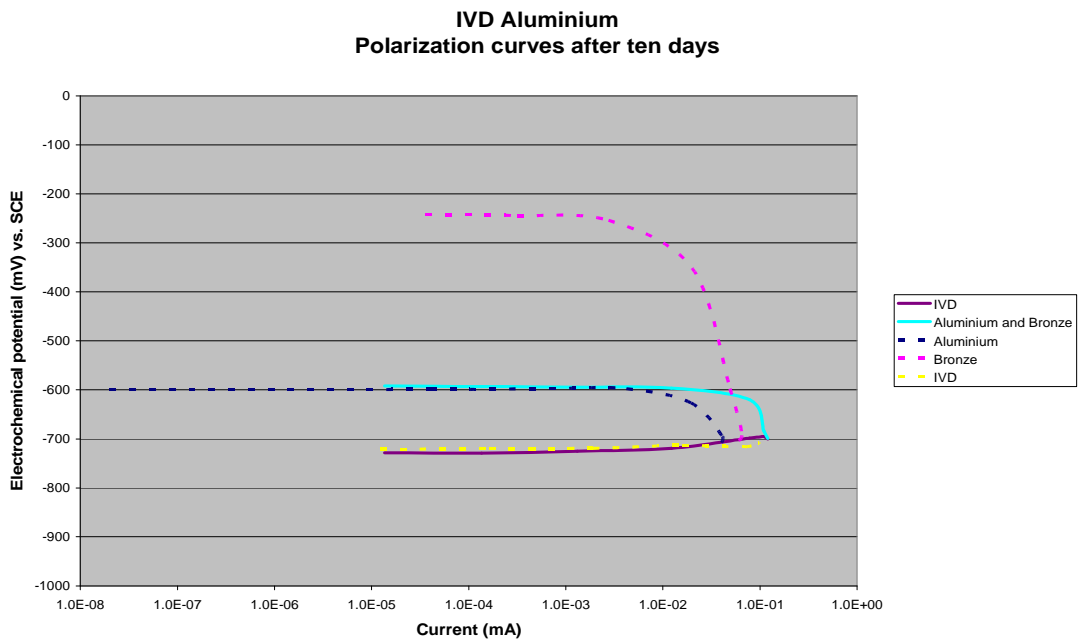


**Figure 128. IVD aluminium, bronze and aluminium. Galvanic currents and mixed potential.**

Polarisation behaviour curves, in Figure 130 and in Figure 131, show that the corrosion is under cathodic control. The aluminium OCP changed considerably after ten days, showing ennoblement from -1036 mV to -731 mV vs.SCE.

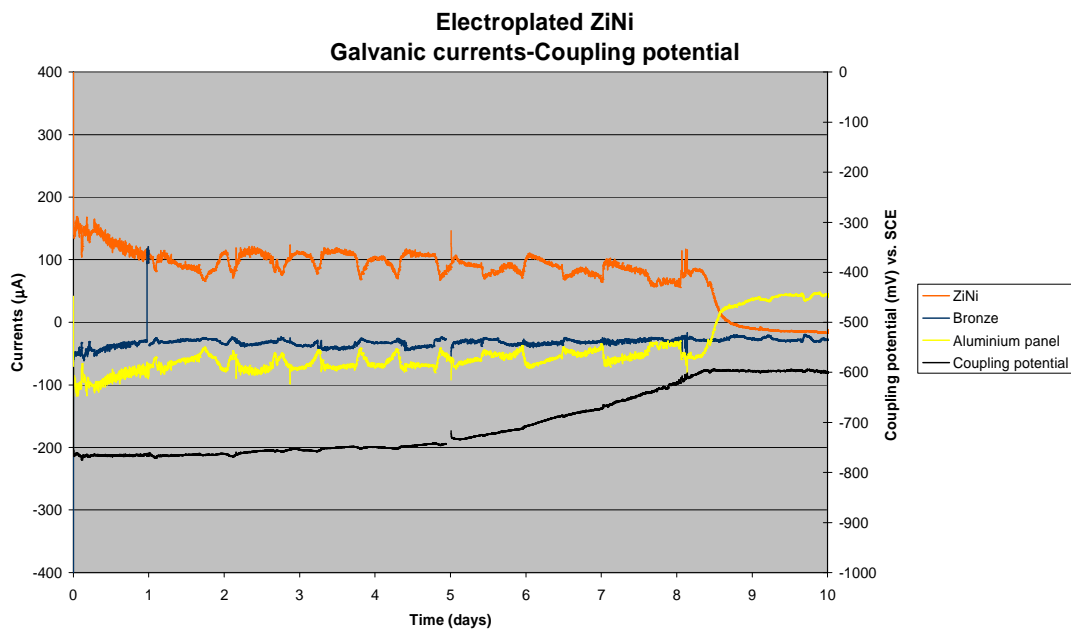


**Figure 129. Polarisation curves after one day of. IVD aluminium, aluminium and bronze. One resistor setup in continuous lines, three resistors setup in dashed lines.**



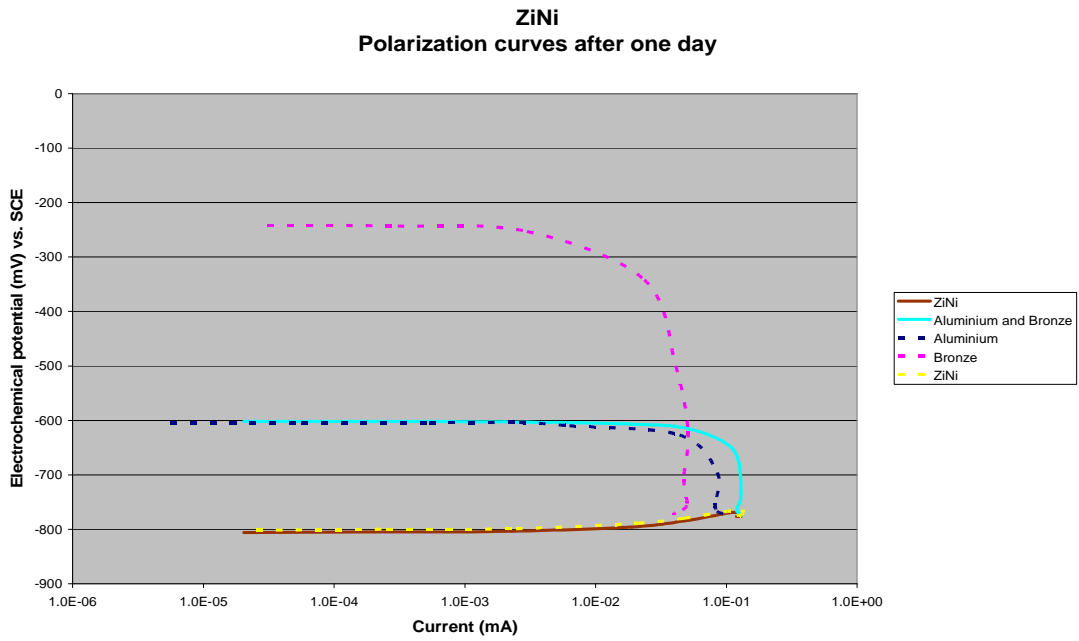
**Figure 130. Polarisation curves after ten days. IVD aluminium, aluminium and bronze. One resistor setup in continuous lines, three resistors setup in dashed lines.**

Figure 131 shows the galvanic corrosion measurements between the Zn-10% Ni, the bronze and the aluminium. The Zn-10% Ni showed a reversal of its polarity after approximately nine days. This result confirmed the first results where the same coating showed a reversal after approximately the same period of time. The mixed potential showed a gradual ennoblement from the beginning of the test to reach a stable value around -600 mV after the reversal of the aluminium and of the Zn-10%Ni.

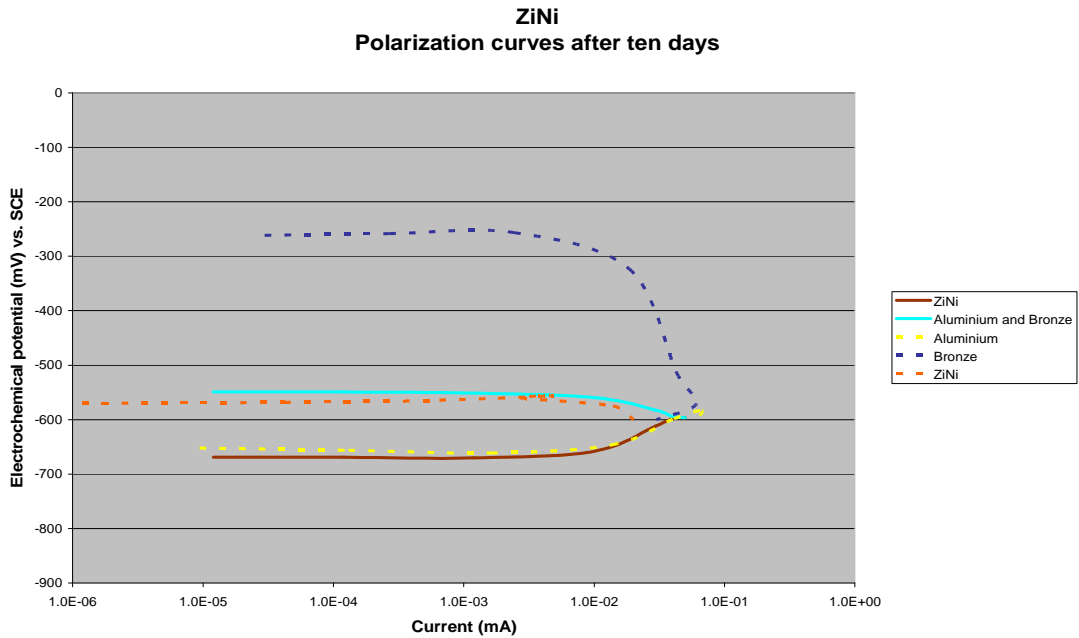


**Figure 131. Zn-10% Ni, bronze and aluminium. Galvanic currents and mixed potential.**

Polarisation curves, in Figure 132 and Figure 133, show an OCP of -800 mV for the Zn-10% Ni after one day with the corrosion process under cathodic control. After the reversal the OCP of the Zn-10% Ni increased to -570 mV and the corrosion changed to a more mixed control. As in the first repetition the ennoblement of the Zn-10% Ni is thought to be due to the depletion of the more active zinc during the test.

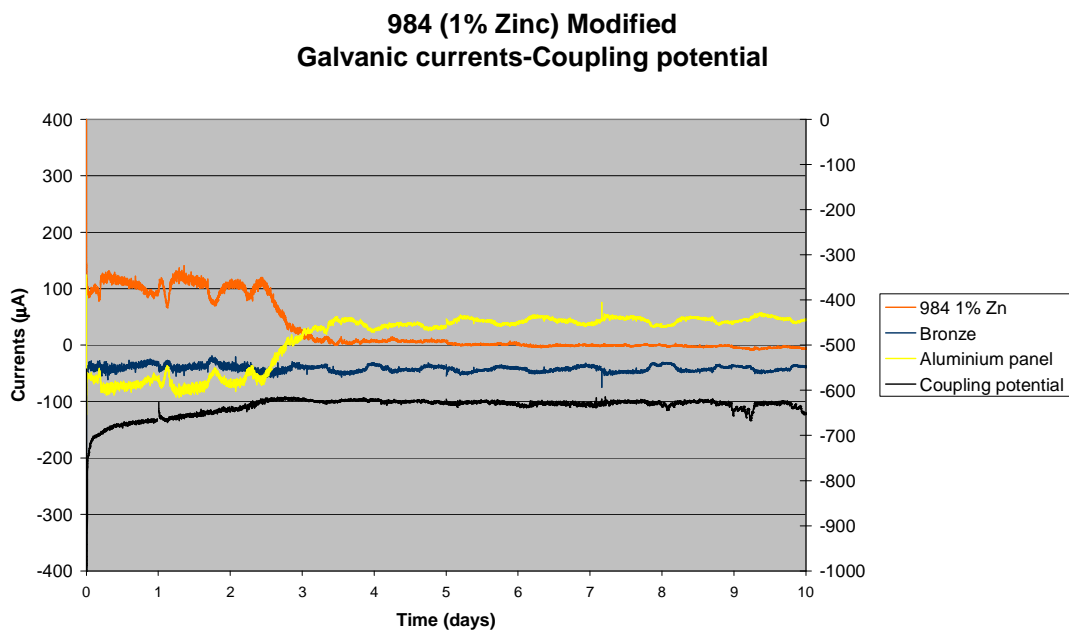


**Figure 132 Polarisation curves after one day. Zn-10% Ni, aluminium and bronze. One resistor setup in continuous lines, three resistors setup in dashed lines.**



**Figure 133. Polarisation curves after ten days. Zn-10% Ni, aluminium and bronze. One resistor setup in continuous lines, three resistors setup in dashed lines.**

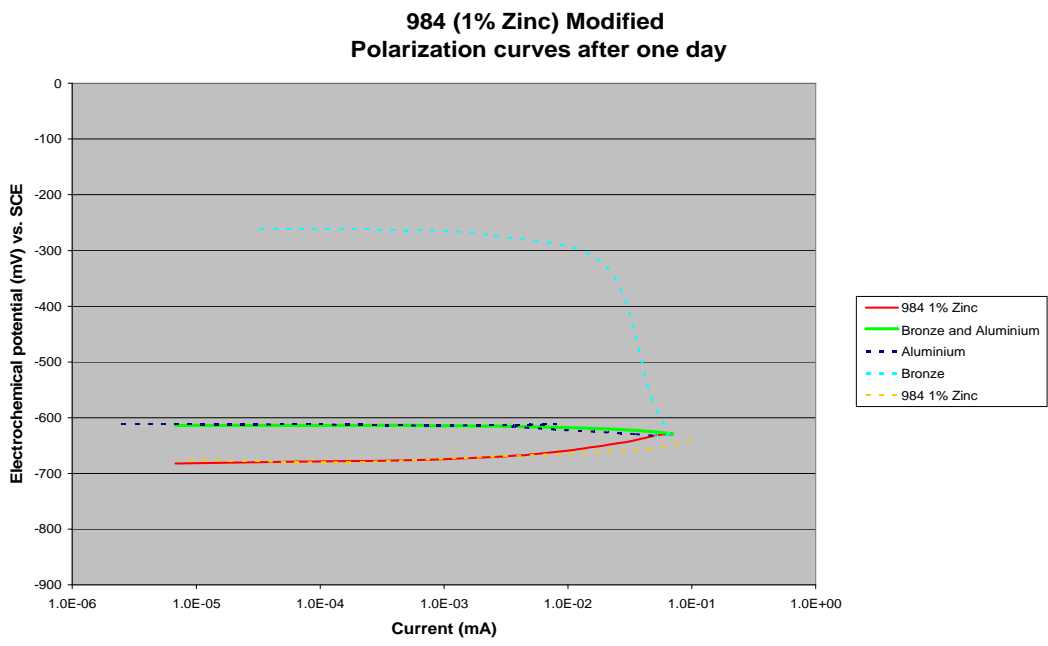
Figure 134 shows the galvanic corrosion measurement between the 984-1% zinc, the bronze and the aluminium panel. The coupling potential increased in two days and a half to a constant value of approximately -620 mV vs. SCE. At the same time the aluminium panel showed a reversal of its polarity changing from a cathodic to an anodic behaviour. The bronze remained a cathode for the entire test while the coating stopped to give protection when the aluminium became the anode. After the reversal of the aluminium the coating stabilized at around 0 mV. This behaviour confirms what was found qualitatively in the first repetition of the galvanic corrosion measurement.



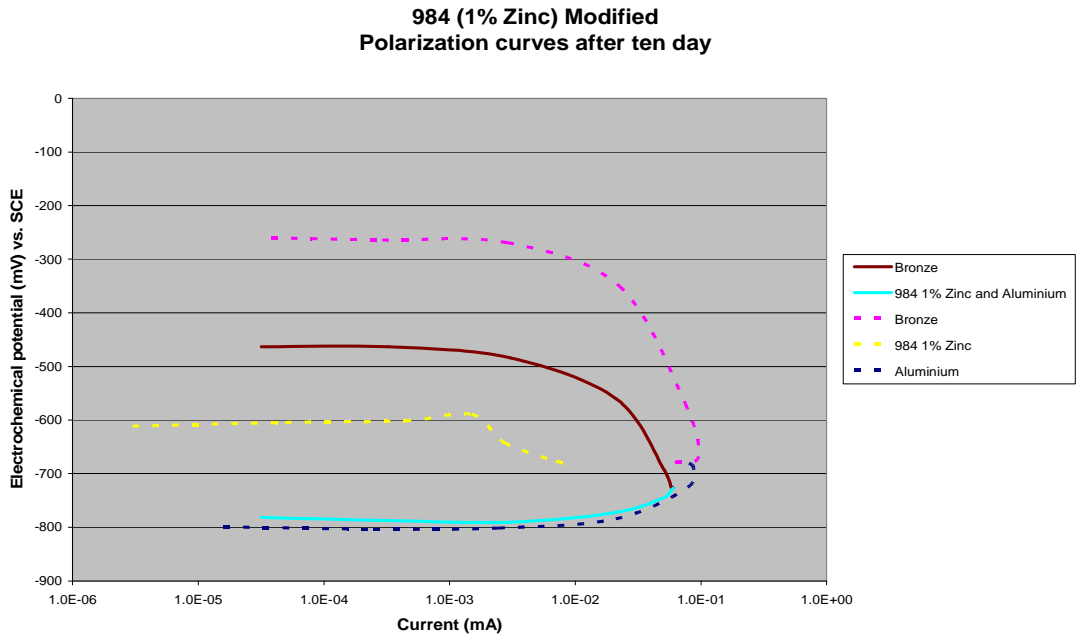
**Figure 134. 984-1% zinc, bronze and aluminium. Galvanic currents and mixed potential.**

Figure 135 and Figure 136 show the polarisation behaviour curves of the three panels after one and ten days. After one day, before the reversal took place, the corrosion process was under mixed control. The two open circuit potentials are very close with -610mV for the aluminium and -680mV for the 984-1% zinc. After the end of the test the OCP of the coating had increased to -610mV and the potential of the aluminium panel had decreased to -800mV. In this new situation the corrosion is under cathodic control. In both the plots the anodic curve were slightly polarized.



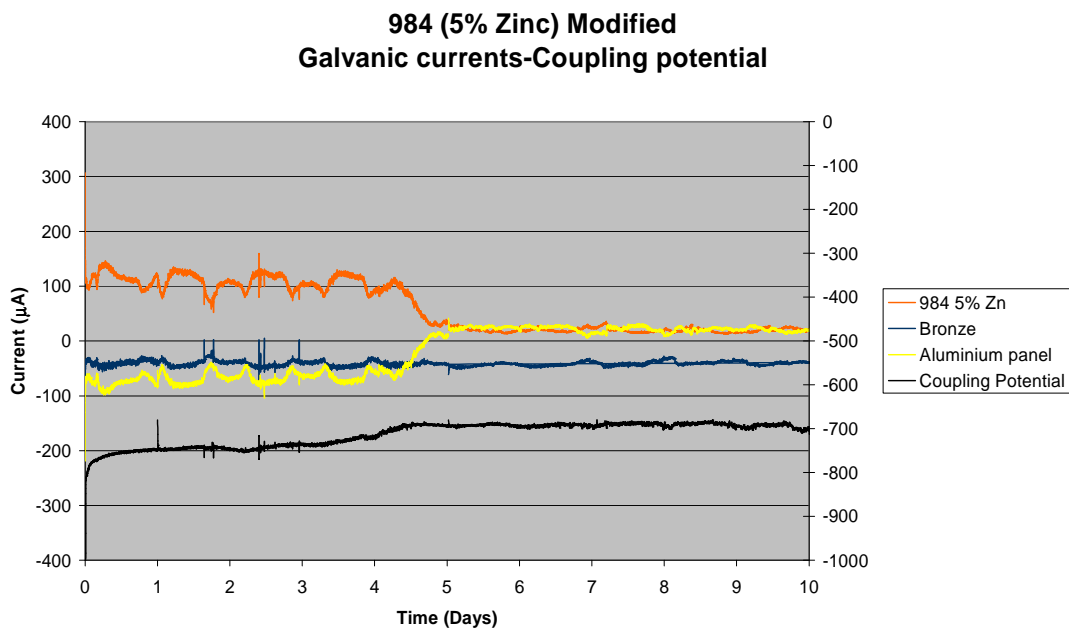


**Figure 135. Polarisation curves after one day. 984-1% zinc, aluminium and bronze. One resistor setup in continuous lines, three resistors setup in dashed lines.**



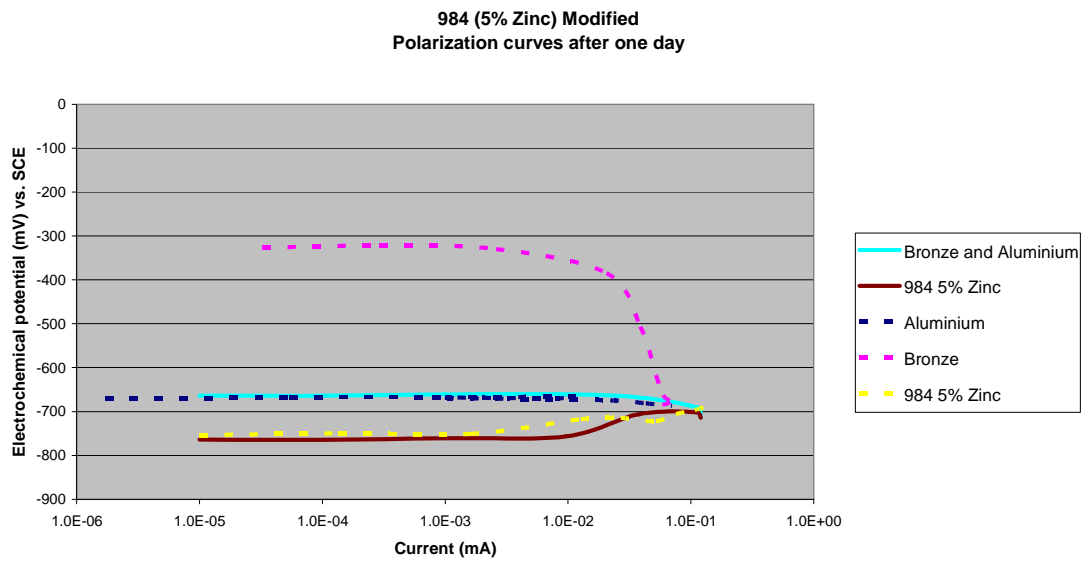
**Figure 136. Polarisation curves after ten days. 984-1% zinc, aluminium and bronze. One resistor setup in continuous lines, three resistors setup in dashed lines.**

Figure 137 shows the galvanic coupling of the 984-5% zinc modified. In this case, the reversal of the aluminium occurred after almost five days. After the reversal of the aluminium, the coating did not become the cathode but remained anodic continuing to give a small current to the bronze panel. The current of the bronze remains constant even after the reversal. This is explained by the Figure 139 where it is clear that the corrosion is strongly under cathodic control. The bronze cannot increase its current because this is limited by the rate of the oxygen that can be reduced on its surface. In this situation an increase of the areas of the anodes does not affect the current provided to the bronze because the reduction of oxygen is limited by its transport to the surface of the bronze.



**Figure 137. Zn-10% Ni, bronze and aluminium. Galvanic currents and mixed potential.**

The increase of the coupling potential before the reversal of the aluminium seems to suggest an increase of the potential caused by the ennoblement of the 984 coating. Once this process stopped the new mixed potential was higher than both the OCPs of the coating and of the aluminium and that is why only the bronze remained cathodic.



**Figure 138. Polarisation curves after one day. 984-5% zinc, aluminium and bronze. One resistor setup in continuous lines, three resistors setup in dashed lines.**

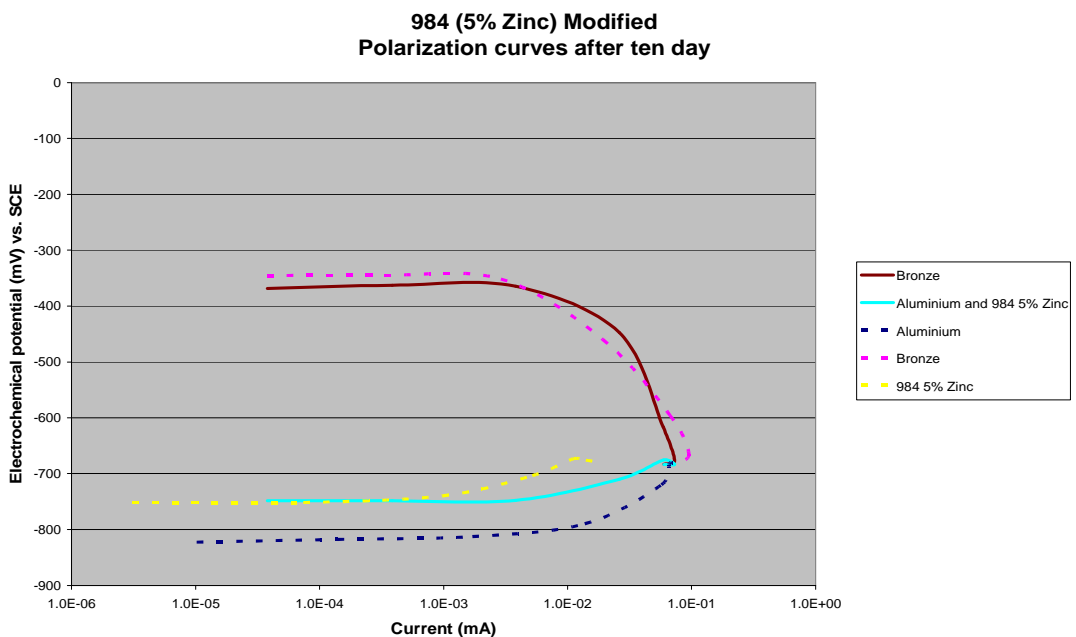
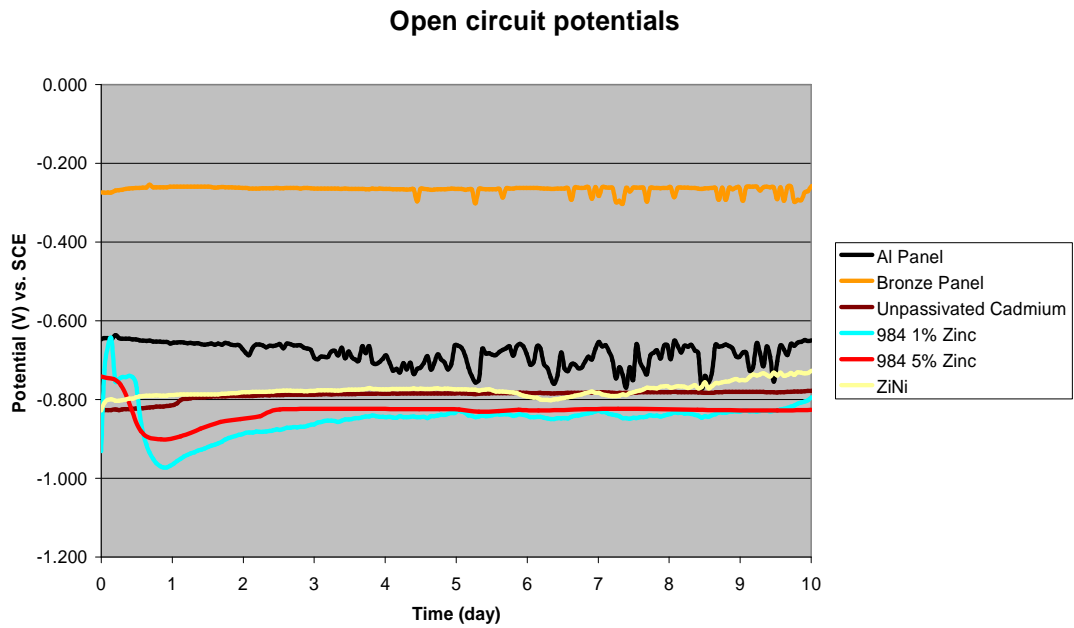


**Figure 139. Polarisation curves after ten days. 984-5% zinc, aluminium panel and bronze panel. One resistor setup in continuous lines, three resistors setup in dashed lines.**

### 3.2.3 Linear polarisation resistance

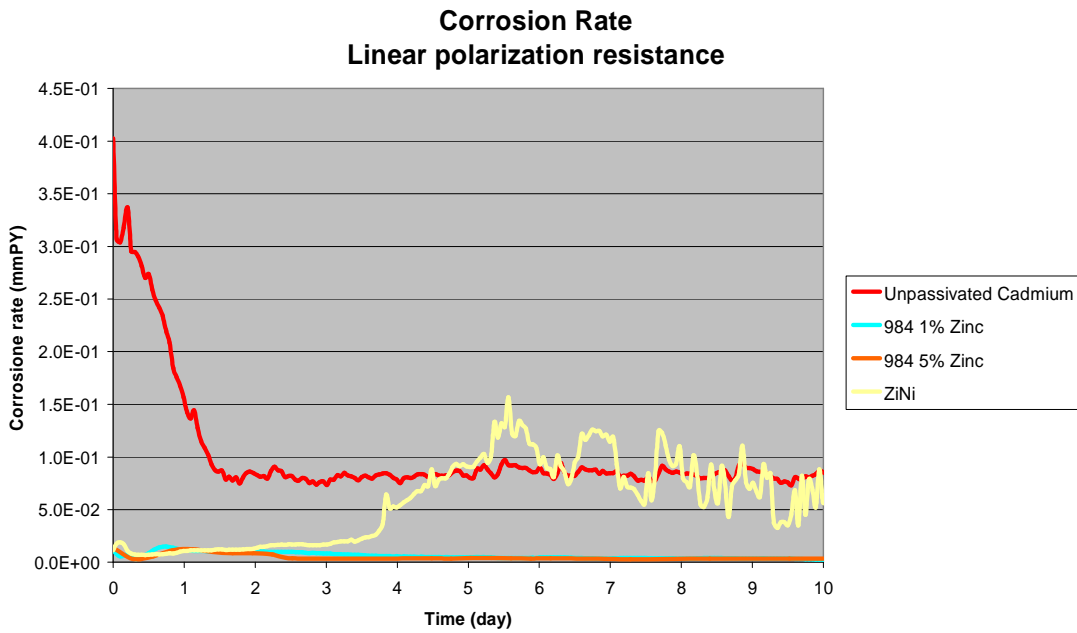
Figure 140 shows the open circuit potentials of unpassivated cadmium, Zn-10% Ni and the two 984 coatings modified with zinc, compared with the OCP of the bronze and the aluminium panels. Bronze was confirmed to be the noblest material, with a stable potential around -260 mV vs. SCE, while the aluminium panel showed a potential around -650 mV vs. SCE. Among the four coatings, 984-5% zinc was the most active at the end of the test, with a final value of 826 mV vs. SCE. 984-1% zinc stabilized more slowly than the 5 % of zinc and it remained more active for a longer period of time. Zn-10% Ni potential stayed at around -760 mV vs. SCE for approximately eight days and after that its potential became more active, to reach -726 mV at the end of the test. The increase in potential confirms what was shown by the galvanic measurement and seems to indicate an ennoblement of the potential due to the depletion of zinc. The Zn-Ni did not reach a potential more noble than the aluminium panel although its potential was still increasing at the end of the test. The galvanic test is more demanding for the coating than the simple self-corrosion test and for this reason its potential did not reach the potential of the aluminium in this test. A longer test would have probably caused a more severe depletion of zinc and would have raised its potential above the aluminium as concluded from the galvanic corrosion results.

Also the potential of the 984-1% zinc was slowly increasing in the last day confirming as for the Zn-Ni the ennoblement due to the preferential oxidation of the zinc particles.



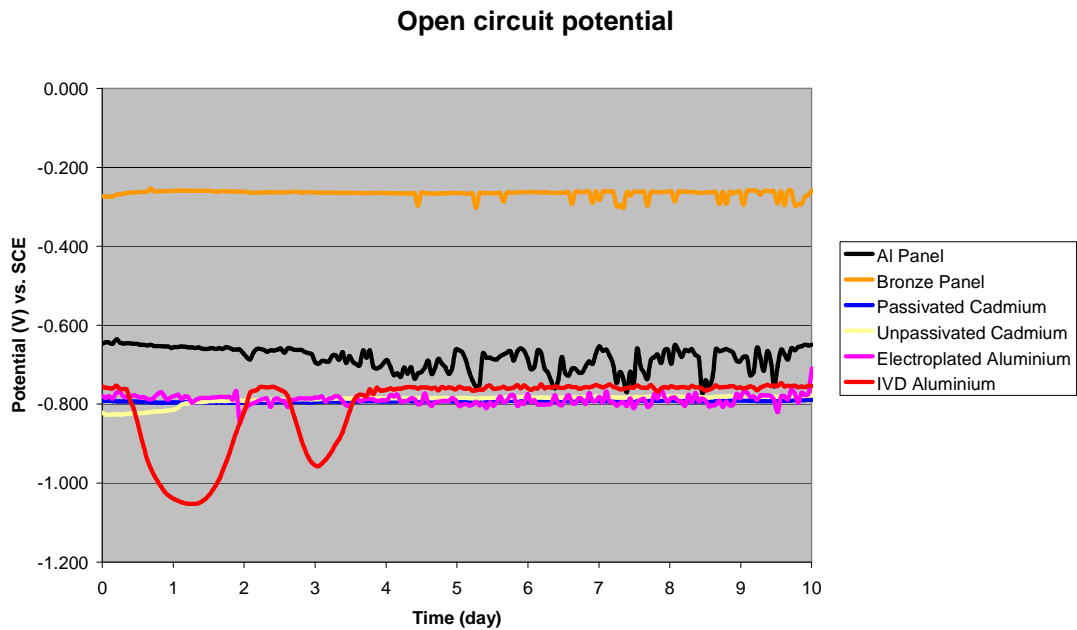
**Figure 140. Open circuit potentials of 984-1% zinc, 984-5% zinc, Zn-10% Ni and unpassivated cadmium compared with the aluminium and the bronze.**

Figure 141 shows the corrosion rates of these four coatings. Cadmium and Zn-10% Ni showed relatively high corrosion rates, with Cd corroding at 80  $\mu\text{m}/\text{y}$  at the end of the test and Zn-10% Ni at 60  $\mu\text{m}/\text{y}$ . 984-5% Zn and 984-1% Zn showed lower corrosion rates during the entire test. After ten days the corrosion rate of 984-5% Zn was 3.5  $\mu\text{m}/\text{y}$  and 2.4  $\mu\text{m}/\text{y}$  for the 984-1% Zn.



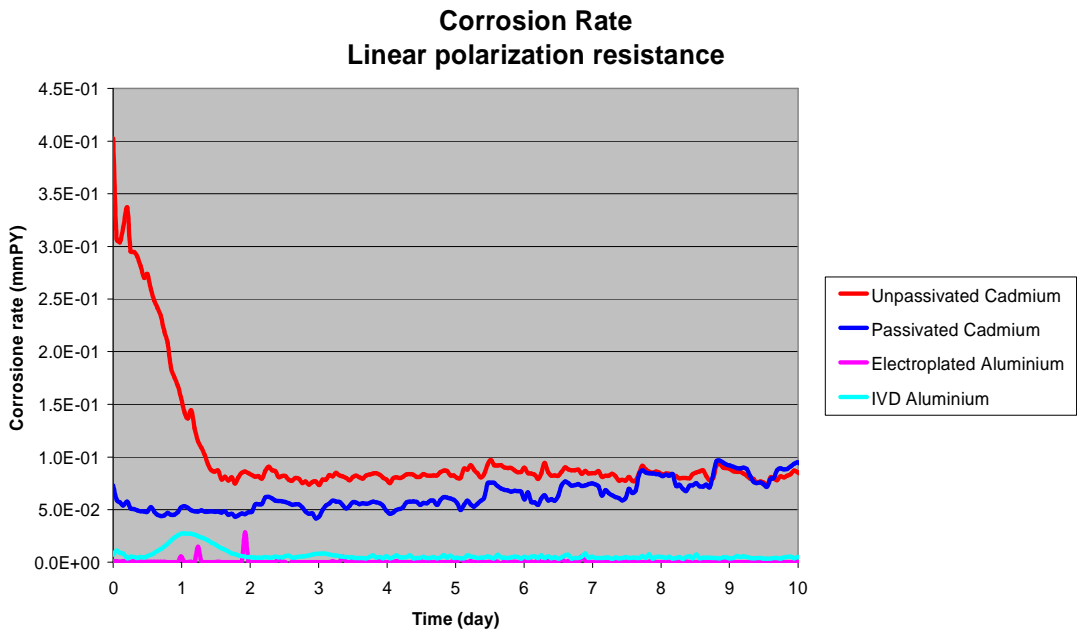
**Figure 141. Corrosion rates for unpassivated cadmium, 984-1% zinc, 984-5% zinc and Zn-10% Ni.**

Figure 142 shows the open circuit potential of the remaining three coatings; electroplated aluminium, IVD aluminium and passivated cadmium, compared with the aluminium panel, the unpassivated cadmium and with the bronze panel. Passivated cadmium was very stable during the entire test, with a potential of -780 mV and confirmed the good quality of this coatings in terms of potential stability. Nevertheless electroplated aluminium also showed a very stable potential around the same values of passivated cadmium. IVD aluminium showed a stable potential after the first four days but was slightly less active than the other coatings. Its potential was measured at -750 mV vs. SCE at the end of the test.



**Figure 142. Open circuit potentials for passivated cadmium, electroplated aluminium and IVD aluminium compared with aluminium and bronze.**

Figure 143 shows the corrosion rates of the same coatings; passivated cadmium, electroplated aluminium and IVD aluminium compared with unpassivated cadmium. Unpassivated cadmium corroded faster than passivated cadmium especially in the first day, reflecting the more active potential measured for this coating compared to the passivated one. Also the corrosion rate of the IVD aluminium reflected the trend of its OCP with higher corrosion rates in correspondence with the more active potentials. At the end of the test its corrosion rate was stable at around  $5\mu\text{m}/\text{y}$ . Electroplated aluminium showed a very low corrosion rate with an average of  $0.6\mu\text{m}/\text{y}$  over the entire test.



**Figure 143. Corrosion rates of passivated cadmium, unpassivated cadmium, electroplated aluminium and IVD aluminium.**



## 4 DISCUSSION

The discussion of the results regarding the sacrificial coating for high strength steel substrate will start with preliminary discussion on the corrosion potentials of the coatings. The corrosion potential of the coatings is the first important value to be discussed and compared with the electroplated cadmium, the coating that has been successfully used as a sacrificial coating for high strength steel [34]. The corrosion potentials can provide a first important indication for the coating selection and on the sacrificial properties of the coatings that will be discussed in the galvanic corrosion section. The variation of the potential of the coating with respect to the steel substrate is relevant since the potential of the coating must remain sufficiently negative to cathodically polarise the steel to a potential at which its corrosion rate is negligible [35].

A good alternative active coating is able to provide the same good cathodic protection to the steel as cadmium without increasing the risk of hydrogen re-embrittlement and also exhibits a low corrosion rate. All the tests were carried out in 3.5% NaCl solution and the assumption is made that while aqueous corrosion is complex and depends on many interrelated factors, useful information can be determined in short-term tests in which the coated steel is immersed in an aqueous solution with a high concentration of aggressive ions. This approach is, to some great extent, justified by the observation that during outdoor atmospheric corrosion the major part of the corrosive attack takes place just before the aqueous film dries out when, through evaporation, the concentration of aggressive ions is greatest [35].

SSRT have been carried out for the evaluation of hydrogen re-embrittlement and the distributions of results compared by using the statistical Student's t-test [36]. The primary use of SSRT is to furnish accepted procedures for the accelerated testing of the resistance of metallic materials to environmental assisted cracking under various environmental conditions [37] like in the case of the production of hydrogen as a consequence of the corrosion reactions.

At the end of this discussion, the galvanic corrosion of the coating has been combined and added to the coating self-corrosion rate, to calculate the total corrosion

of the coating in order to provide a useful indication on the possible duration in service of the coating.

The dissolution rates of the anode ( $r_a$ ) in a galvanic couple [38] can be obtained by adding the corrosion rate of the uncoupled alloy ( $r_0$ ) in the same environment to the galvanic rate ( $r_g$ ). The selection of the best alternative coating will be made on the basis of its ability to provide good sacrificial protection, to reduce the consequential risk of hydrogen re-embrittlement and to reduce its self-corrosion rate, expressed in terms of metal loss.

Figure 144 schematises the effect of the coating potential on the corrosion rate of the steel substrate and on the risk of hydrogen re-embrittlement

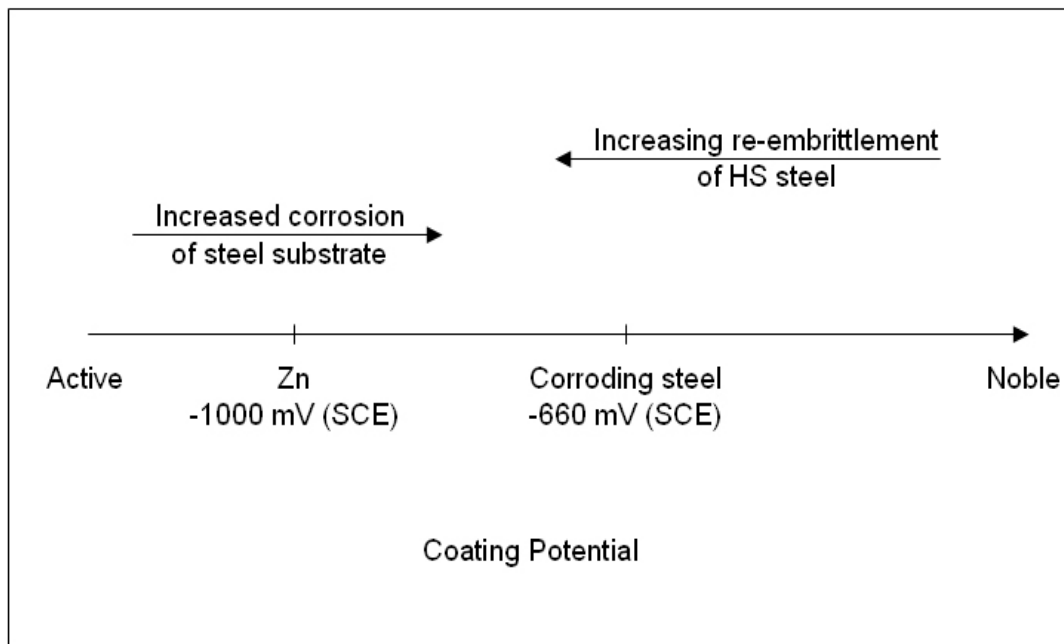


**Figure 144. Effect of the sacrificial coating potential on the corrosion of the steel and on the risk of hydrogen re-embrittlement**

SSRT results will be compared with similar results found in literature [39] and a new mechanism that influences the absorption of the hydrogen in presence of a sacrificial coating will be proposed.

The discussion will continue with the case of the study of the compatibility coating for the aluminium bronze assembly. Differently from the high strength steel substrate, the risk of hydrogen re-embrittlement has not been studied for the bronze substrate since it is not a concern for this material. The discussion will show the beneficial effect of the use of the coating in reducing the corrosion between the uncoated bronze and the aluminium.

The author will consider the ability of the coating to provide a good sacrificial protection in comparison with the self-corrosion rate of the coating that should be minimised. The galvanic corrosion will be added to the self-corrosion following the same procedure described by Mansfeld [38] and already used for the steel substrate. The importance of the equivalent weight and the density of the sacrificial compatibility coating will be explained in the calculation of the metal loss from the galvanic corrosion expressed in terms of current.

The overall discussion will provide useful guidelines explaining different approaches in the choice of sacrificial coating for steel substrate or for the selection of a compatibility coating for the assembly.

In the second case it will be explained as two different criteria that can be considered and the coating that could behave either as sacrificial to both the assembly component or could have a potential in between the two components. In this second case the coating will act as a compatible coating minimising the total corrosion of the system bronze-coating-aluminium but without totally preventing the corrosion of the aluminium component.

#### 4.1 SELECTION OF SACRIFICIAL COATINGS FOR HIGH STRENGTH STEEL SUBSTRATE

The first part of this project was to extend the life of the commercial 984 SermeTel coatings by additions of more active particles like Zn and Mg without significantly

increasing the risk of hydrogen re-embrittlement that can be caused by more active coatings. Zn and Mg addition to aluminium coatings have been studied before [22] by the addition of Mg and Zn ions to ion-beam-assisted deposition coatings, which proved to be beneficial in improving the sacrificial protection of the coatings. The sacrificial protection of the high strength steel substrate was evaluated and compared with the reference coating to be replaced – the electroplated cadmium coating. Together with the modified commercial 984 SermeTel, three more coatings were included in the project; the IVD aluminium that has been previously proposed [7, 40-42] as an alternative to cadmium and a 984 SermeTel without chromates, in order to evaluate the importance of the presence of chromates in the 984 binder. An additional coating similar to the unmodified 984 but containing 100% 7075 aluminium alloy particles was included in the group of alternative coatings to be studied in order to compare the characteristics of the coatings produced with aluminium/zinc and aluminium/magnesium particles, with a coating produced with aluminium alloy particles containing Zn and Mg as alloying elements.

#### 4.1.1 Extent of the problem

Commercial aluminium 984 SermeTel coating has been studied before as an alternative to cadmium replacement but concerns have arisen about its sacrificial protection characteristics and tendency to passivation [1].

Electrochemical tests and marine atmosphere exposure tests carried out in previous work [1] have shown that the coating is prone to passivate and not able to provide the same protection as electroplated cadmium. In this work a 12 month marine atmosphere exposure test on scribed 984 SermeTel and electroplated Cd showed signs of red rust on the SermeTel scribe marks. Cd scribed panels did not display any signs of corrosion degradation either on their surfaces or on their scribed marks. Differently from the SermeTel 984, the electroplated Cd was able to provide protection to the substrate in the scribed region. The signs of red rust on the 984 SermeTel scribed regions showed that the coating is not able to provide sacrificial protection for the same period of time as electroplated Cd.

Laboratory tests carried out at Cranfield University in 3.5% NaCl solution have shown that SermeTel 984 does not remain sufficiently active for the same duration as electroplated cadmium. The potential of electroplated Cd in 3.5% NaCl solution, -800mV vs. SCE, can be considered as a reference potential to be achieved by the alternative coatings in order to provide similar sacrificial protection to the steel.

#### 4.1.2 Corrosion potentials of the alternative coatings

Table 16, Table 17 and Table 18 show the initial, final and average potentials of the coatings during the test. Together with the average potentials over ten days, the standard deviations have been calculated to evaluate the stability of the potential in the same period. Addition of zinc or magnesium lowered the potential of the unmodified coating but only the 50% Zn, the 30%Al/Mg and the 50%Al/Mg remained significantly more active than the unmodified 984 until the end of the test, as seen Figure 12, Figure 15 and Figure 19 in section 3.1.1.

Coating	50%Zn	10%Zn	3%Zn	0.5%Zn	50%Al/Mg	30%Al/Mg	CF1725
mV(SCE)	-1110	-1020	-760	-750	-1250	-1150	-720
Coating	IVD1	IVD2	IVD3	7075	CR984	El Cd	
mV(SCE)	-750	-750	-760	-720	-700	-820	

**Table 16. Initial corrosion potential of the coatings**

Coating	50%Zn	10%Zn	3%Zn	0.5%Zn	50%Al/Mg	30%Al/Mg	CF1725
mV(SCE)	-1050	-770	-760	-750	-1040	-940	-690
Coating	IVD1	IVD2	IVD3	7075	CR984	El Cd	
mV(SCE)	-740	-740	-760	-730	-740	-800	

**Table 17. Corrosion potential of the coatings after 10 days**

Coating	50%Zn	10%Zn	3%Zn	0.5%Zn	50%Al/Mg	30%Al/Mg	CF1725
mV(SCE)	-1070	-810	-790	790	1090	970	680
St Dev %	1.0	4.7	6.2	7.6	5.3	7.1	2.0
Coating	IVD1	IVD2	IVD3	7075	CR984	El Cd	
mV(SCE)	810	740	790	-730	-780	-810	
St Dev %	8.8	2.2	7.0	3.6	5.5	0.4	

**Table 18. Corrosion potential average in ten days and standard deviation in percentage**

The initial corrosion potentials of the 984 coatings modified by the addition of magnesium are more active than the SermeTel 984 and more than the electroplated cadmium. The addition of magnesium particles led to the same effect as the zinc particles but with an increased effect due to the greater activity of magnesium compared to zinc. At the end of the test, all the zinc or magnesium modified coatings were more active than the commercial 984 and the standard deviation shows that the coating with more active particles was more stable during the test.

After 10 days only the 50%Zn, the 50%Mg/Al and the 30%Mg/Al resulted in more activity than the electroplated cadmium. The IVD coating showed an initial potential more active than the 984 but the values became closer after ten days of exposure.

The corrosion potential tests carried out on the 7075 coating showed that the zinc and the magnesium contained in the alloy, not as different particles, did not have the same effect on the modification of the SermeTel 984 potentials. The 7075 coating corrosion initial potential was slightly more active than the SermeTel 984 (-20mv) but at the end of the test the 7075 was less active than the 984. In the 7075 commercial aluminium alloy, the zinc is normally contained in percentages between 5.1 and 6.1 in weight and the magnesium between 2.1 and 2.9 in weight. The small addition of less active elements such as copper present in a composition of 1.2-2.0% in weight could, in part, mitigate the effect of the magnesium and zinc addition. In

the past [22] it was noted that addition of magnesium and zinc by addition to aluminium coating with a ion-beam-assisted deposition (IBAD) shifted the corrosion potential of the pure film to more active values.

The elimination of chromium from the 984 binder did negatively affect the tendency to passivation of the coating. The test showed that the initial corrosion potential of the 1725 coating was 20 mV more active than the commercial 984 but at the end of the test the chromium free coating was 50 mV less active than the 984, far from the electrochemical potential of the electroplated cadmium. In terms of final electrochemical potential, the CF1725 showed the least active potential.

The corrosion potential measurements have shown that the potential of the unmodified 984 is not as stable as the electroplated cadmium which is by far the most stable coating. The 984 was very active during the first 5 days of the test. Although this behaviour seemed to be related to the coating activity during the first days due to the active surface, on the basis of all the tests on the modified SermeTel coatings, it seems it could be also related to the presence of chromates in the binder. This seems to be suggested by the behaviour of the chromium free 1725 – the only coating that did not show any active behaviour in the first days. This coating showed a very stable corrosion potential but probably was not active enough to provide a sufficient sacrificial protection to the steel. Although it has not a sufficiently active potential, the CF 1725 would be an optimum coating for further development of a chromium free coating. Its stable potential could be lowered by the addition of zinc and magnesium which have been shown to work in this direction.

The standard deviation shown in Table 18 is a useful parameter to express the stability of the electrochemical potential during the test. It shows that a greater addition of active particles tends to stabilise the corrosion potential.

#### 4.1.3 Summary of self-corrosion rates

Corrosion currents have been integrated over the exposure time to calculate the charge passed as a function of time. The total charge density passed in ten days is proportional to the metal loss through constants such as the element valence and the

metal density. At this stage the total charge passed after ten days is an important parameter to be linked to the composition of the coatings. Figure 145 shows a comparison of the charge passed for all coatings and this can be regarded as an indicator of the relative rates of self-corrosion metal loss.

Of the zinc containing 984, the highest charge density occurred in the 50%Zn composition and reduced systematically with lower zinc contents. Similarly, the addition of Mg/Al powders increased the charge passed.

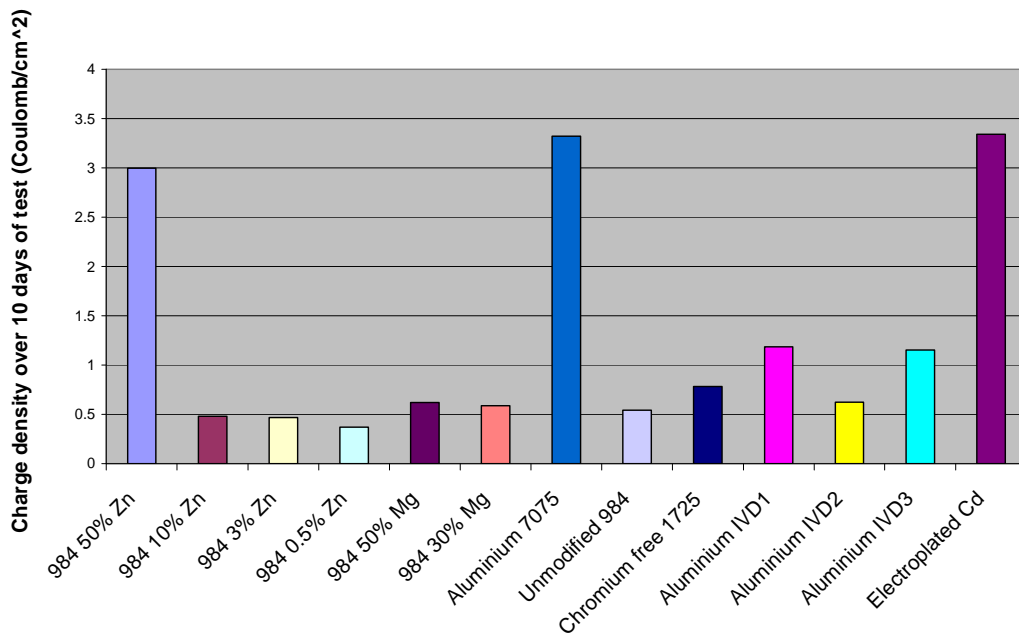


**Figure 145. Total charge density passed by self-corrosion of coatings in 10 days in quiescent 3.5% NaCl solution**

The self-corrosion rate of 7075 was particularly high, presumably due to the effect of copper rich precipitates and other intermetallics in the microstructure. These intermetallics are presumably [43] Al<sub>7</sub>Cu<sub>2</sub>Fe that may serve as a local cathode in the evolution of localised corrosion of aluminium alloy 7075 and is capable of sustaining oxygen reduction reactions at rates of several hundreds of  $\mu\text{A}/\text{cm}^2$ . It is thought that while the 7075 is less likely to passivate than 984, the rate of self-corrosion would limit the coating life. Interestingly, the 1725 chrome free had a higher charge density than the chromium containing 984.



Of the three IVD coatings, the wax layer on IVD2 appeared to have acted as a barrier and reduced the charge density.

High self-corrosion rates are generally unwanted for the coatings. The galvanic corrosion of the coatings to the steel represents the current provided by the coating for protection; the self-corrosion rate has only the effect of limiting the life of the coating. In section 4.1.10 the galvanic corrosion of the coatings will be compared to the self-corrosion rate in terms of charge density. Successively the same comparison will be made on the basis of the metal loss.

#### 4.1.4 Appearance of red rust

A summary chart of galvanic measurements after one day of exposure is shown in Figure 146. The time of the comparison was chosen in one day to be able to compare the coating before any of the coatings or the steel panels showed signs of corrosion. Higher zinc contents resulted in more active average potentials in the first day. Excluding the potential of the 0.5%Zn 984, it is possible to identify a trend in the addition of the more active particles, zinc and magnesium, with the current and the mixed potential of the coating during the first day.

As expected, the more active potentials generally corresponded to higher galvanic currents being supplied to the steel – this providing a greater degree of corrosion protection. This protection has been compared by plotting the time of appearance of the first red rust and within each category of coating there is a fairly systematic trend.

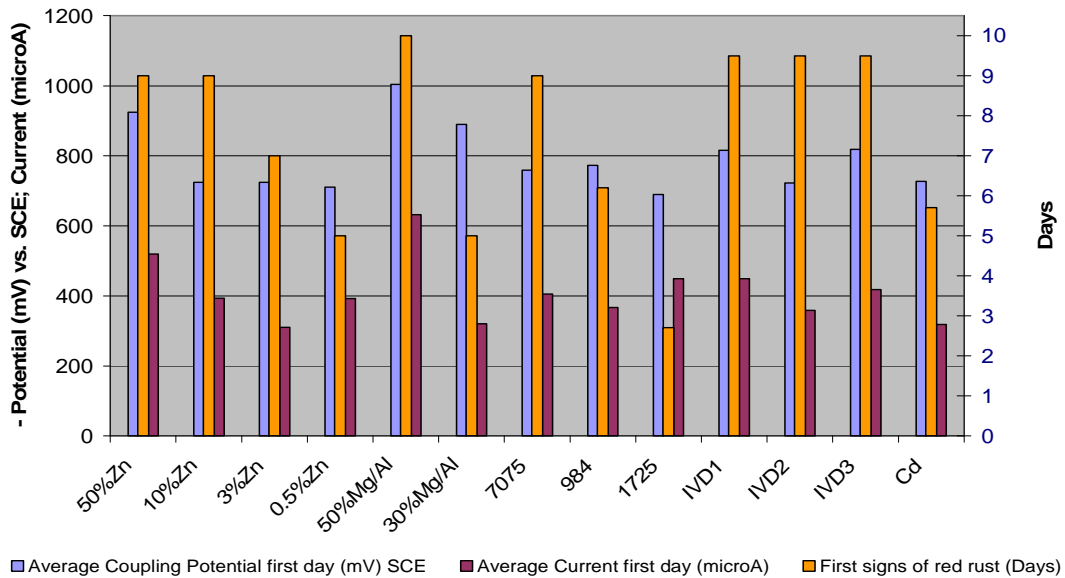


**Figure 146. Average coupling potential during the first day, average current over the first day and time of appearance of signs of red rust.**

For example, the higher zinc contents corresponded to the longer times to red rust. Of the Mg containing coatings, the 50%Mg coating had a longer time to red rust than the 30%Mg coating. The 7075 coating performed very well in this aspect, although it was noticed earlier that the self-corrosion rate would limit the coating life. The three IVD coatings all performed well but cadmium had a relatively short time to red rust, due, it is thought, to the high rate of self-corrosion. In each case the life of these coatings could be improved with the use of an appropriate passivation treatment.

#### 4.1.5 Hydrogen re-embrittlement risk

From the Weibull plot in Figure 147 it is clear that a statistical analysis is necessary to distinguish between different mean failure times. If we consider as an example the 0.5%Zn984 and 3%Zn984 coatings, the means of times to failure for these coatings were 11.1 hours and 11.7 hours. We would like to know if these two coatings promote different amount of hydrogen re-embrittlement i.e. if the different amount of Zn really influences coating characteristics or if the difference in the two means

simply belongs to a normal statistical variation of the mean. The Student's t test, on the basis of the two means, their standard deviations and the number of specimens tested for each set of coatings, allows an assessment of whether the two sets of coatings really belong to different populations.

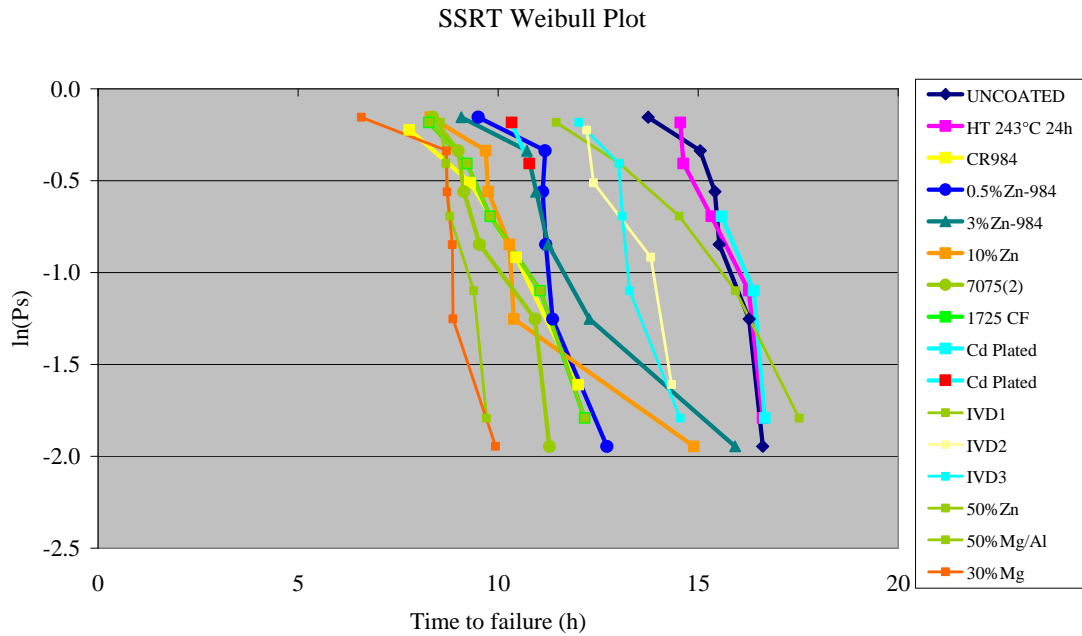


**Figure 147. Weibull Plot of all the coatings**

The five 50%Zn 984 specimens tested failed in an average time of 9.03 hours showing evidence of hydrogen re-embrittlement. 50%Mg/Al 984 specimens failed with an average of 8.56 hours and 30%Mg/Al 984 with 8.62 hours. IVD coatings showed better results with 14.49 hours for IVD1, 13.18 for IVD2 and 13.19 for IVD3. However, the coating showed evident signs of rust after the test, suggesting that the good results (in terms of re-embrittlement) probably hide a low corrosion cathodic protection. The SEM analysis on some of the SSRT IVD specimens after the test, has shown a large area of the specimen where the coating has been removed. Since the electrochemical tests had not shown a particular problem with the IVD coating, this suggests that the coatings might have bad mechanical characteristics and are unable to follow the specimen deformation during the SSRT.

Embrittlement indices have been calculated from Equation 26 to provide a more practical value to compare the different coatings. However, the number itself could lead to wrong conclusions if not supported by a statistical test. It is important to provide the embrittlement indices together with a statistical test on the different distributions. Student's t-test was selected to support analysis of the embrittlement indices.

$$EI = 1 - \frac{Ttf_{coated}}{Ttf_{uncoated}}$$

26

Re-embrittlement indices are shown in Figure 148. 50%Mg/Al 984 has shown a higher index than 30%Mg/Al 984 as expected. 984A 50%Zn has shown the highest re-embrittlement index, 0.41, among the Zn modified coatings tested as expected from its active electrochemical potential. 50%Mg/Al 984 has shown the highest re-embrittlement index, 0.44, among all the coatings tested also as expected according to its potential, as the most active among all the coatings tested.

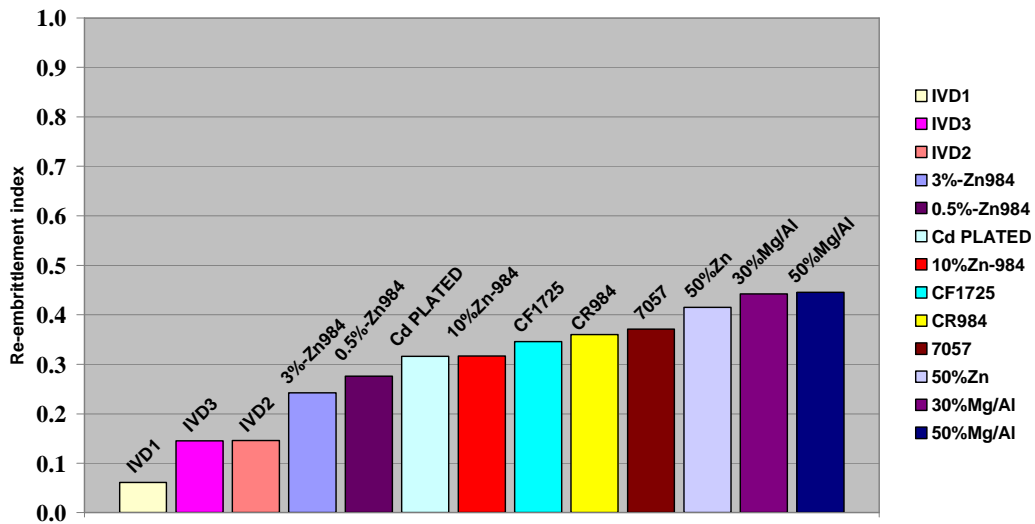


**Figure 148. Re-embrittlement indices of all the coating.**

When using the Student's t-test to study whether the distributions of results belong to different populations, the level of confidence for that affirmation must be declared.

By increasing the level of confidence it becomes more difficult to be able to distinguish between different sets of coatings. A larger number of specimens for each set would be useful to increase the level of confidence. The following tables show the results for the Student's t-test for all the coatings, compared with the uncoated specimens, the HT 243 and the electroplated cadmium. The tables have been made using  $\alpha=0.05$ , i.e. a level of confidence of 95%. When the cell is green it means that the Student's t-test has shown that, with a level of confidence of 95%, the two distributions of results belong to different populations. In this case, it appears that compositions influence their behaviour to hydrogen re-embrittlement. The power of the test,  $\beta=0.1$ , must be taken into consideration when the two distributions do not belong to different populations. If this is the case it is possible to assert that with a power of the test of 90% the two distributions belong to the same population.

	Uncoated	HT	984	984 0.5Zn	984 3Zn	984 10Zn	984 50Zn	
Uncoated								
HT								
	984 30Mg	984 50Mg	7075	1725	IVD1	IVD2	IVD3	Cd Plated
Uncoated								
HT								

**Table 19. Student's t-test on time to failure means for a 95% level of confidence. Green=coatings distributions belong to different populations; Red=coatings distributions do not belong to different populations**

In Table 19 the comparison between the uncoated specimens and the HT shows that that the two distributions belong to the same population with 90% of probability. This means that the heat treatment at 243<sup>0</sup>Celsius did not cause hydrogen re-embrittlement in the steel. Since all the SermeTel coatings were cured at this temperature this allows for the exclusion of any effects of re-embrittlement caused by the heat treatment.

The same table shows that, compared to the uncoated steel, all the coatings caused re-embrittlement in the steel, except the IVD1. As will be explained later, the IVD1

aluminium detached from the steel during the SSRT, probably because of bad adhesion to the substrate, and the absence of re-embrittlement can be attributed to this. The IVD2 and IVD3 remained probably in part attached or close to the substrate because of the additional external wax and PFTE layers.

	984	984 0.5Zn	984 3Zn	984 10Zn	984 50Zn	984 30Mg	984 50Mg
Cd Plated							
	7075	1725	IVD1	IVD2	IVD3		
Cd Plated							

**Table 20. Student’s t-test on time to time to failure means for a 95% level of confidence. Green=coatings distributions belong to different populations; Red=coatings distributions do not belong to different populations**

Table 20 shows the results of the Student’s t-test for the electroplated Cd and the alternative coatings. Comparing the test with the calculation of the re-embrittlement indices shown in Figure 148, there is a probability of 95% that the three IVD coatings can cause less re-embrittlement and the same probability that the 50%Zn 984, the 30%Mg 984 and the 50%Mg 984 can cause more re-embrittlement. The test shows that on a statistical analysis a small addition of zinc to the commercial 984 did not lead to an increase in the risk of re-embrittlement compared with cadmium. The same result was obtained with the three coatings without addition of zinc, i.e. the 7075, CF1725 and the 984.

#### **4.1.5.1 IVD coating detachment**

IVD coatings showed unexpectedly good results in terms of re-embrittlement but all the IVD series coating showed evident signs of corrosion during the SSRT. Despite the fact that this coating had not shown such a fast corrosion during the corrosion tests, the SSRT in the 3.5%NaCl solution seemed to be very demanding for the coating. SEM analysis has shown the almost total absence of re-embrittlement in the IVD1 and this was probably due to a severe detachment of the coating from the substrate that has reduced the cathodic protection and the amount of hydrogen produced. Figure 149 shows the surface of one IVD1 SSRT specimen after the test

with the mapping of the iron. Several similar areas were found everywhere on the specimen surface that might suggest a severe detachment of the coating during deformation.

Other works for the study of Cd replacement by aluminium based coatings have shown that the IVD aluminium has shown poor adhesion of this coating on high strength steel substrate [44]. In the cited report the coating showed “significant flaking/peeling” damages as a result of the bend adhesion test.

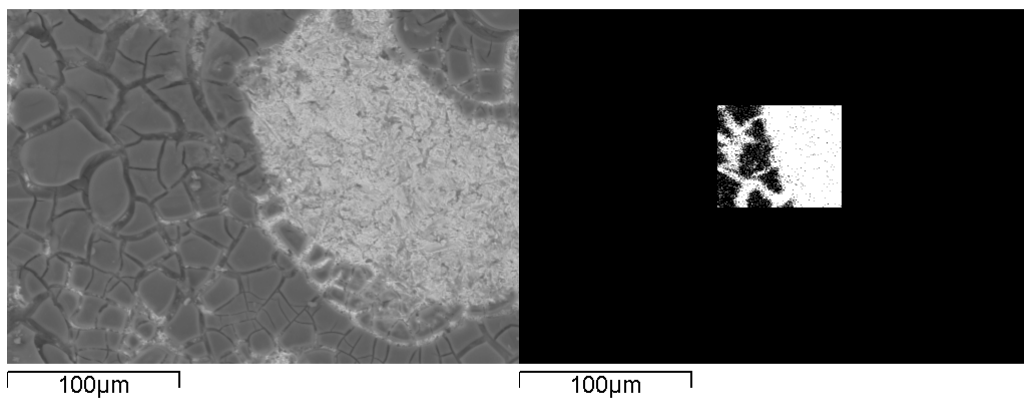


**Figure 149. IVD1. Secondary electrons SEM image on the left and iron mapping on the right. Bias 15kV.**

#### 4.1.6 Effect of applied cathodic potential

The results of the re-embrittlement test were compared with other studies on SermeTel coatings, electroplated cadmium and electroplated aluminium. In a previous work [4] the effect of hydrogen re-embrittlement on AISI 4340, caused by holding uncoated specimens at a range of cathodic potentials in 3.5% NaCl solution, was compared with the amount of re-embrittlement caused by the application of a sacrificial coating on the steel substrate as shown in Figure 150. The mean times to failure were compared with the potential applied for the uncoated specimens and with the coating potentials for the coated specimens.

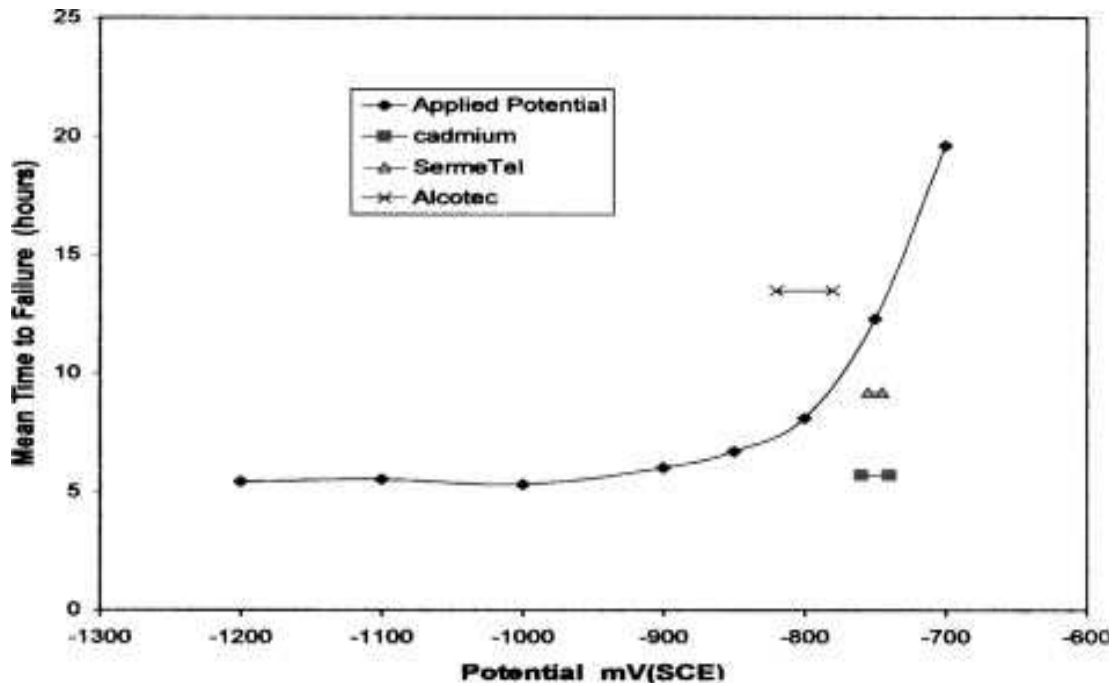


Figure 150. Comparison of mean failure times for specimens with freely corroding coatings and applied cathodic potentials. From [4] fig.7 p.31.

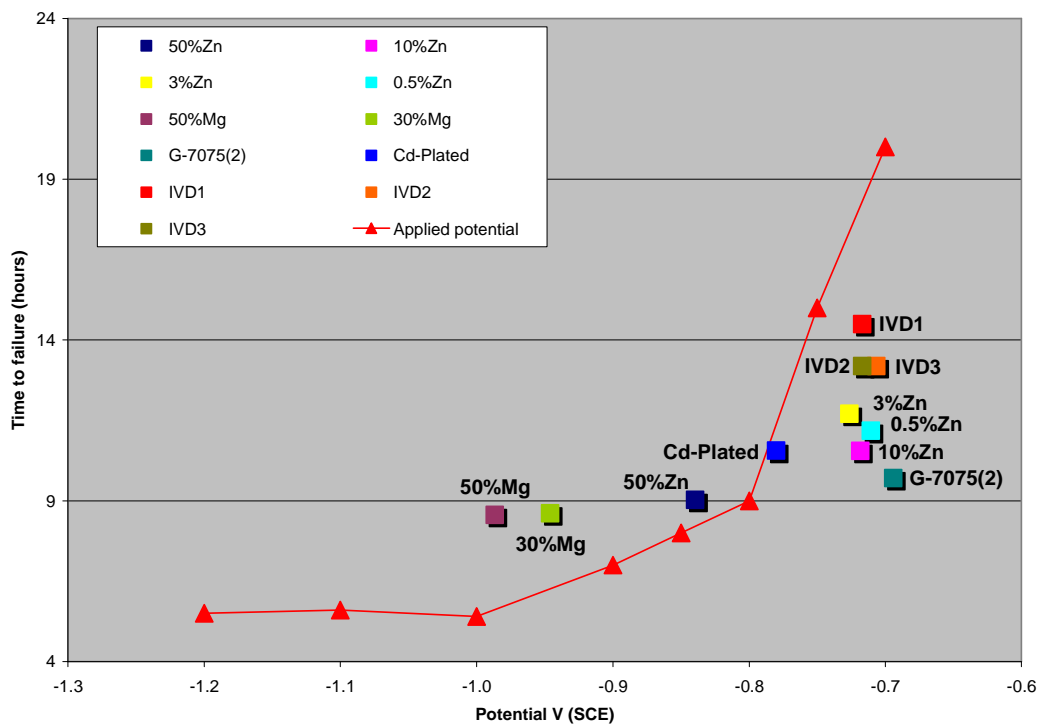


Figure 151. Comparison of mean failure times for specimens with freely corroding coatings and applied cathodic potentials.



The same comparison was made in this work and the results are shown in Figure 151. Like in the work cited some of the coatings, 50%Mg, 30%Mg and 50% Zn caused less re-embrittlement than the equivalent potential applied to the uncoated steel. Many others caused more re-embrittlement lying below the applied potential curve. The point above the curve can be explained by considering the effect of the coating barrier mentioned by the author while, in order to explain the presence of points under the curve, an additional mechanism that coexists with the consideration of the barrier effect of the coating will be proposed in the next section.

When considering the hydrogen re-embrittlement of coated high strength steel under tensile stress, the extent to which re-embrittlement occurs in a particular test depends on several factors [39]:

- a) the electrochemical potential of the coating and the resulting couple potential with the steel
- b) the presence of through-thickness flaws in the coating, which leave areas of steel exposed
- c) the rate of hydrogen uptake by the exposed steel
- d) hydrogen transport and trapping within the steel
- e) the susceptibility of the steel's microstructure to crack initiation and propagation

The electrochemical potential of the coating and the resulting couple potential with the steel is one of the parameters that determine the amount of hydrogen produced in the reactions. Furthermore the steel and coating exchange current densities also determine the amount of hydrogen produced on the two surfaces which is responsible for the re-embrittlement. This will be discussed in more details in section 4.1.7.

The presence of through-thickness flaws in the coating, which leave areas of steel exposed, increases the area of substrate exposed to the corrosive environment. The substrate exposed in correspondence with the coating flaws is directly exposed to the hydrogen accelerating hydrogen uptake in these sites. Less porous coatings give the advantage of leaving fewer areas of the steel exposed to corrosion with an added

advantage in the life of the coating, reducing at the same time the number of sites where the steel is directly exposed to the hydrogen.

The rate of hydrogen uptake by the exposed steel, the hydrogen transport and trapping within the steel and the susceptibility of its microstructure to crack initiation and propagation are characteristics belonging to the substrate and common to all the specimens. Therefore, they are not responsible for the differences in hydrogen re-embrittlement observed between the different coatings tested.

#### 4.1.7 Effect of the exchange current density on the hydrogen re-embrittlement

When considering an aluminium coating and a steel substrate, the hydrogen density produced per unit area is higher on the steel than on the coating. In this situation, an uncoated specimen, held at the same potential of the equivalent coating should suffer a higher re-embrittlement than the coated specimen. For instance, the sample G7075 in Figure 151 failed in 9.7 hours with a potential of -694 mV (SCE) while the uncoated specimen held at the same potential hardly showed any re-embrittlement, failing in 20 hours. In this case, if the hydrogen produced on the aluminium was higher than that produced on the steel, a coating with a bad barrier effect to the hydrogen would let the hydrogen permeate and easily reach the steel substrate, increasing the re-embrittlement. Figure 152 shows an illustration of a similar situation for an aluminium coating on the steel substrate. The exchange current density of the aluminium is  $10^{-3}$  times smaller than that of the steel, so even in the case of a fast permeation through the coating the higher re-embrittlement would remain unexplained.

The exchange current density values are dependent on the materials as reported from different authors [45, 46].

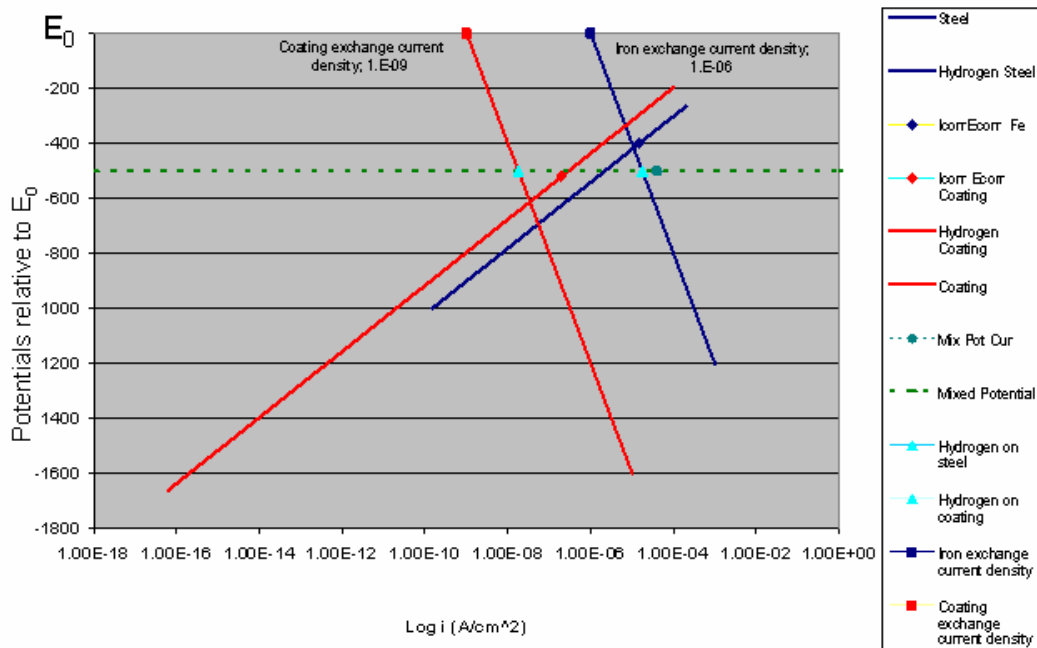


**Figure 152. Effect of the exchange current density on the hydrogen production.  $E_0$  is the equilibrium electrode potential at the pH of the experiment**

The plot in Figure 152 has been drawn using a mix of experimental values and literature values and is meant to be an illustration. The exchange current density for following the reaction



was considered to be  $1 \times 10^{-9}$  Amp/cm<sup>2</sup> for the coating and  $1 \times 10^{-6}$  Amp/cm<sup>2</sup> for the steel. These values are reasonable if considering aluminium or zinc coatings on the basis of the data that can be found in literature [table 3.2, p.98 [46]]. The mixed potential  $E_{\text{CORR}}$  used in the illustration and the value for  $I_{\text{CORR}}$  is -500 mV vs. SHE and  $4 \times 10^{-5}$  Amp/cm<sup>2</sup> are the experimental values for the couple steel/IVD aluminium. The free corrosion potentials and the free corrosion current in the example were also taken from the experimental result for the steel and IVD aluminium.

#### 4.1.8 Increase of the amount of the hydrogen absorbed in the porosity of the coating

The amount of hydrogen formation, adsorption and consequential absorption has been proposed by many authors [28, 47-49] and reported by others [39, 50]. The mechanism has been proposed to follow a reaction sequence at the cathode surface in the form:

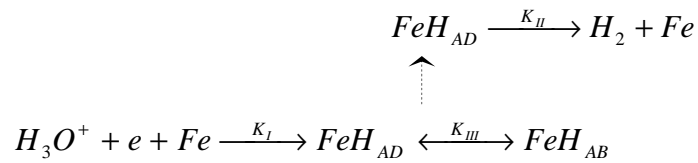


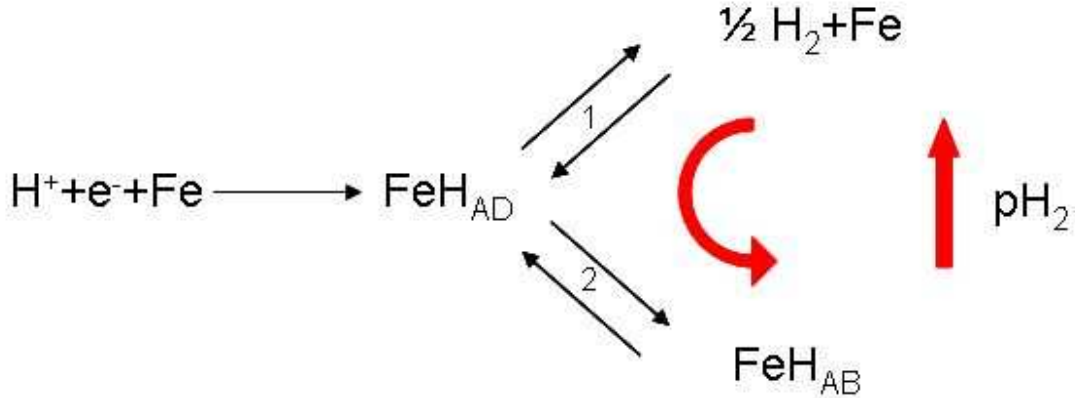
**Figure 153. Hydrogen formation, adsorption and absorption on the steel substrate**

where  $FeH_{AD}$  refers to adsorbed hydrogen on the metal surface,  $FeH_{AB}$  refers to absorbed hydrogen directly beneath the metal surface,  $k_I$ ,  $k_{II}$  and  $k_{III}$  are the rate constants for the corresponding reactions.

This mechanism shows that after hydrogen is adsorbed on the metal surface, two possible reactions may take place: firstly the subsequent absorption of hydrogen below the metal surface which could be a reversible process; secondly, the reaction with additional atomic adsorbed hydrogen to generate molecular hydrogen that escapes from the metal surface.

The new mechanism is based on that proposed by the previous authors but it also considers the effect of the coating's porosity on the equilibrium reactions and the role of the partial pressure of the hydrogen in the gas above the solution entrapped in a pore and how that would increase the amount of hydrogen absorbed. Inside the porosity, the hydrogen can remain trapped with a resulting increase of its pressure. A bubble of hydrogen that is generated into a small open porosity connected to the external through a thin capillary, should, to escape from the pore, have a pressure greater than the external partial pressure of the hydrogen plus an additional pressure

necessary to win the surface tension of the solution in the capillary. Smaller radius of the capillary would result in a greater additional pressure. In the situation the mechanism described in Figure 153 should be completed as follows



where the rate of the reaction 1 is controlled, at the equilibrium, by Equation 28

$$K_{eq1} = \frac{[Fe]_{solid} \cdot (pH_2)^{\frac{1}{2}}}{\gamma_1[FeH_{AD}]} = \frac{(pH_2)^{\frac{1}{2}}}{\gamma_1[FeH_{AD}]} \quad (28)$$

and the reaction 2, at the equilibrium, by Equation 29.

$$K_{eq2} = \frac{\gamma_2[FeH_{AB}]}{\gamma_1[FeH_{AD}]} \quad (29)$$

If the pressure of the hydrogen increases,  $FeH_{AD}$  will consequently reach the new equilibrium. From the second equilibrium  $FeH_{AB}$  will also increase, amplifying the risk of re-embrittlement.

When comparing two coatings with a different number of pores of the same size, the substrate covered with the more porous coating would fail in a shorter time. On its surface a larger number of sites, with a concentration of hydrogen absorbed higher than the uncoated steel held at an identical potential, would increase the amount of hydrogen that permeates into the steel causing its failure.

A change in the area of steel exposed to the solution through the porosity would not change the current density of the cathodic reaction of the hydrogen on the steel and the hydrogen produced inside the pore per unit of area would be the same.

Theoretically a different number of pores contained in two different coatings, all with the same shape and dimension, would all reach identical condition at the same time and the more porous coating would be disadvantageous for the substrate.

A different cause of the modification of the hydrogen entry kinetics into the steel, proposed in the literature, is known by the generic terms “cathodic poison” and “cathodic promoter” [51].

Different authors have reported that hydrogen entry into steel in the presence of promoters is facilitated by formation of a promoter hydride [52, 53], which thereby weakens the Fe-H bond. The order of effectiveness of the promoters studied [52] is S > P > Se > Te > As, but the authors refer, in their publication, to previous studies in which a different order was found.

SermeTel coating contains phosphates in the binder but if this could explain the results for these coatings, the high re-embrittlement on Cd electroplated, compared to the charged uncoated specimen would remain unexplained.

#### 4.1.9 Advantage of the use of aluminium in terms of metal loss

The corrosion rate of the coating expressed in terms of metal loss is dependent on the charge density; the equivalent weight and density is shown in Equation 30.

$$\text{CorrosionRate} = \frac{I_{\text{corr}} \cdot \text{EqWeight}}{\text{Density}} \quad (30)$$

Table 21 reports the equivalent weights and the density of the pure elements contained in the coatings. The calculation of the ratios EqWeight/Density and the gain of the coatings compared to Cd, calculated with Equation 31, is shown in Table 22.

Physical characteristics	Equivalent Weight (g/equivalent)	Density (g/cm <sup>3</sup> )
Cadmium	56.2	8.6
Aluminium	8.9	2.7
Zinc	32.7	7.14
Magnesium	12.2	1.7

**Table 21. Physical characteristics of some of the main elements of coatings**

$$GainOnCadmium = \frac{(EqWeight / Density)_{Coating} - (EqWeight / Density)_{Cadmium}}{(EqWeight / Density)_{Cadmium}} \cdot 100 \quad (31)$$

	EqWeight (g/equivalent)	Density (g/cm <sup>3</sup> )	EqWeight/Density (cm <sup>3</sup> /equivalent)	Compared to cadmium
Aluminium	8.9	2.7	3.3	- 49%
Zinc	32.6	7.1	4.5	- 29%
Cadmium	56.2	8.6	6.5	---
Magnesium	12.2	1.7	7.1	+ 10%
984 50% Zinc-50% Al	20.8	4.9	4.2	- 35%
984 10% Zinc-90% Al	11.4	3.1	3.6	- 44%
984 3% Zinc-97% Al	9.7	2.8	3.4	- 47%
984 0.5% Zinc-99.5% Al	9.1	2.7	3.3	- 48%
984 50% Mg/Al	9.6	2.5	3.8	- 40%
984 30% Mg/Al	9.3	2.6	3.6	- 44%

**Table 22. Physical characteristics of the coating for the calculation of the metal loss**

In the calculation of the metal loss, mixed values have been used for the 984 coatings modified with zinc and magnesium, using a weighted mean, where the weights are the composition of the aluminium, zinc or magnesium. It is interesting to note that

the aluminium has the smallest EqWeight/Density value, with 3.3 while 6.5 is the value for the cadmium. In the calculation of the metal loss from the current, aluminium would lead to a metal loss -49% smaller than the value for the cadmium and the other coatings whose values are shown in Table 22.

Considering the same protection provided by aluminium and a cadmium coating there is an advantage, in terms of metal loss, in using aluminium coatings to increase the durability in service. The results in Table 22 are plotted in the bar chart in Figure 154. This is a theoretical calculation assuming the protection in terms of current provided by the coatings is the same.

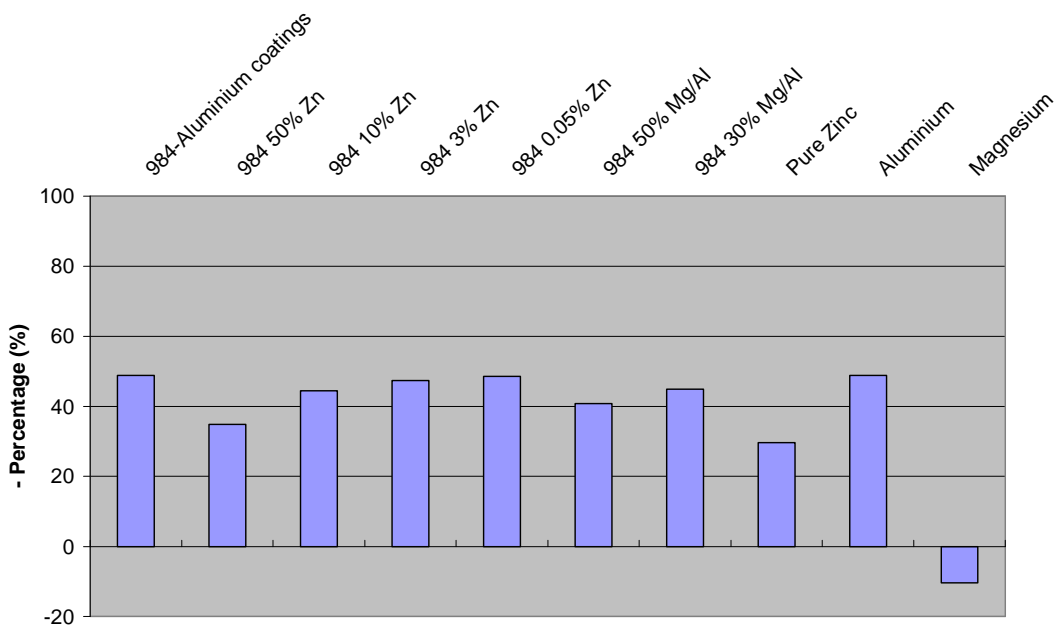


**Figure 154. Decrease of metal loss of the alternative aluminium-based coatings compared to electroplated cadmium in terms of metal loss expressed in percentages**

#### 4.1.10 Total corrosion

The total corrosion of the coatings was calculated by adding the self-corrosion to the galvanic corrosion. Figure 155 and Figure 156 report the calculation in terms of charge density and metal loss. The results were compared after one day, before any



of the coatings showed any signs of corrosion. A small addition of the active element seems to be insufficient to improve the galvanic protection provided by the 984. Among all the coatings, the highest galvanic protection was provided in order by, the 50% Mg 984, the 50% Zn 984 and the IVD1. It is important to note that in this test the IVD aluminium is not exposed to any mechanical stress and it would be a mistake to analyse this result together with the hydrogen re-embrittlement test. In fact, the IVD coatings showed the ability to provide a good protection for the steel but because of the poor adhesion of the coating to the substrate it was not possible to evaluate the amount of re-embrittlement that they would cause to the steel.

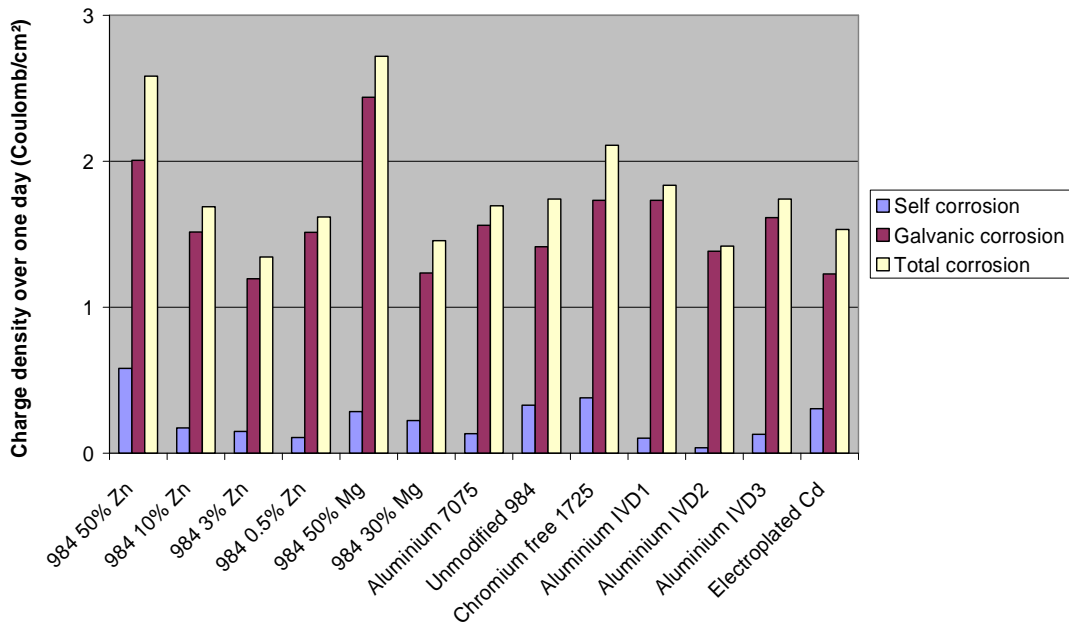


**Figure 155. Charge density for self-corrosion, galvanic corrosion and total corrosion calculated over a period of one day**

For the reasons discussed previously, when calculating the total corrosion in terms of metal loss, the cadmium coating has the disadvantage due to its equivalent weight and density. This leads to the conclusion then even a large addition of zinc or magnesium, which could provide very good cathodic protection, would be competitive with the cadmium in terms of duration in service.

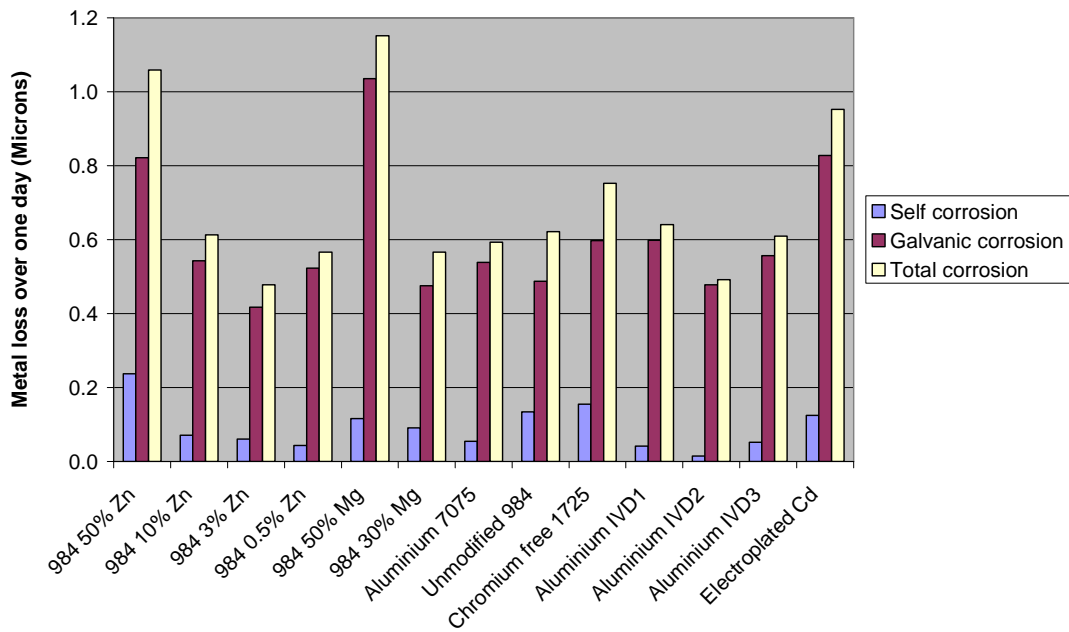


**Figure 156. Metal loss for galvanic corrosion and total corrosion calculated over a period of one day**

#### 4.1.11 Selection of the coating

On the basis of the results obtained during the experimental work, three values have been determined as fundamentals for the selection of the alternative coating, the appearance of red rust, the self corrosion rate and the hydrogen re-embrittlement indices. These values are summarised in Table 23.

	Appearance of red rust in the galvanic test (days)	Self corrosion rate In metal loss in ten days (microns)	Hydrogen re-embrittlement index (EI)
984 50% Zn	9	1.29	0.41
984 10% Zn	9	0.17	0.32
984 3% Zn	7	0.16	0.24
984 0.5% Zn	5	0.12	0.27
984 50% Mg/Al	10	0.41	0.45
984 30% Mg/Al	5	0.29	0.44
984	6	0.18	0.36
CF 1725	2.5	0.27	0.35
7075	9	1.15	0.37
IVD1	9.5	0.41	Coating detachment
IVD2	9.5	0.21	Coating detachment
IVD3	9.5	0.40	Coating detachment
Electroplated Cd	5.5	2.25	0.32

**Table 23. Appearance of red rust in the galvanic test, metal loss caused by self-corrosion rate and hydrogen re-embrittlement indices**

The three IVD coatings, although they performed well in terms of cathodic protection and without showing (as in the case of the IVD2) an excessively high self-corrosion rate, cannot be compared with the other coatings and considered as an alternative to electroplated cadmium because of their poor mechanical adhesion that led to the coating detachment from the steel substrate during the SSRT.

During the test. the CF 1725 showed a very stable potential but was not sufficiently active to provide a good protection. The time of appearance of red rust was measured in 2.5 days and is the lowest value recorded. Its self-corrosion rate was greater than most of the zinc modified 984 coating with the exception of the 50% Zn. In terms of re-embrittlement, the coating did not show an EI substantially different from the

electroplated cadmium so there would be no advantage in the replacement of the cadmium with this coating.

The 7075 was an interesting coating. It showed good cathodic protective coatings with EI not greater than the electroplated cadmium but its performance is penalised by the high self-corrosion rate. Compared to cadmium this value is still lower, as a consequence of the better ratio EqWeight/Density that is favourable to the aluminium coatings, and lower than the 50%Zn 984 that also showed a similar EI. Although there is a difference between these two coatings in the EI values, the Student's t-test between the couple has shown that there is no statistical difference between the two means. Comparing the 7075 with other coatings that provided similar cathodic protection, such as the 10%Zn 984, the 7075 would still have the disadvantage of the high self-corrosion rate that would limit the duration in service.

The zinc modified 984 coatings showed interesting and consistent results with trends depending on the different addition of zinc particles. The appearance of red rust, and the EI increased with the increase of zinc particles contained in the coating as expected. The self-corrosion of the coatings still showed a trend linked to the amount of zinc but with an increase of the coating self-corrosion rate for the coating containing more zinc. A greater addition of zinc can provide longer protection to the steel but increases the self-corrosion of the coating and the risk of hydrogen re-embrittlement. Although the Student's t-test has shown that among the four zinc modified coatings only the couple 50%Zn 984/3%Zn 984 and 50%Zn 984/0.5%Zn 984 are statistically different, the trend of the EI clearly shows that the addition of zinc causes more re-embrittlement and the same was noticed for the addition of the Mg particles.

When comparing the results of the zinc modified 984 coatings with the original 984, the addition of zinc greater than 3% or 10% but smaller than 50% can improve the coating's sacrificial protection characteristics without increasing the self-corrosion rate and the EI. By comparing the same coatings with the electroplated Cd, all the coatings can provide a smaller corrosion rate and a longer protection while maintaining, apart from 50%Zn 984, a similar risk of EI. The values calculated for

the EI indices seem to suggest that the 50%Zn 984 caused more re-embrittlement than the cadmium. The Student's t-test carried out with a level of confidence of 90% has shown that there is a statistical difference between the electroplated cadmium and the 50%Zn 984 but not between the electroplated cadmium and the 10%Zn 984, the 3%Zn 984 or the 0.5Zn 984. Therefore an amount of zinc between 50% and 10% seems to be able to enhance the duration of the cathodic protection without increasing too much the self-corrosion of the coatings and the EI.

The addition of magnesium caused a similar effect on the 984 to the addition of zinc, showing a positive trend between the additions of the active element and the self-corrosion rate, the time of appearance of red rust and the EI. The 50%Mg/Al coating provided the best protection to the steel, providing protection until the end of the test. The composition analyses of the magnesium 984 coatings have shown that the amount of magnesium in the coating is 20% for the 50%Mg/Al 984 and 10% for the 30%Mg/Al 984. These two values were used to calculate the metal loss of the coatings from the measurement of the currents. When comparing the 50%Mg/Al 984 with the 50%Zn 984, the first coating provided a better sacrificial protection but at the same time showed a lower corrosion rate. Despite its good corrosion behaviour the EI was, as for the 50% zinc coating, still greater than the cadmium one and the result was confirmed by a Student's t-test with a level of confidence of 95%.

The three IVD aluminium coatings provided a very good sacrificial protection and a self-corrosion rate comparable to the 50%M/Al 984, except for the IVD2 which also showed a smaller self-corrosion rate. IVD aluminium coatings have been studied for years as good alternatives for cadmium replacement. Some coating manufacturers of IVD aluminium refer to the coating as able to give cathodic protection almost without causing any re-embrittlement to the steel. Similar results were apparently obtained during this study but a further analysis of the IVD coating on the tensile specimen after the test has shown that the good results in terms of re-embrittlement were in reality caused by poor adhesion of the coating to the steel which left the steel almost without protection because of the detachment of the coating.

## 4.2 SELECTION OF THE COMPATIBILITY COATINGS FOR ALUMINIUM/BRONZE ASSEMBLY

### 4.2.1 Extent of the problem

Table 24 shows the average galvanic corrosion currents that have been measured in these tests between aluminium and the uncoated bronze (258  $\mu\text{A}$ ). This relatively high current is an indication of the potential problem that needs to be overcome.

	Current ( $\mu\text{A}$ )
Uncoated – Bronze/Aluminium coupling	258
IVD Aluminium	255
Passivated Cadmium	155
Electroplated Aluminium	147
Unpassivated Cadmium	141
Zn-Ni	135
984 1% Zinc	133
984 5% Zinc	128

**Table 24. Current averages over the first three days.**

### 4.2.2 Effect of applying a coating

Coating the bronze has been shown to reduce the average galvanic current to approximately half its previous value. In addition, the coating became the anode, instead of the aluminium, which was then sacrificially protected. Table 24 shows that the average anodic currents on the coatings were all quite similar, for the first three days, with the exception of the IVD aluminium. However, over a ten day period the average currents began to differ. The reasons for these changes are described below.

### 4.2.3 Comparison of the charge produced by each coating

The charge produced by the coatings in protecting the aluminium and exposed areas of bronze are compared in Figure 157. The graph confirms that all the coatings, except the IVD, had similar behaviour for the first three days.

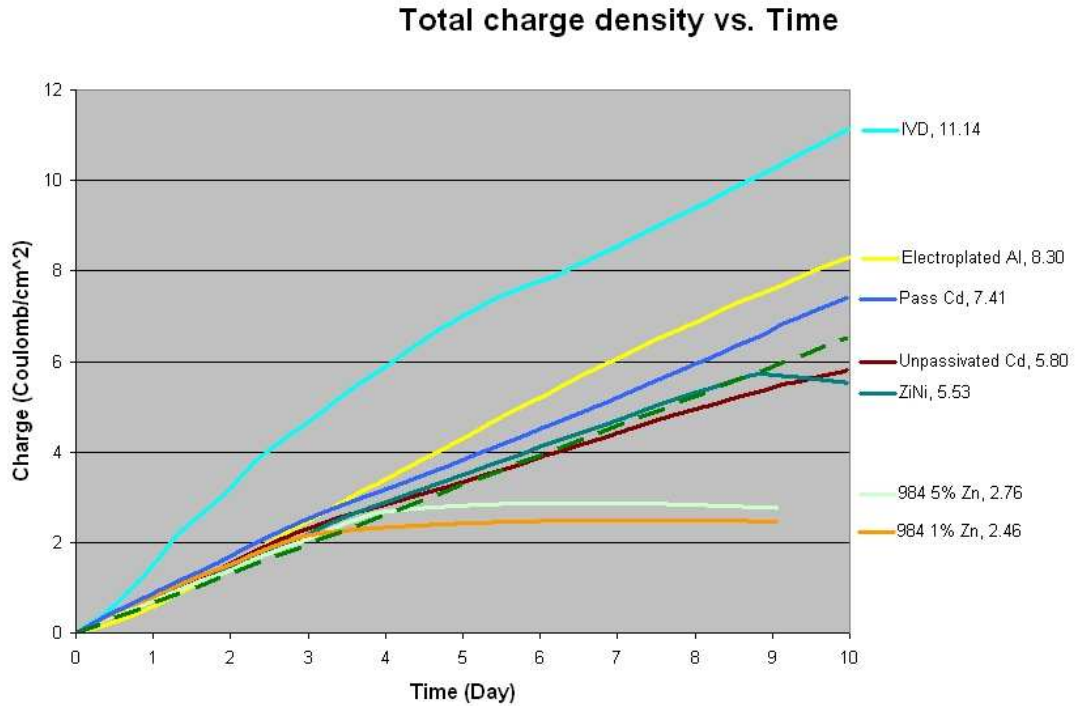


**Figure 157. Total charge density provided by the coatings during the galvanic test.**

At three and five days, the charge produced by 984-1Zn and the 984-5Zn levelled off and no further anodic current was produced by these coatings. It is thought that the formation of corrosion products on the surface and the presence of the inorganic binder acted as a barrier to the aluminium and zinc particles in the coating and prevented further corrosion from taking place.

It can also be seen in Figure 157 that the Zn-Ni coating produced no further charge after 9 days' exposure. This is thought to be due to the selective dissolution of zinc from the coating and progressive ennoblement due to the enrichment of nickel. After nine days the Zn-Ni coating was no longer anodic to the aluminium and sacrificial protection ceased.

The high rate of charge production from the IVD aluminium coating was quite different from that of the other coatings. It is known that this coating has high porosity and the effective surface area, at which the anodic reaction took place, was therefore higher than on the other types.

#### 4.2.4 Time to coating reversal

The loss of sacrificial protection provided by the 984-1Zn, 984-5Zn and Zn-Ni coatings is confirmed by the results in Table 25, which shows the times at which polarity reversal took place and the aluminium became the anode.

	Pass Cd	Un Cd	984 1% Zn	984 5% Zn	Zn-Ni	IVD	El Al
1 <sup>st</sup> test	No rev	No rev	3 days	4 days	9 days	No rev	No rev
2 <sup>nd</sup> test	4 days	No rev	3 days	5 days	8 days	No rev	No rev
3 <sup>rd</sup> test	No rev	No rev	7 days	9 day	9 days	No rev	No rev

**Table 25. Summary of times to current reversal**

The behaviour of passivated Cd (test 2) is regarded as untypical. In contrast to the three zinc containing coatings listed above, the electroplated Al, IVD aluminium and unpassivated Cd remained protective to the aluminium during the entire test.

#### 4.2.5 Potentials of the coatings

A further factor that influences the extent of sacrificial protection conferred by the coating is its potential, compared to that of the aluminium. The Open Circuit Potentials (OCPs) after one day of testing are compared in Table 26. All of the coatings were sufficiently active to sacrificially protect the aluminium.



	Coating	Aluminium	Bronze
984 1% Zinc	-675	-612	-261
984 5% Zinc	-753	-670	-326
Electroplated Al	-998	-567	-208
IVD Al	-1036	-585	-231
Passivated Cd	-811	-633	-295
UnpassivateCd	-782	-580	-242
Zn-Ni	-802	-605	-242

**Table 26. OCPs of the coating, aluminium and bronze after one day of testing.**

The potentials after 10 days are shown in Table 27. With the exception of the 984-1Zn, the 984-5Zn, the Zn-Ni and passivated Cd, all the coatings had more active (electronegative) potentials than the aluminium. Therefore, they acted as anodes, as intended.

	Coating	Aluminium	Bronze
984 1% Zinc	-611	-799	-260
984 5% Zinc	-751	-822	-345
Electroplated Al	-951	-585	-225
IVD Al	-721	-599	-242
Passivated Cd	-477	-806	-287
Unpassivated Cd	-773	-575	-334
Zn-Ni	-570	-652	-261

**Table 27. OCPs of the coating, aluminium and bronze after ten days of testing.**

984-1Zn, 984-5Zn and Zn-Ni had more active potentials for the first three days and the values reported here (-611, -751 and -570 mV (SCE)) indicate that after 10 days they had become noble to the aluminium (-799, -822 and -652 mV (SCE)) and that polarity reversal had taken place. After ten days the potential of the electroplated

aluminium was still exceptionally active, indicating the excellent sacrificial protection that can be expected from this coating.

#### 4.2.6 Corrosion control

The polarisation behaviour test has shown that the corrosion is often under cathodic control. 984-1% Zn has shown anodic control, 984-5% Zn and the electroplated aluminium have shown mixed control and all the remaining coatings have shown cathodic control. Table 28, Table 29, Table 30 and Table 31 summarise the results obtained from the polarisation curves.

The tables report the OCPs of the bronze, the aluminium and each coating measured after one day. The tables report the mixed potentials between the coupled aluminium and the bronze and finally the mixed potentials between the three coupled coatings. The last line of the table reports a comment regarding the type of corrosion control observed.

Zi-Ni			IVD		
OCP Bronze mV (SCE)	OCP Aluminium mV (SCE)	OCP Coating mV (SCE)	OCP Bronze mV (SCE)	OCP Aluminium mV (SCE)	OCP Coating mV (SCE)
-227	-599	-746	-242	-599	-728
Al and Bronze mixed potential mV (SCE)			Al and Bronze mixed potential mV (SCE)		
-596			-593		
Mixed potential mV (SCE)			Mixed potential mV (SCE)		
-722			-700		
Cathodic control			Cathodic control		

**Table 28. Zn-Ni and IVD coatings OCPs and mixed potentials after one day. Type of corrosion control after one day.**

Passivated Cadmium			Unpassivated Cadmium		
OCP Bronze mV (SCE)	OCP Aluminium mV (SCE)	OCP Coating mV (SCE)	OCP Bronze mV (SCE)	OCP Aluminium mV (SCE)	OCP Coating mV (SCE)
-295	-633	-812	-334	-575	-785
Al and Bronze mixed potential mV (SCE)			Al and Bronze mixed potential mV (SCE)		
-633			-572		
Mixed potential mV (SCE)			Mixed potential mV (SCE)		
-787			-772		
Cathodic control			Cathodic control		

**Table 29. Passivated Cadmium and Unpassivated Cadmium OCPs and mixed potentials after one day. Type of corrosion control after one day.**

984 1% Zn			984 5% Zn		
OCP Bronze mV (SCE)	OCP Aluminium mV (SCE)	OCP Coating mV (SCE)	OCP Bronze mV (SCE)	OCP Aluminium mV (SCE)	OCP Coating mV (SCE)
-257	-615	-681	-326	-670	-753
Al and Bronze mixed potential mV (SCE)			Al and Bronze mixed potential mV (SCE)		
-608			-663		
Mixed potential mV (SCE)			Mixed potential mV (SCE)		
-626			-713		
Anodic control			Mixed control		

**Table 30. 984-1% Zn and 984-5% Zn OCPs and mixed potentials after one day. Type of corrosion control after one day.**

Electroplated aluminium		
OCP Bronze mV (SCE)	OCP Aluminium mV (SCE)	OCP Coating mV (SCE)
-225	-585	-951
Al and Bronze mixed potential mV (SCE)		
-585		
Mixed potential mV (SCE)		
-728		
Mixed control		

**Table 31. Electroplated aluminium OCP and mixed potential after one day. Type of corrosion control after one day.**

Although some of the coatings have shown cathodic control, the corrosion currents have shown different values. Theoretically, when under cathodic control, a variation of the mixed potential should not change the value of the corrosion current. In this situation, due to the diffusion of the oxygen through the solution, the cathode has reached the  $i_c$ . In practice, in the author's experimental conditions, the cathodic curve does not reach its vertical limit, showing a negative gradient that is responsible for different values of currents resulting from the intersection with the anodic curves. The corrosion of the anode is dependent on the intersection of the anodic curve with the cathodic curve. The gradient  $\beta$  of the cathodic curve has been calculated in -661 mV/decade in the case of IVD aluminium after one day of testing, assuming the linearity in the region of interest. This value has been calculated from the cathodic curve of the couple aluminium/bronze in Figure 129 considering the gradient of the line intersecting the points  $P_1(-593 \text{ mV}; 42 \mu \text{ A})$  and  $P_2(-939 \text{ mV}; 140 \mu \text{ A})$ . This particular case has been chosen to calculate the gradient of the galvanic curve. All the coatings have been coupled to the same cathode aluminium/bronze and for this reason the value calculated from the IVD plot has been also used for the calculation related to the other coatings.

In particular this plot has been preferred to other because of the wide difference between the mixed potential of the three panels and the OCP of the aluminium/bronze couple cathodic curve.

This value has been used for a prediction of the corrosion current from the measured mixed potential. The current I has been calculated using equation 32 and the results are shown in Table 32

$$\log I = (E - E_0) / \beta + \log I_0 \quad (32)$$

where  $E_0$  and  $I_0$ , equal to -622mV and 128  $\mu$ A, are the mixed potential and the corrosion current of the last coating in the table, the 984 5% Zinc that has been chosen arbitrarily as the starting point for the calculation. Table 32 shows the comparison between the calculated values for the current and the measured one over ten days of testing. Apart from the IVD aluminium that has shown a current that is particularly high when compared to the calculated, the trend of the calculated currents for the other coating is close to the trend of the measured data. An important error in the calculation is thought to be related to the value of  $\beta$  that to simplify the calculation has been considered constant over the whole duration of the test.

	Mesured mixed potential (mV)	Calculated current ( $\mu$ A)	Measured current ( $\mu$ A)
Uncoated – Bronze/Aluminium coupling			258
IVD Aluminium	-876	309	255
Passivated Cadmium	-760	206	155
Electroplated Aluminium	-737	190	147
Unpassivated Cadmium	-766	211	141
Zn-Ni	-766	211	135
984 1% Zinc	-633	133	133
984 5% Zinc	-622 ( $E_0$ )	128	128 ( $I_0$ )

**Table 32. Comparison between calculated current and measured current on the basis of the experimental Tafel constant**

The situation explained is illustrated in Figure 158, where the brown curve represents the cathodic curve of the IVD aluminium obtained from the polarisation behaviour test after one day. The two anodic lines, in light blue and yellow are only illustrative

for two different cases. The dashed blue line represents the vertical trend of the cathodic curve when controlled by the dissolution of the oxygen in the solution. In this situation the interception of the yellow and the light blue line with the dashed line would lead to two different mixed potentials but the same value of the current. In our experimental conditions, in the range of interception with the anodic curves, the experimental cathodic line has a very high gradient but not infinite, leading to values of currents that are still considerably different. In the illustration the interception between the brown and the yellow line is  $94 \mu\text{A}$  and  $-720 \text{ mV}$  (vs. SCE); the interception between the brown and the light blue line is  $128 \mu\text{A}$  and  $-855 \text{ mV}$  (vs. SCE). The interception with the dashed line would be  $62 \mu\text{A}$  and  $740 \text{ mV}$  (vs. SCE) for the yellow line and  $62 \mu\text{A}$  and  $-900 \text{ mV}$  (vs. SCE) for the light blue line.

The illustration leads to the conclusion that an increase of the cathodic control leads to a general decrease of the corrosion current, a general decrease of the mixed potential and to values of the currents closer to the limiting  $I_l$ . This also means that, when under cathodic control, the activity of the coating plays a secondary role as its dissolution is controlled by the cathode. In practice, in our experimental conditions, this situation has not been really reached and more active coatings have provided a greater current to the cathode.

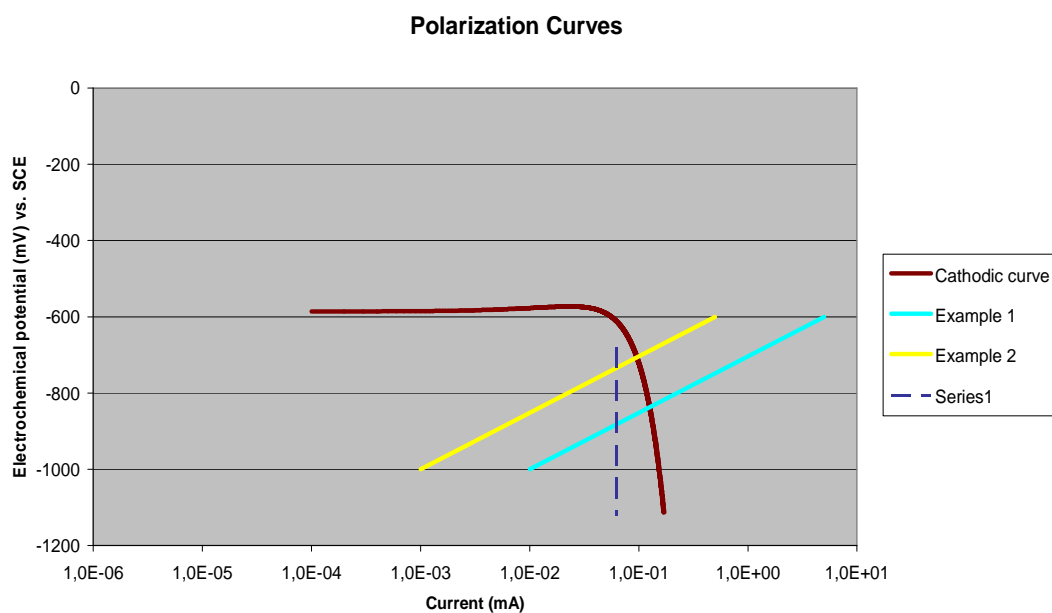


**Figure 158. Illustration of the effect of the cathodic curve gradient on the corrosion currents compared with a situation of complete cathodic control (dashed line)**

#### 4.2.7 Lifetime of the coatings

The coatings are depleted not only by providing sacrificial protection to the aluminium but also as a result of self-corrosion. The total corrosion metal loss, expressed as the sum of the galvanic and self-corrosion contributions, is shown in Figure 159 and Figure 160.

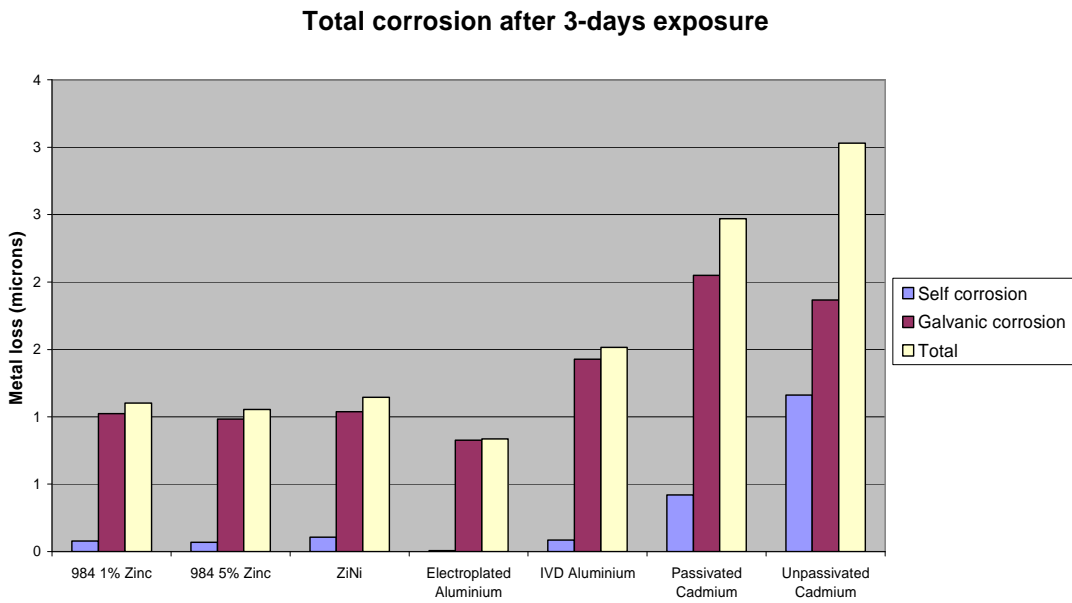


**Figure 159. Total corrosion after 3-days' exposure before reversal of any coating took place.**

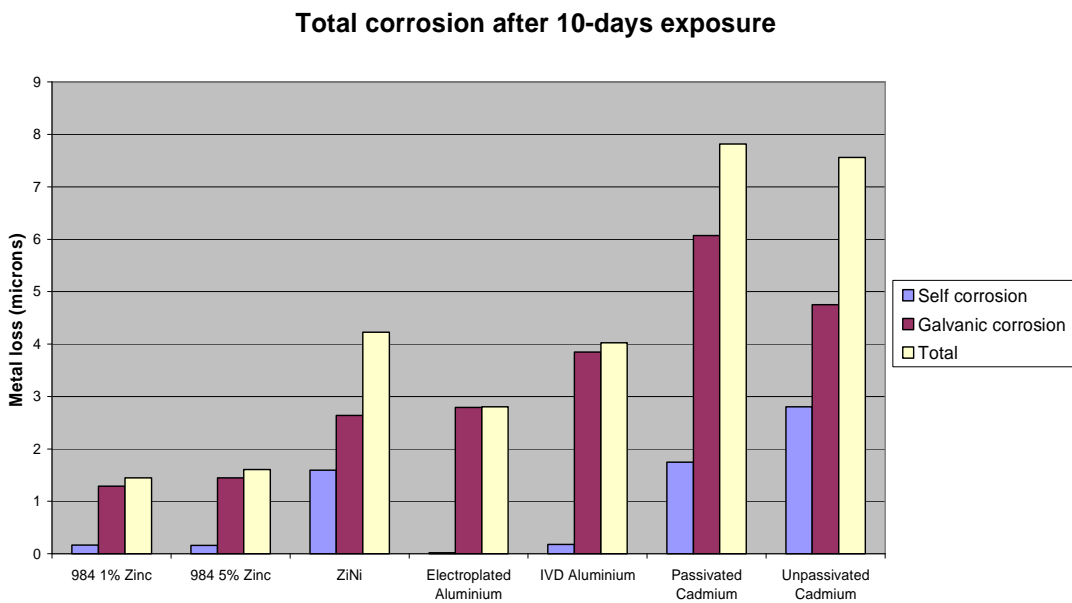


**Figure 160. Total corrosion after 10-days' exposure**

Figure 159 shows the metal loss after 3-days' exposure before reversal of any coating took place. The results might be expected to be similar for each coating as the



charges produced were shown to be similar in Figure 157. However, when expressing corrosion in terms of mass, rather than current, higher values are seen for the cadmium and Zn-Ni compared to the aluminium-based coatings. The reason is the higher mass of these coatings and the Cd, Zn and Ni having a valency of 2 compared to 3 for Al.

Figure 160 compared the metal loss after ten days. In this case, lower values are seen for the two 984 coatings as they only acted as anodes for the first 3-5 days of the test. Referring again to Figure 157, the 984-1, 984-5 and the Zn-Ni are considered the least favourable coatings as they failed to provide protection to the aluminium throughout the test. Of the remaining coatings, all provided satisfactory protection. The choice, therefore, is between the two cadmium replacements; IVD and electroplated aluminium.

The very low self-corrosion rate and the lower total metal loss of the electroplated aluminium are both favourable properties. In addition, its active potential and dense, pore-free structure make it a good choice.

### 4.3 OVERALL DISCUSSION

In the selection of a sacrificial coating to high strength substrates it has been seen that the following characteristics are important for the selection:

- the coating electrochemical potential must be active in order to provide protection to the steel
- the coating self-corrosion rate to extend the life in service of the coating
- the ratio equivalent weight/density of the coating must be low to minimise the metal loss when considering equal sacrificial protections
- the porosity of the coating should be minimised to increase the barrier effect of the coating and to minimise the accumulation of hydrogen in the porosity that would consequentially increase of the amount of hydrogen absorbed.

In the selection of the coating for the bronze/aluminium assembly there are two different approaches that can be followed for the selection of the coating. The first,

on which the discussion has been based, is similar to the one for the high strength steel substrate. The best coating has the following characteristics:

- active potential to provide good sacrificial protection both to the aluminium and to the bronze component
- low self-corrosion rate to minimise the total corrosion of the coating and to extend its life in service
- low ratio equivalent weight/coating density to minimise the metal loss of the coating and extend its life in service

On the basis of these considerations the SermeTel modified 984 coatings with a small addition of zinc have shown to be good alternatives to cadmium for the high strength steel substrate coating, and the electroplated aluminium seems to be the most suitable coating for the substitution of the cadmium in the case of bronze/aluminium assemblies. The electroplated aluminium has not been tested for the steel substrate but it might result in a good alternative for that application and should be tested in the future work.

A second alternative approach for the selection of the compatibility coating has been suggested by some of the results obtained during the experimental work. The 984 1%Zn and the 984 5%Zn after a few days reached a “neutral position” between the aluminium and the bronze without exchanging any current with them. This unusual behaviour suggested an alternative approach with the coating that is not more active than the two other components and exchanges very small galvanic currents with them. In this different situation the coating covers most of the bronze thus avoiding contact with the aluminium. The only galvanic corrosion in this situation would be between the big anodic area of the aluminium and the small cathodic area of the bronze, which would be exposed in correspondence of the possible damages of the coating. In these conditions, and if the corrosion is under cathodic control, the dissolution of the anode (aluminium component) would be proportional to the area of the cathode that is relatively small. According to Mansfeld and Kenkel [54] the corrosion current density on the aluminium, in this case the anode, would be:

$$i_g^A = i_{0_2}^L \frac{A^C}{A^A} \quad (33)$$

where  $i_{0_2}^L$  is limiting c.d. for diffusion of oxygen on the bronze that is constant and it is dependent on the material. If the coating is not taking part in the corrosion and its effect is only to reduce the area of the cathode exposed, in condition of diffusion control, it would result in being beneficial to the aluminium, because its corrosion would be proportional to the area of cathode exposed.

The two cases can be summarised as follows:

a) the coating is the only anode, the aluminium and the bronze are both cathodes.

If the electrochemical potential of the coating is more active than the potentials of the bronze and the aluminium, the coating would be the only anode. In this condition the galvanic corrosion that would occur between the uncoated bronze and aluminium is completely “transferred” to the aluminium. The coating is now giving protection to the same area of aluminium and to the small area of bronze not covered by the coating.

In these conditions, with the areas considered in the experimental work, that have been assumed as representative of the real conditions, the corrosion on the coating would be smaller than the corrosion on the aluminium coupled with the uncoated bronze.

In this case an increase in the area of the exposed bronze could cause a significant increase in the corrosion on the compatibility coating.

b) the coating is in a neutral position and the aluminium is the anode.

If the coating has an electrochemical potential close to the mixed potential of the coupling aluminium-bronze without the coating, it would exchange very small galvanic currents with the two other materials if added to the couple.

In these conditions, the coating would cover most of the bronze, leaving a smaller area of the cathode exposed, with an advantage for the corrosion of the anode as described by Equation 33. The galvanic corrosion would be on the

aluminium but considerably reduced if compared with the situation without the compatibility coating.

In case (a), the coating is coupled to a small area of a strong cathode, the bronze, plus a large area of a weak cathode, the aluminium. In case (b) the coating does not exchange any galvanic current and the aluminium, the anode, is only coupled to the small area of the strong cathode, the bronze. In case (a), the additional disadvantage for the anode would be its more active electrochemical potential compared to case (b), as the coating must be more active than both the bronze and the aluminium to be the cathode. In terms of total galvanic corrosion of the system, case (b) is advantageous.

Depending on the applications of the compatibility coating, the two cases, (a) and (b) can be considered desirable or not. In the specific assembly setup studied in this project, even a small amount of corrosion on the aluminium component is undesired since the aluminium one is a structural component. In other situations, a small corrosion on the uncoated component could be tolerated, and the use of a coating with a potential in between the potential of the two other components could be beneficial in the reduction of the total galvanic corrosion of the system. These considerations clearly depend on the use of the two components and on the possibility of replacing the less noble component rather than the coating and on the costs involved.

Despite practical considerations, it seems clear that the perfect compatibility coating used to cover the cathode in a galvanic assembly should have a potential in between the two components. In particular this potential should be very close to the mixed potential of the two components coupled without the coating, taking into account the reduction of the area of the more noble component after the coating has been applied.

The use of a sacrificial coating as a compatibility coating is an interesting use that must be conveniently selected or designed by changing its electrochemical potential to make it compatible with the assembly considered.

The two cases studied in this project show the different uses that can be made of sacrificial coatings on the basis of specific needs and applications by trying to limit the side effects caused by the hydrogen, in the case of a high strength steel substrate, or to limit the galvanic corrosion between the assembly of two components acting more as a compatibility coating.

## 5 CONCLUSIONS

### 5.1 ALTERNATIVE SACRIFICIAL COATINGS FOR HIGH STRENGTH STEEL SUBSTRATE

[A] Additions of small quantities of alloying elements were effective in improving the corrosion performance of commercially available CR984-LT coating. They avoided the tendency to passivation and in some cases extended the times at which red rust appeared.

[B] Addition of zinc particles systematically lowered the potential of the coatings, increased the sacrificial current to protect exposed areas of steel and extended the time of protection. Similar effects were observed with addition of Mg/Al powder.

[C] IVD coatings performed well both in terms of galvanic protection of the steel substrate and in the self-corrosion rates.

[D] 7075 displayed promising corrosion potentials but led to a high rate of self-corrosion which would limit the coating life. Similarly the self-corrosion rate of the Cd coating was high.

[E] Despite the improvements in corrosion performance provided by the addition of Zn particles, no increase in re-embrittlement of the high strength steel substrate was observed during corrosion of the coatings.

[F] All the coatings showed self corrosion rates smaller than electroplated cadmium although aluminium. Over a period of ten days aluminium 7075 coating and SermeTel 984 5% Zn showed the greatest corrosion rates but smaller the electroplated cadmium. The self corrosion rates were 2.1 microns/year for cadmium, 1.1 microns/year for the aluminium 7075 and 1.2 for SermeTel 984 5% Zn. All the remaining coatings showed self corrosion rates smaller than 0.4 microns/year.

[G] In terms of galvanic protection all the coatings except CF1725, SermeTel 984 0.5% Zn and SermeTel 984 30% Mg, performed better than electroplated cadmium, increasing the time of appearance of red rust from 5.5 days to 9 days in the case of SermeTel 984 50% Zn SermeTel 984 10% Zn and aluminium 7075, 9.5 days in the case of IVD coatings, 10 days in the case of Sermetel 50% Mg.

## 5.2 ALTERNATIVE COMPATIBLE COATINGS FOR ALUMINIUM/BRONZE ASSEMBLIES

[A] Each of the coatings investigated was effective in reducing the galvanic corrosion between bronze and aluminium and in providing sacrificial protection to the aluminium.

[B] The charge produced by all the coatings in protecting the aluminium was similar for the first three days, with the exception of the IVD aluminium, due to its porosity and higher effective surface area.

[C] The effectiveness of the zinc-containing coatings was lost when polarity reversal took place: 984-1%Zn (3 days), 984-5%Zn (5 days), Zn-10%Ni (9 days). The aluminium and, in general, the cadmium coatings remained protective during the entire 10-day tests.

[D] The aluminium coatings displayed lower rates of metal loss than cadmium, due in part to their higher charge capacity (valency of 3, compared to 2 for Cd) and their lower density.

[E] Both the aluminium coatings offered the advantage of a very active initial potential close to -1000 mV (SCE) and, in the case of the electroplated aluminium, this was maintained for most of the test period.

[F] The very low self-corrosion rate of the electroplated aluminium, combined with its active potential and dense, pore-free structure makes it a good alternative to cadmium for this application.

### 5.3 GENERAL CONCLUSIONS

[A] The project has shown that the same coatings can be used with a different approach on active substrate or noble substrate.

In the case of active substrates, which have high corrosion rates, the use of a coating with a more active potential is beneficial to protect the substrate from the corrosion, providing cathodic protection. The amount of protection provided has to be balanced with the self-corrosion characteristics of the coating to find the optimum compromise between corrosion protection, duration of the coating in service and, in the case of HSS, the risk of hydrogen re-embrittlement.

[B] In the case of noble substrates, which are less prone to corrode than active materials, the use of a metal coating is recommended when the noble material is in contact with a more active component and galvanic corrosion could occur. In this case the noble material can be covered with a more active coating, which would act as a compatibility coating, reducing the galvanic corrosion between the noble component and the active component.

[C] The potential of the compatibility coating should be as close as possible to the potential of the active material in the coupling. This would reduce the galvanic corrosion between the active component and the coating. The possibility to select coatings with potentials slightly more active or less active than the active component has been evaluated in the project.

[D] A coating more active than the active material would reduce the galvanic corrosion between the two components. In correspondence of possible damages on



the coating surface, with consequent exposure of small areas of the noble substrate, the coating would provide sacrificial protection to the active component avoiding its galvanic corrosion. This approach is important when the active component needs to be preserved from galvanic corrosion, while a certain amount of galvanic corrosion is considered acceptable on the coating.

[E] Nevertheless, in terms of minimisation of the total galvanic corrosion between the noble component, the active one and the compatibility coating, it has been shown that a coating with a potential slightly more active than the active component would be beneficial. In this case the ideal potential of the coating would be the mixed potential generated by the surface areas of the two components in contact. For the noble component, the surface area to be considered should be the one eventually exposed in correspondence of damages on the compatibility coating.

## 5.4 FUTURE WORK

From the findings of this research programme several important topics have been identified which should be investigated further in order to use these novel aluminium based coatings in service.

### **[A] Beneficial effects of a nickel layer beneath sacrificial coatings for HSS**

A thin layer of nickel electrodeposited onto high strength steel before applying a coating of cadmium could virtually eliminates the problem of hydrogen re-embrittlement. The reason for this improvement is that the nickel acts as a barrier to hydrogen generated during corrosion of the cadmium so that little hydrogen enters the steel. The diffusion coefficient for hydrogen in nickel is  $8 \times 10^{-10} \text{ cms}^{-1}$  compared to a value of  $2 \times 10^{-7} \text{ cms}^{-1}$  for the unprotected steel.

Whether a nickel layer is also effective in controlling hydrogen re-embrittlement caused by corrosion of aluminium-based sacrificial coatings could be further investigated. Whether this approach has any detrimental effects should be considered. For example, could the nickel layer adversely affect the corrosion of the steel component when the sacrificial coating approaches the end of its life?

A nickel layer could be electrodeposited as a nickel strike and its effect on both SermeTel metal particle and IVD aluminium coatings could be investigated.

**[B] Study of chromium-free aluminium coating modified by additions of active elements for HSS**

CF 1725 would be an optimum coating for further development of a chromium free coating. Its stable potential could be lowered by the addition of zinc and magnesium which have been shown to work in this direction.

## APPENDIX

### A) INTERPRETATION OF POLARISATION CURVES

Figure 161 shows the polarisation curves of a 24 cm<sup>2</sup> panel of copper and 8 cm<sup>2</sup> panel of steel. The corrosion is under cathodic control, the reduction reactions on the cathode have reached their limit and they cannot occur at a higher rate. This is shown by the fact that an increase in the area of the anode, in Figure 162, does not change the current. The cathode has reached its limit in terms of the number of electrons that can be consumed by the reduction of the oxygen. In contrast, an increase in the area of the cathode, shown in Figure 163, increased the current exchanged, because a larger cathodic surface would be able to consume a greater number of electrons in the cathodic reduction of oxygen. It can be seen that in this case, some anodic polarisation has occurred and the current shows signs of being limited by the concentration of metal ions (Fe<sup>2+</sup>) accumulating at the anode. Situations where polarisation of both the cathodic and the anodic reactions takes place are termed mixed control.

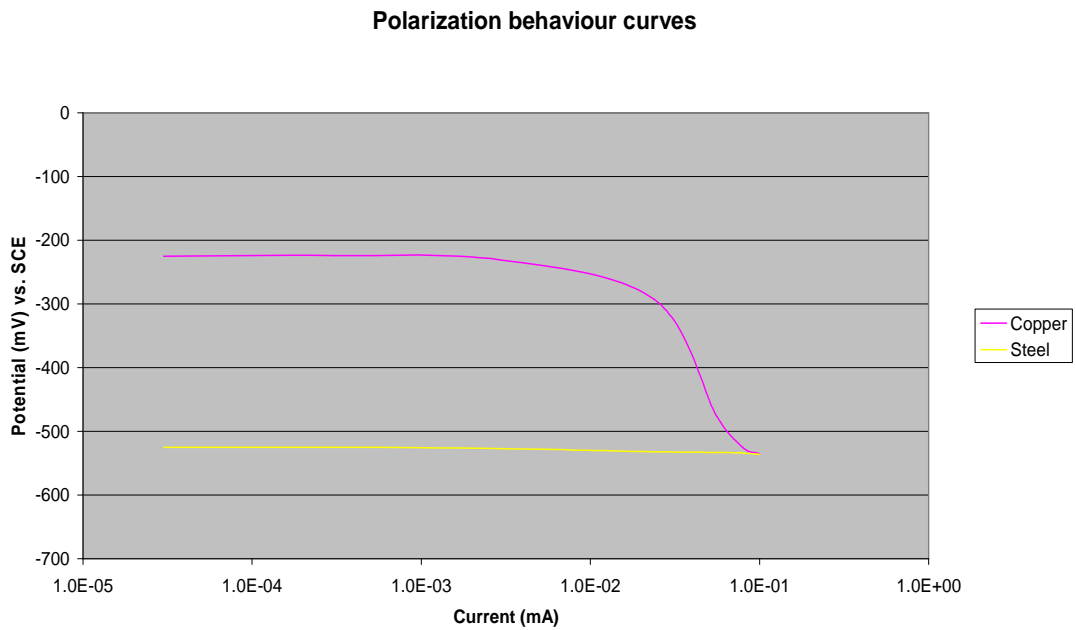


**Figure 161. Polarisation behaviour curves between copper and steel. Area steel  $24 \text{ cm}^2$ , area copper  $8 \text{ cm}^2$**

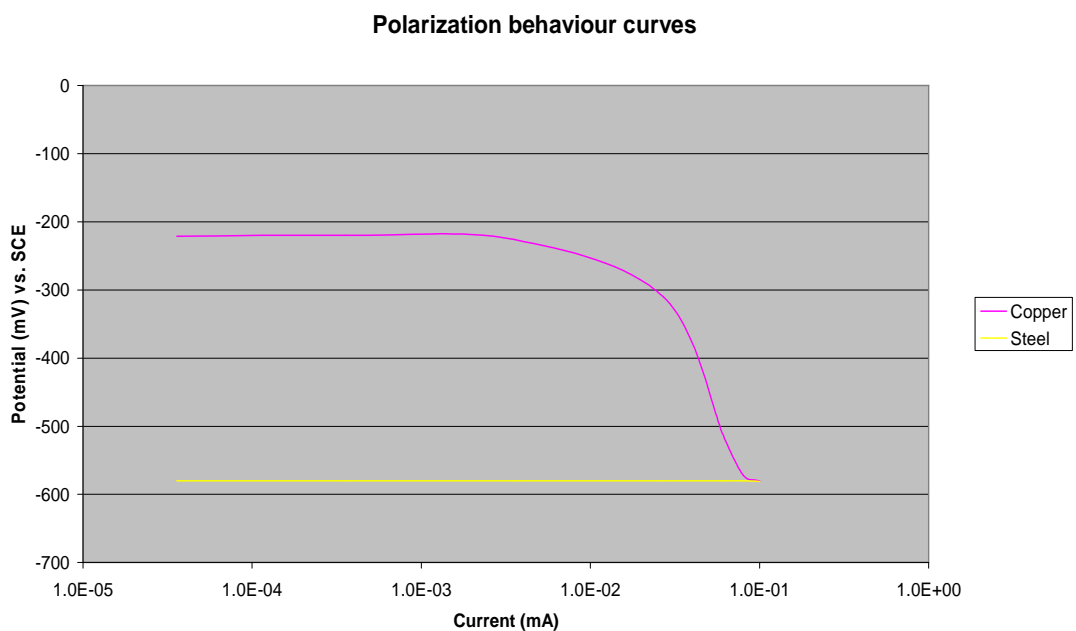


**Figure 162. Polarisation behaviour curves between copper and steel. Area steel  $48 \text{ cm}^2$ , area copper  $8 \text{ cm}^2$**

Study of the corrosion control makes it possible to evaluate whether the protective coating would be able to provide more current without changing its potential. It shows whether the corrosion of coated components is dominated by the effect of the environment or by the coating itself. In a situation in which the corrosion process has already moved to a mixed control, as in the situation shown in Figure 163, an increase of the area of the cathode would move the mixed potential to a more noble value with a consequent decrease of the protection provided to the anode.

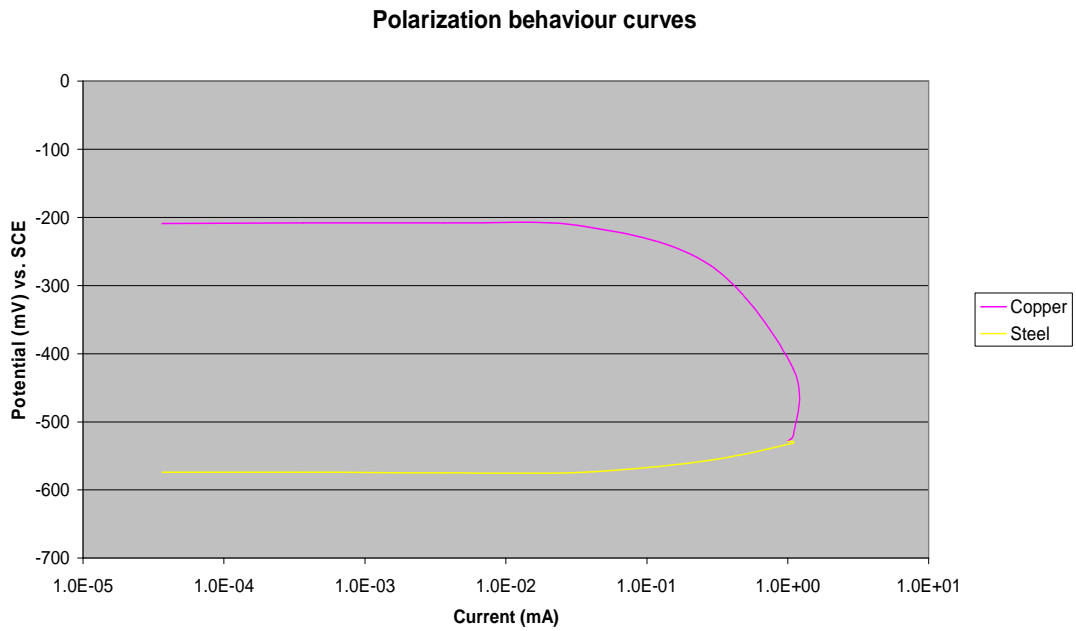


**Figure 163. Polarisation behaviour curves between copper and steel. Area steel 24 cm<sup>2</sup>, area copper 24 cm<sup>2</sup>**

The implication in the case of diffusion control has been studied in literature [54] and they showed, as in the example, that the galvanic c.d.  $i_g^C$  with respect to the cathode is independent of the area ratio since

$$I_g = I_c^C(E_g) = i_{O_2}^L A^C \quad (34)$$

and

$$\frac{I_g}{A^C} = i_g^C = i_{O_2}^L = const \quad (35)$$

where  $A^C$  is the area of the cathode,  $I_c^C(E_g)$  is the cathodic current on the cathode,  $i_{o_2}^L$  is the limiting c.d. for diffusion of oxygen.

The galvanic c.d. with respect to the anode is described by:

$$i_a^A = i_{o_2}^L \left( 1 + \frac{A^C}{A^A} \right) \quad (36)$$

and in case of diffusion control

$$i_c^A = i_c^C = i_{o_2}^L \quad (37)$$

so that

$$i_a^A = i_s^A \left( 1 + \frac{A^C}{A^A} \right) \quad (38)$$

## B) STERN-GEARY VALUES

The Stern-Geary values used in the calculation of the corrosion rate were calculated from the Tafel coefficients  $b_a$  and  $b_c$ . These values cadmium [1] and for aluminium [55] are shown in Table 33

	$b_a$ , mV	$b_c$ , mV	$\beta$
Cadmium	-	-	16
Aluminium	45	600	18

**Table 33.  $b_a$  and  $b_c$  values used to calculate the Stern-Geary constants**

The same values were used for all the Al-based coatings. In the work it was chosen to use values published in the scientific literature rather than measuring the values by mean of potentiodynamic scan measurements. The experimental difficulties in the

determination of the correct values to be used in calculation of the corrosion rates are listed below:

- the anodic and cathodic constants,  $b_a$  and  $b_c$  change over time
- $b_a$  is not linear
- the diffusion control of the cathodic control makes difficult the determination of  $b_c$

For these reason it was preferred to refer to published values that are the results of comparisons between different published studies.

### C) WEIBULL MODEL OF FAILURE TIMES

It is common for replicate hydrogen embrittlement tests carried out under apparently identical experimental conditions to result in a range of times to failure due to the variation in the number, size and distribution of microstructural defects in the specimens. For this reason, Weibull statistics was used in order to distinguish between the effects of each of the experimental variables.

For a Weibull model the probability,  $P_s$ , of a specimen not failing within time  $t$  is given by equation 39

$$P_s = 1 - P_f = e^{-x(t-t_i)} \quad (39)$$

where  $P_f$  is the probability of failure and  $x$  is a shape parameter termed the Weibull slope, which represents the probability per unit time that during time  $t$  a crack will develop in the specimen of sufficient size to cause failure. The value of  $x$  gives the scatter of failure times and is an indication of the range of defect sizes within the specimens. The term  $t_i$  is the minimum crack incubation time below which there are no failures (i.e. when  $P_s = 1$ ). A schematic plot of failure times is shown in Figure 164.

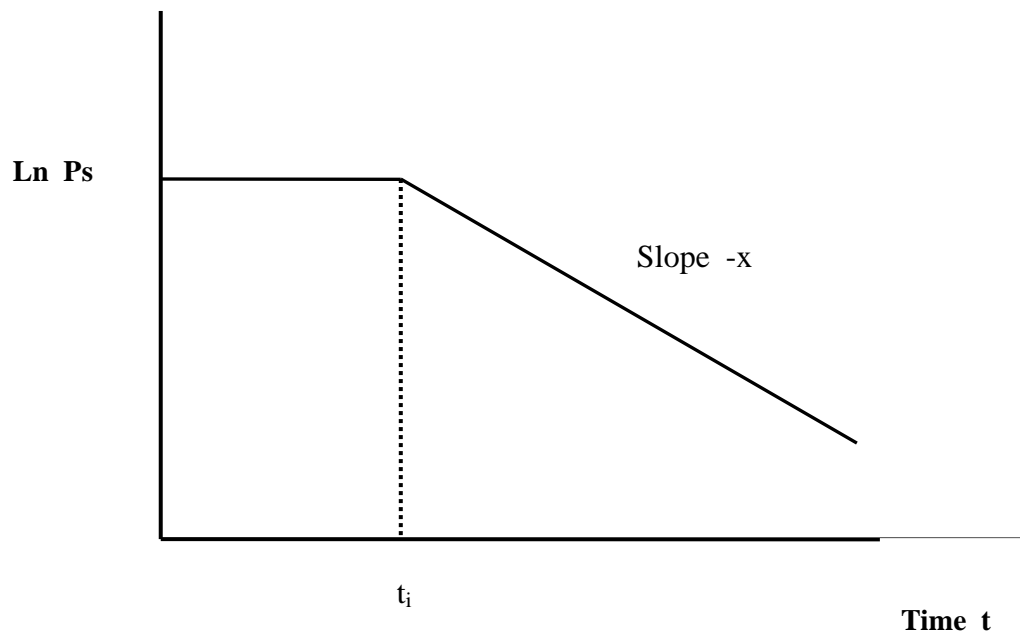


**Figure 164. Schematic Weibull plot of failure times**



## REFERENCES

1. Chalaftris, G. and M.J. Robinson, *Evaluation of Aluminium-Based Coatings for Cadmium Replacement*, in *School of Industrial and Manufacturing Science*. 2003, Cranfield University: Cranfield. p. 242.
2. Hillier, E.M.K. and M.J. Robinson, *Hydrogen embrittlement of high strength steel electroplated with zinc-cobalt alloys*. *Corrosion Science*, 2004. **46**(3): p. 715-727.
3. Figueroa, D., *Hydrogen Embrittlement Susceptibility of Ultra High Strength Steels*, in *School of Industrial and Manufacturing Science*. 2005, Cranfield University: Cranfield. p. 315.
4. Chalaftris, G. and M.J. Robinson, *Hydrogen re-embrittlement of high strength steel by corrosion of cadmium and aluminium based sacrificial coatings*. *Corrosion Engineering, Science and Technology*, 2005. **40**: p. 28-32.
5. Baldwin, K.R., et al., *Aluminium-magnesium alloys as corrosion resistant coatings for steel*. *Corrosion Science*, 1996. **38**(1): p. 155.
6. Baldwin, K.R., M.J. Robinson, and C.J.E. Smith, *The corrosion resistance of electrodeposited zinc-nickel alloy coatings*. *Corrosion Science*, 1993. **35**(5-8): p. 1267.
7. Yu, Q., J. Deffeyes, and H. Yasuda, *Corrosion protection of ion vapor deposition (IVD) Al-coated Al alloys by low-temperature plasma interface engineering: Part I. DC cathodic polymerization with anode magnetron enhancement*. *Progress in Organic Coatings*, 2001. **42**(1-2): p. 100.
8. Wynn, P.C. *Zinc Nickel Electroplating in the New Millennium*. [cited; Available from: [http://www.atotech.com/data/publications/ZnNi\\_Electroplating\\_SurFin\\_2001.pdf](http://www.atotech.com/data/publications/ZnNi_Electroplating_SurFin_2001.pdf).
9. *116. Chronic toxicity studies on cadmium and chromium*. *Food and Cosmetics Toxicology*, 1963. **1**: p. 131.
10. Suzuki, I. and M. Enjuzi, *The development of the corrosion resistance of an Fe-Zn alloy coating on the basis of the behaviour of the corrosion product*. *Corrosion Science*, 1986. **26**(5): p. 349.
11. Baldwin, K.R., M.J. Robinson, and C.J.E. Smith, *Corrosion rate measurements of electrodeposited zinc-nickel alloy coatings*. *Corrosion Science*, 1994. **36**(7): p. 1115.
12. Stein, M., et al., *Dealloying studies with electrodeposited zinc-nickel alloy films*. *Corrosion*, 1997. **43**(1-2): p. 223.
13. Gavrilu, M., et al., *Corrosion behaviour of zinc-nickel coatings, electrodeposited on steel*. *Surface and Coatings Technology*, 2000. **123**: p. 164-172.
14. Forsgren, A., *Corrosion Control Through Organic Coatings*. 2006: CRC Press.
15. Twite, R.L. and G.P. Bierwagen, *Review of alternatives to chromate for corrosion protection of aluminium alloys*. *Progress in Organic Coatings*, 1998. **33**: p. 91-100.
16. Edeleanu, C. and U.R. Evans, *The causes of the localized character of corrosion on aluminum*. *Trans. Faraday Soc.*, 1951. **47**: p. 1121-1135.
17. Kendig, M.W., A.J. Davenport, and H.S. Isaacs, *The mechanism of corrosion inhibition by chromate conversion coatings from x-ray absorption near edge spectroscopy (Xanes)*. *Corrosion Science*, 1993. **34**(1): p. 41.
18. Zhao, J., et al., *Effects of chromate and chromate conversion coatings on corrosion of aluminum alloy 2024-T3*. *Surface and Coatings Technology*, 2001. **140**(1): p. 51.
19. Rosenfeld, I.L., *Zashch. Met.*, 1979. **15**: p. 349.
20. Largin, B.M. and I.L. Rosenfeld, *Zashch. Met.*, 1981.
21. Kautek, W., *The galvanic corrosion of steel coatings: aluminum in comparison to cadmium and zinc*. *Corrosion Science*, 1988. **28**(2): p. 173.
22. Enders, B., H. Martin, and G.K. Wolf, *Corrosion and wear properties of multipurpose coatings deposited by ion-beam-assisted deposition*. *Surface and Coatings Technology*, 1993. **60**(1-3): p. 556.
23. Oriani, R.A., *Hydrogen-the versatile embrittler*. *Corrosion*, 1987. **43**(7): p. 390-397.
24. Shreir, L.L., *Corrosion*. 3rd ed. 1994: Butterworth-Heinemann.
25. N. Eliaz, A.S., *Charateristics of Hydrogen embrittlement, stress corrosion cracking and Tempered Martensite Embrittlement in High-Strenght Steels*. *Engineering Failure Analysis*. Vol. 9. 2002.

26. Szklarska-Smialowska, Z. *Various Forms of Localized Corrosion Common Features and Differences*. in *Stress Corrosion Cracking and Hydrogen Embrittlement of Iron Base Alloy*. 1973. Unieux-Firminy: NACE.
27. Barth, C.F. and A.R. Troiano, *Cathodic Protection and Hydrogen in Stress Corrosion Cracking*. *Corrosion*, 1972. **28**(7): p. 274-279.
28. J. O'M. Bockris, J.M., L. Nanis, *The Hydrogen Evolution Kinetics and Hydrogen Entry into alpha-Iron*. *Journal Electrochemical Society*, 1965. **112**: p. 1025-1031.
29. McCright, R.D. *Effects of Environmental Species and Metallurgical Structure on the Hydrogen Entry into Steel*. in *NACE-5 Conference*. 1973: Unieux-Firminy.
30. Oriani, R.A., *Acta Meter.*, 1975. **72**: p. 1065.
31. Speiser, R. *Hydrogen in Metals*. in *NACE-5 Conference*. 1973: Unieux-Firminy.
32. Choo, W.Y., et al., *Hydrogen solubility in pure iron and effects of alloying elements on the solubility in the temperature range 20 to 500°C*. *Journal of Materials Science*, 1981. **16**.
33. Organization, I.L. [cited Cadmium ICS 0020]; Available from: <http://www.ilo.org/public/english/protection/safework/cis/products/icsc/dtasht/icsc00/icsc0020.htm>.
34. Brooman, E.W., *Corrosion performance off environmentally acceptable alternatives to cadmium and chromium coatings: Chromium--Part I*. *Metal Finishing*, 2000. **98**(7): p. 38.
35. Watkins, K.G., R.D. Jones, and K.M. Lo, *Electrochemical investigation of the corrosion rate of sacrificial coatings on steel*. *Materials Letters*, 1989. **8**(1-2): p. 21.
36. Mendenhall, W., *Statistics for engineering and the sciences*, t. ed., Editor. 2007, Upper Saddle River, N.J.
37. *Standard Practice for Slow Strain Rate Testing to Evaluate the Susceptibility of Metallic Materials to Environmentally Assisted Cracking*. ASTM G129-00(2006).
38. Mansfeld, F., *The Relationship Between Galvanic Current and Dissolution Rates*. *Corrosion*, 1973. **Vol. 29**: p. 403-405.
39. D. Figueroa, M.J.R., *The effects of sacrificial coatings on hydrogen embrittlement and re-embrittlement of ultra high strength steels*. *Corrosion Science*, In press.
40. Yu, Q., et al., *Corrosion protection of ion vapor deposition (IVD) Al-coated Al alloys by low-temperature plasma interface engineering: Part III--DC cathodic polymerization in a closed reactor system*. *Progress in Organic Coatings*, 2002. **44**(1): p. 37.
41. Brooman, E.W., *Corrosion Behavior of Environmentally Acceptable Alternatives to Cadmium and Chromium Coatings: Cadmium, Part I*. *Metal Finishing*, 2000. **98**(4): p. 42.
42. Navinsek, B., P. Panjan, and I. Milosev, *PVD coatings as an environmentally clean alternative to electroplating and electroless processes*. *Surface and Coatings Technology*, 1999. **116-119**: p. 476.
43. Birbilis, N., M.K. Cavanaugh, and R.G. Buchheit, *Electrochemical behavior and localized corrosion associated with Al<sub>7</sub>Cu<sub>2</sub>Fe particles in aluminum alloy 7075-T651*. *Corrosion Science*, 2006. **48**(12): p. 4202.
44. Beck, E.N., *Joint test report for execution of phase of phase I of "high strenght steel joint test protocol for validation of alternatives to low hydrogen embrittlement cadmium for high strenght steel landing gear and component application-of July 2003"*. 2007, Department of the navy. Naval air warfare center aircraft division. Patuxent River, Maryland. p. 59.
45. Fontana, M.G., *Corrosion engineering*. 1986, New York: McGraw-Hill. 556.
46. Jones, D.A., *Principles and prevention of corrosion*. 1992, New York: Macmillan Publishing. 568.
47. R. N. Iyer, H.W.P., *Analysis of Hydrogen Evolution and Entry into Metals for the Discharged-Recombination Process*. *Journal of the Electrochemical Society*, 1989. **136**: p. 2463-2470.
48. R.D. Mc.Cright. *Effect of Environmental Species and Metallurgical Structure on the Hydrogen Entry into Steel*. in *Stress Corrosion Cracking and Hydrogen Embrittlement of Iron Base Alloys*. 1973. Unieux-Firminy: NACE.

49. Stachurski, M.A.V.D.Z., *The Mechanism of Hydrogen Evolution on Iron in Acid Solutions by Determination of Permeation Rates*. Journal of the Electrochemical Society, 1964. **111**: p. 615-623.
50. Figueroa, D., *Hydrogen Embrittlement Susceptibility of Ultra High Strength Steels*. 2003, Cranfield University.
51. Allcock, B.W., *Hydrogen concentration measurements using a gel-filled electrochemical probe*. 1993, Cranfield University, UK. p. 259.
52. Newman, J.F. and L.L. Shreir, *Role of hydrides in hydrogen entry into steel from solutions containing promoters*. Corrosion Science, 1969. **9**(8): p. 631.
53. McCright, R.D. and R.W. Staehle, *Effect of Arsenic upon the Entry of Hydrogen into Mild Steel as Determined at Constant Electrochemical Potential*. Journal of the Electrochemical Society, 1974. **121**(5): p. 609-618.
54. Mansfeld, F. and J.V. Kenkel, *Galvanic corrosion of Al alloys--III. The effect of area ratio*. Corrosion Science, 1975. **15**(4): p. 239.
55. Treseder, R.S., R. Baboian, and C.G. Munger, *NACE Corrosion Engineer's Reference Book*. 2nd ed. 1991, Houston: NACE International.